Outcrop-Based Correlation Of Magnetic Susceptibility With Spectral Gamma-Ray Spectrometry In The Woodford Shale Of South-Central Oklahoma

By

Michael Gordon Aufill

Bachelor of Science in Secondary Science Education

Oklahoma State University

Stillwater, Oklahoma

2004

Submitted to the Faculty of the
Graduate College of the
Oklahoma State University
in partial fulfillment of
the requirements for
the Degree of
MASTER OF SCIENCE
December, 2007

Outcrop-Based Correlation Of Magnetic Susceptibility

With Spectral Gamma-Ray Spectrometry In The

Woodford Shale Of South-Central Oklahoma

Thesis Approved:

Dr. Alex Simms

Thesis Adviser

Dr. Stanley Paxton

Dr. James Puckette

Dr. Anna Cruse

Dr. Darwin Boardman

Dr. A. Gordon Emslie

Dean of the Graduate College

Acknowledgements

I would like to gratefully acknowledge the efforts of both my Thesis Advisors. First, I thank Dr. Stanley Paxton, who caused me to become curious about MS and black shale in general. As a 50 year-old nontraditional student with arthritis, he was my mentor and my co-worker in the field. I will remember fondly all the nights we spent camping in the Arbuckle Mountains and the days we spent making measurements and discussing geology at the outcrop face. Dr. Paxton always treated me as much like a colleague as a student. Second, I owe an immense debt of gratitude to Dr. Alex Simms who agreed to be my Advisor as Dr. Paxton left Oklahoma State University to work at the USGS. Dr. Simms' willingness to take on the task of bringing this thesis to completion as my new Advisor was very generous. It would be difficult to express sufficient thanks for the patient manner in which Dr. Simms guided me through that traumatic transition. To the rest of my Committee, I express appropriately similar gratitude. Dr. Anna Cruse was my staunch defender and endless wellspring in questions of geochemistry. Dr. Jim Puckette gleefully applauded my efforts to make sense of the Hass B outcrop, even when my observations and hypotheses did not agree with published reports. Dr. Darwin Boardman helped me navigate the complexities and muddy waters of stratigraphic nomenclature. All of my Committee Members encouraged me to regularly present on-going study results in professional venues.

I would like to thank Dr. Ibrahim Çemen my former Department Head and Professor who later became my financial champion as I began pursuing an MS in geology. I assume he was intrigued that a “non-geologist” would have the unmitigated gall to take Structural Geology, as an elective no less. I would also like to thank Newfield Exploration and the Boone Pickens School of Geology for the research and teaching opportunities I enjoyed at Oklahoma State University. Without their generous support I would have been unable to complete my thesis.

I would like to thank my mother who would have been proud to see her son earn a Maters Degree in Geology. My thanks are insufficient for the patience and longsuffering of my wife Melody and my sons Matthew and Gordon. My family has steadfastly endured the financial hardship woefully associated with college students. My sons cheerfully acquiesced on the occasions when they were conscripted to help their half-crippled father in the field. I owe humble thanks to Mr. Larry Rhodes who gave me the privilege to explore the amazing beauty and geology of his ranch in the Arbuckles, the location of the Hass A outcrop and Henry House Falls. I am grateful to the staff of the YMCA camp at Lake Classen who not only gave me repeated access to Camp Classen, but also petitioned their neighbors on my behalf so I could wander adjacent properties as well. I will always remember that Dr. Robyn Hannigan trusted me to digest my own samples while her brilliant PhD students (Matt and “Leo”) performed the ICP-MS on the samples

I would like to thank all of my teachers especially Dr. Brian Carter, Dr. Todd Halihan, Dr. Surinder Sahai, Dr. Jack Vitek, Dr. Gary Stewart, Dr. Richard Marston, and Dr. Jeff Crabaugh. It would be treachery if I did failed to acknowledge several of my

fellow students. In no particular order, I owe a debt of gratitude to Patrick Kamann, Grant Heard, Carl Rapson, Ali Jaffri, Tim Samson, Eric Gerding, Emiko Konishi, and Cody Winchester, Cody Manek, Aaron Grunau, Alischa Krystyniak, and Manish Singh.

TABLE OF CONTENTS

LIST OF TABLES

LIST OF FIGURES

Figure Page

CHAPTER I

INTRODUCTION

Hypothesis and Research Problem:

The magnetic susceptibility (MS) of marine sediments (Liu et al., 2003; Vlag et al., 2004) and sedimentary rocks is thought to be controlled by inputs of terrestrial sediments containing detrital iron mineral particles (Ellwood et al., 2000). Although a strong relationship has been reported between the content of detrital material and increased MS in carbonates, little work has been conducted to show the same relationship in shales (Ellwood et al., 2000). Despite this shortfall, researchers have suggested the use of magnetic susceptibility (MS) to correlate important historical geologic boundaries on a global basis using both carbonate and siliciclastic rocks (Ellwood et al., 2000; Crick et al., 1997, 2002). One global MS correlation of the Frasnian/Famennian (F/F) boundary correlated radioactive black pyrite-rich Woodford shale with carbonates, shales, and marls (Crick et al., 2002). Although the section of Woodford Shale (Hass B) was reported to contain no carbonates, researchers correlated it with various F/F carbonate dominated and mixed lithology sections around the world, including the Global Stratotype and Stratigraphic Position (GSSP) near Coumiac, France.

All study sections in this global study, except the Woodford Shale, are composed predominantly of limestone and marl (Crick et al., 2002). In assuming detrital control of MS in the Woodford Shale, the significance of abundant (Kirkland et al., 1992)

authigenic (Lyons and Severmann, 2006) paramagnetic minerals, especially pyrite (Nagata, 1961), is overlooked.

The characteristic enrichment of black marine shale in authigenic pyrite, uranium, and several transition metals not normally associated with carbonates, is reported by Berner (1970), Berner et al. (1979), Cruse and Lyons, (2004), Lyons and Severmann, (2006). The enrichment in uranium, along with potassium and thorium (Swanson, 1961), results in the characteristically high gamma-ray magnitude (Fertl, 1979; Fertl and Chingilarian, 1989) in Devonian/Mississippian shale units, such as the Woodford Shale (Olsen, 1982).

Due to its characteristically high gamma-ray magnitude, the petroleum industry has used gamma radiation as the basis for stratigraphic correlation of Woodford Shale sections throughout the Anadarko Basin since the 1930's (Fertl and Chingilarian, 1989). The Woodford Shale contains large concentrations of the three radioactive elements in the gamma-ray specific elemental assemblage (GSEA), thorium (Th), potassium (K), and uranium (U) (Adams and Weaver, 1958; Bloxam, 1964). In general, the GSEA varies with lithology (Ellis, 1987) or geochemical facies (Adams and Weaver, 1958); (Table 1). Within the Chattanooga Shale, (Schmoker, 1980, 1981, 1993) and the Woodford Shale specifically, gamma-ray magnitude and GSEA variation as a function of lithology is well documented (Lambert, 1991, 1992, 1994; Hester et al., 1988, 1990, 1992; Dennis, 1997).

Moving basinward in a marine depositional setting, one might expect a decrease in the abundance of detrital iron-bearing minerals such as magnetite, reported as the dominant control on MS (Crick et al., 2002), with a corresponding increase in both authigenic iron concentration and iron aluminum ratios (Fe/Al); (Taylor and McClennan, 1985; Cruse and Lyons, 2004).

Table 1. Gamma-ray specific elemental assemblages and iron valences in idealized mudrock depositional environments. Shale elemental assemblages based on Swanson (1961), Bloxam, (1964), several shale standards including: NASC (Gromet et al., 1984), PAAS (Taylor and McClennan, 1984), and BSC (Vine and Tourtelot, 1970). MS strength is based on reports of MS dependence on iron valence state in iron oxides (Nagata 1961, Retallack et al. 2003). Iron valence state and stability is based on reports by Berner (1970), Berner et al. (1979), Faure (1991), Rimmer (2004a, 2004b) and Lyons and Severman (2006).

Idealized Mudrock Depositional Environment (excluding diagenesis)	**Spectral Gamma-Ray Elemental Assemblage**	**Gamma-Ray relative to other mudrocks**	**Common Fe Valence(s)**	**Iron Source (provenance)**	**predicted MS relative to other mudrocks**
terrestrial shale	**lowest U, very high K, highest Th**	**low gamma**	**Fe (III) hematite**	**detrital low Fe/Al**	**high**
marine marginal reducing shale (underclays)	**low U, very high Th and K**	**med gamma**	**Fe (II) pyrite (from siderite)**	**mixed provenance**	**?**
marine marginal oxidizing (shale)	**low U, high Th and K**	**med gamma**	**Fe (III) hematite**	**detrital low Fe/Al**	**high**
marine oxidizing/reducing (shale) (hemi-pelagic)	**med U, high Th and K**	**high gamma**	**Fe (II) pyrite and Fe (III) hematite magnetite**	**mixed provenance med Fe/Al**	**varies environmentally with oxygen and Fe valence**
deep Marine Reducing (Pelagic)	**highest U, lowest Th, med K**	**highest gamma**	**Fe (II) Pyrite Fe III unstable**	**authigenic pyrite high Fe/Al**	**low**

Enrichment in total iron (e.g. authigenic pyrite) and uranium, both precipitated directly from seawater in anoxic depositional environments, tends to limit the importance of detrital iron in black shale depositional environments associated with extremely high gamma magnitudes (Olson, 1982; Lyons and Severmann, 2006). The finding that MS is roughly controlled by detrital iron predicts that MS magnitude based on detrital minerals containing iron should decrease as one moves basinward, as previously reported by Ellwood et al., (2000). Conversely, in clastic sedimentary rocks such as the Woodford Shale, gamma-ray magnitude and concentration of authigenic uranium increase as one moves basinward (Swanson, 1961). Thus, it has been suggested that high gamma-ray magnitude is characteristic of environments containing little or no detrital iron component (Lyons and Severmann, 2006) in environments where Fe (III) is not chemically stable (Faure, 1991).

Research Questions:

This study will test the hypothesis that "magnetic susceptibility magnitude will vary inversely with gamma-ray magnitude in the Woodford Shale". Another aim of this study is to estimate the control that detrital iron exerts on magnetic susceptibility in the Woodford Shale. In addition to testing the aforementioned hypothesis, this study will provide a perspective on other economically important and scientifically significant questions. These include:

1.) Does MS or gamma- ray magnitude vary with the well studied mineralogy, particle size (Kirkland et al., 1992), and broad lithofacies divisions of the Woodford Shale (Lambert, 1991, 1992, 1993)? The ability to predict Woodford

facies changes with MS could have direct bearing on predicting shifts in location, quality, thickness, or number of conventional and unconventional reservoirs in the Anadarko Basin.

2.) Is the iron in the Woodford Shale detrital (Crick et al., 2002), or is it authigenic (e.g. pyrite); (Kirkland, et al., 1992)? Using iron/aluminum (Fe/Al) ratios it is possible to estimate enrichment of authigenic iron vs. detrital iron relative to the NASC and other shale standards, (Vine and Tourtelot, 1970; Gromet et al., 1984; Taylor and McClennan, 1985; Quinby-Hunt et al., 1989).

3.) Is the Lake Classen Spillway exposure of the Woodford Shale at Hass B an appropriate magnetic type section for the Frasnian/Famennian (F/F) Boundary in North America? If shale and carbonate are found to be fundamentally different in their MS responses, perhaps a section of Devonian carbonates would be a more appropriate type section for MS correlations.

4.) Does magnetic susceptibility vary with lithology or lithofacies? The ability to predict subtle or large lithologic changes through MS variation, extended through MS correlation across the Anadarko Basin, could have the potential to aid petroleum production. The previously cited use of spectral gamma-ray analysis to delineate large and subtle changes in Woodford Shale lithology is already widely employed (Hester et al., 1988, 1990, 1992).

The simultaneous measurement of gamma-ray specific elemental concentrations and magnetic susceptibility at previously studied Woodford Shale outcrops (Krystyniak, 2003; Krystyniak et al., 2005; Paxton et al., 2006a, 2006b, 2007) will be used to determine if there is a predictive correlation between MS and gamma-ray magnitude in

the Woodford Shale. The concentrations of iron, aluminum, and other trace elements in Woodford Shale samples will be measured by the method of inductively coupled plasma-mass spectrometry (ICP-MS). The provenance of iron in the Woodford Shale, either detrital or authigenic, will be determined through comparison of observed iron/ aluminum ratios (Fe_{ppm}/Al_{ppm}) to established shale standards such as, the Marine Sciences Group Black Shale Composite (BSC); (Vine and Tourtelot, 1970), the North American Shale Composite (NASC); (Gromet et al., 1984), and the post Archean Australian Shale Standard (PAAS); (Taylor and McClennan, 1985).

Location of Study Area (Outcrops):

The Chattanooga Shale and its equivalent the Woodford Shale occur over a large portion of the United States (Lambert, 1991). This study will focus on two well studied Woodford Shale outcrops in south-central Oklahoma. The most complete section is the outcrop exposed in the quarry and on the west side of Henry House Creek in Carter County, Oklahoma, Section 30, T. 2S., R.1E. I.M. (Figure 1). This outcrop is also known as Hass A (Hass and Huddle, 1965). The second outcrop is located at the Lake Classen Spillway in Murray County, Oklahoma, Section 24 T. 1S., R. 1E. I.M. (Figure 1). The second outcrop, also known as Hass B, is located approximately 7 miles from the first outcrop (Hass and Huddle 1965). Both outcrops are located in the Arbuckle Mountains where long sequences of Paleozoic rocks are exposed in the Arbuckle Anticline (Ham, 1986); (Figure 2).

During a preliminary survey for this study, several Woodford Shale outcrops other than Hass A and Hass B, were visited, photographed, and sampled. The present

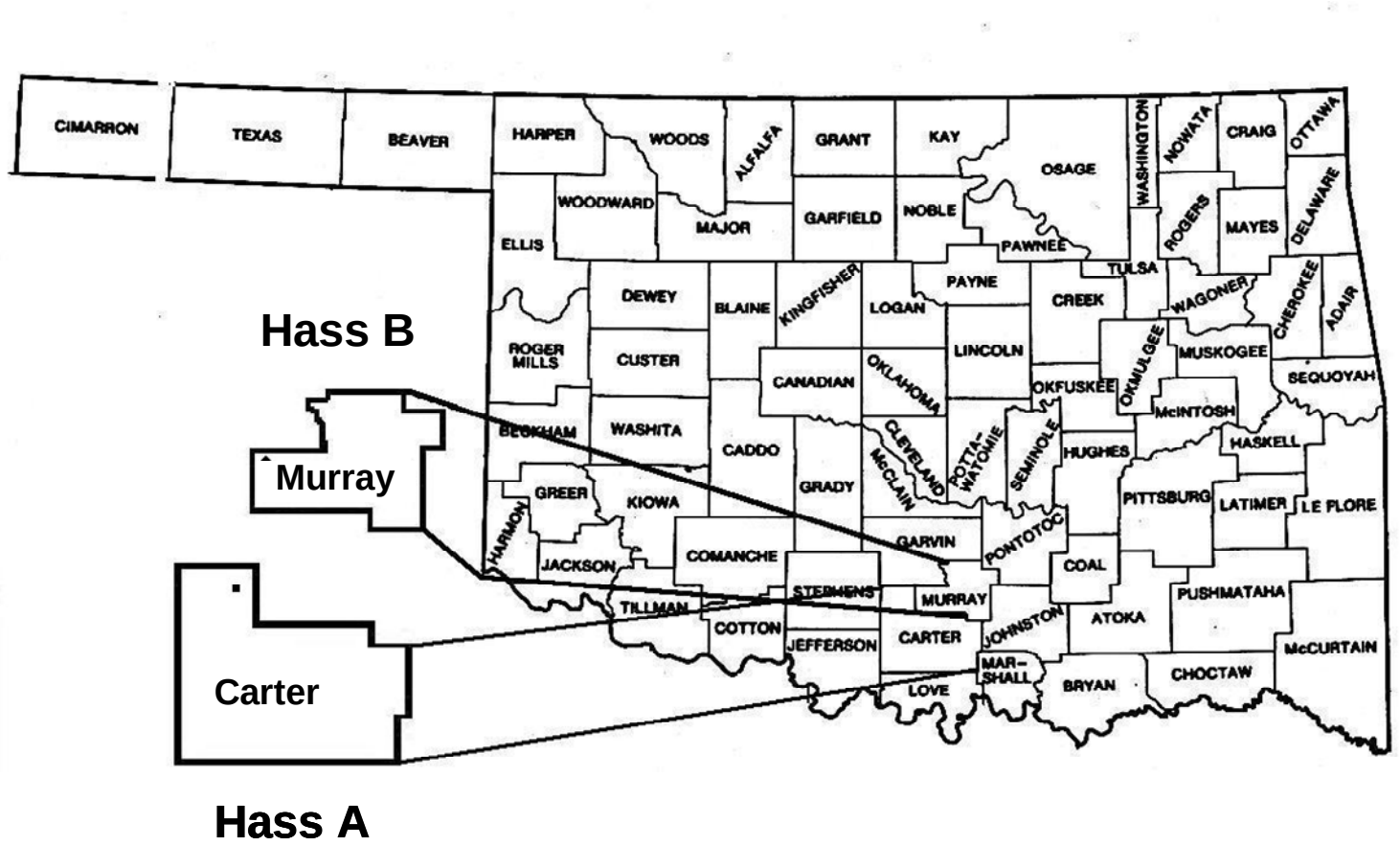

Figure 1. Locations of study outcrops.

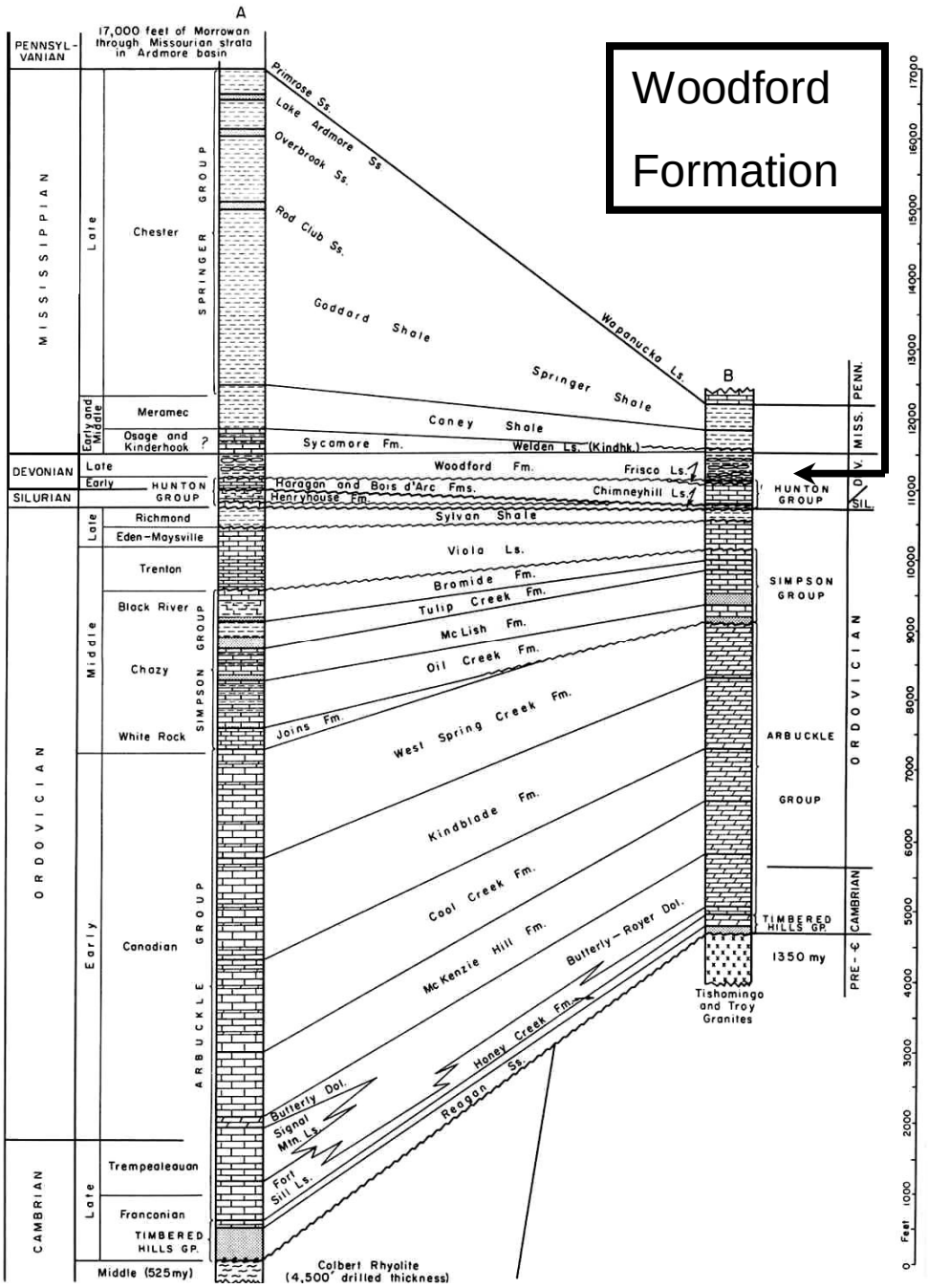

Figure 2. Lithologic cross-section of study area (Ham, 1986).

study will also incorporate observations from other Woodford Shale outcrops including: the former Woodford Shale type section (Gould, 1925) exposed west of Hass A near the town of Woodford, Oklahoma in Carter County, Oklahoma, Section 34, T. 2S., R. 1W. I.M., the I-35 southbound exposure of the Woodford on the southern limb of the Arbuckle Anticline, west of Hass A, Carter County, Oklahoma, Section 36, T. 2S., R. 1E. I.M., the current Woodford Shale type section, the I-35 northbound outcrop of the Woodford near Turner Falls (and Hass B) in Murray County, Oklahoma, Section 30, T. 1 S., R. 1E. I.M (Fay, 1989), the exposure in the Hunton Quarry near Daugherty, Oklahoma, Section 6, T. 2S., R. 3E. I.M. and the exposure in the McAlister Cemetery pit near Ardmore Oklahoma, Section 36, T. 5S., R. 1E. I.M.

Scope and Limitations:

The main focus of this study is 2 outcrops: Hass A (Figure 3) and Hass B (Figure 4), or Henry House Creek and Lake Classen Spillway, respectively. Although no cored sections of the Woodford are included in the study, significant amounts of spectral gamma-ray data are available for the Woodford Formation and it has been shown that gamma-ray lithocorrelation across the Anadarko Basin is a straightforward process (Fertl and Chingilarian, 1989; Hester et al., 1990; Dennis, 1997).

Woodford lithofacies changes have been documented in the form of petroleum industry gamma-ray logs (Hester et al., 1990; Lambert, 1993) and resistivity logs (Hester et al., 1988) prepared in conjunction with Woodford petroleum production (Dennis, 1997). In addition to data collected during this study, data from other Woodford Shale

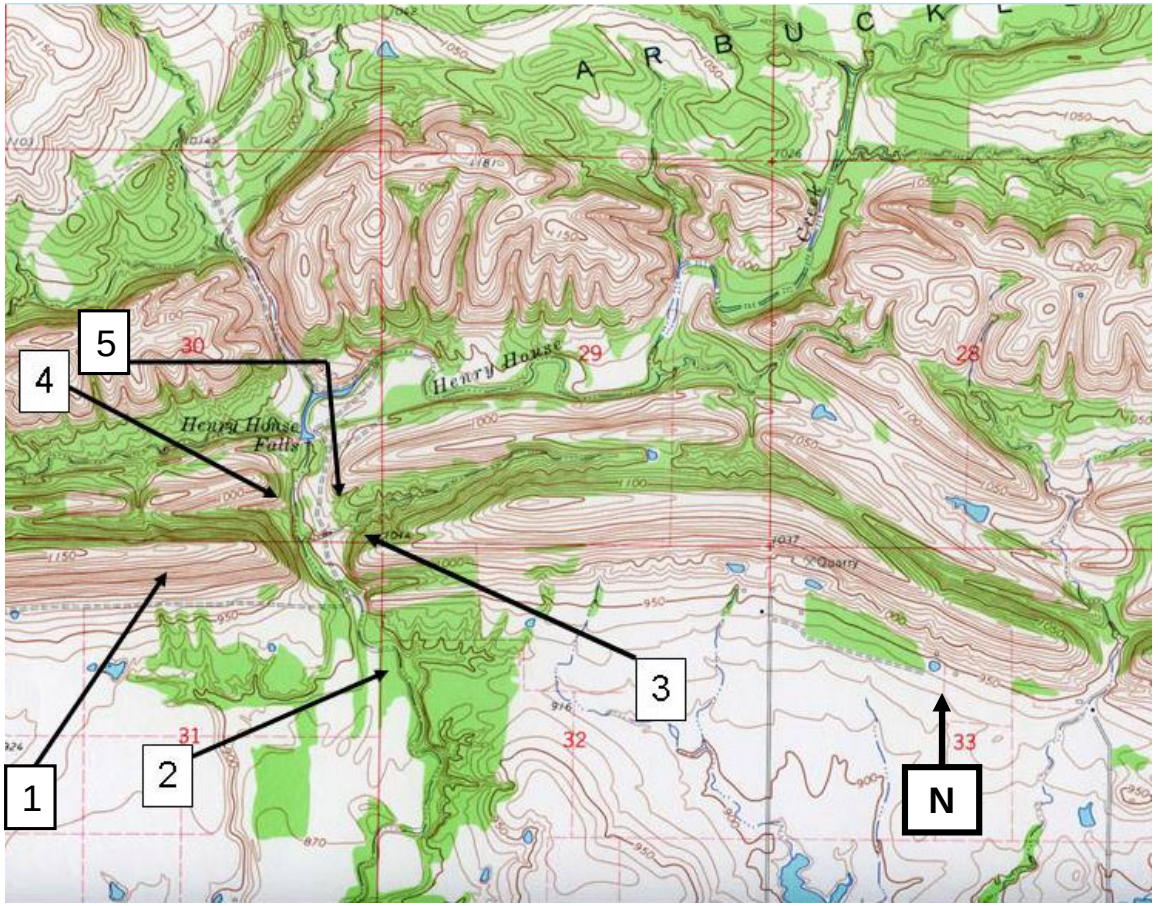

Figure 3. Modified USGS topographic map of the Hass A, Henry House Creek study area. Woodford Shale beds strike 266^{o} and dip 49^{o} SE. Note the roughly E-W trend of the Sycamore Limestone hogback and the southern limb of the Arbuckle Anticline (1), an outcrop of Caney Shale (2), the top of the Woodford Shale in the ranch quarry (3), the basal contact between the Hunton Limestone (Bois d'Arc Limestone) and the Woodford Shale at the confluence of Henry House Creek and an unnamed ephemeral creek dubbed "Rattlesnake Creek" in this study (4). The largest silicified logs were located near the basal contact between the Hunton Limestone and the Woodford Shale in the ranch quarry (5).

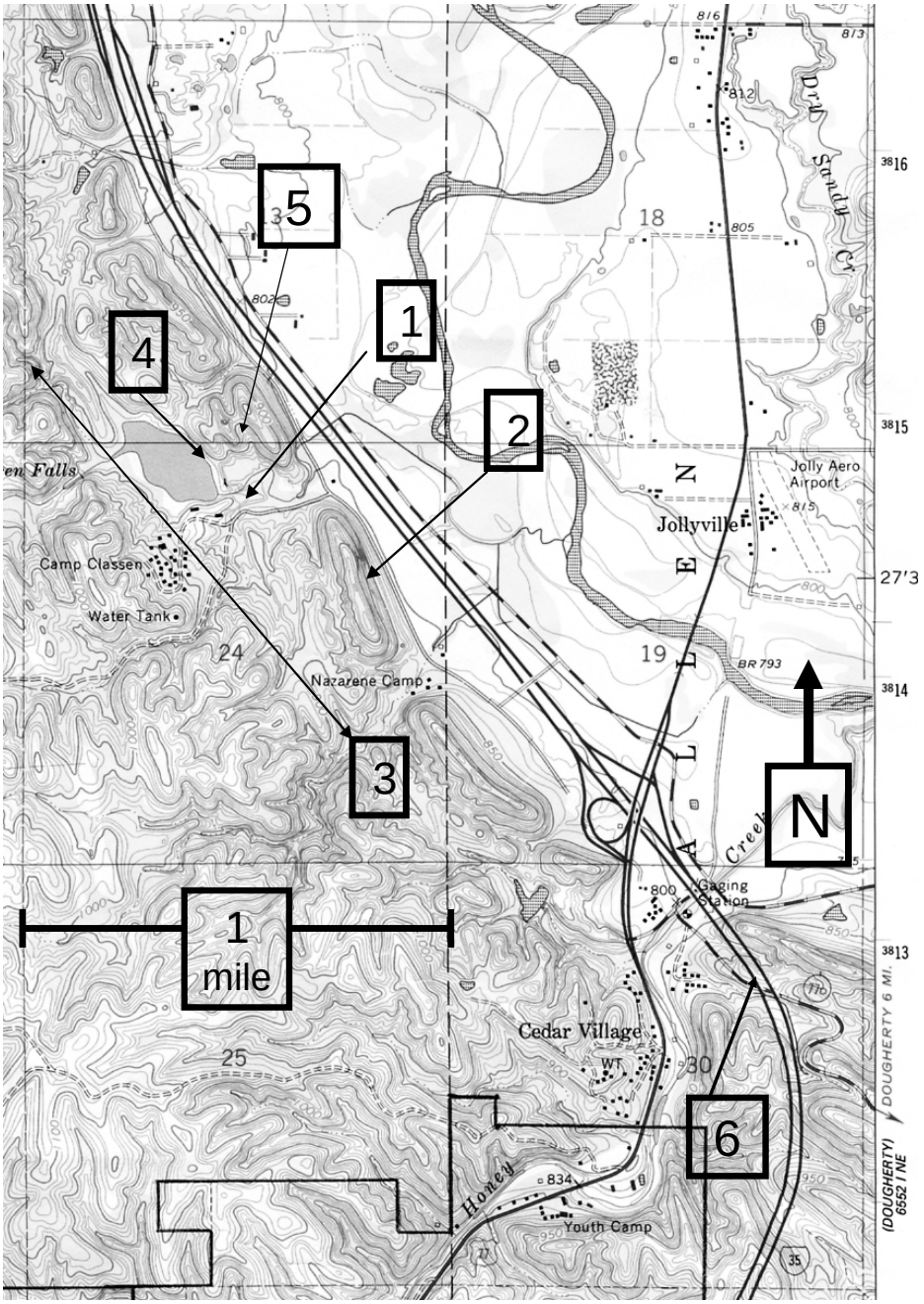

Figure 4. Modified USGS topographic map of the Hass B, Lake Classen spillway study area. Important features include: (1.) the Lake Classen Spillway outcrop of Woodford Shale at Hass B, (2.) the resistant hogback of Sycamore Limestone (3.) the approximate trend of Washita Valley Fault-Zone, (4.) the location of an unfaulted basal contact between the Henryhouse-Harragan Limestone and the Woodford Shale (**Ph_l**) (5.) the approximate location of contact between (**L_l**) and (**Ph_R**) repeat section of phosphatic Woodford Shale, and (6.) the approximate location of the I-35 north Woodford Shale outcrop on the north limb of the anticline.

studies found in the literature will be used to test study results. Biostratigraphic control for these outcrops is provided by other studies (Hass and Huddle, 1965; Over and Barrick, 1990; Over 1992a, 1992b, 2002; Schwartzapfel and Holdsworth, 1996).

The most complete outcrop at Hass A has been divided into 969 separate beds of varying thickness in this study (Figure 5). This sub-division of the outcrop into this large number of sub-units is well beyond the scope of any published Woodford Shale studies (Table 2). Likewise, this study provides a detailed description of the lithologic succession at Hass B (Figure 6); (Table 3). Most Woodford studies subdivide the formation into three main intervals based on kerogen content and well log properties (Lambert, 1991, 1992). Other workers have noted the absence of, and need for, detailed Woodford Shale outcrop lithostratigraphy (e.g. Hester et al., 1990).

The magnetic susceptibility (MS) employed in this study is volume specific MS (κ). It offers distinct advantages over other forms of MS employed in previous studies. Volume specific MS (κ) is easily measurable in the field or laboratory, allowing repeated measurements to be made very rapidly. Due to the rapid manner in which κ can be measured, several lateral MS measurements were made at each point.

One limit on this study was the occurrence of thin covered intervals at the top and base of the Hass A section (Hass and Huddle, 1965). More significantly, the Hass B section contains large intervals that are completely covered or altered by soil forming and tectonic processes. The upper portion of Hass B has been altered by a combination of soil forming and tectonic processes, or covered by modern stream deposits. In these intervals, meaningful MS measurements could not be obtained. In these covered intervals, the study was often limited to measurements of bed thickness, lithology, and/or gamma-ray magnitude.

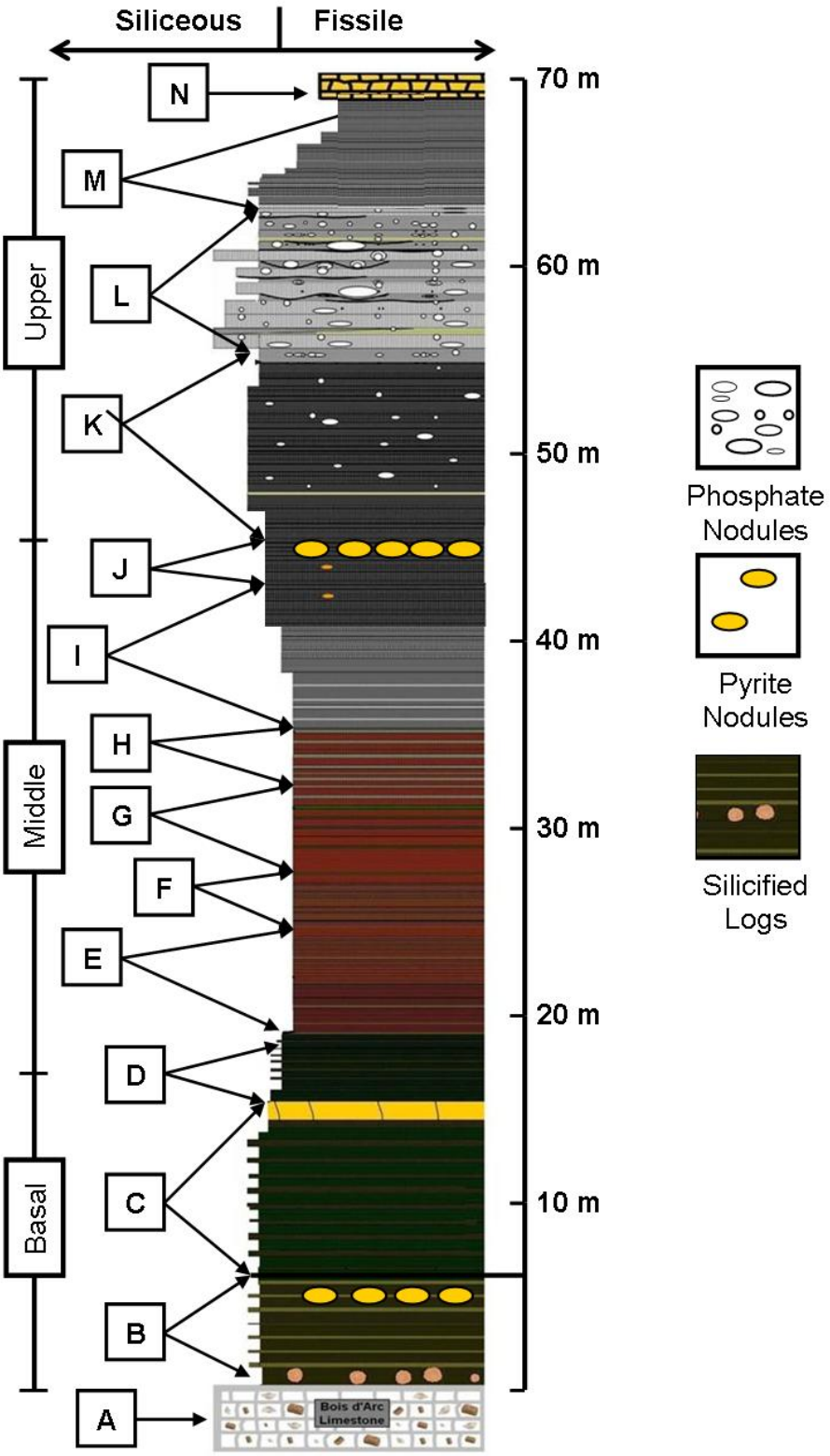

Figure 5. Detailed stratigraphy of the Woodford Shale at Hass A, Henry House Creek (Carter County, Oklahoma). A key and detailed description of stratigraphic units at the Hass A outcrop are located in Table 2.

Table 2. Detailed lithological description of Woodford Shale at **Hass A**

Unit	**Lithology (**Notes)	**height** (m above Bois d'Arc Limestone base)
N	(Mississippian) Transitional Unit → Sycamore Limestone	above Woodford Shale
M	Cyclic black fissile shale with corresponding thick black blocky siliceous beds - Phosphate nodules present but less common up to 65.5 m of section – easily erodible (U/Th = 2.1 - 15.3)	62.9-69.6
L	Very thin beds cyclic dark blue/gray fissile shale with corresponding and numerous extra blue/gray blocky and undulating chert, phosphate, and dolomitic beds- Spherical, oblate, and elliptical phosphatic nodules coalescing into undulating continuous beds-Phosphate nodules throughout-Easily erodes to lag of phosphate nodules- Contains Devonian/Carboniferous Boundary (U/Th = 2.1 - 15.3)	56.4-62.9
K	Very thin beds cyclic black-blue/gray fissile shale with corresponding and numerous extra very thin beds blue/gray blocky chert and laminated hydrocarbon-rich dolomitic beds- Spherical phosphatic nodules common in basal beds-Thick (12.2 cm) laminated dolomitic shale at top-Very well indurated (U/Th = 4.0 – 10.8) (24-32 beds/m)	45.7-56.4
J	Thick beds cyclic black fissile shale with thin beds of very well indurated black blocky siliceous shale- Contains common large (5 – 10 cm) pyrite nodules. Thin pyrite bed Near *formation* U-maximum concentration (U ppm = 112.6) (U/Th = 6.6 – 11.6) pyrite weathers with rust-colored residue	43-45.7

Table 2. Detailed lithological description of Woodford Shale at **Hass A** (cont.)

I	Thick beds cyclic black fissile shale with few very thin beds of blocky siliceous shale- Contains large (5 – 10 cm) pyrite nodules. (U/Th = 3.1 – 10.7)	36-43
H	Thick beds cyclic black fissile shale with corresponding thin black blocky siliceous beds-Erodes easily	32.1-36
G	Very thick beds cyclic brown/black fissile shale with corresponding and very thin brown/black blocky siliceous beds. Very poorly indurated. (U/Th = 3.4 - 7.6)	27.5-32.1
F	Thick (< 1m) beds cyclic brown/black fissile shale with corresponding and very thin brown/black blocky siliceous beds. Very poorly indurated. (U/Th = 3.6 - 7.6)	25.6-27.5
E	Thick beds cyclic brown fissile shale with corresponding and very thin brown/black blocky siliceous beds. Very poorly indurated. (U/Th = 3.1 – 6.5)	19.5-25.6
D	Thick (< 1m) beds cyclic dark green/black fissile shale with corresponding and extra thin brown blocky siliceous beds. Very poorly indurated. (U/Th = 4.2 – 8.1)	16.6-19.5
C	Thick (< 1m) beds cyclic dark green fissile shale with corresponding brown blocky siliceous beds. Fissile intervals are poorly indurated. Thick (19.4 cm) blocky yellow carbonate bed at top (U/Th = 2.8 – 8.3)	6.2-16.6
B	Brown/green fissile cyclic (4-11 cycles/m) shale with inter-bedded brown blocky siliceous shale high K (1-3 ppm)-green weathered mudstone, chert pebbles, chert nodules and silicified wood (*Callixylon sp)* at/near base- Pyrite nodules common-(U/Th ratio =2.0 – 8.0)	0-6.2
A	(Devonian) Bois d'Arc Limestone (Hunton Group)	Below

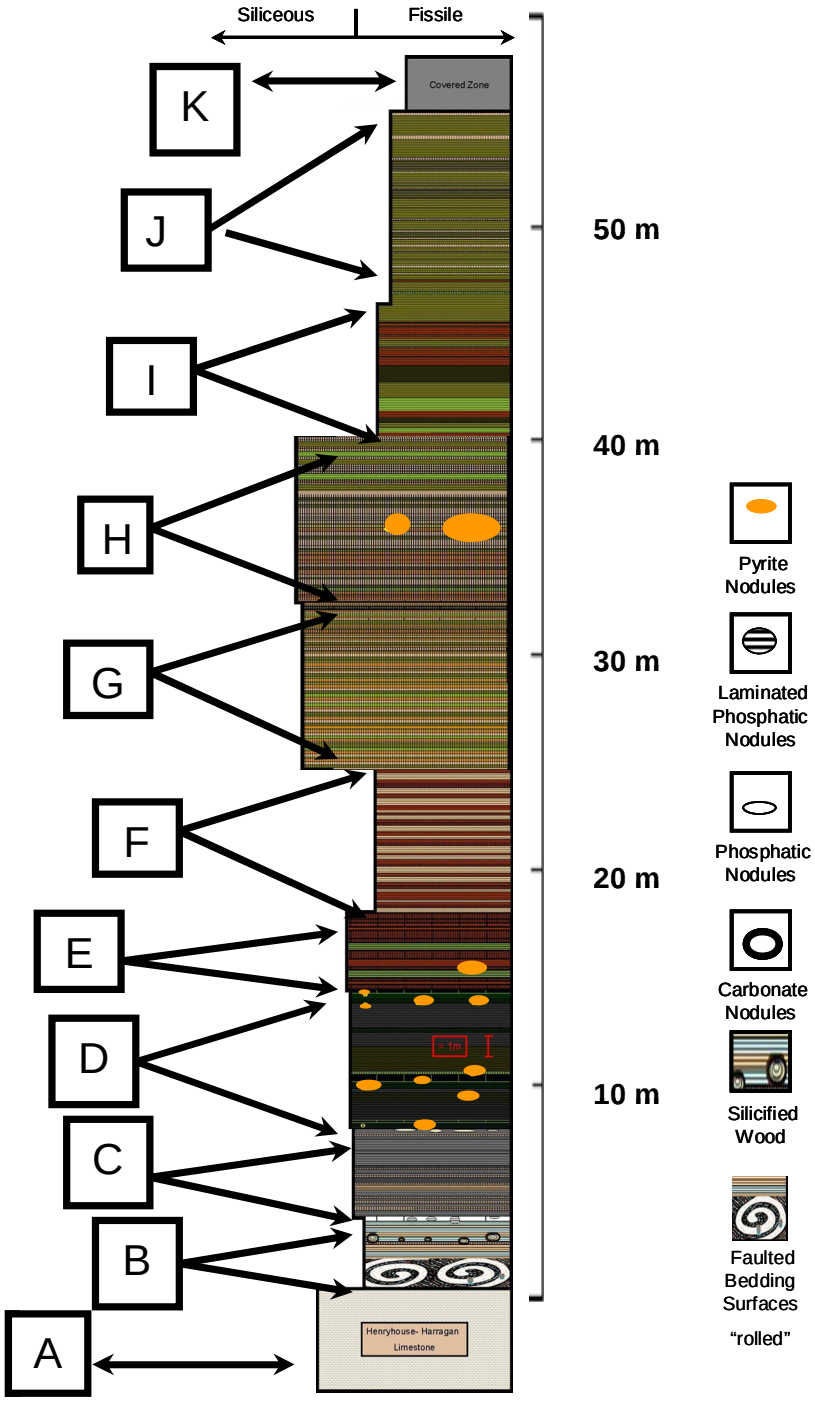

Figure 6. Detailed stratigraphy of the Woodford Shale at Hass B, Lake Classen Spillway (Murray County, Oklahoma). A key and detailed description of stratigraphic units at the Hass B outcrop are located in Table 4.

Table 3. Detailed lithological description of Woodford Shale at **Hass B***

Unit		**Lithology (**Notes)	height (m above **Henryhouse Harragan** base)
CZ Or (K*)	**L_R**	Sycamore Limestone. Multiple beds of gray/green fresh (yellow-weathered) wackstone with fine sand-size grains of silica residue. No macro-fossils, no laminations. Beds are parallel and blocky and pervasively shattered. Individual clasts have subconchoidal fracture, some with slicken lines.	55.8 m-109.1 m
	W	Welden Type Woodford Shale contains grey, pink, and tan beds of massive silty shale with septarian calcareous nodules (vigorous acid reaction). Contains thin discontinuous siliceous beds. Bedding features or continuous laminations absent. Blocky siliceous Woodford Shale beds *in situ* at top with oblate and spherical phosphatic nodules.	
	Ph_R	Fractured beds of black siliceous and brown-gray phosphatic Woodford Shale with oblate and spherical phosphatic nodules. Siliceous beds trend roughly 330^o. Curved plates of thin deformed siliceous shale breccia (no acid reaction) occur as float.	
	L_1	Multiple beds of grey/green fresh (yellow-weathered) wackstone (vigorous acid reaction) with fine sand size grains silica residue. Beds dip roughly 90^o and strike roughly 330^o. No macro-fossils or laminations observed. Beds are parallel, blocky and pervasively shattered. Individual clasts have subconchoidal fracture, some with slicken lines, and calcite fracture-fill. Phosphatic Woodford Shale *in situ* at base of interval.	

Table 3. Detailed lithological description of Woodford Shale at **Hass B** (cont.)

CZ Or (K*)	**Ph_1**	Woodford Shale. Fractured beds of welded breccia. Original lithology is black siliceous and blue-gray phosphatic Woodford Shale with oblate and spherical phosphatic nodules. Curved plates of thin deformed siliceous shale breccia (no acid reaction) occur as float.	
K		Covered zone in spillway (CZ)	
J		Cyclic fissile and siliceous thinly bedded green/ brown shale. (U/Th = 1.5 – 6.2). Gamma-ray Measurements impossible after 55.8 m of section. MS measurements impossible after 48.2 m of section. Creek widens balance of outcrop missing, faulted, or under water in creek. (U/Th = 1.5 – 6.2)	55.8 – 47.1
I		Very thick beds of brown/green fissile, fissile siliceous, and thin blocky siliceous shale. Near top of interval shale becomes more fissile and fissile packages become thicker. Formation is fractured and eroded. Weathers easily. (U/Th = 3.6 – 7.8)	40.2 – 47.1
H		Couplets of cyclic light brown/green siliceous-laminated and siliceous thinly bedded shale and blocky chert separated by multiple extra repeated chert beds. Fissile beds becoming thicker at top of interval. Interval (.3 m) of small pyrite nodules and thin discontinuous pyretic layers at approx 35.7 m of section. Outcrop is stained with iron oxide. Gamma-ray magnitude maximum at 36.6 m of section (U/Th = 4.0 – 6.5).	32.7 – 40.2
G		Cyclic light brown/green fissile, siliceous-laminated and siliceous thinly bedded shale with corresponding and multiple repeated chert beds (i.e. no fissile beds intervening). Highly fractured and sheared. Fissile beds very thin relative to balance of outcrop. (U/Th = 2.8 – 8.2)	25.0 – 32.7

Table 3. Detailed lithological description of Woodford Shale at **Hass B** (cont.)

F	Cyclic packages of thickly bedded light brown/green fissile and thinly bedded siliceous-laminated shale with corresponding blocky chert beds. Zone of highly fractured and sheared chert and siliceous shale at 20.2 – 21.3 m of section. Weathers very easily. Site of second pool below dam begins between reference beds "A8"and "A9". (U/Th = 2.9 – 8.8)	17.4 – 25.0
E	Cyclic light brown/green fissile siliceous and laminated shale with corresponding very thick blocky siliceous beds. Resists erosion and forms fall in spillway. Contains Frasnian / Famennian (F /F) boundary (Over, 2002). (U/Th = 3.3 – 8.7)	13.7 – 17.4
D	Dark gray or black paper-thin fissile or green cyclic fissile and laminated siliceous shale. Contains corresponding thick blocky beds green blocky siliceous shale. Small (≈ 1.5 cm) pyrite nodules occur at fissile siliceous contacts at several levels within interval. Insoluble nodule at approx. 12 m of section (U/Th = 1.9 – 6.5)	7.3 – 13.7
C	Dark gray or black cyclic fissile shale. Contains several thick blocky beds tan siliceous shale. Elliptical septarian carbonate concretions at top of interval. (U/Th ratio = 3.1 – 6.9).	3.2 – 7.3
B	Pink (Munsell 10R 8/4) and light blue/gray (Munsell 5G 8/1) gleyed claystone. Abraded *in situ* carbonate clasts and *Callixylon sp* within 1m of base. Spillway exposure chaotically folded, disrupted and faulted. First blocky bed siliceous shale (pink, Ibid.) at approx 1.3m of section. Thin laminated dolomite and elliptical laminated carbonate nodules at top of interval. Site of first pool below dam, from carbonate base to reference bed "A". Contains Acadian Unconformity surface. (U/Th ratio = 0.5 – 3.5).	0 - 3.2

Table 3. Detailed lithological description of Woodford Shale at **Hass B** (cont.)

A	Harragan Formation, Henryhouse Limestone, Hunton Group. Thickly bedded blocky tan (fresh) dark gray (weathered) wackstone. Calcite rich (vigorous acid reaction). Contains sand and silt-size insoluble silica residue. Contains middle Devonian Conodonts (Hass & Huddle, 1965). No fossils observed. Strike measured azimuth 315^{o} dipping 85^{o} NE. Nearly vertical beds partially covered by alluvium and colluvium containing clasts of weathered Collings Ranch Conglomerate.	below basal contact
	* Intervals A thru J are observed and described in the spillway outcrop. Interval K corresponding to a covered zone (CZ) is observed north of the spillway and is composed of zones Ph_1 thru L_R are described based on exposures immediately north of the spillway outcrop. Zones L_1 thru L_R are described based on exposures immediately south of the spillway outcrop (Ham, 1986; Fay, 1989; Pybus, 1995).	

Table 4. Spectral gamma-ray measurements in basal beds of Woodford Shale at Hass A and Hass B.

Height (cm) Above/ Below Base	K (wt.%)		U (ppm)		Th (ppm)		U/Th Ratio (ppm/ppm)		Gamma-Ray Magnitude (API units)	
	Hass A	Hass B	Hass A	Hass B	Hass A	Hass B	Hass A	Hass B	Hass A	Hass B
152.4	2.3	6.1	32.4	10.4	11.0	18.5	2.9	0.6	340.	255
137.2	2.0	5.0	30.4	10.7	10,4	20.8	2.9	0.5	317	249
121.9	2.1	5.4	28.1	10.0	11.8	15.7	2.4	0.6	306	229
106.7	2.1	4.2	30.5	10.4	12.1	19.2	2.5	0.5	326	227
91.4	2.0	3.4	33.5	7.9	9.4	13.9	3.6	0.6	338	173
76.2	1.6	3.4	21.5	10.6	12.5	11.4	1.7	0.9	248	185
61.0	2.2	3.8	25.4	10.9	11.0	16.0	2.3	0.7	262	212
45.7	1.6	3.7	20.7	9.0	7.2	13.4	2.9	0.7	220	185
30.5	1.1	2.9	16.6	6.5	9.2	11.3	1.8	0.6	187	144
15.2	1.1	2.8	13.0	7.3	6.4	9.9	2.0	0.7	147	143
-30.4	0.8	Hunton Limestone	2.9	Hunton Limestone	4	Hunton Limestone	0.7	Hunton Limestone	55	Hunton Limestone
-60.8	0.7		0.9		4.3		0.2		38	

The scope of this study is largely limited to MS in the marine clastic rocks of the Woodford Shale. As a result, conclusions and interpretations will be limited by the relatively few studies specific to MS in marine clastic sedimentary rock. Well studied MS in clastic terrestrial sediments (Retallack et al., 2003) may be a poor analog for testing our results because by definition, sediment is unlithified. Recent studies have reported significant magnetic alteration in sediment by compaction, cementation, diageniesis, and redox changes (Liu et al., 2003; Vlag et al., 2004, Evans and Elmore, 2006).

Conclusions in this study are further limited by enigmatic differences between modern oceans and the so-called Strangelove Oceans or *Kellwasser* Events (kill-water) of the Frasnian/Famennian boundary (House, 2002). Even the most anoxic modern oceans are a poor analog to the oceans of the Devonian (Sepkowski, 1986).

CHAPTER II

REVIEW OF LITERATURE

Magnetic Susceptibility:

Two common types of magnetic susceptibility reported in the literature are volume specific magnetic susceptibility (κ) and anhysteric magnetic susceptibility (χ). Both are dependent on the strength of magnetic induction or magnetic flux density (*B*), which is defined by the equation;

$$B = H + 4\pi J \text{ (Eq. 1)}$$

where, *J* is the magnetic moment or strength of magnetization caused by the magnetic field of the material per unit volume (Nagata, 1961), and *H* is a uniform magnetic field produced by a magnetic bridge instrument such as the *MS2K* manufactured by Bartington Industries. Volume specific magnetic susceptibility (κ) is defined by;

$$\kappa = J/H \text{ (Eq. 2)}$$

dividing the volume-specific magnetic susceptibility (κ) by the density of the material (ρ) in either CGS or SI units, yields χ, or mass specific susceptibility;

$$\kappa / \rho = \chi \text{ (Eq. 3).}$$

Mass-specific magnetic susceptibility, or χ, is not as easily affected as volume-specific MS by the size of particles (Nagata 1961, Banerjee et al., 1981, Sachs and Ellwood, 1981). Because it is less influenced by size, χ can be employed as a method of estimating grain size. Banarjee et al. (1981) reported that volume-specific MS is

disproportionately affected by very fine particles of iron minerals relative to mass-specific MS. Mass-specific magnetism takes into account the mass of the particle and may be a better measure of magnetism if particle size variability is suspected. Furthermore, Banarjee et al. (1981) reported that the ratio of anhysteric remnant magnetism to mass-specific MS is a better method of characterizing fine particles of magnetite than mass-specific MS or volume-specific MS alone. Ledbetter (1986) used this magnetic ratio to determine travel pathways of fine magnetite particles in the Argentine Basin.

Ledbetter (1986) concluded that in poorly energetic basins, circulation currents are capable of transporting and reworking deposits of magnetic detritus. He and Banarjee et al. (1981) concluded that magnetic susceptibility is not homogenous in a single modern basin because some parts of basins receive disproportionate quantities of magnetite or varied particle-size distributions of magnetite. Neither study concluded that pyrite was an important control on MS (Banarjee et al., 1981; Ledbetter, 1986).

Scheiber (1994) and Scheiber and Baird (2001) describe the reworking of large quantities of detrital pyrite in the Devonian Chattanooga Shale (Woodford Shale equivalent). Scheiber (1994) and Scheiber and Riciputi (2004) concluded that detrital pyrite, originally deposited as authigenic pyrite, was the most abundant iron species present. Scheiber and Elwood (1993) used MS to determine particle pathways in Proterozoic shale, reporting that MS variation was evidence of reworked iron particles.

Volume-specific magnetic susceptibility (κ) is dimensionless. Materials with negative κ on the order of 10^{-6} are called diamagnetic or very weakly magnetic. Those materials which have a positive magnetic susceptibility, on the order of 10^{-6}, are defined

as paramagnetic or weakly magnetic. Materials with strong κ on the order of $10\text{-}10^5$ are defined as ferromagnetic (Nagata, 1961). Typically, iron III is ferromagnetic, while iron II is paramagnetic (Table 1), and substances such as carbonate and silica are diamagnetic (Nagata, 1961).

Both volume-specific and mass-specific MS have been used in a variety of sediment studies for varied purposes including: characterizing paleosols (Nagata, 1961; Ďurža, 2004; Retallack, et al, 2003), relative dating of cave sediments (Ellwood et al., 2003b), inferring paleoclimate at an archeological site (Ellwood et al. 1995), inferring climate change (Liu et al., 2003; Vlag et al., 2004), characterizing particle sizes and currents in modern basins (Ledbetter, 1986), defining sediment provenance (Lui et al., 2003), studying enhanced reduction of iron oxide by sulfate reducing bacteria (Li et al., 2006), studying enhanced methane flux at gas hydrate vents (Novosel et al., 2005), studying control and concentration of magnetic particles in the Argentine Basin (Sachs and Ellwood, 1988), studying hydrocarbon contaminated aquifers (Zachara et al., 2004), studing sediment diagenesis in modern deep-sea fans (Dillon and Bliel, 2004), and correlating MS changes in lake sediments along with pollen to determine timing of glaciation and thresholds of anthropogenic erosion (Banarjee et al., 1981).

The sediment-specific studies of MS cited above can be divided into two groups. The first group, generally earlier MS studies, often does not take into account the effects of lithification, sediment mineralogy and provenance, basin redox trends and diagenesis. Instead, early studies focus on sediment particle size, environmental energy and morphology of depositional basins. This group of studies concluded that global MS is a function of eustatic sea-level change or weathering of magnetic minerals in soil forming

processes and dependent mainly on detrital iron-bearing minerals (Crick et al., 2002). Redox alteration of iron minerals by any cause or precipitation of authigenic minerals such as pyrite is not considered in these studies and the importance of pyrite as an MS control is specifically minimized (Ellwood et al, 2000; Crick et al., 2002). The second group, or more recent MS literature, tends to conclude that MS variation is a function of, strongly influenced by, or later changed through environmental geochemistry (Liu et al., 2003), biological modifications (neogenesis) of sediment after deposition (Zachara et al., 2004), and rock diagenesis, long after lithification (Retallack, 2003).

MS has been studied in rocks for many reasons including: searching for middle Devonian asteroid impacts (Ellwood et al., 2003c), searching for K/T impacts (Ellwood et al. 2003a), for global lithocorrelation at several Devonian stage boundaries (Ellwood et al., 2001; Crick et al. 1997; Ellwood et al., 2006; Crick et al. 2002), studying MS variation as a function of detrital content in carbonates (Ellwood et al., 2000; Gersl and Hladil, 2003), correlating *in situ* outcrops to petroleum well bit cuttings (Ellwood, et al., 2000), studying Milankovitch cyclicity in the Kimmeridge Clay (Weedon et al., 2004), and studying the effect of ferromagnesian calcite cement in sandstone (Nash and Pittman, 1975). Like MS sediment studies, earlier rock-specific studies appear to focus on magnetic detrital particles and particle transport mechanisms and ignore the effects of geochemical and biological alteration of sediment, the effects of compaction and cementation during the process of lithification, and any subsequent rock diagenesis. In effect, early rock MS studies rely heavily on sediment studies without considering the differences between rock and sediment or all the physical and chemical changes that occur during the process of lithification. Later rock-specific studies tend to emphasize

biogeochemical alterations to sediment after deposition (Li et al., 2006) and modification of MS through rock diagenesis (Retallack, 2003; Evans and Elmore, 2006).

Studies of MS in terrestrial sedimentary rock are largely limited to descriptions of paleosols, where large fluctuations and cyclicity in MS is used as evidence to infer the presence of paleosols (Retallack et al., 2003). MS in Cambrian and early Paleozoic sediments allows detection of paleosols despite the destruction of soil structures such as root traces (Retallack, et al., 2003). Volume-specific MS is particularly sensitive to maghemite which is an iron oxide commonly produced by soil forming processes (Nagata, 1961). Paleosol identification using MS to detect soil-formed magnetite is often made problematic due to pervasive reduction of soil-formed iron minerals and reduced MS magnitudes due to burial gleization, surficial gleization prior to burial, or groundwater gleization (Retallack et al., 1997, 2001, 2003). Paleozoic MS signatures are similar to profiles in modern gleyed soils. However, Quaternary paleosols exhibit MS magnitudes that are an order of magnitude higher than Paleozoic soils (Retallack, et al., 2003).

Many MS studies of marine sedimentary rocks emphasize the importance of detrital content, particularly in carbonates (Ellwood et al., 2000). The global studies of Devonian rocks conclude that MS is a function of detrital input with little discussion of MS alteration through redox change, diagenesis, or biological sediment modification after deposition of sediment (Crick et al., 1997, 2002; Ellwood et al., 1995, 2000, 2001, 2003a, 2003b, 2003c, 2006). Carbonate MS control by detrital fragments of minerals such as clay and biotite (Ellwood et al., 2000) is inferred in a study of Silurian carbonates and

may have limited application to the carbonates of the Frasnian/Famennian boundary and global correlation of upper Devonian Rocks (Crick et al., 2002).

One practice specific to the global-scale rock MS studies is MS-based global correlation between strata of different lithologies (Crick et al., 2002). In many cases, the possibility of lithologically controlled MS variation is not discussed (e.g. Ellwood et al., 2000, 2001). MS correlation is also reported in studies where sequences of mixed lithology are MS correlated with other sequences of mutually variable lithology (Ellwood et al., 2000) or a study in which strata of mixed lithology are correlated to strata of a single lithology such as the Woodford Shale (Crick et al., 2002) (Figure 7).

One important carbonate MS study found magnetic susceptibility to vary directly with detrital content in limestone (Elwood et al., 2000). In this study, MS response was reported to be the result of detrital particles that did not contain detrital or soil-formed magnetite, reported as the main control in earlier MS studies (e.g. Crick et al., 1997). Ellwood et al. (2000) reported the rocks contained little magnetite, and that the largest control on MS magnitude was abundance of detrital particles of paramagnetic materials, such as clay, ferromagnesian silicates such as biotite, iron sulfides such as pyrite, and other materials. The possibility that the iron sulfides observed in the study were authigenic or diagenetic, or the product of reduced iron III, was not discussed.

While iron sulfides are paramagnetic (Nagata, 1961; Ellwood et al., 2000), the iron that produces pyrite is often originally deposited in terrestrial sediments as magnetite or hematite in an oxidizing environment (Banarjee et al., 1991, Ledbetter, 1986; Retallack et al., 2003),

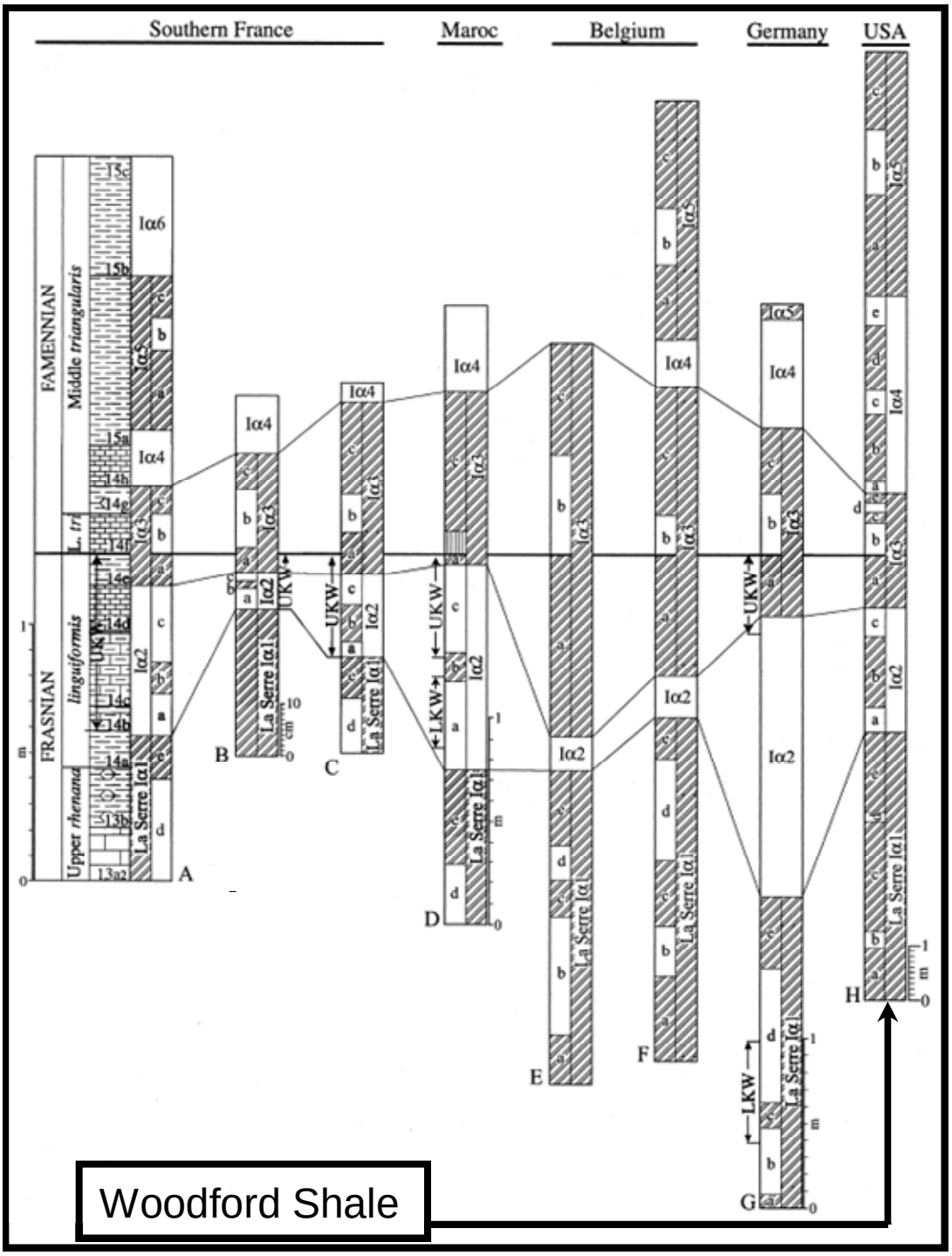

Figure 7. MS based global correlation across the Frasnian/Famennian boundary. Important to this study are: (A) the section used for comparison in the recent global MS study at the La Serre C in the Montagne Noir, southern France, near (B) the Global Stratotype Stratigraphic Position (GSSP) of the Frasnian/Famennian Boundary at Coumiac, France, and (H) the Oklahoma Woodford Shale at Hass B, (Crick et al., 2002).

or may originate as an authigenic precipitate from iron scavenged from continental shelves (Berner, 1970; Berner et al., 1979 Raiswell, et al., 2001; Lyons and Severmann, 2006). Important potential sources of iron in authigenic pyrite that have been overlooked in global MS studies (Crick et al., 1995, 2002; Ellwood et al., 1995, 2000, 2001, 2003a, 2003b, 2003c, 2006) include: dissolved iron (Fung et al., 2000) and dissolved or suspended iron (Cruse and Seewald, 2001; Seewald et al., 2003; Cruse and Lyons, 2004) with hydrogen sulfide (Seewald, et al., 2003) also sourced from hydrothermal fluids at mid ocean ridges or oceanic rift systems.

It is important to note that calcite, and therefore limestone, may have large and variable proportions of a ferromagnesian component that results from the burial diagenesis or alteration of primary limestone to dolomite (Nash and Pittman, 1975; Sternbach, 1984; Weedon, 2004). This type of alteration is common (Deer, et al., 1999) and variable in extent (Evans and Elmore, 2006). Diagenetic enhancement of iron concentration in primary limestone is reported to result from pressure solution (Evans and Elmore, 2006) and interaction of fresh water and seawater along an interface (e.g., Dorag Model; Badiozamani, 1973). The process of dolomitization in all models mentioned above involves additions (Deer et al., 1999) of paramagnetic transition metals to diamagnetic (Nagata, 1961) primary limestone, thereby diagenetically altering the original MS of the carbonates.

The magnetic susceptibility of carbonates appears to be generally lower than shale and other sedimentary detrital rocks (Nash and Pittman, 1975; Ellwood et al., 2000; Weedon, 2004). In studies specific to the subject of global MS correlation, shifts in MS at study outcrops are reported to be global-scale shifts, yet the largest reported

fluctuations in MS occur at lithologic transitions and could also be reasonably explained as functions of local changes in lithology or facies changes in individual stratigraphic successions reported at study sites (Crick et al., 1997, 2002; Ellwood et al., 1995, 2000, 2001, 2003a, 2003b, 2003c, 2006); (Figure 8).

Due to the occurrence of large pyrite nodules and framboids in the Woodford and Chattanooga Shale (Kirkland et al, 1992) and the generally authigenic provenance of pyrite (i.e. reduced iron) in black shale (Lyons and Severmann, 2006), it is reasonable to suspect that reducing processes may have suppressed the MS magnitude of any detrital iron which was originally deposited in the oxidized ferromagnetic form (Berner, 1979; O'Brien, 1995; Crick et al., 1997, 2002). Precipitation of authigenic iron pyrite in shale has been reported by many authors (Berner et al., 1979; Rickard, 1970; Cruse and Lyons, 2004; Lyons and Severmann, 2006). Three possible methods of pyrite precipitation are replacement of bacteria and other microorganisms, crystallization of inorganic gels, and pseudomorphic replacement of small gas bubbles in sediment (Berner et al., 1979).

The geochemical ratio of pyrite to pyrite plus reactive iron is called the degree of pyritization (DOP) and is employed as a method of inferring euxinic or anoxic environmental conditions (Berner et al., 1979; Rimmer, 2004a, 2004b) associated with carbon sequestration in Devonian black pyrite-rich marine shales (Leventhal and Hosterman, 1982; Russell, 1985). Reactive iron includes iron oxides and some minor silicate phases. Further, Devonian age Chattanooga Shale was found to contain only iron in the (II) state; even though the iron had often been deposited in the (III) valence state (Leventhal et al., 1983). The interpretation of MS signature in landward portions of

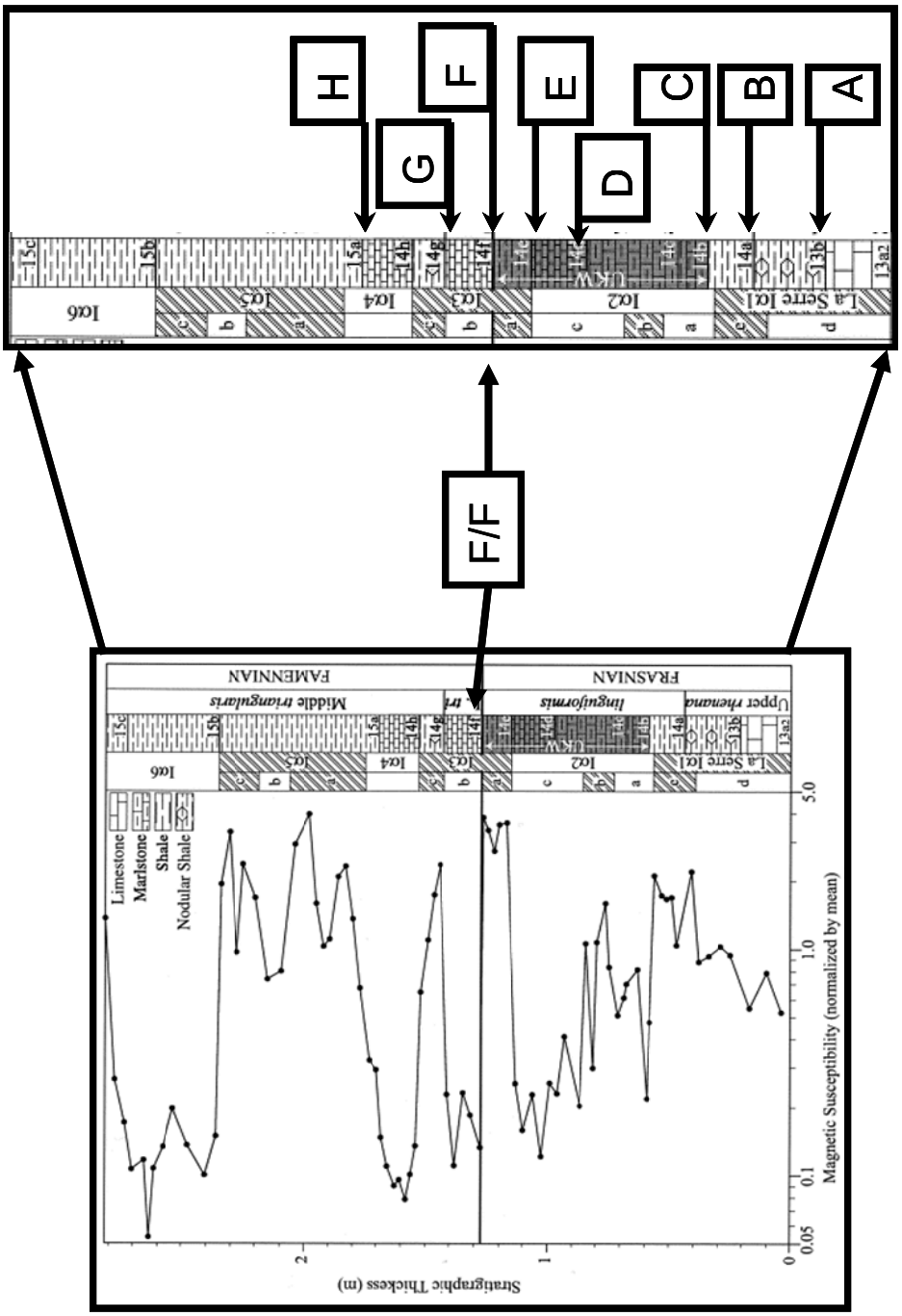

Figure 8. Magnetic susceptibility and lithology at the Frasnian/Famennian (F/F) boundary at Frasnes, France. This F/F magnetic comparison section (<3 m) was correlated with the Woodford Shale (25 m) at Lake Classen Spillway (Hass B) in Oklahoma. The largest changes in (normalized) MS, reported as global cycles appear to coincide with lithofacies changes (A thru H) in the stratigraphic colomn (Crick et al., 2002). Note MS scale is not linear.

basins is even more problematic with rapid, repeated, or oscillatory changes in soil and rock MS through burial, gleization and flooding gleization (Retallack et al., 2003), repeated oscillations in the presence and depth of any oxygen minimum zone (OMZ) (Larasoaña et al., 2006), changes in oxygen abundance through corresponding changes in global circulation, changes in elevation of thermoclines, and changes in biological productivity (Wignall and Myers, 1988).

Many locations in the Chattanooga Shale and its equivalents have been observed to undergo oscillations in marine oxygen content (Scheiber, 1994), which have been found to be partially controlled by paleobathymetry (Russell, 2004) and differing rates of tectonic uplift (Hester et al., 1992) in Devonian basins of North America (Charpentier and Schmoker, 1982; Ettensohn, 1983; Hester et al., 1990; Schmoker, 1980, 1983). Geochemical studies of the Chattanooga Shale suggest that time equivalent Woodford Shale outcrops will differ in their depositional oxygen content (Leventhal and Hosterman, 1982; Leventhal, 1983, Beier and Hayes, 1989). Other studies infer variable oxygen content in Devonian black shale from the following: degrees of pyritization (Rimmer, 2004a, 2004b), presence of pyrite spheres and framboids (Kirkland et al., 1992; Gordon and Baird, 2001), petroleum source rock quality (e.g. total organic carbon, Hester et al., 1992), gamma-ray magnitude through varying uranium concentration (Hester et al., 1988), occurrence and thickness of carbonate intervals (Amsden et al., 1968), conodont assemblage and occurrence (Over, 1992a, 1992 b, 2000, 2002), total thickness of black shale intervals, number of benthic faunal species (Wignall and Myers, 1988), and shale lamination recording the suppression of bioturbation (Hallam, 1966, Cluff, 1980). Sediments rich in organic matter are particularly susceptible to alteration of original MS

signatures, especially terrestrial sediment subjected to immersion in water, burial, or other processes which might change the amount of available oxygen (Retallack et al., 2003).

Variation of environmental oxygen content and degree of pyritization have significance in petroleum exploration because time-equivalent units are variable in carbon content (Leventhal and Hosterman, 1982) and hence, source rock potential in time-equivalent units is variable (Klemme and Ulmishek, 1991; Tissot and Welte, 1984). Oxygen content and DOP have direct bearing on the alteration of MS magnitude through reduction of primary magnetite to pyrite as anaerobic bacteria reduce soil-formed iron oxides during metabolism of soil-formed organic carbon by anaerobes in terrestrial environments (Retallack, 2003) or similar reduction of iron oxides during metabolism of carbon in marine environments (Fung et al., 2000).

Abundant pyrite in the form of framboids, layers, ooids, and nodules is reported in black shales (Berner et al, 1979; O'Brien, 1995) and Devonian shales (Scheiber and Riciputi, 2004). The Woodford Shale contains large pyrite nodules (Kirkland et al., 1992). The majority of pyrite that occurs in marine shale is authigenic or diagenetic (Scheiber and Baird, 2001). Some of the largest values of MS in the Woodford Shale may be accounted for by large nodules and layers of apparently authigenic pyrite (Kirkland et al, 1992) since black shale is reported to contain little or no magnetite (Crick et al., 2002). Scheiber and Baird (2001) concluded that accumulations of authigenic sand-sized pyrite grains were often reworked far from basin margins, and the only important local sources of sand-sized or larger sediment in black shale. Neither authigenic pyrite precipitated from seawater (Lyons and Severman, 2006), reworked

authigenic pyrite, originally precipitated from seawater (Scheiber and Baird, 2001), nor diagenetic nodules of pyrite (Kirkland et al., 1992) strongly relate to primary deposition of soil-formed detrital iron (Crick et al., 2002). Anoxic and euxinic environments, associated with high degrees of pyritization, were favorable to deposition of high quality petroleum source rocks during: the Silurian and Devonian (Lüning et al., 2000), the Pennsylvanian (Coveney et al., 1991), the Mississippian (Montgomery et al. 2005), and the Jurassic (Raiswell et al, 2001).

Thick accumulations and high concentration of authigenic iron is also possible in marginal marine siliciclastic sediments (Adams et al., 2006) or as bog ore associated with coal deposits and wetland soils (McCarthy, 2002). In brackish environments, siderite is precipitated from pore water as rhizoconcretions in association with sulfate reducing bacteria (Adams et al., 2006). This concentration of iron may not alter the total mass of iron in a given system, but it would have the effect of altering the MS pattern by enhancing MS in some strata while simultaneously diminishing MS in other strata. Altering iron in the (III) valence state to the (II) valence state may diminish the MS of the whole system, (Retallack, 2003) and depending on occurrence of impermeable layers of sediment, affect some strata disproportionately as compared to others (Sternbach, 1984). Differences in basin morphology, supertidal erosion, tectonic uplift, flooding, or any other processes not absolutely homogeneous over time and space could enhance or diminish iron concentrations and alter MS magnitudes or overprint MS signatures in sedimentary rock (Sternbach, 1984).

Little definitive evidence exists as to whether the higher global MS signal is produced during eustatic highstand or eustatic lowstand. MS magnitude is reported to be

generally low during highstand and high during lowstand while being highest at maximum flooding surfaces (Crick et al., 1997, 2002; Ellwood et al., 1999, 2000, 2006). Changes in biological diversity and carbonate production are found to cause changes in MS magnitude and rock composition (Ellwood et al., 2000). Carbonate occurrence and content in marine depositional environments at all scales has been inferred to result from changes in water temperature as a function of regional paleolatitude, changes in ocean currents, changes in water oxygen content, excessive hydrogen sulfide, biological extinction, biological succession, rifting, changes in sediment-source detritus which destroy filter-feeding organisms, basin opening or closure in areas near or below mean sea level, and changes in glaciation induced by tectonic drift of a land mass into or out of high latitude positions exclusive of global climate change (McGee, 1996). These controls on the organisms that produce carbonates can work in combinations causing complexity in geologic interpretations described by Schumm (1991). In moving from one basin to another or from one lithology to another, environmental, biological, sediment-source mineralogy, and energy regime changes to original MS magnitude may render MS pattern correlation between basins difficult.

In general, global rock-specific MS studies employ interpretations dependent on conclusions from sediment and paleosol studies as lines of evidence in MS interpretations of rock (Crick et al., 1997, 2002; Ellwood et al., 1999, 2000, 2006). Contradictions between sediment-specific MS studies are present in the literature. In a paleosol study by Ellwood et al. (1995) the enhanced magnetic susceptibility measurements of hearth sequences at an archeological site are attributed to reduction of hematite by fire. This report of MS increase through iron reduction conflicts with other reports that reduced

iron compounds are paramagnetic and soil-formed hematite is ferromagnetic, or more specifically, canted antiferromagnetic (Nagata, 1961). Chemical reduction of iron compounds has been reported elsewhere to diminish the MS magnitude rather than increase it (Retallack et al., 2003; Novosel et al, 2005).

Lithification may have the potential to increase or dampen various types of magnetic susceptibility as a function of increased aggregate size of magnetic substances contained in rock (Nagata, 1961). Differential compaction in the Woodford Shale (Rottman, 2000) and other shales (Baldwin and Butler, 1985) has the potential to affect volume specific MS, dependent on the volume of magnetic material in a unit volume. Introduction of dissolved magnetic iron and other metals to sediment (Cruse and Lyons, 2004; Lyons and Severmann, 2006) or rock (Nash and Pittman, 1975; Evans and Elmore, 2006) is reported. Likewise, removal (Retallack et al., 2003), and chemical alteration of magnetic material in sediment (Retallack et al, 2003; Li et al., 2006) and rock (Zachara, 2004) have been reported. When the valence of iron in sediment is altered by sediment oxidation (Larasoaña et al., 2006) or reduction (Fung et al., 2000) either chemically (Novosel et al., 2005) or biogeochemically (Zachara, 2004; Li et al., 2006), MS values may be affected by orders of magnitude (Nagata, 1961).

For example, Sternbach (1984) reported that burial diagenesis in the Anadarko Basin decreased the iron concentration of the Sylvan Shale while increasing the iron concentration, up to 5 weight percent, of the overlying Hunton Limestone. Sternbach (1984) reported that these simultaneous diagenetic alterations were gradational in individual well-cores and not homogeneous across the Anadarko basin and controlled by a complicated combination of: distance above or below the Sylvan Shale/Hunton

Limestone, the variable depth of burial of the Sylvan Shale-Hunton Limestone contact across the Anadarko Basin, the original basin morphology, the smectite-illite ratios in the primary Hunton Limestone, the extent and distribution of prior dolomitization which had replaced calcium with magnesium, thereby preventing further diagenetic increases in iron content and preservation of primary porosity in the Hunton Limestone.

While this study (Sternbach, 1984) was not directly focused on MS, it reported simultaneous diagenetic increases and decreases in the concentration of iron, the dominant magnetic substance in rock (Nagata, 1961) and dominant control on rock MS (Crick et al, 2002, Retallack, 2003). Of direct importance to this study, Sternbach (1984) reported that the Woodford Shale had not contributed significant quantities of iron in the observed economically important diagenesis of Hunton Limestone. Sternbach (1984) concluded that flow of iron-rich fluids and hydrocarbons had been upwards stratigraphically in nearly horizontal strata. Because the Anadarko Basin contains other simlar stratigraphic successions (e.g. Woodford Shale succeeded by Sycamore Limestone), it is possible that the MS pattern of the Anadarko Basin may have several important diagenetic controls not considered in global models of MS controlled by detrital sediment alone (Crick et al., 2002).

Global MS studies, in focusing on detrital iron, may have overlooked several significant sources of iron in sediment and rock. Hydrothermal vents can provide a source of authigenic iron in marine depositional environments in dissolved or suspended form (Cruse and Lyons, 2004). Hydrothermal vents in modern oceans are associated with magmatic arcs (Cruse and Lyons, 2004), ocean trenches (Ballard et al., 1984) and mid-ocean ridges (Crane and Ballard, 1980, Ballard et al. 2001). Studies of modern

oceans indicate that up to 9% of the ocean's total iron budget is dissolved in seawater (Fung et al., 2000), while dissolved iron accounts for increases in MS during diagenesis of carbonate (Evans and Elmore, 2006). These findings demonstrate significant marine sources of non-detrital paramagnetic iron in sediment and the ability of marine depositional systems to alter carbonate magnetism. Dissolved iron also provides a potential source for precipitation of authigenic pyrite in black marine shale (Rimmer, 2004a, 2004b; Cruse and Lyons, 2004) in environments where dissolved iron is the largest or only significant source of iron (Lyons and Severmann, 2006). Although Evans and Elmore (2006) reported diagenetic MS changes in carbonates, they concluded that assemblages of iron minerals present and therefore MS strength were primarily due to presence or differences in redox conditions during burial and deformation. Novosel et al. (2005) found methanogenisis caused detrital magnetite in marine sediment, to be reduced to pyrite, inducing a corresponding decrease in MS strength of 35 n-T (nano Teslas). Zachara et al. (2004) found that bioavailable iron (III) was reduced to iron (II) as the result of bacterial methanogenesis of oil contaminants in an aquifer, while significant alteration of paleosol MS was reported to be due to both the reduction of iron (III) and the dissolution of soil-formed magnetite and the subsequent diagenesis of rock after lithification (Retallack, 2003). Unless rocks or sediments have similar histories, even rocks or sediments with similar ages and identical compositions will likely yield vastly different MS measurements. In focusing on detrital iron, some MS studies have effectively ignored the importance and widespread precipitation of authigenic pyrite and other iron (II) compounds in black shale, black limestone (Wendt and Belka 1991), and coals (McCarthy, 2002).

Authigenic pyrite or reworked authigenic pyrite has been concluded to imply reducing or anoxic conditions prevalent in Devonian black shales (McGee, 1996; Scheiber and Baird, 2001; Dunk et al., 2002; Lüning and Kolonic, 2003; Lüning et al, 2004; Scheiber and Riciputi, 2004) and Devonian limestone (Wendt and Belka, 1991). In Europe especially, global MS studies (Crick et al., 2002) appear to have overlooked the importance of pyrite contained in *Kellwasser* (kill-water) limestones (Joachimski and Buggisch, 1993). Global occurrence of pyrite-rich black shale (e.g. petroleum source rock) at important Devonian stage boundaries has been reported by Klemme and Ulmishek (1991). Similar reports in: America (Beier and Hayes, 1989), Africa (Lüning et al., 2003), and South America (Moretti and Martinez, 1995) underscore the importance of pyrite in Devonian interpretations. The rocks associated with the F/F boundary imply extraordinary if not unique geochemical conditions and anoxia (Joachimski and Buggisch, 1993; Gĕrsl and Hladil, 2004) associated with mass extinction of the marine organisms (McGee, 1996) that produced carbonates (Sepkowski, 1986; Sorauf and Pedder, 1986), anomalous concentrations of pyrite in black carbonates (Wendt and Belka, 1991), and global-scale deposition of petroleum source rocks like the Woodford Shale (Lüning and Kolonic, 2003; Lüning et al., 2003). Black shales, as petroleum source rocks, undergo significant and variable biogeochemical changes associated with high TOC (Olsen, 1982), during natural gas generation in shale (Broadhead et al., 1982), and thermal petroleum source-rock maturation (Cardott and Lambert, 1987). Some portions the Woodford Shale are both a source rock and minor reservoir for oil and natural gas, underscoring the economic and scientific importance of the diagenetic changes in the Anadarko Basin.

The relative contributions of detrital and authigenic iron in marine shales are commonly estimated by measuring the concentrations of iron and aluminum in shale samples and then comparing the calculated Fe/Al ratios to standard values from the Post Archaean Australian Shale Standard (PAASS), the North American Shale Composite (NASC), and the Marine Sciences Group Black Shale Composite (BSC) (Vine and Tourtelot, 1970; Gromet et al., 2004, Taylor and McLennan, 1985; Quinby-Hunt et al., 1989, Cruse and Lyons, 2004; Doveton and Merriam, 2004; Lyons and Serverman, 2006; Tribovillard et al., 2006). Aluminum as a constituent in shale has been treated as a conservative tracer in siliciclastic deposition with the degree of iron enrichment estimated by comparisons to Shale Standard (Taylor and McClennan, 1985). Lyons and Severmann (2006) concluded that iron provenance in black shales such as the Woodford Shale was exclusively authigenic, originating as pyrite precipitated directly from seawater. Kirkland et al. (1992), reported that the Woodford Shale was minimally influenced by terrestrial sediment, with a particle size distribution dominated (98%) by particles smaller than silt, predominantly radiolarian tests of opaline silica. These observations conflict with several reports in Global MS correlation studies that iron in Devonian black shale from the Frasnian/Famennian, (Crick et al, 2002), Eifelian/Givetian (Crick et al., 1997), and middle Devonian (Ellwood et al., 2006) has a detrital provenance and MS is controlled by detrital minerals containing iron (Ellwood et al., 2000) or detrital magnetite (Crick et al, 1997). Large numbers of studies in black shale (Berner et al., 1979; Cluff, 1980; Leventhal, 1983; Leventhal and Hosterman, 1982; Algeo, 2004; Rimmer, 2004a, 2004b) report that Fe II (i.e. sulfide) is the dominant iron species and not Fe III (i.e. oxides) because iron (III) is relatively soluble in water (Retallack, 2003) and very

unstable in environments with low concentrations of oxygen or low pH (Faure, 1991).

Gamma-Ray Spectrometry

Shale bulk gamma-ray studies (Ellis, 1987) and spectral gamma-ray analysis (Fertl and Chingilarian, 1989) both commonly measure total gamma-ray magnitude in API units (Belknap et al., 1959; Schmoker, 1981; Doveton and Merriam, 2003). The gamma radiation measured by the logging tools results from the radioactive decay of uranium, thorium, and potassium, and their respective daughter products (Adams and Weaver, 1958). Gamma radiation measurements are a function of the energy liberated when unstable nuclei disintegrate (Ivanovich and Harmon, 1982). Although the composition of shales varies widely, the gamma-ray magnitude and gamma-ray specific elemental assemblage of shales remains strikingly different from other clastic sedimentary rocks or carbonates (Swanson, 1961). Black marine shale in particular is very radioactive (Swanson, 1961). Shale gamma-ray magnitude has been used as a proxy for organic richness in the Woodford Shale (Olson, 1982).

As a common practice, gamma-ray logs are not plotted full scale (e.g. above 150 API) and the individual contributions of Th, U, and K are combined by use of an algorithmic equation (Doveton and Merriam 2004). The equation for gamma-ray magnitude expressed in API units (American Petroleum Institute) is:

$$\gamma_{API} = 4[Th] + 8[U] + 16\,[K] \quad \text{(Eq. 4)}$$

where γ_{API} is the gamma-ray magnitude measured in API units, Th and U represent the concentrations of these elements in parts per million (ppm), and K is expressed in terms of weight-percentage (Ellis, 1987). Gamma-ray magnitude in API units, historically employed to define relative stratigraphic position of the more important sandstone and

carbonate petroleum reservoirs, is calibrated using an artificial concrete formation in Houston, Texas (Ellis, 1987). The artificial formation of known composition (24 ppm Th, 12 ppm U, and 4% K) generates 200 API units (Belknap, 1959). By differentiating rocks based on these three constituents, it is possible to infer facies changes through differences in their respective abundances in rocks, controlled by lithology and depositional environment (Adams and Weaver, 1958).

Much information can be lost on bulk gamma-ray logs (e.g. the use of the API equation) and spectral gamma-ray analysis has been successfully used to locate previously unrecognized productive basal intervals of uranium-rich, oil-rich, Misener Sandstone in the Woodford Formation (Dennis, 1997). Gamma-ray logging of well bores has been used to correlate productive zones and identify lithologies in exploration for petroleum since the 1930's (Fertl and Chingilarian, 1989). Additionally, spectral gamma-ray detectors measure the separate contributions of uranium (U), potassium (K), and thorium (Th) in rocks and sediments (Ellis, 1987). Petroleum engineers routinely use the gamma-ray specific elemental assemblage to determine clay composition (Ellis, 1987). Specific clay composition and preservation of original rock porosity have been shown to be affected by alteration of clay composition and iron content through diagenesis (Sternbach, 1984). Original depositional environment, sediment source, and particle size can be estimated from the quantity and composition of clay minerals in well-bores (Ellis, 1987). In petroleum exploration, inferred depositional facies changes often relate to primary porosity, permeability and diagenetic changes in reservoirs (Sternbach, 1984). Oil production potential is commonly evaluated as functions of clay content, mineralogy,

and facies change of sedimentary rocks through spectral gamma-ray analysis (Ellis, 1987).

Spectral gamma-ray logs, like older gamma-ray magnitude logs, are commonly used in petroleum exploration to correlate strata, evaluate lithology, and evaluate changes in depositional environment (Ettensohn, 1979; Fertl, 1979; Schmoker, 1980, 1981; Charpentier and Schmoker, 1982; Schmoker and Charpentier, 1983; Sullivan, 1985; Hester et al., 1988 1990, 1992; Lambert, 1991 1992, 1993; Dennis, 1997; Rottman, 2000). Spectral gamma-ray analysis of petroleum logs is commonly used to infer lateral thinning and thickening of shale units (Ettensohn et al., 1979; Ettensohn, 1995; Lambert, 1993). When used in conjunction with other well-log parameters such as resistivity, spontaneous potential, etc., conclusions based on gamma-ray log data provide additional evidence related to porosity and permeability in petroleum exploration (Fertl and Chilingarian, 1989), and aquifer evaluation (Christenson et al., 1998). In addition to evaluating saturated thickness of an aquifer, Cristenson et al. (1998) were able to predict water quality through gamma-ray logs. Cristenson (1998) found that hazardous trace metals including cadmium and arsenic in the Central Oklahoma Aquifer were preferentially accumulated in shale intervals, which are then easily identified on gamma-ray logs.

Spectral gamma-ray analysis is a non-destructive technique (Chenourd and Lalou, 1969) used to make inferences about rocks and stratigraphic sequences to study the following: depositional environment, density of water saturated sediment (Whitmarsh, 1971), lithological variation of core from units of interest in petroleum exploration (Chenouard and Lalou, 1969), stratigraphy in well bores (Ettensohn, 1979), magnetic

susceptibility (Gĕrsl and Hladil, 2004), petroleum source rock characteristics (Hester et al., 1990), benthic levels of oxygen through variation in uranium content (Wignall and Myers, 1988), organic carbon in Devonian petroleum sourcerocks in Africa (Lüning and Kolonic, 2003b), carbon content of the Devonian Bakken Shale of the Williston Basin, (Schmoker and Hester, 1983), and organic carbon content of Devonian shales in the western Appalachian Basin (Schmoker et al., 1993). Other uses of spectral gamma-ray analysis with applications specific to petroleum exploration include: detailed, identification of subtle changes in lithofacies, presence of secondary porosity and natural fracture systems, paleogeographic trends and facies changes across oilfields, location of watered-out intervals in reservoirs under enhanced recovery, determination of reservoir net shale percentage, and in-situ potash concentration (Fertl, 1979).

Although marine black shales are somewhat enriched in thorium and potassium, black shale, especially Devonian Shales, often contain anomalously large concentrations of uranium (Adams and Weaver, 1958, Coveney et al., 1991; Lüning et al., 2003, 2004; Lüning and Kolonic, 2003). Terrestrial shales generally have higher concentrations of potassium and thorium and lower uranium concentration relative to marine shales (Bloxam, 1964). Uranium has been strongly correlated with organic carbon concentrations in marine shale through geochemical techniques, well log studies, and studies utilizing portable gamma-ray detectors in automobiles and airplanes (Adams and Weaver, 1958; Swanson, 1961, Hallam, 1966; Ettensohn, 1979, 1995; Watson and Plant, 1979; Leventhal and Hosterman, 1982; Charpentier and Schmoker, 1982; Russell, 1985; Wignall and Myers, 1988; Barnes and Cochran, 1989; Beier and Hayes, 1989; Postma and ten Veen, 1999; Lüning and Kolonic, 2003; Lüning et al., 2003; 2004; Algeo, 2004;

Rimmer, 2004a, 2004b; Tribovillard et al., 2004; Weedon et al., 2004). Strong correlations between total organic carbon and uranium are reported in the Chattanooga Shale (Schmoker, 1980, 1981, 1982; Schmoker and Hester, 1983; Leventhal et al., 1983), Pennsylvanian shales (Coveney et al., 1991; Fisher and Wignall, 2001), Jurassic shales (Pearson et al., 2004; Tyson, 2004; Morgans-Bell and Cohen, 2004), and the Woodford Shale specifically (Olson, 1982; Fertl and Chilingarian, 1989; Kirkland et al., 1992; Hester et al., 1988, 1990, 1992).

In addition to the gamma-ray based correlation between uranium and organic carbon by Hester et al. (1990); (Figure 9), another black shale (e.g. Woodford Shale) study of bulk density derived from well logs found an inverse correlation between bulk density and organic carbon concentrations (Figure 10); (Schmoker, 1993). This finding is consistent with reported inverse relationships between gamma-ray magnitude or uranium concentration and bulk density (Figure 11); (Schmoker, 1980, 1981; Schmoker and Hester, 1983; Meyer B. and Nederlof M., 1984; Fertl and Chilingarian, 1989; Hester et al., 1990, 1992; Kirkland et al., 1992; Lüning, et al., 2003). "Hot" uranium-rich black shales with high organic carbon content are important source rocks (Klemme H., and Ulmishek G, 1997; Ormiston and Oglesby, 1995) and minor reservoirs for oil production (Schmoker, 1980; Comer, 1991, Dennis, 1997). Recently, the recognition that black shales are important natural gas reservoirs has led to a new interest in characterizing shale at a more detailed level in terms of reservoir characteristics (Charpentier and Schmoker, 1982; Schmoker, 1980, 1993). Because gamma-ray magnitude, uranium concentration, and bulk density are often plotted on the same well log, three properties are available to characterize source-rock potential.

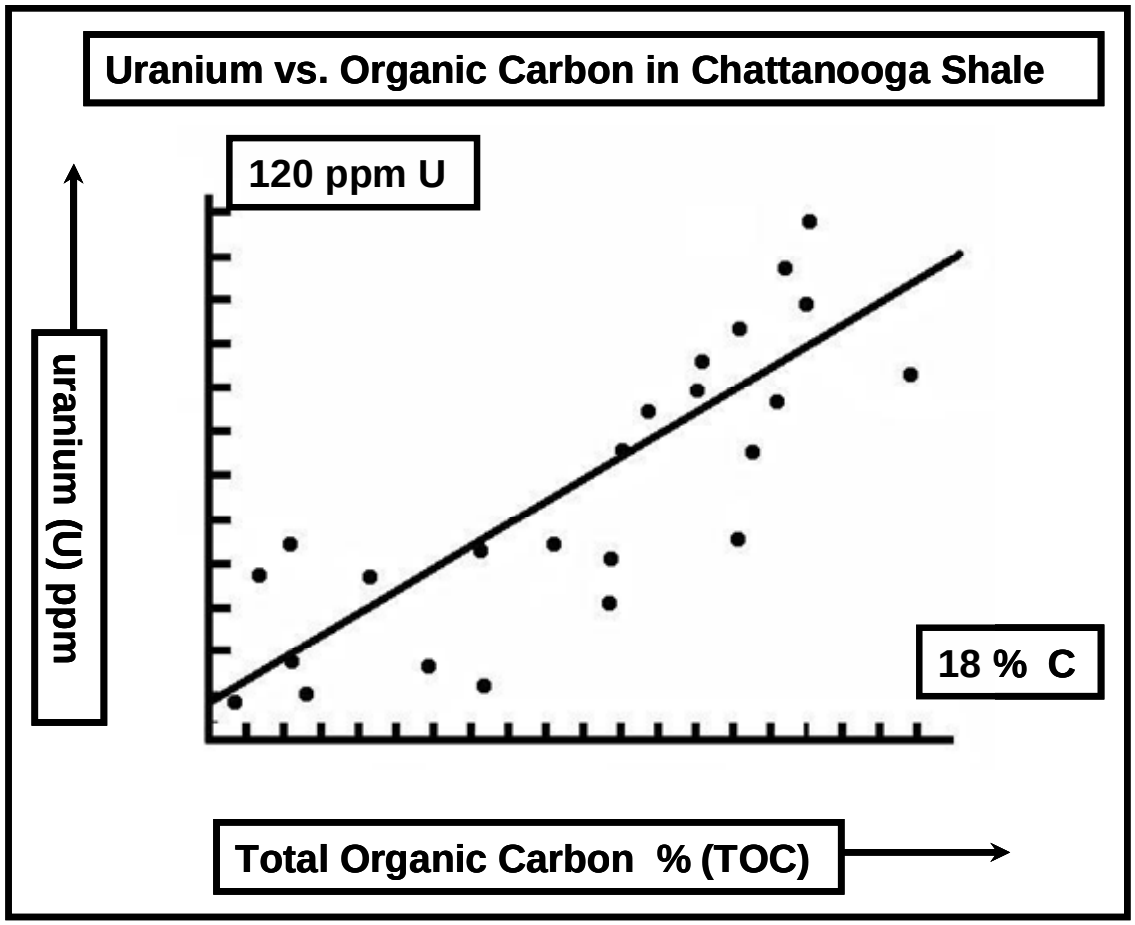

Figure 9. Gamma-ray log derived plot of uranium concentration vs. total organic carbon in the Chattanooga Shale (Woodford Shale equivalent) (Hester et al., 1990).

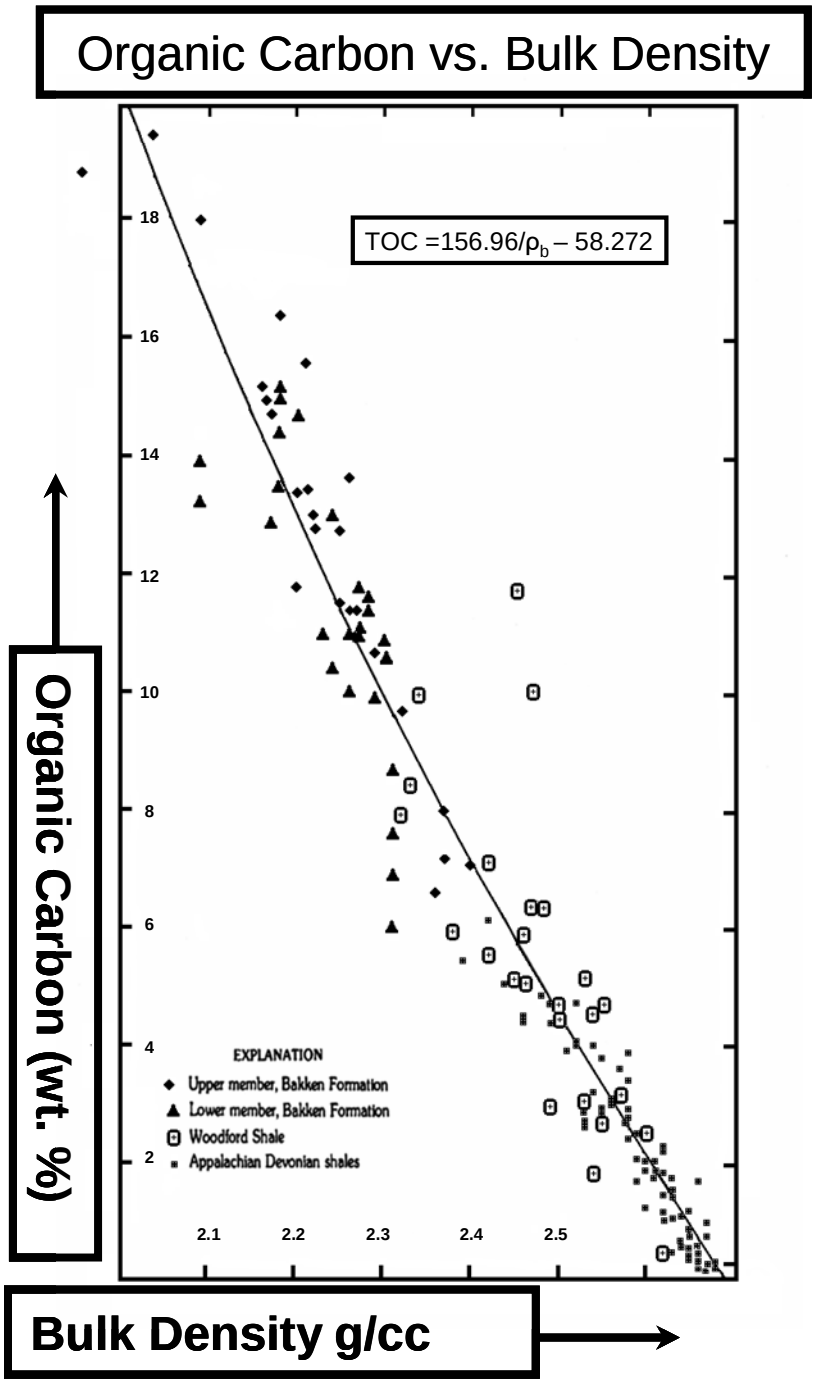

Figure 10. Plot of total organic carbon (TOC) vs. bulk density in Devonian black shales of North America including the Woodford Shale (Hester et al., 1990).

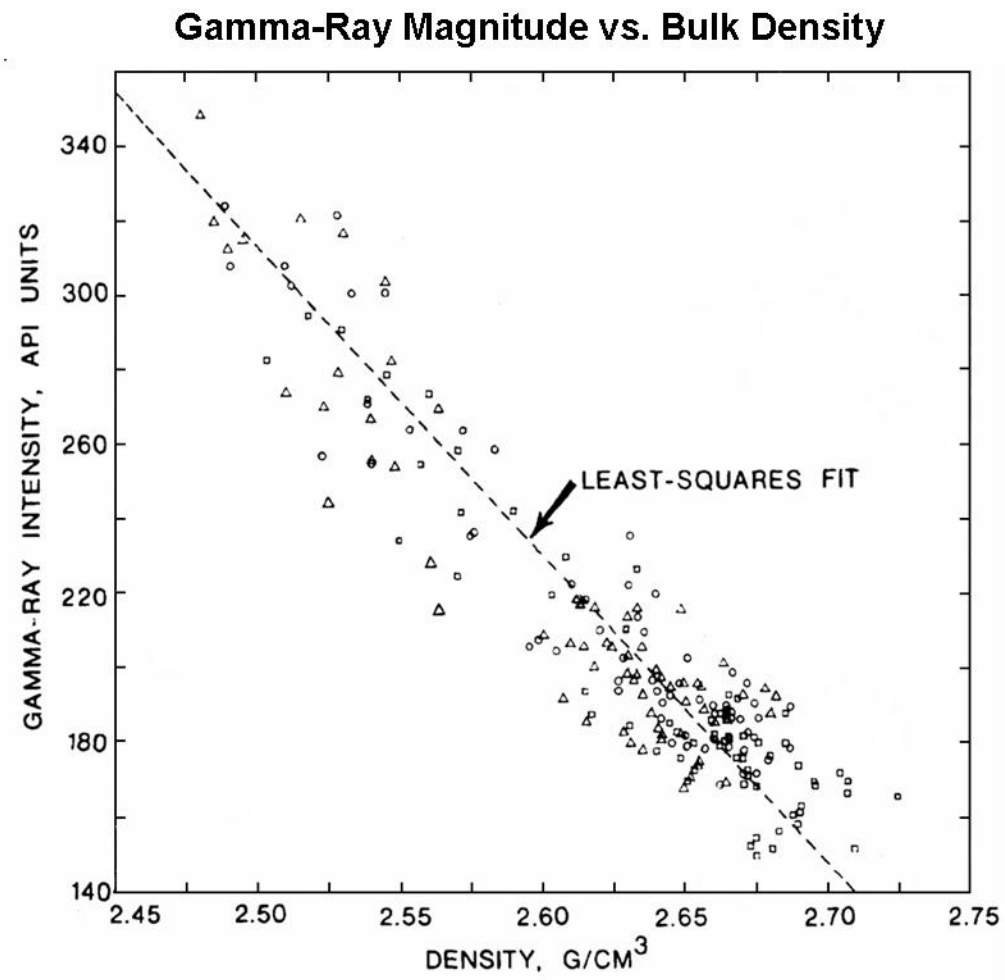

Figure 11. Log-derived plot of gamma-ray magnitude (API units) vs. bulk density (cgs units) in Devonian black shales of Appalachia including the Chattanooga Shale (Schmoker, 1993).

As shales became more important as reservoirs, the ability to characterize reservoir characteristics such as lithology on gamma-ray logs (Charpentier and Schmoker, 1982; Schmoker, 1980, 1993) was reported, along with the continued use of gamma-ray logs to identify and characterize source rock potential in black shales (Ettensohn, 1995). Delineating subtle changes in shale depositional facies has become economically critical (Sullivan, 1985). Adams and Weaver (1958) originally proposed the concept of geochemical facies changes in shales as a function of changes in the concentrations of Th, U, and the uranium / thorium (U/Th) ratio. The gamma-ray specific radioactive elements arrive in the shales by different mechanisms and in varying quantities as the result of facies changes (Adams and Weaver, 1958; Bloxam, 1964), different redox properties (Dypvik and Harris, 2001), and differing chemical properties which respond to changes in redox conditions (Ivanovich and Harmon, 1982).

In sedimentary rocks, potassium is commonly found in insoluble clays whereas thorium is commonly found in insoluble detrital fragments (Adams and Weaver, 1958) and resistate minerals such as zircon or monazite (Ivanovich and Harmon, 1982). Both thorium and potassium are more abundant than uranium in terrestrial or hemipelagic shale (Swanson, 1961). Uranium appears to be fixed in ocean sediments in reducing or anoxic conditions (Barnes and Cochran, 1990; Dunk et al., 2002). It is possible to temporarily bind uranium to clay and organic particles under oxic conditions (Ivanovich and Harmon, 1982). Uranium (VI) is highly soluble and in all but highly dysoxic conditions. Uranium is often remobilized in oxic environments or by environmental shifts that increase available oxygen (Larasoaña et al., 2006) through increased Eh, or increased pH (Faure, 1991). Therefore, unless uranium (IV) is fixed and remains in a

reducing environment it will remobilize (Postma and ten Veen, 1999). Dark shales in the Devonian Old Red Sandstone are known to have abnormally high concentrations of uranium relative to other terrestrial shales (Watson and Plant, 1979) but are confined to units containing high concentrations of organic carbon or petroleum (Michie and Cooper, 1979). Aerobic microorganisms feed on organic detritus. Therefore, uranium and carbon do not remain in high concentrations in oxic to dysoxic depositional environments (Wignall and Myers, 1988). This is one reason why large concentrations of organic carbon, associated with high quality Devonian (Ettensohn, 1995) petroleum source rock, are highly though not perfectly correlated with uranium (Lüning, and Kolonic, 2003) especially in the Woodford Shale (Olson, 1984).

Under oxidizing conditions, a variety of trace elements typically do not precipitate from seawater or are remobilized because they are electron acceptors and are only precipitated under reducing conditions (Dunk et al., 2002). Because reducing conditions favor the sequestration of organic carbon, transition elements elements, and uranium, it is possible to describe facies changes in shale (Adams and Weaver, 1958; Russell, 1985; Tyson, 2004). Red or brown shales containing iron oxides are interpreted as being deposited in oxic conditions under terrestrial influence and commonly have low concentrations of uranium with relatively high values of thorium and potassium (Doveton and Merriam, 2003). These terrestrial shales will register above the shale baseline on a standard gamma-ray log and spectral gamma-ray log (Ellis, 1986). Pelagic shales represent basinal depositional conditions with elevated uranium content fixed in a relatively anoxic environment and are usually gray or green in color, caused by slightly elevated concentrations of organic carbon or pyrite (Beier J. and Hayes J., 1989; Doveton

and Merriam, 2003; Morgans-Bell and Cohen, 2004). The shales most distal to terrestrial environments are typically black with high concentrations of organic carbon, pyrite, and uranium (Swanson, 1961; Cochran and Barnes, 1990). Processes such as storm deposits and wind may still send potassium and thorium detritus to the deep basin (Adams and Weaver, 1958). As a general trend these deep-water shales are hottest in uranium and lower in potassium and thorium (Weaver and Adams, 1958).

Because redox geochemistry exerts control on uranium's solubility, its patterns of enrichment/depletion are easily interpreted (Cochran and Barnes, 1990). Like uranium, iron III is a common electron acceptor at sediment interfaces in microbially mediated reducing environments (Cochran and Barnes, 1990). The theoretical redox potentials (pe) of iron and uranium reduction are very comparable (Cochran and Barnes, 1990), partially accounting for high concentrations of uranium, organic carbon, and precipitation of authigenic pyrite in black marine shale (Fisher and Wignall, 2001). The ecology of anaerobic organisms is highly dependent on the presence and redox behavior of iron and hydrogen sulfide in coupled-cycling, a major pathway for the reductive dissolution of iron oxides whereby iron oxides (Fe III) are reduced to iron sulfides (Fe II) in sediment (Li, et al., 2006). This partially explains why black or pelagic shales are often enriched in authigenic uranium only fixed in reducing conditions, enriched in organic carbon preserved in reducing conditions, and have high degrees of pyritization, interpreted as evidence of at least reducing conditions and possibly euxinic conditions (Rimmer, 2004a, 2004b; Tribovillard et al., 2006).

Marine shales can be differentiated from terrestrial shales on the basis of spectral gamma-ray logs (Coveney et al., 1991) or bulk gamma-ray magnitude, (Adams and

Weaver, 1958). The North American Shale Composite (Gromet et al., 1984) has a gamma-ray magnitude of ≈ 122 API units and a gamma-ray specific elemental assemblage of 3.2% K, 2.7 ppm U, 12.3 ppm Th (Doveton and Merriam, 2004). A marine shale standard, the Marine Sciences Group Black Shale Composite (Vine and Tourtelot, 1970) has a gamma-ray magnitude of ≈ 216 API units and a gamma-ray specific elemental assemblage of 3% K, 15.2 ppm U, 11.6 ppm Th (Quimby-Hunt et al., 1989; Doveton and Merriam, 2004). High concentrations of uranium represent the largest compositional difference between idealized terrestrial and marine shale end-members (Doveton, and Merriam, 2004).

Woodford Shale:

Woodford deposition persists in a deep water marine environment (Kirkland et al., 1992; Lambert, 1991, 1992, 1993) or in an epieric sea (Scheiber, 1994; Ettensohn, 1995) from middle Devonian (Hass and Huddle 1965) until early Mississippian (Kinderhookian); (Schwartzapfel and Holdsworth, 1996; Over and Barrick, 1990; Over, 1992a, 1992b, 2002). Woodford deposition continues without major hiatus or unconformity in the Appalachian Foredeep (Klemme and Ulmishek, 1991; Ettensohn, 1995) caused by tectonic loading during the Acadian Orogeny (Ettensohn, 1995; Ormiston and Oglesby, 1995). The persistence of deep water conditions in the Devonian, without hiatus, constrains environmental conditions for a long and economically important period of earth's geologic history when as many as 14 of the 15 highest quality source rocks in North America were deposited (Comer., 1991; Ormiston and Oglesby, 1995).

Reports that the Woodford (Chattanooga Shale equivalent) was deposited in deep or anoxic water include evidence such as: conodont assemblages (Over, 2002), the lack of bioturbation as evidenced by reports of: continuous laminations or varves (Hallam, 1967, Pearson et al., 2004), undisrupted primary sedimentary structures (Cluff, 1980), low sedimentation rates (Cruse et al., 2006) estimated at 1 cm per thousand years and abundant pyrite (Kirkland et al., 1992), and high concentrations of organic carbon evenly divided among its three informal divisions in excess of .6% (Schmoker and Hester, 1983). The Woodford Shale is an important petroleum source rock, above the (.5%) cutoff value for TOC established by (Tissot and Welte, 1984).

The Woodford Shale was described by J.A. Taff as the Woodford Chert in 1902 and was included in the Index to the Stratigraphy of Oklahoma (Gould, 1925). It was originally described as a limy chert and shales of upper Devonian age correlated with the Chattanooga Shale of Oklahoma, Arkansas, and Tennessee with occurrence in several counties and average thickness of 625 feet (Gould, 1925). The description includes the following geomorphologic reference to a weathering pattern, “The outcrop usually forms rough lowlands covered with jack oak timber” (Gould, 1925). Since none of the individual outcrops described in the literature report Woodford Shale thicknesses approaching 625 feet, this number may possibly originate from drilling reports.

Later descriptions of the Woodford Shale are more detailed. The Woodford Shale in the Anadarko Basin is a carbonaceous and siliceous dark-gray to black radioactive shale that yields gamma-ray magnitudes of more than 160 API units (Sullivan, 1985). The upper Woodford Shale is characterized by phosphatic nodules up to 2 inches in diameter, blocky chert, dolomitic shale (Siy, 1988). In the Arbuckle Mountains the

Woodford contains thin dark chert beds, cherty shale, and black fissile, bituminous shale (Sullivan, 1985). The McAlester Cemetery Quarry near Ardmore Oklahoma contains large (5 foot diameter) calcite concretions which based on information from quarrymen; occur near the base of the zone of phosphate nodules (Kirkland et al, 1992). Neither the original type locality of the Woodford Shale (Gould, 1925) located on the south limb of the Arbuckle Anticline near the town of Woodford, Oklahoma nor the new type locality (Fay, 1989) on the north limb of the Arbuckle Anticline on I-35 are included in more recent biostratigraphic studies.

In a biostratigraphic study, Hass and Huddle (1965) made detailed descriptions of measured sections at several Woodford Shale outcrops including Hass A and Hass B. The descriptions of Hass A and Hass B may be the most accurate and detailed contained in the literature. Over (2002) described both study outcrops and several other Woodford outcrops at exposures in southern and eastern Oklahoma (1992a, 1992b). Over (2002) extended and refined previous biostratigraphic constraint of Woodford Shale to include several additional locations in Oklahoma and across the U.S. in the Chattanooga Formation and several equivalents. The placement of the F/F boundary in the Over (2002) study within the Woodford Shale was included in a recent global study of MS (Crick et al., 2002). The most recent Chattanooga Shale correlations by Over (2002) included volcanic ash layers associated with late Devonian volcanism in the Eastern U.S. to define the several Woodford equivalents including: the Java Formation in the Northern Appalachian Basin of New York, the Hanover Member of the Appalachian Basin Chattanooga Shale, the upper Olentangy Shale of Ohio, the Boyle Formation in the Illinois Basin and the New Albany Shale (Over and Rhodes, 2000; Over, 2002). No ash

beds have been reported in the Woodford Shale of Oklahoma. The location of such ash beds would likely help sub-divide Woodford into intervals of known age.

The upper Woodford Shale is mid-upper-Devonian to lower Mississippian (Hass and Huddle, 1965; Over and Barrick, 1990; Over, 1992a, 1992b,, 2002; Schwartzapfel and Holdsworth, 1996). The Woodford Shale is equivalent to several North American black marine shales including: portions of the Chattanooga, the Antrim Shale of the Michigan Basin, the New Albany Shale of the Illinois Basin, the lower and upper members of the Bakken Formation of the Williston Basin, the Exshaw Formation of the Alberta Basin and the Devonian shales of the Appalachian Basin (Schmoker and Hester, 1983). The Frasnian/Famennian boundary typically occurs in lower Woodford Shale intervals (Hass and Huddle, 1965, Amsden and Klapper, 1972; Over, 2002). The F/F boundary is well-known because of the mass extinctions (Sepkoski, 1986; Sorauf and Pedder, 1986) when two (Raup and Sepkoski, 1982) or three (House, 2002) distinct extinction events have been reported to result in the loss of up to 70% of global biological diversity (McGee, 1996). Anoxic and euxinic water conditions and multiple marine transgressions are often cited as highly probable causes of Devonian extinctions (House, 1983).

The Woodford Shale is an important petroleum source rock in the Anadarko Basin (Cardott and Lambert, 1985), New Mexico, Texas (Comer, 1991), and Kansas (Lambert, 1991, 1994). In the Southwest, the Woodford Shale is equivalent to the Houy Formation of the Llano uplift in central Texas, the middle division of the Arkansas Novaculite in the Ouachita Mountains in southeastern Oklahoma and west-central Arkansas, the upper part of the Caballos Novaculite in the Marathon region of west

Texas, the Percha Formation in the Hueco and Franklin Mountains of west Texas, and the Sly Gap Formation in the Sacramento Mountains of southeastern New Mexico (Comer, 1991).

One member of the Woodford Shale, the Misener Sandstone is an important reservoir when it discontinuously occurs at the base of the Woodford Formation in Oklahoma and Kansas (Amsden and Klapper, 1972). The Misener has been correlated with the Sylamore Sandstone of eastern Oklahoma and a siltstone which outcrops at the base of the Woodford Shale in Turkey Creek at the top of the Turkey Creek Limestone (Amsden, 1960), which is regarded as an atypical facies of the Woodford Shale (Amsden et al., 1968). The report that the Misener Sandstone is absent in the Arbuckle Mountains (Amsden and Klapper, 1972), agrees with other reports that the pre-Woodford channel sandstones do not cross the axis of a paleotopographic high (Hester et al., 1992) associated with the Acadian Orogeny (Hester, 1992; Ettensohn, 1995).

Uplift during the Acadian Orogeny (Ettensohn, 1995) and erosion resulted in the post-Hunton/pre-Woodford unconformity (Tarr, 1955; Ham, 1955, 1986; Rottman, 2000). The most compelling evidence for the post-Hunton/pre-Woodford unconformity is the observation that Woodford Shale immediately overlies rocks as old as late-Cambrian to early Ordovician in southern Oklahoma (Tarr, 1955; Maxwell, 1959; Amsden, 1960). At Hass B the lower mid-Devonian Henryhouse Formation outcrops at the stratigraphic base of the Lake Classen Spillway Woodford outcrop (Barrick and Klapper, 1990; Hass and Huddle; 1965, Over, 2002). The Bois D'Arc Formation of the Hunton Limestone is upper-Devonian-age in the Arbuckle Mountains and underlies the Woodford at Henry House Creek (Hass A); (Hass and Huddle, 1965; Over, 2002);

(Figure 15). The basal post-Hunton pre-Woodford unconformity (Maxwell, 1959) is not obvious at the outcrop level because discordance in dips of strata does not occur (Amsden, 1960, Kirkland et al., 1992).

The basal Woodford contains conglomerate at some locations in the Arbuckles which is further evidence of an unconformity (Amsden, 1960; Hass and Huddle, 1965; Comer, 1991). One possible cause of past confusion associated with this unconformity is the discontinuous nature of the thin mantle of sediments (e.g. Misener Sandstone) that is deposited on rocks of variable age (Tarr, 1955). The thickness of the basal Woodford deposits does not appear to fully account for the volume of missing rock. Another perplexing observation is the widely disparate ages reported in basal deposits over short distances. Basal beds at Hass A and Hass B are reported to be lithological equivalents (Kirkland et al., 1992) despite large differences in conodont ages and assemblages (Hass and Huddle, 1965) and no observed hiatus in Woodford Deposition.

The unconformity surface in the Arbuckle Mountains contains chert pebbles, carbonate pebbles, and silicified wood (*Callixylon sp*); (Hoskins and Cross, 1952, Chitaly and Chongyang, 2001). Some basal Woodford Shale exposures contain tasmanites, fructifications, spores, and bones (Kirkland et al., 1992). The preservation of wood fossils in the Arbuckle Mountains in conjunction with pyrite nodules (Kirkland, 1992; Aufill et al., 2006, 2007) indicates persistent anoxic bottom waters in the Anadarko Basin (Schmoker, 1980), and the Chattanooga Shale (Schmoker, 1990). Other geochemical evidence of anoxia in basal Woodford includes abundant organic carbon (Cardott and Lambert, 1987), high concentrations of uranium (Olson, 1982; Hester et al., 1990, 1992),

and elevated gamma-ray magnitude caused by high concentrations of uranium (Olson, 1982; Dennis, 1997).

A model of Woodford deposition in an epieric sea proposes concurrent deposition of Woodford Shale on both sides of a paleotopographic high trending roughly southeast to northwest (Hester et al.1988, 1990, 1992). The portion north and east of this paleotopographic high received mostly terrestrial sediments (Hester et al., 1990) such as the quartzose Misener Sandstone with thicknesses of up to 20ft (Amsden and Klapper, 1972, Dennis, 1997). Hester (1990) used the paleotopographic high to divide the Woodford Formation into southwest and northeast depo-centers. The southwest depo-center accumulated the greatest thickness of Woodford Shale, perhaps as the result of greater accommodation or long-term continued subsidence. The basin south and west of the paleotopographic high received mostly marine sediment on a karsted surface (Hester et al., 1992) with discontinuous Misener Sandstone deposition, commonly less than a foot thick (Amsden and Klapper, 1972).

Woodford Shale in the Anadarko Basin, south and west of the above mentioned paleotopographic high, was deprived of terrestrial sediment by a migrating tectonic forebulge (Hester et al; 1990, 1992). The foredeep created by the forebulge caused sediment starvation and siliceous detrital particles greater than silt-size were limited to 2% or less in corresponding lithology (Kirkland et al. 1992). North of the forebulge Misener Sandstone was deposited discontinuously (Amsden and Klapper, 1972) and occurrence is mostly limited to channel-fill deposits in channels eroded in post-Hunton time (Tarr, 1955: Maxwell, 1959).

Hester et al., (1988, 1990) describe the Woodford Shale in Oklahoma as 2 similar shale units separated by a more radioactive and resistive middle member. The 3 main Woodford Shale intervals have mean log-derived TOC in the lower, middle, and upper members of 3.2, 5.5, and 2.7 weight percent respectively (Hester et al, 1988). Total organic carbon does not appear to vary with member thickness but is observed to vary with thermal maturity. Most hydrocarbons have been generated in the lower and middle members (Hester et al., 1990). Mean vitrinite reflectance value (R_0) generally increases from northeast to southwest with mean values ranging from .5-2.0% (Cardott and Lambert, 1985). Comer and Hinch (1987) estimate 27-33% of Woodford's hydrocarbon potential has already been expelled.

The Woodford Shale is an unconventional reservoir for natural gas (Hester et al., 1992), when fracturing, man-made or natural, provides effective porosity for significant ongoing production (Fertl and Chingilarian, 1989). Fracture systems appear to be the most significant fluid pathways providing functional porosity and permeability (Fertl and Chingilarian, 1989). Siliceous intervals of the Woodford are reported to be better targets for manmade fracturing and directional drilling (Fertl and Chingilarian, 1989). Fertl and Chingilarian (1989) reported successful well recompletions in uranium rich intervals with low concentrations of thorium and potassium and silty fissile shale near dolomite beds.

The overall thickness of the Woodford Shale is reported to be dependent paleotopography of the Acadian Unconformity surface (Rottman, 2000). Complete removal of the Woodford Shale in the Arbuckle Mountains was caused by two uplifts in Pennsylvanian time followed by erosion (Tarr, 1959). The first Pennsylvanian uplift, the Wichita Uplift, came in the Morrowan and the second, the Arbuckle Uplift, occurred

during the Virgillian (Braun, 1959; Ham, 1955, 1986). Various conglomerates record the timing of the uplifts (Pybas, et al., 1995). One notable result of tectonism in the Pennsylvanian is significant crustal shortening on the north limb of the Arbuckle Anticline along the Washita Valley Fault Zone (Pybas et al., 1995). During the series of uplifts, Paleozoic rocks near Lake Classen Spillway (Ham, 1955, 1986; Fay, 1989) were tilted or overturned and later covered by the Collings Ranch Conglomerate (Pybas et al., 1995). Rocks as old as Cambrian are exposed in the center of the largest fold in the anticline (Ham, 1986). This series of Paleozoic rocks is an eroded anticline that acts as a tectonic window (inlier), allowing one easy access to over eleven thousand feet of strata which are of scientific interest and economic significance (Ham, 1986).

Woodford Shale deposition ended in the early Mississippian (Hass and Huddle, 1965). The end Devonian-Mississippian boundary is reported to occur near the top of the Woodford Shale near the zone of round phosphatic nodules (Kirkland et al., 1992) on the basis of conodonts (Hass and Huddle, 1965; Over and Barrick, 1990; Over, 1992a) and radiolarians (Schwartzapfel and Holdsworth, 1996). Woodford Shale in some locations is succeeded stratigraphically by the pre-Welden Shale (Culp, 1959), or an easily eroded transitional unit (Hass and Huddle, 1965) separating the Woodford Shale from the Sycamore Limestone (Prestridge, 1957). Pre-Welden Shale is latest Kinderhookian in age (Over and Barrick, 1990). Welden or pre-Welden deposition is variable, absent, and discontinuous (Braun, 1959). The use of the terms Welden-Sycamore and Sycamore-Mayes describes units older than Sycamore and younger than Woodford (Culp, 1959; Braun, 1959). Welden units have been dated as Osagean in age on the basis of conodonts (Barrick et al, 1990; Over and Barrick, 1990). Reported confusion in early literature

arises from incomplete stratigraphic understanding and the use of oilfield and nonstandard nomenclature (Gould, 1925). The Welden or transitional interval (Hass and Huddle, 1965) grades into the Sycamore indicating uninterrupted marine deposition. Literature reports of an unconformity between the Woodford Shale and the overlying Sycamore Limestone are based on broken and eroded phosphate nodules found in the Sycamore Limestone at some locations (Siy, 1988; Cole, 1989). No obvious erosional surface is described at Hass A or Hass B (Hass and Huddle, 1965).

The Sycamore Limestone, named by J.A. Taff in 1903 (Cooper, 1926), is often described as a fine-grained detrital limestone and concentrations of undifferentiated silica sponge spicules (Coffey, 2001) leading to its description as a spiculite (Schwartzapfel and Holdsworth, 1996). The type location for the Worthey (upper) Member of the Sycamore Limestone is located on the Worthey Farm in section 33, T.2S, R.1E. I.M., approximately 3 miles from the Hass A outcrop, Section 30 T. 2S. R. 1E. I.M (Prestridge, 1957). The type locality of the lower member nearby is also located on and named for the Cornell Ranch in Section 25, T. 2S., R. 1E. I.M., approximately one mile from Hass A and two miles from the first Woodford Shale type section near Woodford, Oklahoma, Section 34, T.2S., R.1E. I.M. (Prestridge, 1957).

The Sycamore Formation contains two erosionally incompetent shale intervals which have been confused with the Caney Shale in certain oilfield terminology (Braun, 1959). The Sycamore was described as 3 dense drab limestones separated by covered intervals (Cooper, 1926). Later, the Sycamore Limestone was described as two distinct units (Prestridge, 1958). Coffey (2001) offered a recent detailed description of the formation with four intervals including basal shale, siltstone, middle shale, upper

pelloidal packstone. Conodont evidence indicates the Sycamore Limestone base is middle Meramecian in age with radiolarian evidence inconclusive due to paucity of specimens (Schwartzapfel and Holdsworth, 1996).

Stratigraphically above the Sycamore Limestone is the Caney Shale (Cole, 1989). The change from Sycamore Limestone to Caney Shale is thought to result from a major transgression resulting in the deposition of organic rich shales (Culp, 1961; Cole, 1989). The basal contact of the Caney Shale is gradational (Culp, 1961; Cole, 1989). Radiolarian and conodont data indicate that the basal Caney Shale is Chesterian in age (Schwartzapfel and Holdsworth, 1996). Although radioactive, standard gamma-ray logs of the Caney Shale do not exhibit the high gamma-ray magnitude typical of Woodford Shale (Cole, 1989, Fertl and Chingilarian, 1989). Therefore extreme uranium enrichment in magnitudes seen on Woodford Shale logs is probably not common in the Caney Shale (Hester et al. 1990, 1992).

The Caney Shale, described by Taff in 1901(Elias and Branson, 1959) consists of three intervals (Prestridge, 1958) of very thinly bedded cyclic silica rich shale. Some Caney beds contain thin elliptical carbonate nodules called bouillon, which are very characteristic of the formation (Elias and Branson, 1959). The three units of the Caney Shale in ascending order are the Ahloso, the Sand Branch, and the Delaware Creek, respectively (Branson and Elias, 1959). Peace (1994) indicated that the Caney Formation was the only pre-Pennsylvanian lithology of post Woodford Shale age that had not produced oil or gas. Recently the Caney Shale has been the object of a “gas play” and has produced natural gas (Forgotson, 2006). Above the Caney Formation are the Chester

and Springer Formations, which may be the last important formations prior to the orogenies of the Pennsylvanian (Braun, 1959; Peace, 1994).

Woodford Shale was deposited on the eroded surface of Hunton Limestone (Maxwell, 1959; Tarr, 1955; Amsden et al., 1968,; Amsden and Klapper, 1972; Hester et al., 1990, 1992; Ettensohn, 1995; Rottman, 2001; Over, 2002). The Hunton Group is divided, oldest to youngest, into three formations including: the Chimneyhill Formation, the Henryhouse Formation (Harragan-Henryhouse Marl), and the Bois d'Arc formation, which consists of Frisco and Bois d'Arc Limestones (Maxwell, 1959; Ham, 1986). In the northern Arbuckles, the Woodford Shale rests unconformably on the Henry House Formation and on the Southern Limb the Woodford rests on Bois d'Arc Limestone (Hass, and Huddle; Ham, 1986; Over, 2002).

CHAPTER III

Research Methods

Outcrop Lithology and Description:

Vertical thickness, strike, and dip measurements were made and recorded at both study outcrops. Individual outcrop beds were sequentially numbered with an alpha-numeric system. Bed numbers were recorded on the outcrop face and in data books. Each individual shale bed thickness was measured and bed lithology was recorded. Occurrence of special features in individual beds, such as pyrite nodules, silicified wood, carbonate beds, and phosphate nodules was recorded. Measured sections and detailed outcrop descriptions were made for both study outcrops including the outcrop data specified above.

Additionally, lithologic information was recorded corresponding to the exact location of each paired MS/gamma-ray measurement point. For the purpose of correlation at Hass A, lithology at individual MS/gamma-ray point was described as either “fissile”, “siliceous”, or “transitional”. The position of each measurement point was recorded with an indelible mark, where possible, indicating the exact position on the outcrop face. In the field books, a unique sequential number was assigned to each measurement point. Bed numbers and special features, from the outcrop descriptions, were also recorded in conjunction with the paired measurement points. Outcrop lithological information in the study was based on the gross appearance of the rock.

Paired Magnetic Susceptibility and Spectral Gamma-Ray Measurements:

In order to measure variation of MS as a function of gamma-ray magnitude and gamma-ray specific elemental assemblage, sequentially ordered, paired measurements of volume specific magnetic susceptibility and spectral gamma-ray response were made at two outcrops of the Woodford Shale. Volume specific magnetic susceptibility measurements and spectral gamma-ray measurements were made at six inch (15 cm) intervals at both the Henry House Creek (Hass A) and Lake Classen spillway (Hass B) outcrops. Measurement pairs were numbered and recorded in bound field/transit notebooks at the outcrops.

Volume specific magnetic susceptibility (dimensionless) was measured in SI units with the MS2k instrument manufactured by Bartington Labs (Figure 12a). Gamma radiation in this study was measured with an Exploranium 320 spectral gamma-ray detector manufactured by SAIC (Figure 12b). At each individual gamma-ray measurement point, the total gamma-ray count was recorded along with the individual concentrations of potassium (K) in per-cent (%), uranium (U) in parts-per-million (ppm) and thorium (Th) in parts-per-million (ppm). Gamma-ray magnitude in American Petroleum Institute units (API) was calculated for each MS measuring point using the standard equation (Eq 4.).

The instrument used in this study to make the volume specific magnetic susceptibility measurements is manufactured by Bartington Labs (Figure 12a). The machine is a magnetic bridge instrument as described by Graham (1954) and Nagata (1961). The sensor induces a weak magnetic field in the specimen. The

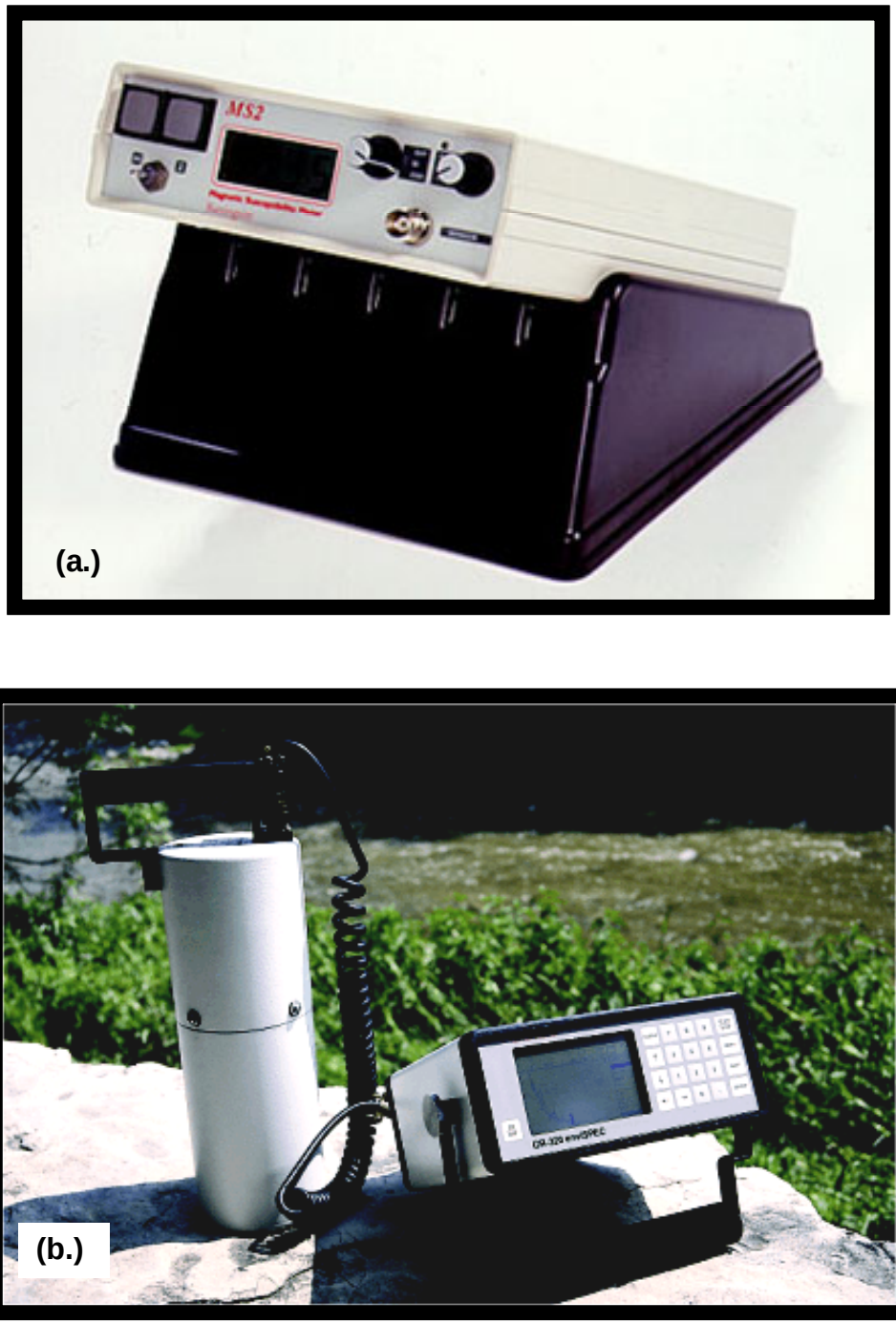

Figure 12. Study instruments. These portable instruments, used in the study were (a.) the MS2K manufactured by Bartington Industries, used to measure magnetic susceptibility (MS) and (b.) the Exploranium 320, used to measure gamma-ray magnitude and individual concentrations of gamma-ray specific elements. Both instruments allow rapid and non-destructive measurements of outcrop lithology *in situ*.

instrument calculates the MS of *in situ* lithology and quickly displays the measurement on a LED (Dearing, 1991).

In practical terms this means no other procedures are required to rapidly measure and record volume specific rock magnetic susceptibility (κ) at the outcrop. The measurement of κ, (dimensionless) is displayed on the LED. This reading can be multiplied by 10^{-5} and 10^{-6} for SI units or CGS units respectively (Dearing, 1991). In order to determine mass specific magnetic susceptibility, it is necessary to calculate the density of a specimen. This requires the physical removal of the specimen from the outcrop to determine the density in a laboratory. Volume specific magnetic susceptibility magnitude is only dependent on the given volume of magnetic material present and its respective magnetic properties (Nagata, 1961). Therefore volume specific MS is easily measured in outcrops and soil profiles that are fairly smooth and on any rock surface provided that sample volume is held constant.

While making preliminary measurements, it was noted that lateral variability in MS magnitude was common. Scraping the surface of outcrops, in order to remove the effect of any accumulation or alterations present, often resulted in consistently lower measured MS value. Higher MS magnitudes were associated with rust-colored stains, weathering rinds, and soil formation. As a result, it was assumed that in the event of lateral variation of MS, the lower MS value represents a better measure of rock MS response. Occasionally, structures such as pyrite nodules up to 8 cm in diameter or pyrite in layers, account for higher MS values. In these situations, the MS measurements were considered to be a true property of the formation and thus the higher values were recorded.

Woodford Shale Samples:

MS and gamma-ray measurements were plotted in an Excel spreadsheet on a personal computer at the outcrop in order to generate curves illustrating the change in gamma-ray and MS magnitudes as a function of the distance above the outcrop base. Based on these curves, generated with paired MS and gamma-ray measurements, researchers collected fresh rock samples at gamma-ray magnitude maximum/minimum points. At each sample point, researchers collected a minimum of six (6) plastic bags containing a minimum of 40 grams of fresh rock. The exact location of the maximum/minimum points was recorded in the field books and on the outcrop face in terms of individual bed number and the sequential number associated with the individual MS/gamma-ray data pair. Additional samples above and below gamma-ray magnitude maximum/minimum points were collected in fissile and siliceous beds. The stratigraphic position of the additional samples (e.g. individual bed #) was recorded in the field notes.

Inductively Coupled Plasma-Mass Spectrometry:

Trace metal composition of one suite of Woodford Shale samples was determined by means of inductively coupled plasma-mass spectrometry at Arkansas State University following digestion with nitric acid. Concentration of aluminum and iron and a calculated iron aluminum ratios (Fe/Al) were used to evaluate enrichment of authigenic iron in the Woodford Shale (Lyons and Severman, 2006). ICP-MS Detection limits were 10 parts per billion (ppb) for major elements and 1ppb for minor and trace elements. ICP-MS results have a 95% reproducibility (RSD > 5%) for all elements.

CHAPTER IV

RESULTS

Outcrop Observations:

Outcrop 1-Henry House Creek (Hass A)

The most complete Woodford section is the outcrop exposed on the west side of Henry House Creek (Figure 3), adjacent to the main ranch road bordering the ranch's shale quarry in Carter County, Oklahoma, Section 30 T 2S R1E IM. A detailed lithologic description of the Hass A outcrop is provided in Table 2. The base of Hass A has been exposed by excavation in the ranch quarry and along an unnamed intermittent stream which feeds into Henry House Creek from the west. The basal contact of the Woodford outcrop is exposed a few feet above the stream-bed which we named "Rattlesnake Creek". This basal contact with the underlying Hunton Formation (Bois d'Arc Limestone) frequently, though intermittently, outcrops along the trace of the contact surface for some distance both east and west of the study outcrop. The Hass A outcrop is a gentle anticline with some beds offset in the quarry.

The basal beds at Hass A contain silicified logs of the fossil fern-tree, *Callixylon sp* (Kirkland et al., 1992). One of the largest *Callixylon* specimens was located *in situ* but not in growth position near the base at Hass A in thinly bedded pink and blue fissile shale. This shale weathers to bright green at the confluence of Henry House creek and "Rattlesnake Creek" where weathered and eroded basal Woodford is partially covered by alluvium.

The shale above the Hunton Limestone-Woodford Shale contact contains clasts of silicified wood and chert clasts apparently weathered from the underlying Hunton group. Some of the smaller clasts of silicified wood are fine-grained and possibly suitable for lapidary purposes. The larger logs of *Callixylon* from Hass A are coarse grained while smaller fragments of silicified wood are more fine-grained (Figure 13). The logs are slightly oblate and rounded on their lower contact surface. Only 1 of the logs was found *in situ.* Although this log does not appear to be in a growth position as described by Retallack (2001), it occurs in a semi-upright position, is partially buried in undisturbed sedimentary layers, and a protrusion at the base could possibly be interpreted as a root or anchoring structure.

A very thin interval of thin pink (Munsell 10R 8/4) and light blue gray (Munsell 5G 8/1) claystone beds occur in basal beds at Hass A. This interval contains weathered pebbles, silicified wood and basal units at Hass A contain relatively high (U/Th) uranium thorium ratios, relatively low concentrations of potassium, uranium and Thorium, and relatively low gamma-ray magnitudes (Table 4). All three radioactive elements, gamma-ray magnitude, and U/Th ratio show marked increases in the lithologic transition from Hunton Limestone to Woodford Shale.

The Hass A quarry surface is unweathered and mostly clear of alluvium. In this regard the quarry closely resembles cored Woodford lithology. We identified three major types of shales: fissile, transitional, and siliceous (Figure 14). Fissile shale was commonly dark green, brown or black and poorly indurated. Fissile beds ($\leq$ 1.3 m) were typically much thicker than siliceous beds ($\leq$ 12.4 cm). Siliceous shale exhibited

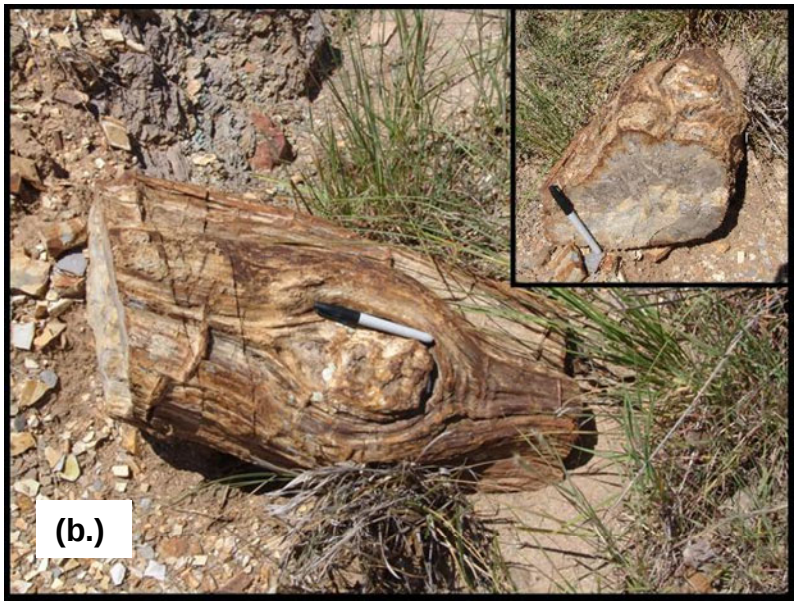

Figure 13. Silicified logs (*Callixylon sp*) from Woodford Shale at Hass A. Small fragments of the wood are common at the base of the quarry at Hass A. Larger pieces such as (a.) are found in the small drainage which heads west of "Rattlesnake Creek" Divisions within scale bar are 0 .1 m. and (b.) a log occurring *in situ* near the base of the Woodford Shale in the Henry House Creek quarry (marker for scale).

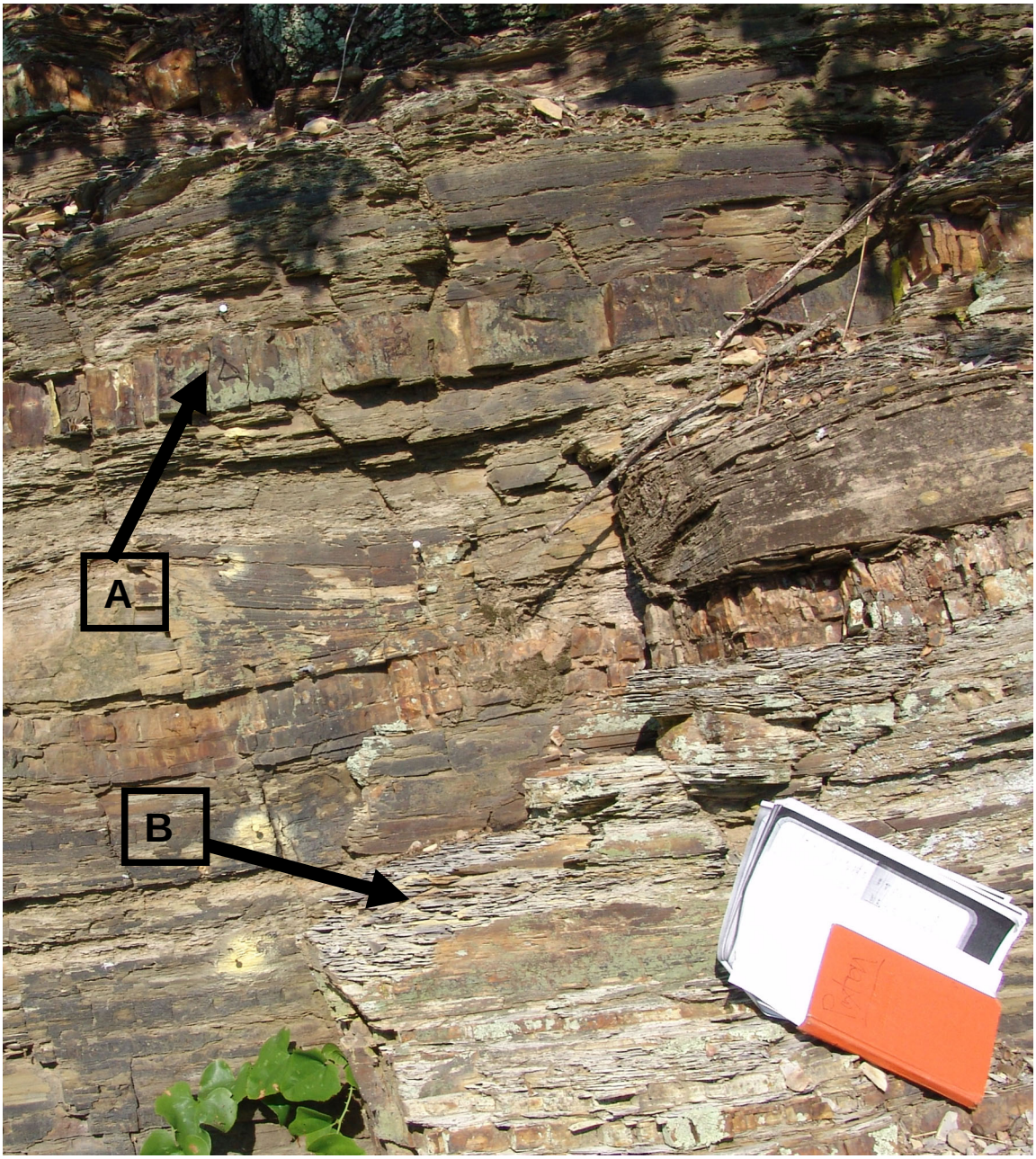

Figure 14. Common lithologies at Hass A. Photograph includes blocky beds of well indurated siliceous shale such as (A) and poorly indurated fissile shale such as (B).

subconchoidal fracture and was black or gray in color. Siliceous beds were typically finely laminated, blocky, and well indurated. The term “transitional shale” was used to describe those measurement points where the MS instrument was under the direct influence of both fissile and siliceous lithologies.

Pyrite nodules were first observed *in situ* near small fragments of *Callixylon sp.* near the base of the Woodford Shale in the quarry. Pyrite nodules (Figure 15), pyrite layers and *Callixylon sp*, all occur at the Hass B creek section, but with decreased size and frequency. The top of the upper-middle fissile interval contains a pyrite layer approximately 1 cm thick near the outcrop MS/gamma-ray magnitude maximum.

The creek section is almost entirely exposed but more weathered relative to the quarry section. Some of the lithological differences at Hass A are observable through differential weathering. Siliceous Shale (Figure 16) and fissile shale (Figure 17) weather at different rates. Erosion, pedogenic processes and soil formation have made the middle fissile unit of the Woodford Shale a preferred plant growth medium relative to the balance of the formation. The middle interval does contain some siliceous beds that are laterally continuous. Siliceous beds, when present, extend into Henry House creek where they form riffles and cascades. Rills and small gullies bring runoff to the creek along the top of erosionally exposed resistant siliceous beds. These resistant beds form the basis of a pattern of angled or diagonal stair-like features, repeated through the outcrop and creek bed.

Gamma-ray magnitude and MS as a general trend appeared to rise and fall in a cyclic fashion. Gamma-ray magnitude was generally observed to be highest (peak) in the middle to top of incompetent fissile beds. MS was also observed to be typically highest in

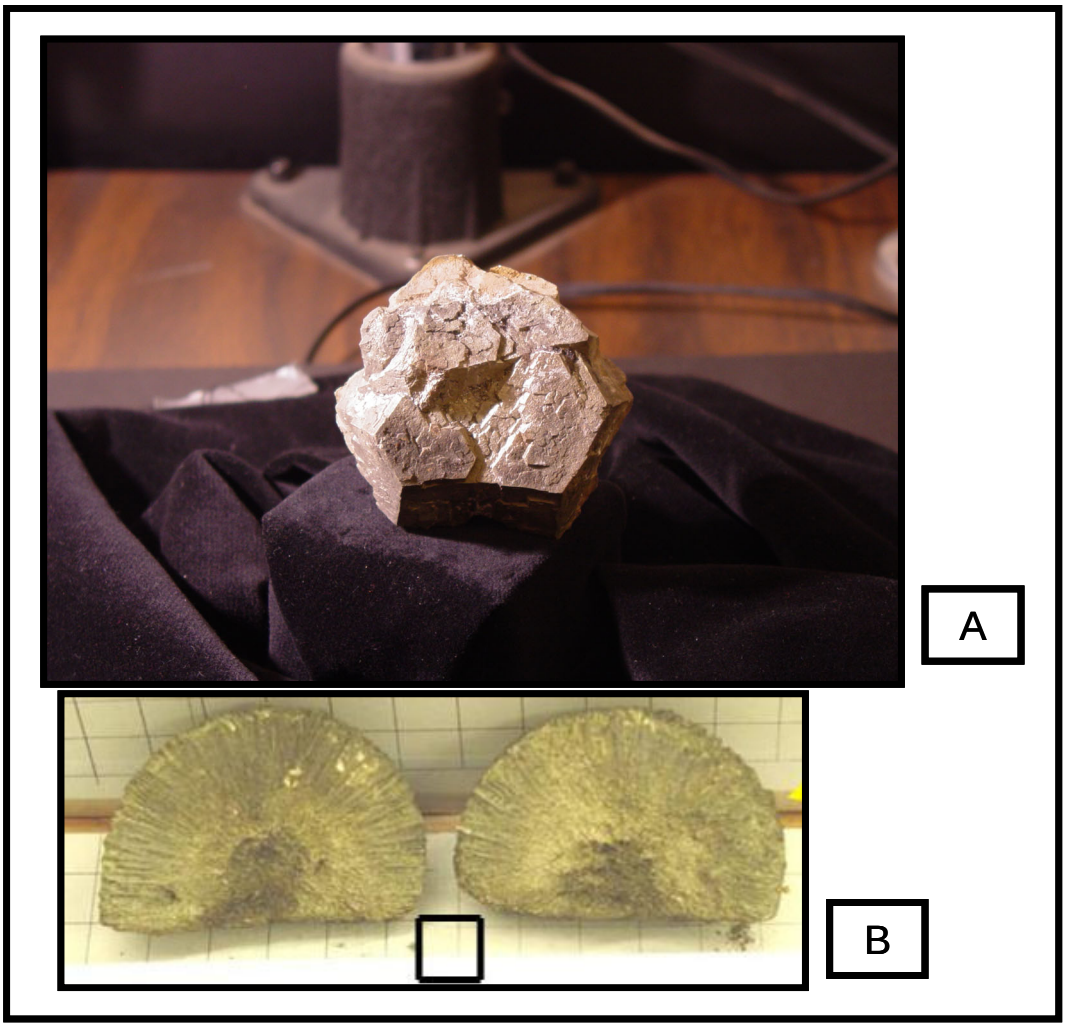

Figure 15. Woodford Shale pyrite/marcasite nodules and crystals. (A) Pyrite nodule with intergrown euhedral crystals located near the base of the Woodford Shale at Hass A. Specimen (A) has a mass of 133.3 g and diameter 8 cm. (B) Radial marcasite nodules (scale = 1.27 cm) were located in two intervals at Hass A and Hass B corresponding to MS/gamma-ray magnitude maxima.

Figure 16, Contact surface between the upper siliceous/middle fissile intervals of the Woodford Shale at Hass A. Perspective view "looking up" along the resistant siliceous bedding and contact surface. Arrow shows general trend of bedding surfaces, with geologist for scale. Resistant siliceous beds extend into stream and form falls or riffles. Above the high water mark, the siliceous beds form sheer walls.

Figure 17. Middle fissile interval of the Woodford Shale at Hass A. Upper arrow in photograph denotes position of upper siliceous/ middle fissile contact where Henry House Creek is deflected by highly indurated siliceous beds forming cliffs in the upper Woodford interval. Lower Arrow and geologist indicate the highly vegetated and poorly indurated middle Woodford Shale interval. Geologist (staff) indicates the position of a local maximum gamma-ray magnitude interval contained in the weathered fissile shale.

fissile beds. Fissile beds contained both local and outcrop maxima for gamma-ray magnitude and MS. The middle interval at Hass A is predominantly composed of fissile beds and has the highest gamma-ray magnitudes (Figure 18). It was observed that outcrop maxima of: uranium concentration (112.6 ppm), MS (18 SI units), and gamma-ray magnitude (980 API) were all contained at the same measurement point (data pair #293). That measurement point was located in a fissile bed near the top of the middle fissile interval (Figure 19).

Hass A Woodford Shale unconformably overlies Bois D'Arc Limestone of the Hunton Formation (Figure 20). Located stratigraphically above the Woodford at Hass A is the Sycamore Limestone which is exposed for nearly forty miles along the southern limb of the Arbuckle Anticline (Cooper, 1926).

Outcrop 2-Lake Classen Spillway (Hass B)

The second main study outcrop of Woodford Shale is located in the Lake Classen Spillway at the Goddard YMCA Camp in Murray County, Oklahoma, Section 24 T.1S., R.1E I.M. (Figure 4). We identified three main types of lithology at Hass B including basal claystone, fissile shale, and siliceous shale. The Woodford Shale at Hass B rests unconformably on Devonian carbonates from the Harragan-Henry House Formation (Hass and Huddle, 1965; Over, 2002) (Figure 25). At Hass B, the early Mississippian conodont forms, documented at Hass A (Over and Barrick, 1990; Over 1992a, 1992b; Schwartzapfel and Holdsworth, 1996) are not documented and the upper Woodford Shale intervals, corresponding to the lower Mississippian Boundary, is covered, eroded, or faulted out in the spillway section (Over, 2002). The highest stratigraphic intervals at Hass B are completely eroded, covered or faulted out in the spillway, (Figure 6).

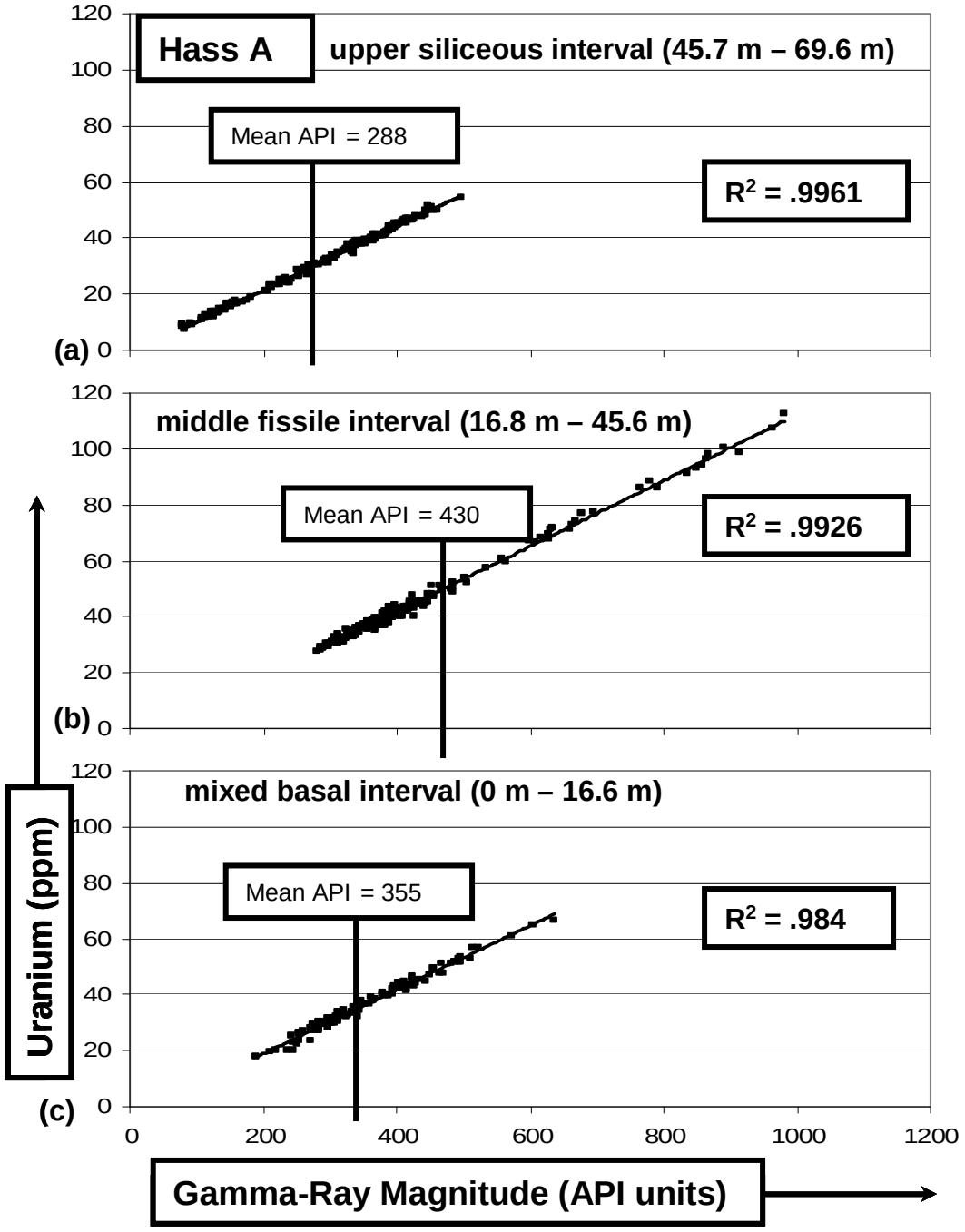

Figure 18. Uranium concentration vs. gamma-ray magnitude in the 3 main lithologic intervals observed at Hass A. Plots include: the upper siliceous interval (a.), middle fissile interval (b.), and basal mixed interval (c.).

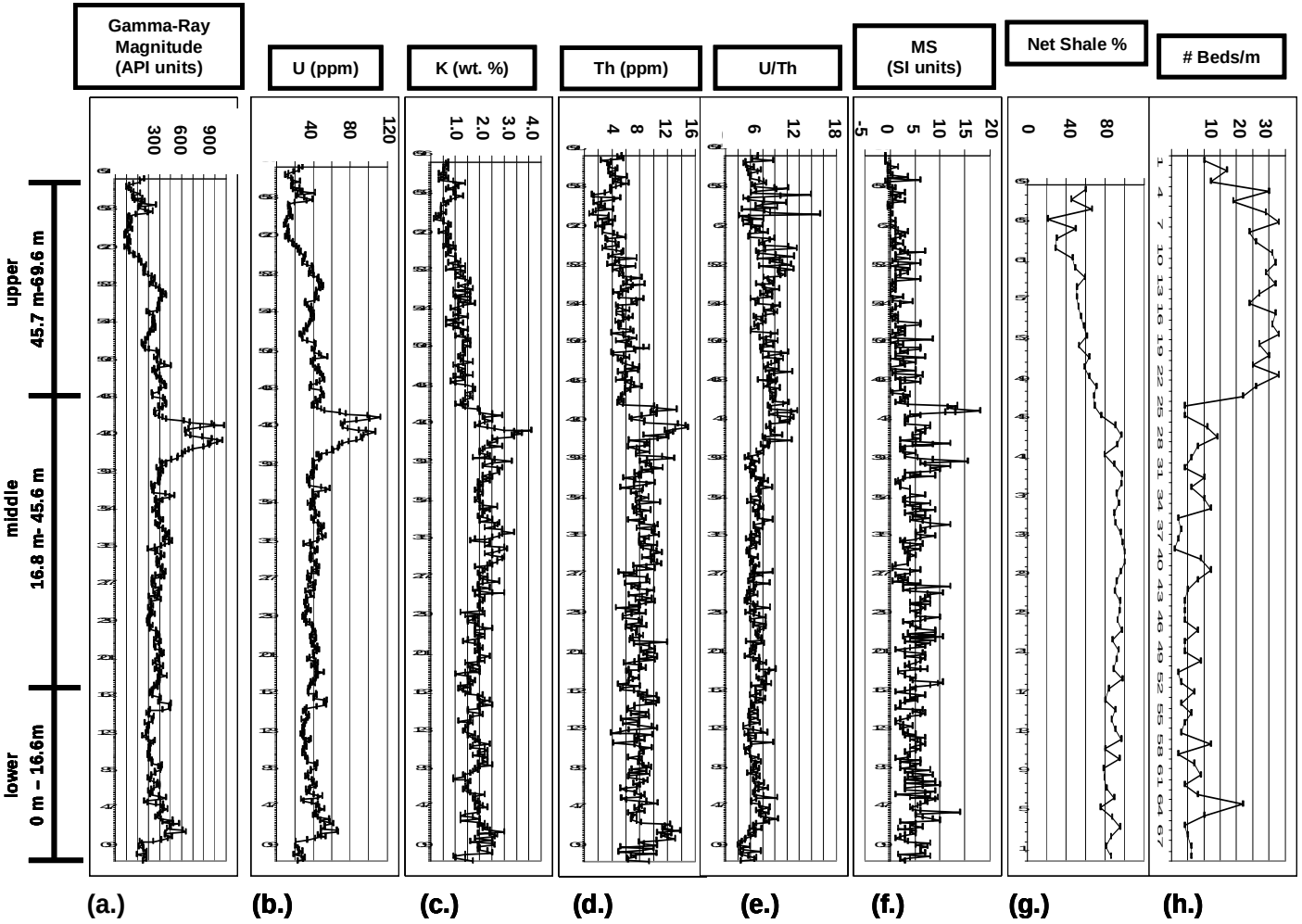

Figure 19. Comparison of profiles for several study variables in three main intervals at Hass A including: gamma-ray magnitude (a.), U (ppm) (b.), K (wt. %) (c.), Th (ppm) (d.), U/Th ratio (e.), MS (f.), net shale % (g.), and # of beds/m (h.).

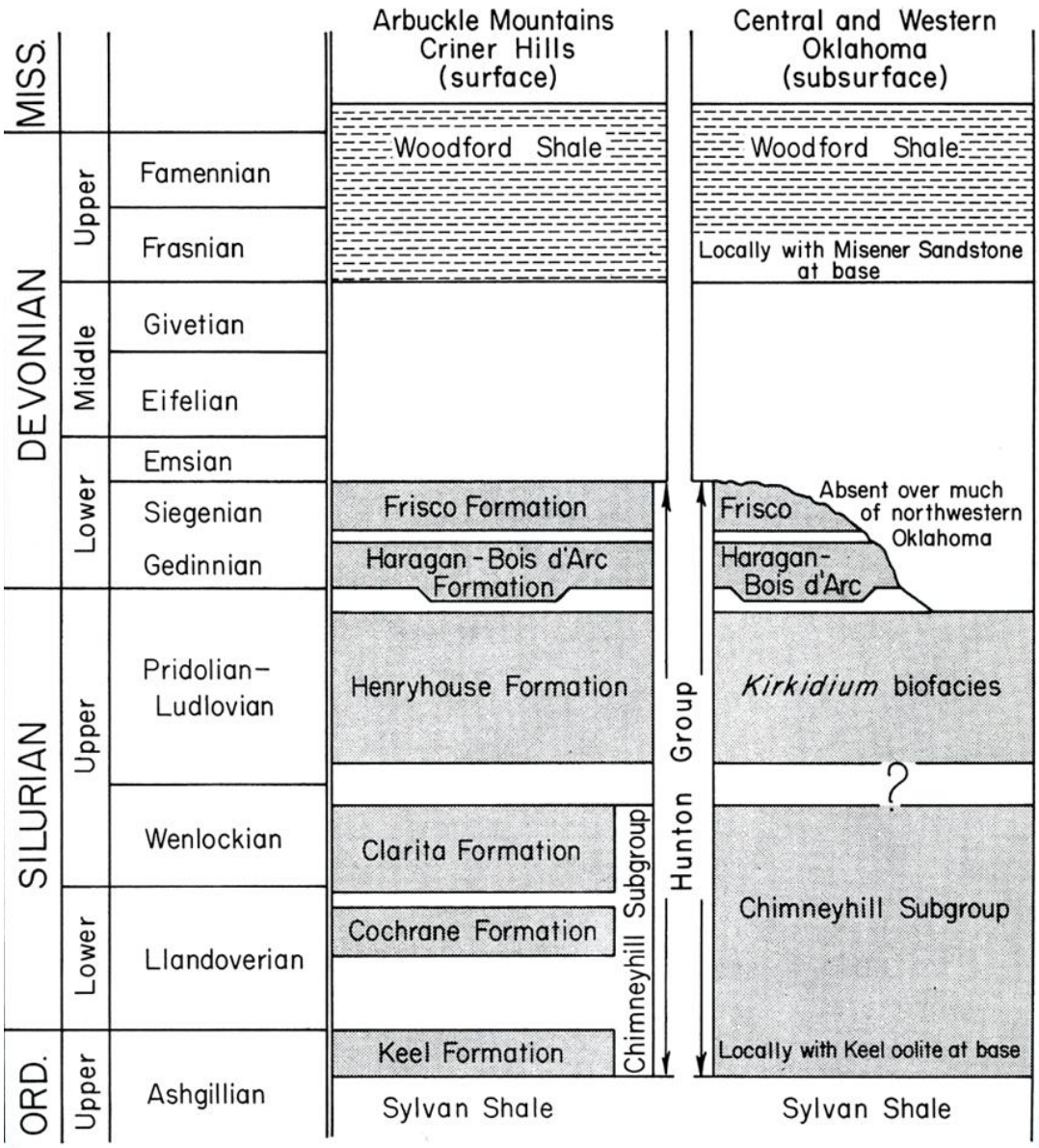

Figure 20. Stratigraphy below the Woodford Shale (Acadian Unconformity surface). Note the missing section below the Woodford Shale and lithology of different ages upon which Woodford Shale deposition occurs (Ham, 1986).

especially the zone of phosphatic nodules associated with proximity to the Devonian-Mississippian boundary (Over and Barrick, 1990; Over, 1992a, 1992b; Schwartzapfel and Holdsworth, 1996; Hass and Huddle, 1965). Phosphatic nodules are observed in this study north of the spillway outcrop at Hass B. This observation implies that the Devonian-Mississippian contact may be present in the general study area around Hass B. North of the Spillway, nearly vertical repeated sections, including a repeated section of Woodford Shale were observed (Figure 21). West of the spillway, stratigraphically below Hass B, nearly horizontal beds of Collings Ranch Conglomerate unconformably occur above steeply dipping pre-Pennsylvanian strata and repeated sections (Ham, 1955, 1986; Fay, 1989, Pybas, 1995) (Figure 22).

Basal Woodford Shale at Hass B contains sparse wood fossils and weathered rock clasts. Some rock clasts from the base of Hass B contain slicken lines indicating a probable tectonic origin. Although not reported in previous studies of Hass B, the first 4.8 m (15.7 ft.) above the base of the Woodford Shale outcrop is chaotically folded and faulted in the spillway (Hass and Huddle, 1965; Over and Barrick, 1990; 1992a, 1992b, 2002; Crick et al., 2002). The basal 2.5 m (97 in.) at Hass B is tectonicly homogenized, with rock fabric and bedding planes almost obliterated. Reproducible MS measurements were impossible in the first 5.6 m (16.5 ft.) The basal contact is offset at least several meters in a fault observed in the spillway. Lateral investigation, north of the Lake Classen Spillway in this study, revealed an unfolded and unfaulted basal Woodford contact. The entire spillway exposure is severely fractured and faulted (Figure 23).

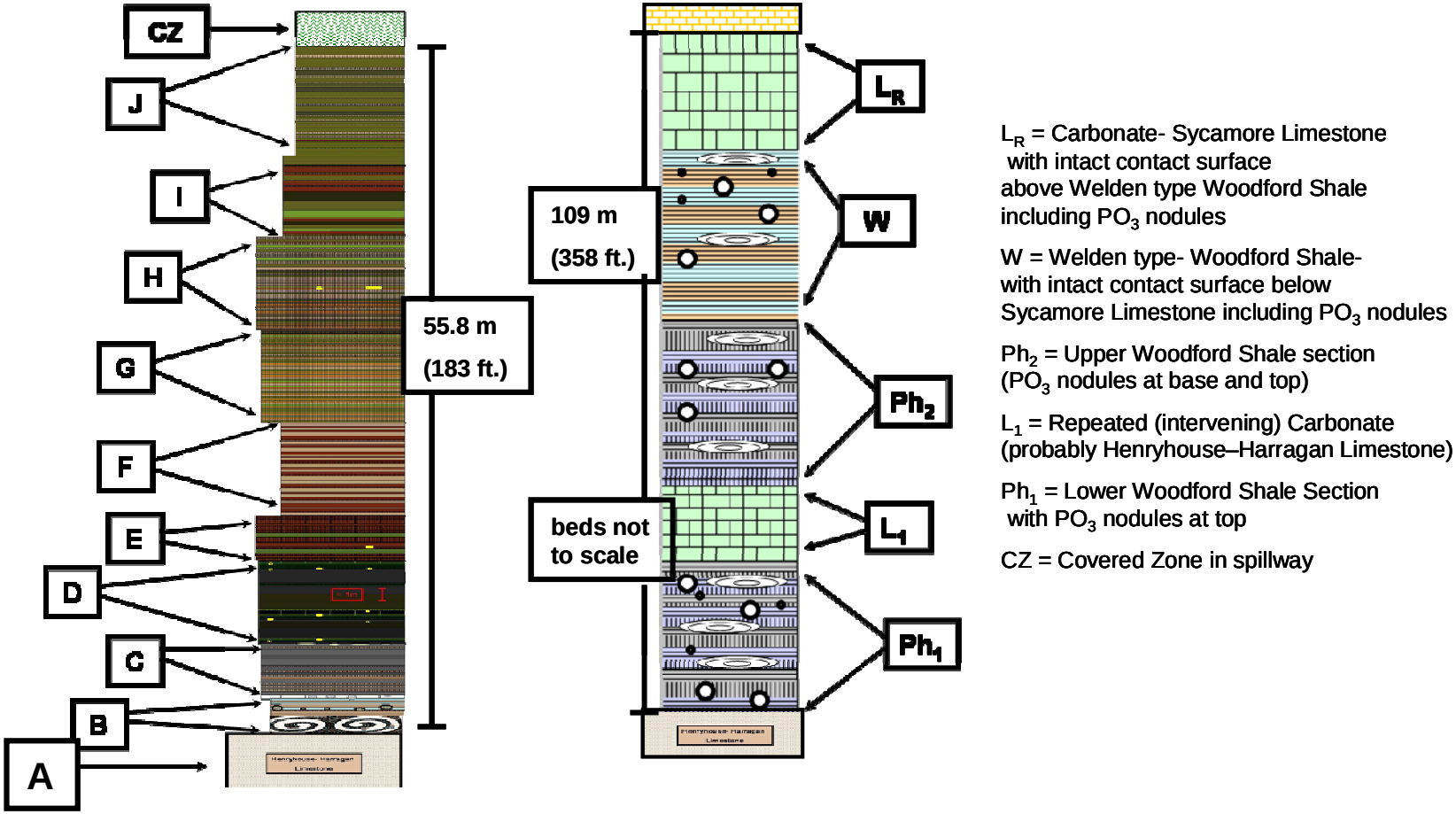

Figure 21. Simplified lithologic column from **Hass B** (Lake Classen Spillway) and observed repeated sections north of the spillway section. Woodford Shale is succeeded by a covered zone not to scale (CZ). A detailed measured section of the Hass B spillway outcrop is found in Figure 6.

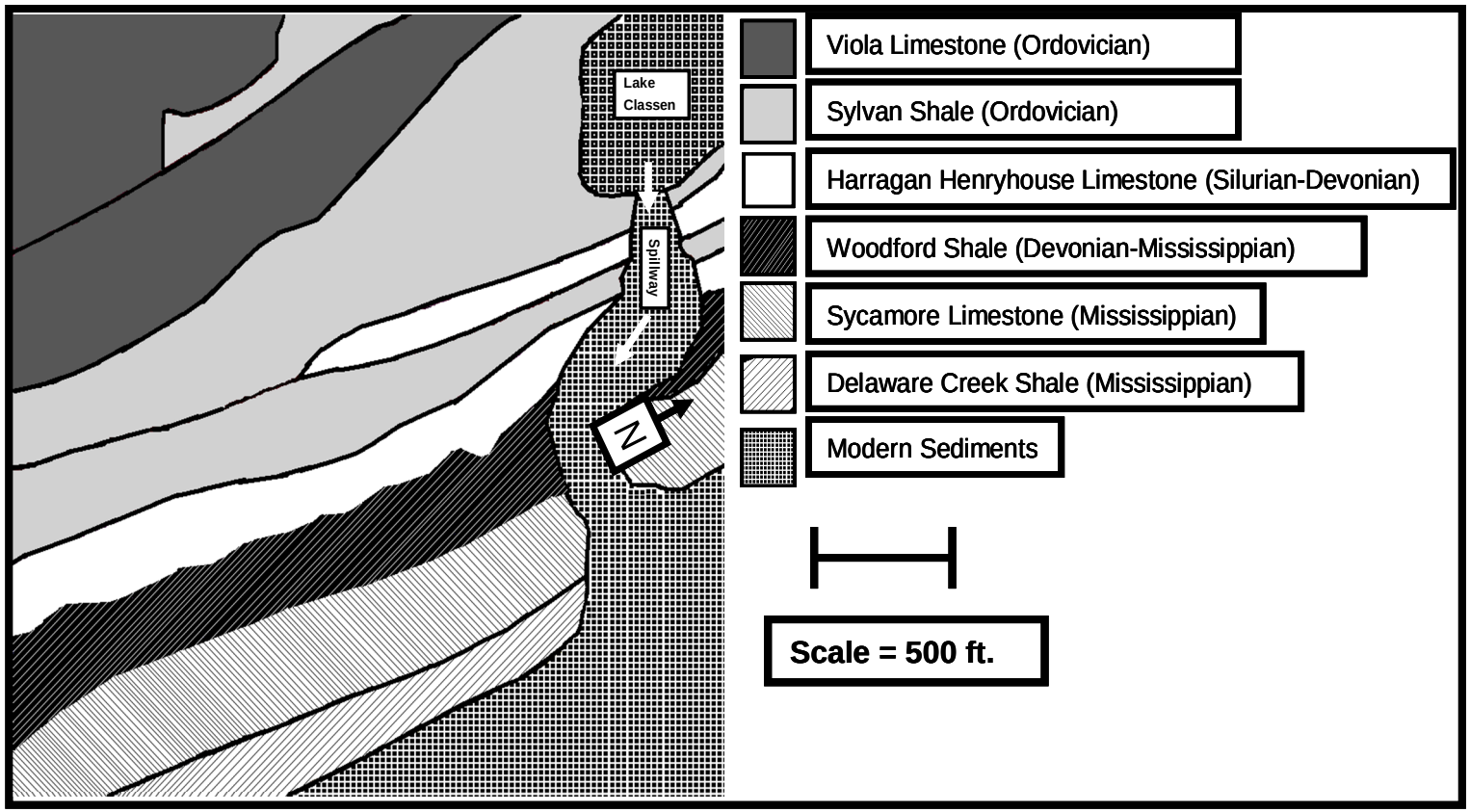

Figure 22. Portions of a regional geologic map of the Arbuckle Mountains modified from Fay (1989) including the Lake Classen Spillway, Hass B outcrop of the Woodford Shale. The repeated lithologies in the Washita Valley Fault Zone (Pybas et al., 1995) become progressively younger from S to N and W to E (Ham, 1955, 1986; Fay, 1989).

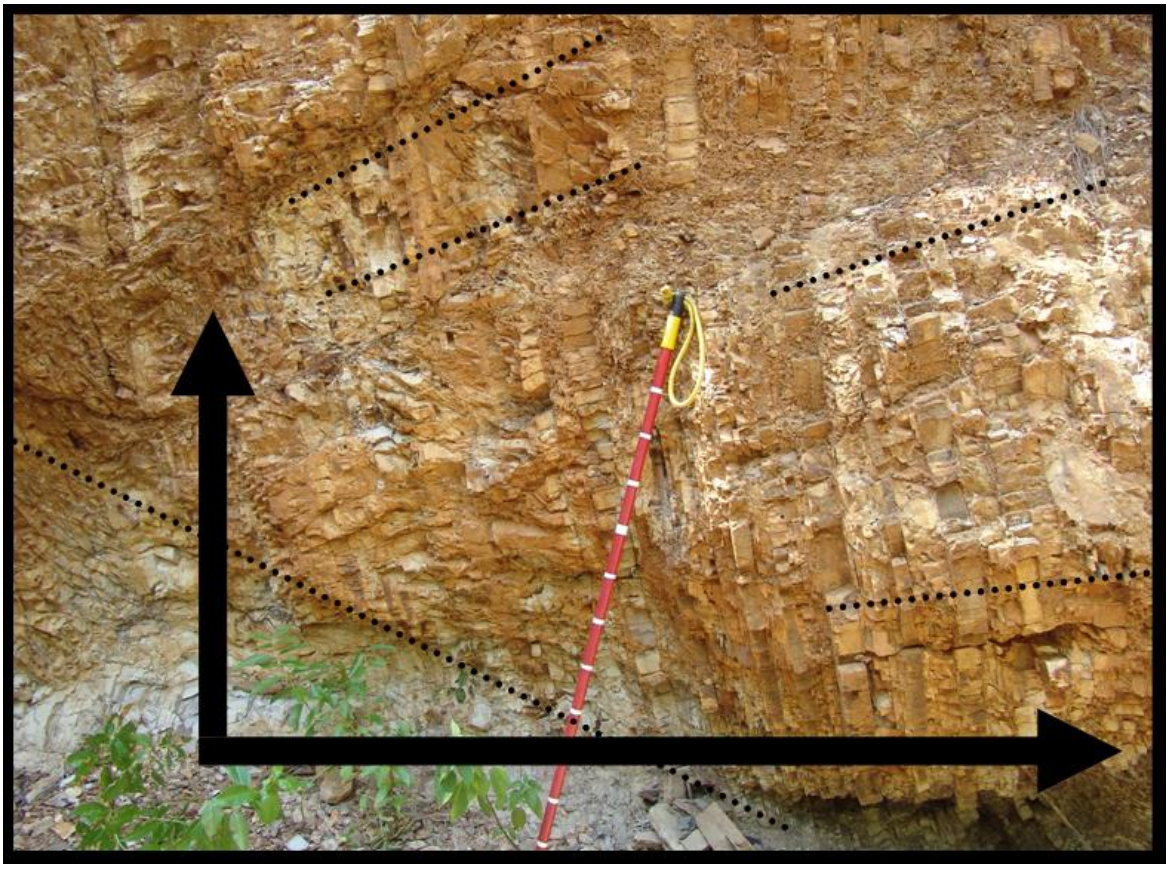

Figure 23. Faulted and fractured lithology at Hass B. The entire Hass B outcrop is badly faulted and fractured. Long arrow indicates stratigraphically up direction (east) and short arrow indicates vertically up direction. Typical faults in the fractured beds are indicated with dotted lines. Staff for scale, rests on pulverized rock typical of the Hass B outcrop (each mark is 0.1 m).

A resistant hogback of the Sycamore Limestone located stratigraphically above the Woodford at Hass B traces the trend of the Arbuckle Anticline in the study area. The trend of this hogback changes from roughly 280° to 340° in approximately 2.4 km (1.5 miles). The attitude of the Woodford at Hass B was observed to strike 315° with a dip of approximately 85° NE. The Woodford Shale at Hass B is tilted nearly upright, but not overturned.

Several lithologies are observed at Hass B in the spillway (Table 3) including claystone, limestone, paper-fissile black shale, brown chert, siliceous coarsely and thinly laminated shale, silty fissile shale, laminated dolomitic shale, black chert, and black fissile shale with pyrite nodules coalescing into thin and discontinuous pyrite layers. The basal Woodford Shale at Hass B on the north side of the Lake Classen dam contains alternating pink and blue beds of claystone.

Structural Observations at Hass B:

Repeated Sections (Hass B)

A partial repeated section of Woodford Shale with cataclastic brecciated siliceous shale was observed north of the spillway at Hass B (Figure 24). Adjacent to and north of the spillway exposure, a (lower) brecciated zone of Woodford Shale beds occurs which contains shattered, welded blocky siliceous shale, round phosphatic nodules, with casts of round phosphatic nodules (**Ph_l**) (Figure 25). These beds trend approximately 340°. The welded brecciated shale beds are vertically overlain by several feet of an intervening (lower repeat) carbonate section (**L_l**) resembling Sycamore Limestone (Figure 26). The Woodford Shale (**Ph_1**) and intervening carbonate (**L_1**) contact is succeeded by another partial exposure (**Ph_R**) of brecciated Woodford Shale. The second, subsequent partial outcrop of Woodford Shale trends approximately 315°.

Figure 24. Pulverized, warped and welded siliceous welded breccia from (**Ph_R**) partial repeated section north of spillway at Hass B. This pulverized welded siliceous shale (a.) is highly indurated and deformed. Original bedding planes of siliceous beds in (b.) are bent nearly 90^o

Figure 25. Fractured blocky siliceous shale welded breccia from **Ph_1** with casts of phosphatic nodules from Hass B north of spillway section. Sample occurs at the top of **Ph_1** and below **L_1**, a repeated carbonate bed of Sycamore Limestone observed in this study *see Figure 21*.

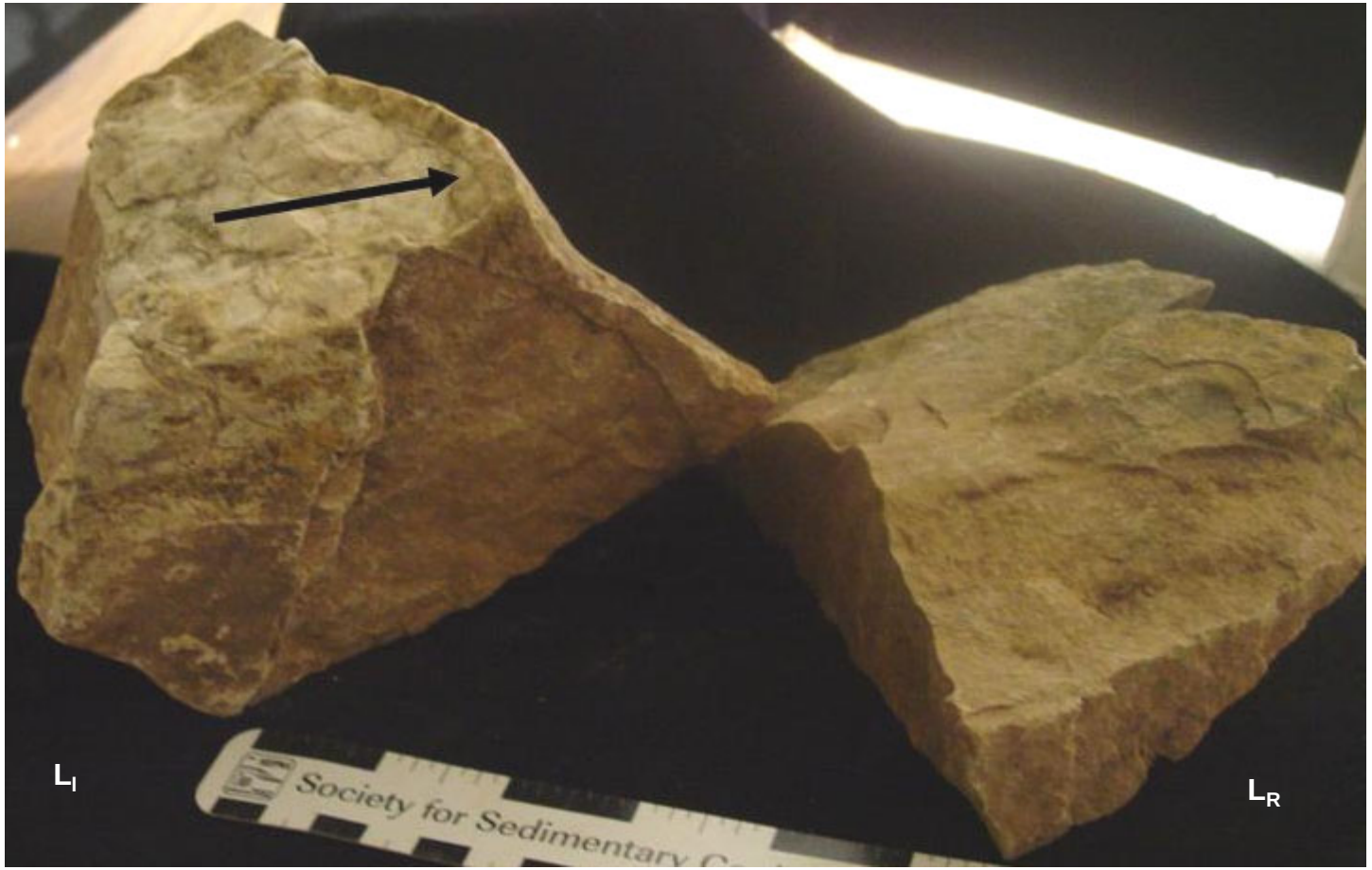

Figure 26. Photographs of limestone clasts $\mathbf{L_1}$ and $\mathbf{L_R}$. Clast $\mathbf{L_1}$ was removed from parallel beds of blocky carbonate located stratigraphically above $\mathbf{Ph_1}$ and stratigraphically below $\mathbf{Ph_R}$. Clast $\mathbf{L_R}$ was removed from the blocky parallel beds of Sycamore Limestone that comprise a resistant hogback in the study area (Ham, 1973; Fay, 1989).

Woodford Formation at all other Woodford Shale outcrops.

We interpret the intervening carbonate (**L_l**) to be Sycamore Limestone based on the gross appearance of the lithology along with structural observations by Ham (1986), Fay (1989), and Pybas et al. (1995) of multiple repeated sections in the Paleozoic rocks in the area of Hass B in the Washita Valley Fault Zone. Those repeated sections become increasingly younger from north to south (Fay, 1989). While, it is possible that the intervening carbonate (**L_l**) between the lower Woodford Shale section (**Ph_1**) and the upper repeated Woodford Shale section (**Ph_R**) is Henryhouse Harragan Limestone, that identification would not effect the interpretation of repeated Woodford Shale sections. The clasts of the (**L_l**) carbonate were observed to contain calcite fracture fill, further evidence of tectonic alteration of the study area.

Exact identification of the intervening carbonate (**L_1**), between the two sections of Woodford Shale (**Ph_1** and **Ph_R**) at Hass B is beyond the scope of this study. However the unidentified carbonate contains mostly calcite and not dolomite based on field tests using 10% HCL. Because the intervening blocky carbonate is limestone and not dolomite, it is improbable that (**L_1**) is an anomalous facies within the Woodford Formation. Unlike the limestone bed (**L_1**) powdered samples of the internal carbonate beds the at all other Woodford Shale outcrops are all weakly reactive with HCl. The upper carbonate (**L_R**) was reported to be Sycamore Limestone by Fay (1989) (Figure 22). The lithology from (**L_R**) appears to be limestone based on our field tests with HCl, where clasts (not powdered) were observed to have a very vigorous reaction. The presence of phosphatic nodules in beds of Welden-Type Woodford Shale *in situ* at the base of **L_R** is strong evidence that the strata are basal beds of Sycamore Limestone.

Repeated sections of Henryhouse-Harragan Limestone are observed immediately south of the Lake Classen spillway outcrop on the road leading to the Camp Caretakers residence as reported by Fay (1989). Also south of the spillway, Collings Ranch Conglomerate occurs unconformably, both stratigraphically and vertically, above the Woodford Shale outcrop and repeated sections of Harragan-Henryhouse Limestone. This conglomerate was described by Pybas et al. (1995) as part of the Washita Valley fault zone in the Lake Classen area.

Outcrop Attitude and Orientation (Hass B)

The occurrence and stratigraphic positions of the upper brecciated zone of phosphatic nodules (**Ph_R**) above the spillway outcrop at Hass B shows that the outcrop is tilted but not overturned. This finding disagrees with a report that the Hass B outcrop is gently overturned (Crick et al., 2002). The attitude of the partial section of Woodford Shale exposed in the spillway generally agrees with the trend of the underlying (older) Henryhouse-Harragan Limestone and the attitude of the overlying (younger) Sycamore Limestone. At all of the Woodford Shale outcrops or Sycamore Limestone outcrops studied by Hass and Huddle (1965), Over (1992a, 1992b, 2002), or Schwartzapfel, and Holdsworth (1996), the zone thick zone of spherical phosphatic nodules occurs at or near the top of the Woodford Shale, near the contact with the Sycamore Limestone (Siy, 1988).

Several observations (see *Outcrop Observations*) imply that the Hass B outcrop is not overturned. In all the study outcrops, the zone of phosphate occurs near the top of the (older) Woodford Shale stratigraphically below the contact with the (younger) overlying

Sycamore Limestone (Coffey, 2001). Stratigraphically below the (younger) Woodford Shale is the (older) Henryhouse-Harragan Limestone (Ham, 1986). Stratigraphically below the Henryhouse-Harragan Limestone are several (older yet), Ordovician and Silurian carbonates and Sylvan Shale (Ham, 1986; Fay, 1989, Pybas et al., 1995). The Harragan-Henryhouse Limestone, Woodford Shale, and Sycamore Limestone are all observed to dip at approximately 85^{o} NE in the area of Hass B, agreeing with reports by by Ham (1986) and Fay (1989).

Missing Lithology (Hass B)

The strata in the area of the Hass B, including the Lake Classen spillway is extremely faulted, eroded, fractured, brecciated, or completely covered. Furthermore, the repeated strata have been tilted to form a half graben structure, now only partially exposed after removal of large thicknesses of Collings Ranch Conglomerate (Pybas et al., 1995). The choice to include the Hass B outcrop in this study, despite the condition of the study area was based on two factors. First, Hass B is very close to the well-exposed and nearly complete Hass A outcrop where recent outcrop-based spectral gamma-ray studies of Woodford Shale have been conducted (e.g. Krystyniak 2003). Second, Hass B was included in a study of global MS correlation and offered as a possible global magnetic type section for the Frasnian/Famennian in the United States (Crick et al., 2002). Unfortunately, a complete description of the outcrop lithology, MS profile, and gamma-ray magnitude profile of Hass B are not possible.

None of the Woodford exposures proximate to Hass B are complete. Therefore, each provides limited information about the area's tectonic history and lithology. The

vertical thickness of the partially exposed (overturned) Woodford Shale section at I-35 north 2.25 km (1.4 miles) from Hass B is 82.3 m (274 ft.), while the thickness of the spillway outcrop is 55.8 m (183 ft.); (Fay, 1989). Assuming that the true Hass B vertical thickness is the same as the I-35 north outcrop, it is possible that at least 27.5 m (91 ft) are missing or unexposed in the Hass B spillway, without accounting for repeated sections of Woodford Shale observed north of the spillway. North of the spillway outcrop, the vertical thickness of the Woodford Shale was measured between the contact surface of the Henryhouse-Harragan Formation and the base of the Sycamore Limestone hogback. The result was a total measured vertical thickness of 109 m (358 ft.).

The thickness difference between Woodford Shale exposed north of the spillway exposure and the spillway exposure of Woodford Shale at Hass B 55.8 m (183 ft) is best explained in terms of literature reports of thrust faulting and repeated Paleozoic sections stratigraphically below the spillway outcrop at Hass B (Ham, 1986; Fay, 1989; Pybas et al., 1995). Woodford Shale has been measured at several outcrops on both limbs of the Arbuckle Anticline within a few miles of Hass B including: I-35 north, at 83.5 m (274 feet), I-35 south, at 88.4 m (290 feet) (Fay, 1989) and Hass A, 69.6 m (230 ft.); (Table 2).

Spectral Gamma-Ray Observations:

Gamma-Ray Specific Elemental Assemblage Variations

The largest observed gamma-ray specific elemental variations occur at the lithologic transition between Woodford Shale and the formations bounding the Woodford Shale (Table 4). The rapid increase in concentration of radioactive elements of the lowest Woodford Shale intervals is used as evidence of the lithologic change from carbonate to

shale, a dependable stratigraphic marker across the Anadarko Basin (Hester et al., 1988). These rapid increases result from fundamental differences between gamma-ray specific elemental assemblages of carbonates relative to those of shales. Measurements at Hass A and Hass B show that the Woodford Shale contains much higher concentrations of all three radioactive elements measured by the spectral gamma-ray analysis relative to the formations bounding the Woodford.

Woodford Shale specific differences in the gamma-ray specific elemental assemblage can be divided into five main categories including: variation at each individual study outcrop where gamma-ray specific elemental assemblages vary between the three main Woodford intervals (e.g. Figure 18), variation at each individual study outcrop, gamma-ray specific elemental assemblages vary within individual main intervals (Tables 5, 6), variation of spectral gamma-ray specific elemental assemblages between individual main intervals at one outcrop and corresponding main intervals at other outcrops (e.g Table 4), variation between spectral gamma-ray specific elemental assemblages, especially potassium and thorium, that vary at the larger or outcrop scale (Figures 19, 27), and variation caused by missing measurements and the observation that Hass B is not a complete outcrop. Moreover, portions of the Hass B outcrop suitable for reproducible spectral gamma-ray measurements are simultaneously unsuitable for MS measurements. If this missing lithology (e.g. low gamma-ray magnitude phosphatic interval) were included, gamma-ray magnitude statistics (e.g. mean, range, etc.) would likely decrease.

Although the observed maximum uranium concentration (ppm) at Hass A is almost double that of Hass B, the mean uranium concentrations of the two outcrops differ by a

Table 5. Gamma-ray magnitudes and gamma-ray specific elemental assemblages in lithologic intervals (*from Figure 5, Table 2*) of Woodford Shale at **Hass A**

Unit	**height** (m above base)	**K** (%) range	**U** (ppm) range	**Th** (ppm) range	**Fissile** interval (cm) thickness	**Siliceous** interval (cm) thickness
N*	above Woodford	1.3	3.0	6.9	Sycamore Limestone *1 measurement	
M	62.9 - 69.6	0.1 - 1.4	7.4 - 41.4	0.6 – 6.3	1.9 – 14.0	.1 - 10.0
L	56.4 - 62.9	0.3 - 1.7	8.8 – 50.1	1.5 - 8.7	0.1 – 25.0	0.1 – 10.0
K	45.7 - 56.4	0.6 – 1.8	24.1 – 54.5	3.9 – 9.3	0.9 - 14.7	0.1 – 3.3
J	43 - 45.7	1.0 – 4.1	39.4 -112.6	4.7 – 14.9	1.9 - 12.8	0.5 – 4.4
I	36 - 43	1.7 – 4.1	32.3 – 98.7	5.1 – 14.9	2.0 – 27.0	0.3 – 0.9
H	32.2 - 36	1.8 – 3.4	33.2 – 52.5	6.2 – 10.9	1.8 – 15.0	0.1 – 0.5
G	27.6 - 32.2	1.6 – 3.1	28.8 – 45.6	4.9 – 11.1	63.5 –127.6	0.9 – 1.8
F	25.6-27.6	1.7 – 3.0	29.3 – 41.3	5.8 – 10.1	2.9 - 15	0.3 - 0.5
E	19.5 - 25.6	1.2 – 2.5	27.8 – 45.4	4.5 – 11.9	2.8 – 28.3	0.9 – 1.5
D	16.7 - 19.5	1.0 – 2.1	33.0 – 51.0	4.8 – 9.0	51.0 –114.0	0.5 – 1.0
C	6.2-16.7	0.9 – 1.7	25.3 – 53.6	3.8 – 10.7	30.0 – 120.0	4.0 – 10.0
B	0-6.2	0.9 – 3.0	17.7 – 66.5	4.9 – 13.8	5.0 – 10.0	2.0 – 5.0
A**	Below Woodford	0.7 – 1. 0	0.1 – 2.9	2.8 – 4.6	Bois d'Arc Limestone ** 12 measurements	

Table 6. Gamma-ray magnitudes and gamma-ray specific elemental assemblages in lithological intervals (*from Figure 6*, *Table 6*) of Woodford Shale at **Hass B**

Unit	**d** (m above base)	**K** (%) range	**U** (ppm) range	**Th** (ppm) range	**Fissile** interval (cm) thickness	**Siliceous** interval (cm) thickness
K (CZ)	Covered zone and repeated sections not described in spillway					
J	47.2 – 55.8	1.4 – 2.7	14.0 – 39.4	5.9 – 11.7	0.2 - 195.6	1.0 - 7.3
I	40.2 – 47.2	1.5 – 2.9	28.4 – 53.2	5.4 – 11.6	2.2 - 228.6	1.1 – 8.1
H	32.7 – 40.2	1.3 – 2.8	40.4 – 60.3	6.4 – 12.5	1.1 - 64.8	0.6 - 10.2
G*	25.0 – 32.7	1.5 – 2.8	25.5 – 57.0	6.2 – 11.8	0.2 - 36.8	1.3 - 40.6
F*	17.4 – 25.0	1.1 – 2.3	31.5 – 48.9	3.9 – 12.4	1.3 - 52.1	1.0 - 78.0
E	13.7 – 17.4	1.0 – 2.7	21.0 – 41.8	3.8 – 10.3	1.3 - 68.6	1.3 - 12.2
D	7.3 – 13.7	1.8 – 4.0	23.8 – 48.9	6.8 – 13.6	0.5 - 134.6	1.6 - 17.8
C	3.2 – 7.3	1.2 – 3.2	30.4 – 57.7	6.2 – 12.9	1.1 - 43.2	1.3 - 6.2
B	0 - 3.2	2.6 – 6.1	6.5 – 37.6	9.9 – 21.4	0.3 - 246.4*	1.9 - 4.8*
A**	Below	2.8 – 2.9	6.5 – 7.3	9.9 – 11.3	Henryhouse- Harragan Limestone	

* Denotes faulted zones with obscured bedding planes. Beds (B) basal claystone, (F,G) tan chert, are pervasively fractured, sheared, and kinked. ** (n = 2) measurements

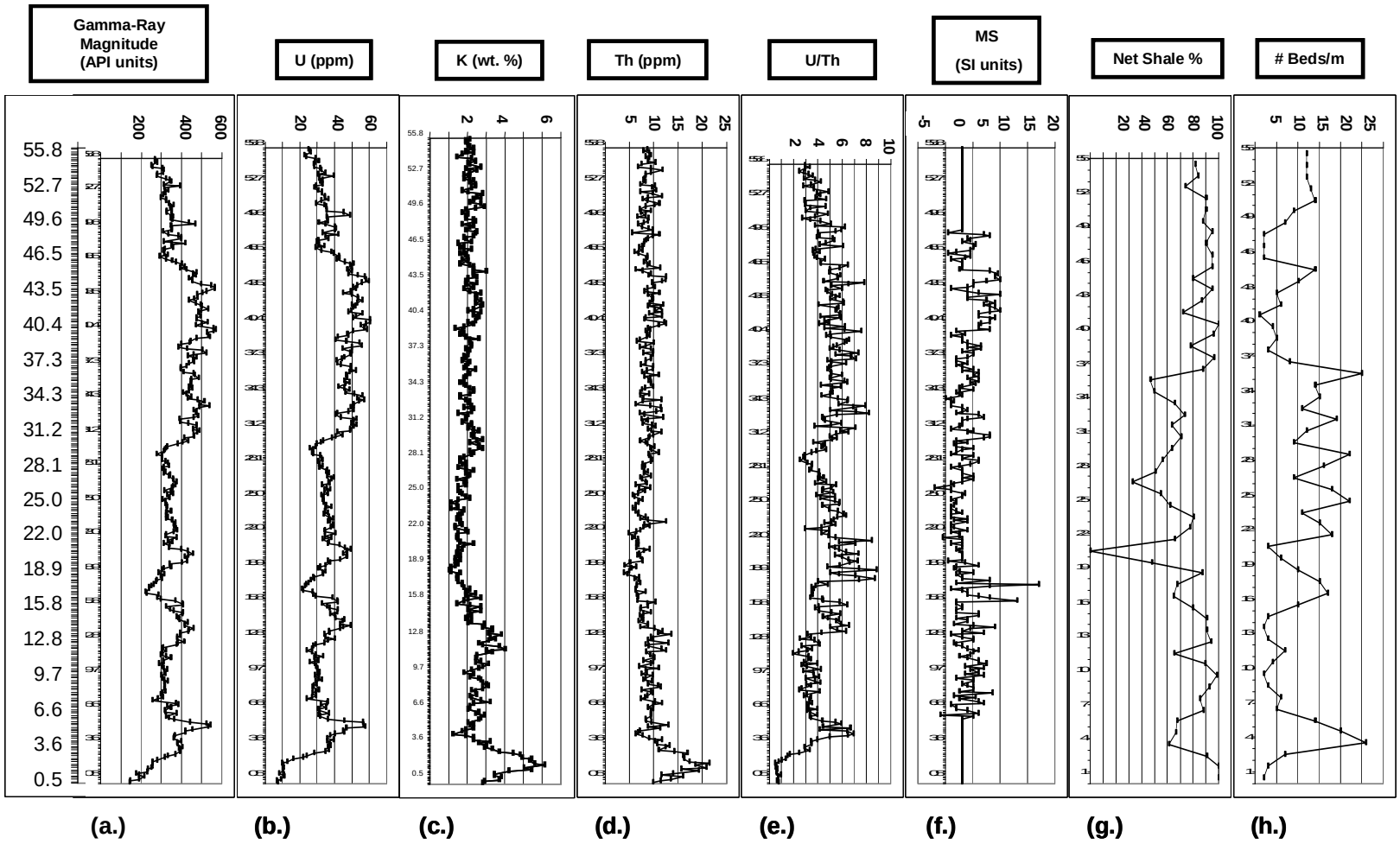

Figure 27. Comparison of profiles for several study variables at Hass B including: gamma-ray magnitude (a.), U (ppm) (b.), K (wt. %) (c.), Th (ppm) (d.), U/Th ratio (e.), MS (f.), net shale % (g.), and # of beds/m (h.).

few parts-per-million. Basal beds at Hass B have a generally lower concentration of uranium relative to Hass A. Hass B is richer overall in thorium relative to Hass A (Table 4). Hass B basal beds have a minimum U/Th ratio of .5 while the corresponding minimum at Hass A is 3.4 times greater (U/Th = 1.7) (Table 4). This difference reflects both the lower Th concentration and higher U concentration at Hass A (Table 7) relative to Hass B (Table 8). Because the base of both outcrops represents the Acadian Unconformity Surface (Hass and Huddle, 1965), the difference between the U/Th ratios of the Woodford Shale and Hunton Carbonate is reflective of differences in lithology.

The relative difference between maximum (4.1) and minimum (0.1) concentration values of potassium at Hass A (41 fold) is the greatest single elemental difference noted among radioactive elements measured by spectral gamma-ray analysis (Table 7). The minimum potassium concentration (weight %) occurs near the respective tops of both formations (Figures 19, 27). The minimum K concentration is an order of magnitude larger at Hass B (1.0) relative to Hass A (0.1), but the difference may be partialy explained by the complete removal of the upper beds in the spillway at Hass B (Tables 7, 8). Potassium concentration (weight %) in basal beds at Hass A is relatively low while the basal beds of Hass B are extremely enriched in K (Table 4). This difference in basal K concentration is possibly evidence of differences between the depositional environments at the two locations at the onset of Woodford Shale deposition. Gamma-ray magnitude comparison between the upper intervals at study outcrops is impractical, due to the complete removal of the upper Woodford Shale interval in the spillway at Hass B. Likewise, the presence of faulting at the basal Woodford Shale contact surface in the spillway at Hass B calls into question whether the basal section is complete.

Table 7. Summary statistics for spectral gamma-ray data at Hass A.

Hass A	Gamma-ray Magnitude (API units)	Potassium (wt. %)	Uranium (ppm)	Thorium (ppm)	U/Th ratio
Mean	363.5	1.7	38.6	7.2	5.4
Standard Error	6.3	0.0	0.7	0.1	0.1
Median	362.4	1.7	38.2	7.2	5.1
Mode	380.4	2.0	37.7	7.9	6.6
Standard Deviation	134.0	0.7	15.1	2.4	2.0
Sample Variance	17955.1	0.5	227.5	6.0	4.2
Kurtosis	4.3	-.01	4.9	0.1	1.5
Skewness	1.2	0.1	1.4	0.1	0.9
Range	902	4	105.2	14.3	13.6
Minimum	77.6	0.1	7.4	0.6	1.7
Maximum	979.6	4.1	112.6	14.9	15.3
count	458	458	458	458	458

Table 8. Summary statistics for spectral gamma-ray data at Hass B.

Hass B	Gamma-ray Magnitude (API units)	Potassium (wt. %)	Uranium (ppm)	Thorium (ppm)	U/Th ratio
Mean	372.3	2.2	36.5	8.9	4.5
Standard Error	4.4	0	0.6	0.1	0.1
Median	357.6	2.1	36.0	8.7	4.4
Mode	304.0	1.9	30.4	8.7	5.0
Standard Deviation	80.5	0.7	10.6	2.4	1.5
Sample Variance	6749.0	0.5	111.8	6.0	2.3
Kurtosis	-.02	7.2	0	5.3	0.4
Skewness	0.2	2.2	-.02	1.7	-.02
Range	424.8	5.1	53.8	17.6	8.4
Minimum	142.8	1.0	6.5	3.8	0.5
Maximum	567.6	6.1	60.3	21.4	8.8
Count	328	328	328	328	328

In summary, Hass B is richer in both thorium and potassium relative to Hass A at both the major interval (Table 4), minor interval (Tables 5, 6), and outcrop scale (Tables 7, 8). The differences in concentrations of the aforementioned elements, is most significant in comparisons between respective basal intervals (Figure 4). These basal differences between the outcrops are important independent of the removal of the upper phosphatic intervals of Hass B. The middle fissile unit at Hass A has the maximum concentration of uranium (112.6 ppm.); (Table 7) more twice the maximum value in Hass B (60.3 ppm); (Table 8). Mean uranium concentrations at Hass A (38.6 ppm) and Hass B (36.5 ppm) are similar in their mean uranium concentration (Tables 7, 8), yet the base of Hass A is enriched in uranium relative to Hass B (Table 4). It is probable that the uranium statistics at Hass B are strongly affected (e.g. higher than actual) by missing data corresponding to the phosphatic interval (e.g upper Woodford Shale) that typically has low gamma-ray magnitude and extremely low concentrations of uranium (e.g. Figure 19).

Gamma-Ray Magnitude: Elemental Control

Uranium exerts the strongest control on gamma-ray magnitude, and this trend is slightly stronger at Hass A relative to Hass B (Figure 28). The R^2 value for the variation of gamma-ray magnitude vs. uranium concentration is .99 and .94 respectively for Hass A (Table 9) and Hass B (Table 10). Plots of gamma-ray magnitude vs. height above outcrop base are virtually indistinguishable from plots of uranium concentration (ppm) vs. height above outcrop base, at Hass A and Hass B (Figures 29, 30). Thorium (Figure 31) and potassium (Figure 32) are also important in determining API magnitude,

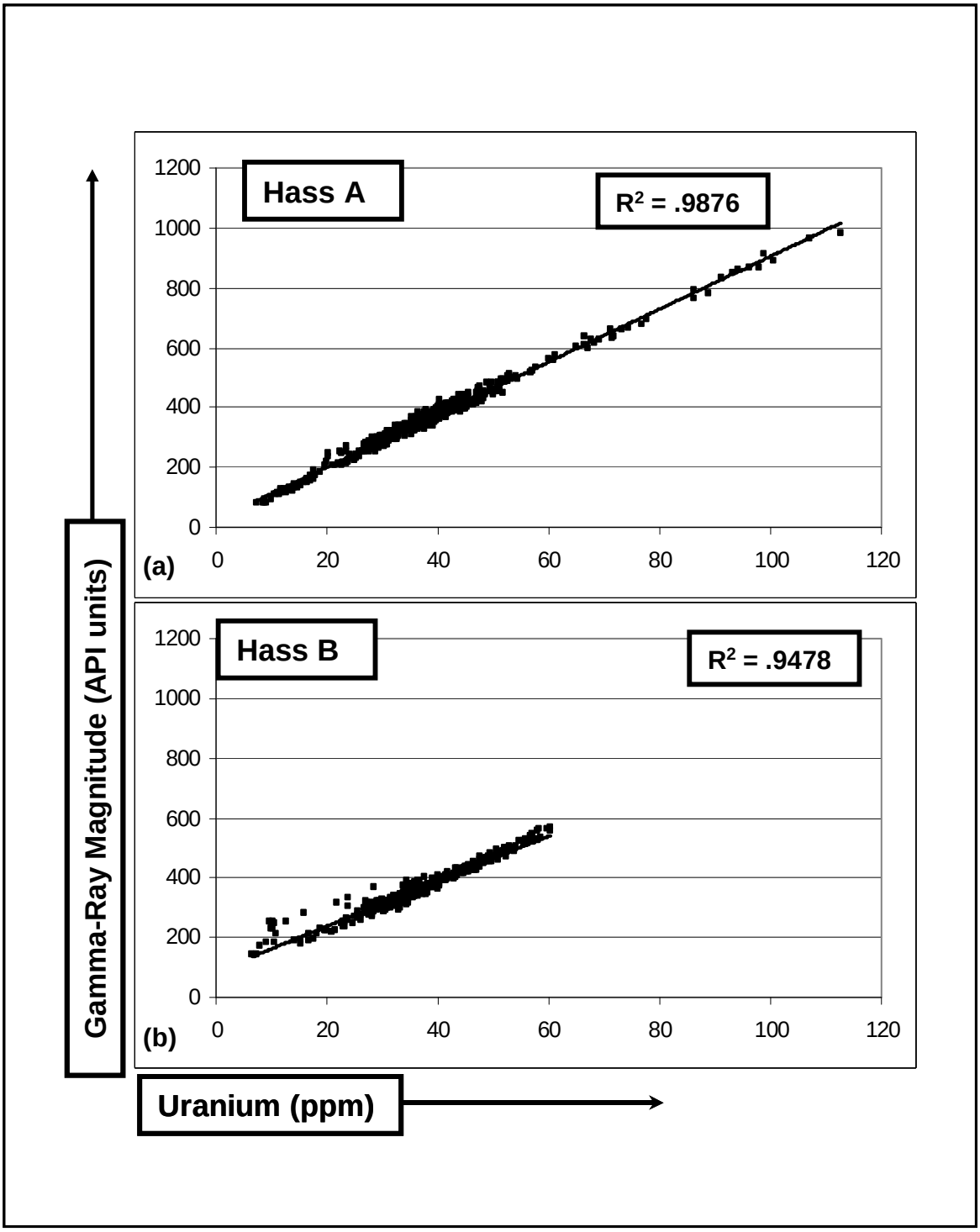

Figure 28. Gamma-ray magnitude vs. uranium concentration in the Woodford Shale at Hass A (a.) and Hass B (b.).

Table 9. R^2 (R-squared) values for relationships between gamma-ray specific elements, MS, and gamma-ray magnitude in Woodford Shale at Hass A.

R^2→ ↓	U (ppm)	Th (ppm)	K (wt. %)	MS (SI units)	Gamma-Ray Magnitude (API units)
Fissile A					
U (ppm)	1	0.32	0.27	0.09	0.99
Th (ppm)	0.32	1	0.50	0.10	0.41
K (wt. %)	0.27	0.5	1	0.12	0.35
MS (SI units)	0.10	0.10	0.12	1	0.10
Gamma-Ray Magnitude (API units)	0.99	0.41	0.35	0.10	1
Siliceous A					
U (ppm)	1	0.40	0.46	0.17	0.99
Th (ppm)	0.40	1	0.66	0.36	0.49
K (wt. %)	0.46	0.66	1	0.35	0.56
MS (SI units)	0.17	0.36	0.35	1	0.21
Gamma-Ray Magnitude (API units)	0.99	0.49	0.56	0.21	1
Transitional A					
U (ppm)	1	0.30	0.20	0.00	0.98
Th (ppm)	0.30	1	0.56	0.01	0.43
K (wt. %)	0.29	0.56	1	0.03	0.42
MS (SI units)	0.00	0.01	0.03	1	0.00
Gamma-Ray Magnitude (API units)	0.98	0.43	0.42	0.00	1

Table 10. R^2 (R-squared) values for relationships between gamma-ray specific elements, MS, and gamma-ray magnitude in Woodford Shale at Hass B.

R^2→ ↓	U (ppm)	Th (ppm)	K (wt. %)	MS (SI units)	Gamma-Ray Magnitude (API units)
Fissile B					
U (ppm)	1	0.04	0.00	0.07	0.98
Th (ppm)	0.04	1	0.27	0.02	0.11
K (wt. %)	0.00	0.27	1	0.04	0.01
MS (SI units)	0.07	0.03	0.04	1	0.09
Gamma-Ray Magnitude (API units)	0.98	0.11	0.01	0.09	1
Siliceous B					
U (ppm)	1	0.07	0.00	0.01	0.98
Th (ppm)	0.07	1	0.19	0.03	0.14
K (wt. %)	0.00	0.19	1	0.03	0.02
MS (SI units)	0.01	0.03	0.03	1	0.01
Gamma-Ray Magnitude (API units)	0.98	0.14	0.02	0.01	1
Claystone B					
U (ppm)	1	0.42	0.51	N/A	0.94
Th (ppm)	0.42	1	0.81	N/A	0.21
K (wt. %)	0.51	0.81	1	N/A	0.20
MS (SI units)	N/A	N/A	N/A	1	N/A
Gamma-Ray Magnitude (API units)	0.94	0.21	0.20	N/A	1

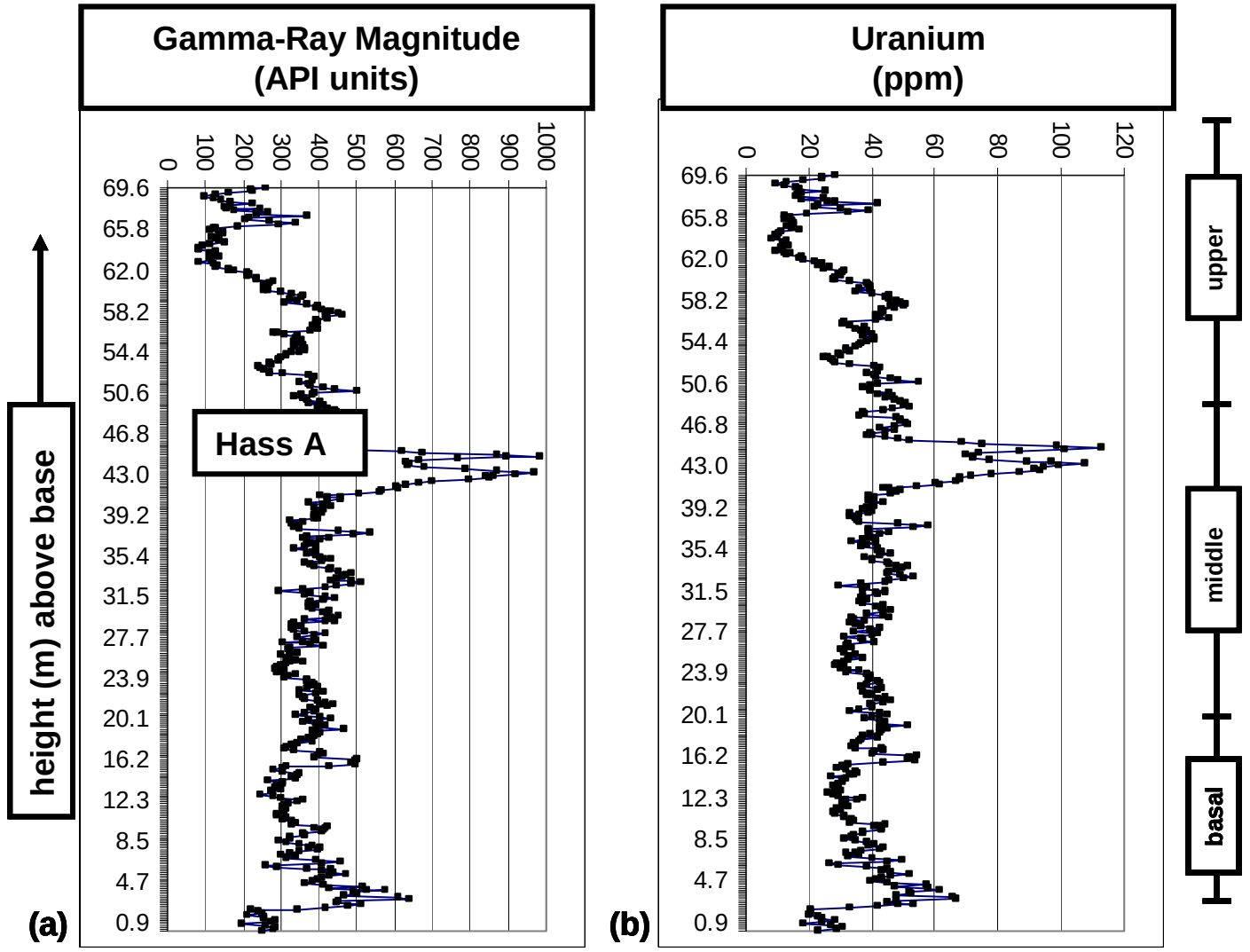

Figure 29. Comparison of gamma-ray magnitude (a.) and uranium concentration (b.) profiles at Hass A.

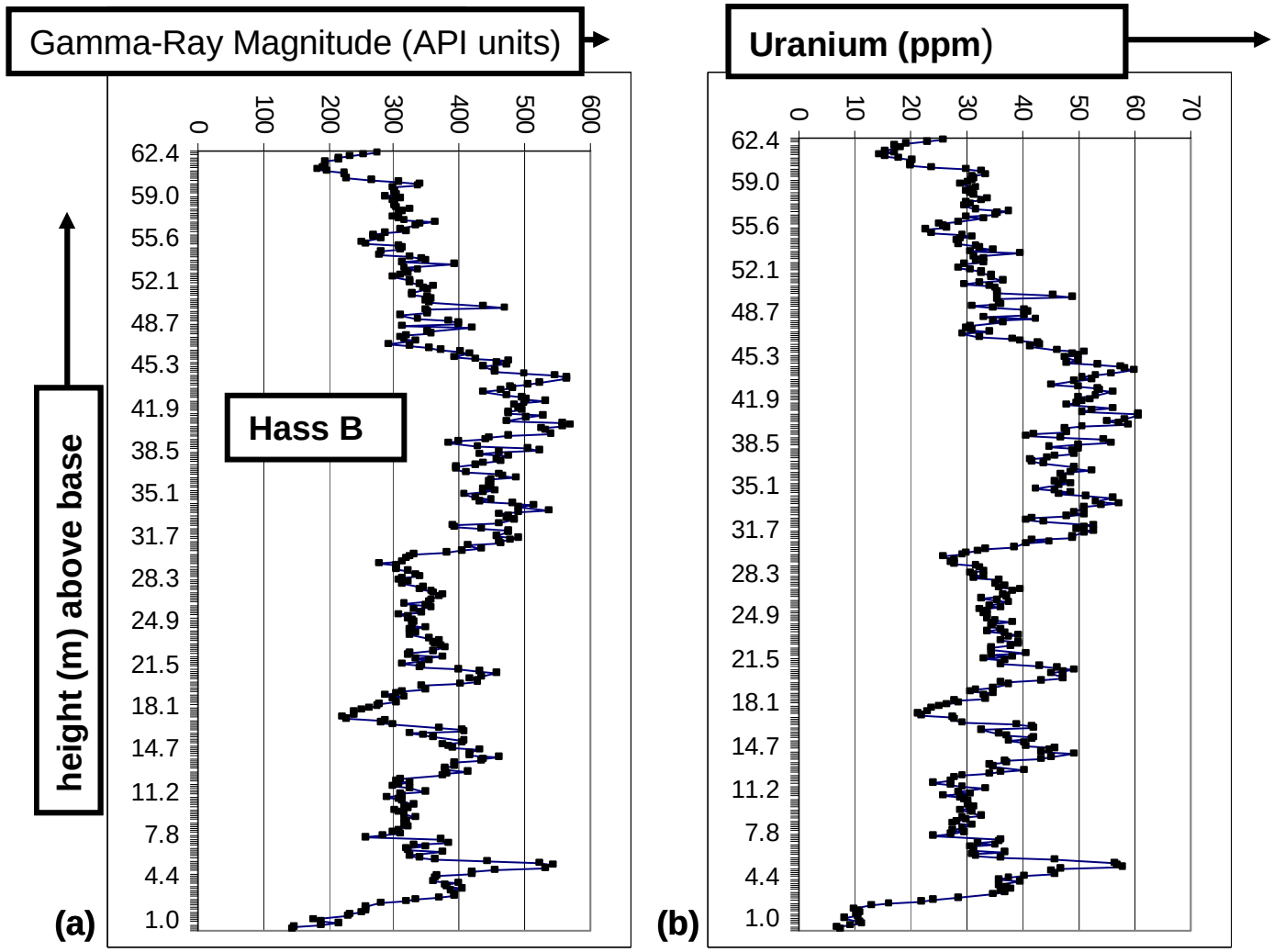

Figure 30. Comparison of gamma-ray magnitude (a.) and uranium concentration (b.) profiles at Hass B.

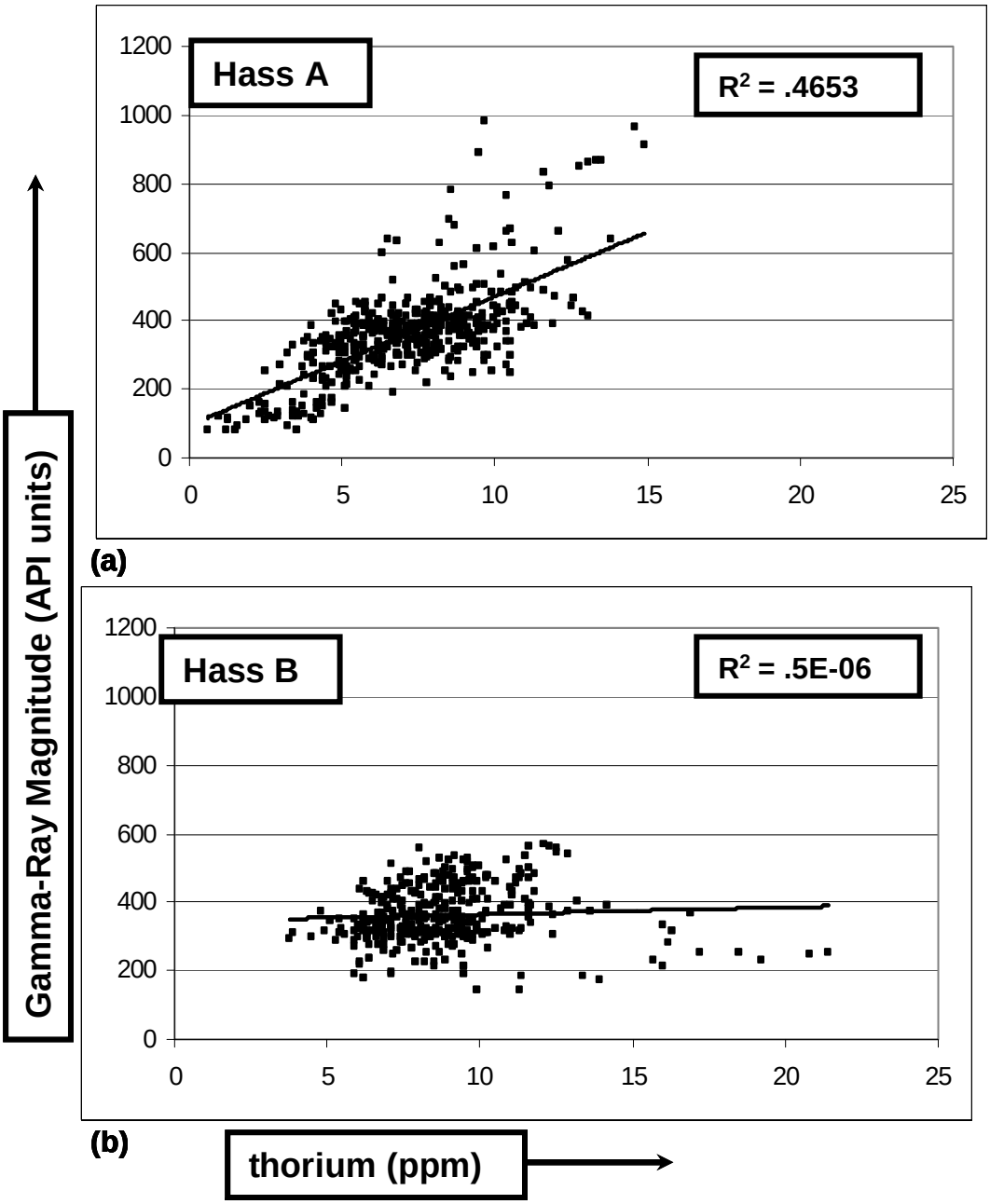

Figure 31. Plots of gamma-ray magnitude vs. thorium concentration in Woodford Shale at Hass A (a.) and Hass B (b).

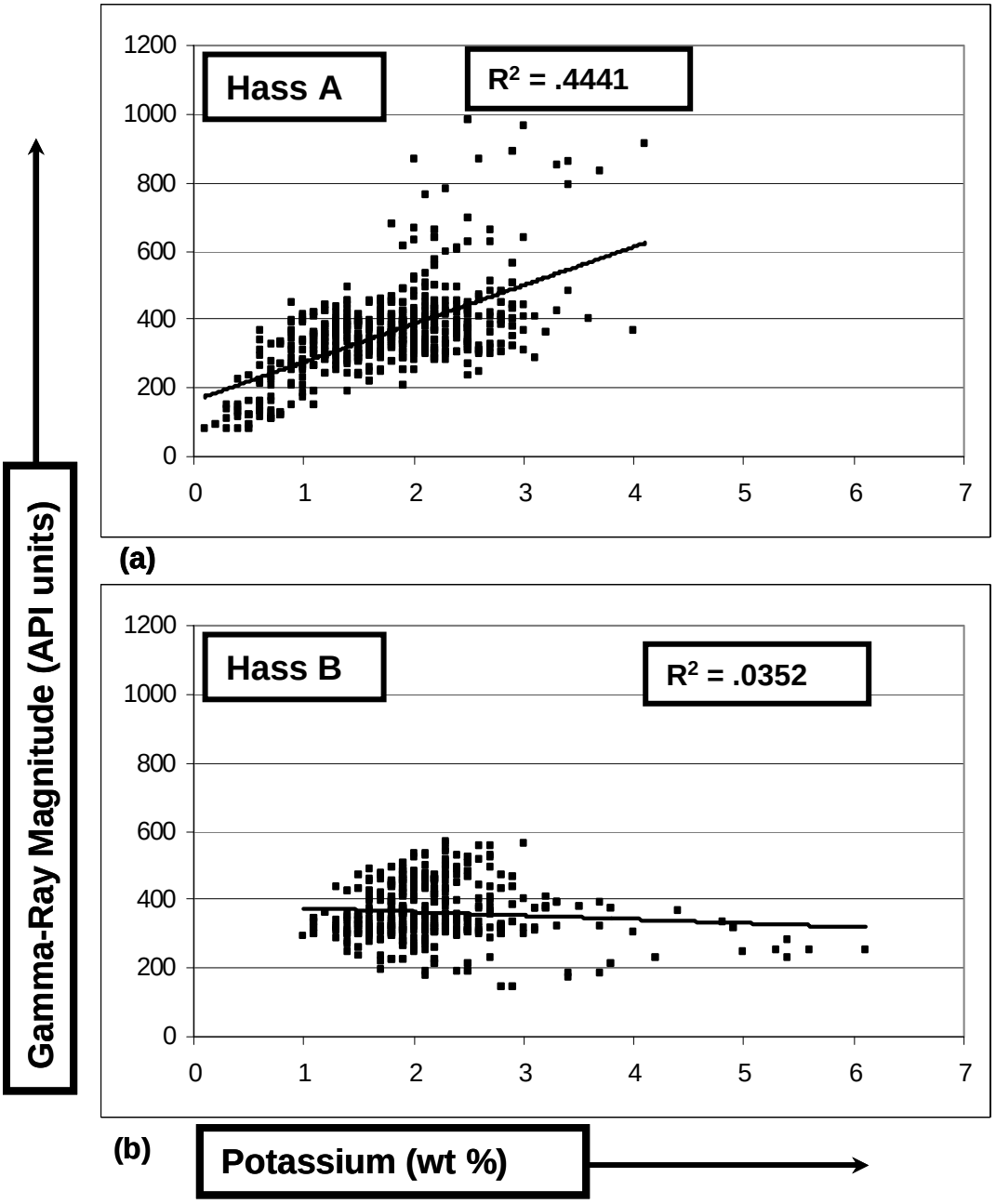

Figure 32. Plots of gamma-ray magnitude vs. potassium concentration in Woodford Shale at Hass A (a.) and Hass B (b).

but R^2 values of thorium vs. gamma-ray magnitude and potassium vs. gamma-ray magnitude are significantly lower relative to those corresponding to uranium vs. gamma-ray magnitude, at both outcrops (Tables 9, 10). The relationship (R^2) or correspondence between potassium vs. thorium seems slightly higher at Hass A (R^2 value =.60) relative to Hass B (R^2 value =.59) (Figure 33). Correlation between uranium vs. thorium and uranium vs. potassium seems to be weak at both outcrops, especially at Hass B (Tables 9, 10).

Spectral gamma-ray derived thorium concentration data imply that uranium is extremely enriched relative to thorium at Hass A. Estimates of detrital and authigenic uranium fractions are calculated by a method developed by Wignall and Myers where thorium and uranium are expressed in parts per million (ppm) (1988):

$$U_{detrital} = 1/3(Th_{total}) \text{ (Eq. 5).}$$

Thorium concentrations derived from spectral gamma-ray data at Hass A range from 0.6 ppm to 14.9 ppm (Table 7). The estimated detrital component of uranium in Woodford Shale samples at Hass A is 1/3 of that range (0.2 ppm to 5 ppm). The mean thorium concentration from Hass A spectral gamma-ray data is 7.2 ppm (Table 7), resulting in an estimated mean detrital uranium fraction of 2.4 ppm. Uranium concentrations from spectral gamma-ray data range from 7.4 ppm to 112.6 ppm. Thus, Hass A Woodford Shale is extremely enriched in authigenic uranium. Total uranium concentrations from spectral gamma-ray data at Hass B range from 7.5 ppm to 60.3 ppm while thorium concentration ranges from 3.8 ppm to 21.4 ppm (Table 8). Detrital uranium at Hass B is estimated at 1/3 of that range (1.3 ppm - 7.1 ppm). Thus, Hass B Woodford Shale is also enriched in authigenic uranium.

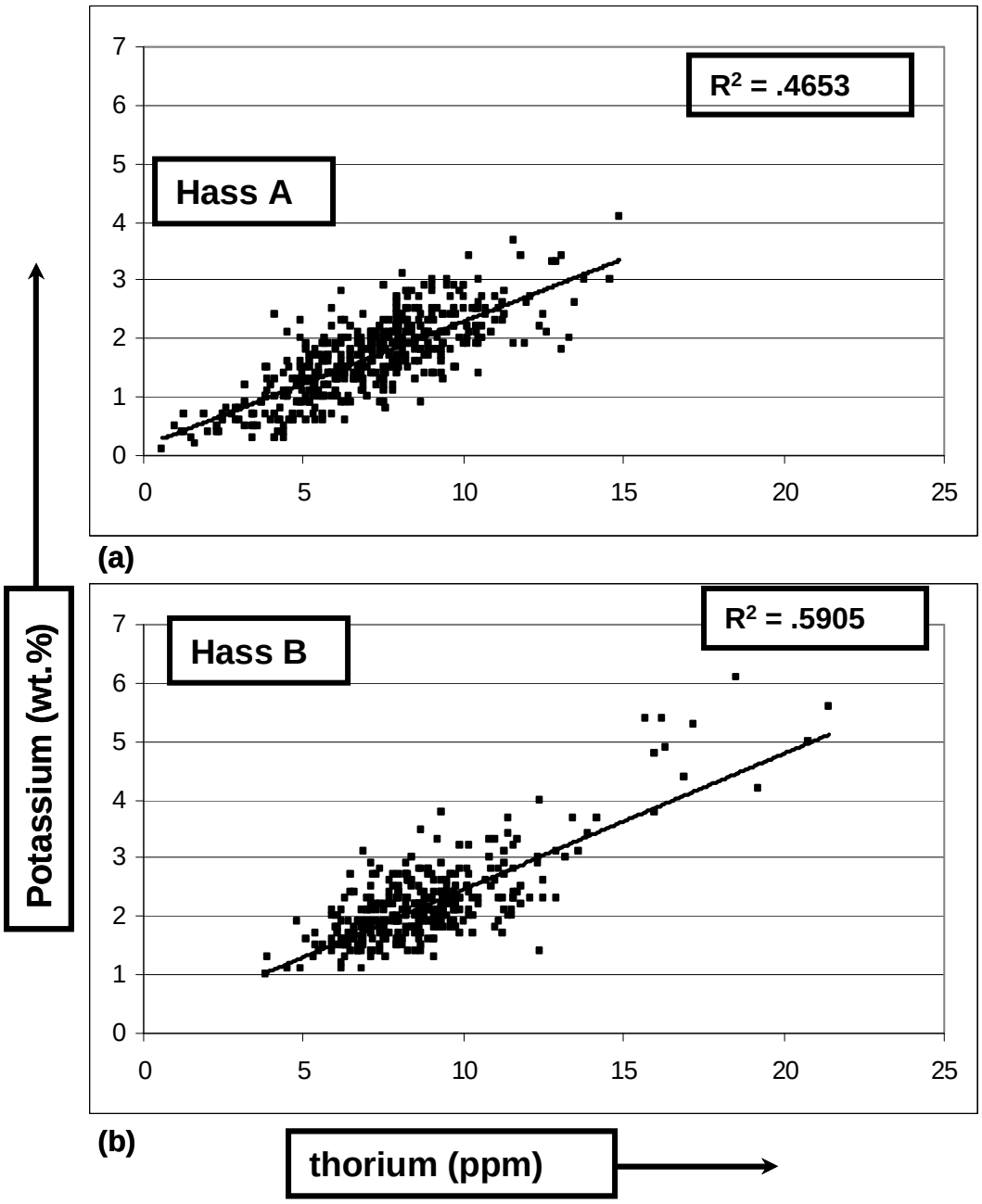

Figure 33. Plots of potassium concentration vs. thorium concentration in Woodford Shale at Hass A (a.) and Hass B (b.).

Gamma-Ray Magnitude vs. Lithology

The largest scale variations in gamma-ray magnitude occur at the lithologic transitions between Woodford Shale and the formations bounding the Woodford Shale, hence the different formations (Table 4). As expected, the gamma-ray magnitude of the Woodford Shale is fundamentally different relative to that of the bounding formations. This result is consistent with the widespread use of gamma-ray magnitude (and gamma-ray specific elemental assemblage) to delineate lithology (Ellis, 1987).

Several parameters, including gamma-ray magnitude and uranium concentration appear to be lithologically controlled (Figures 19, 27). These parameters include: outcrop and interval stratigraphic thickness (m), outcrop and interval net shale % (thickness shale/ total lithologic thickness) plotted as a function of distance (d) above the outcrop base, outcrop and interval net silica % (blocky siliceous thickness/total lithologic thickness) plotted as a function of distance (d) above the outcrop base, and an inferred index of cycle thickness, total number of fissile and siliceous beds per meter (# beds/m), plotted as a function of distance (d) above the outcrop base.

Uranium concentration is highest, resulting in highest gamma-ray magnitude (Figure 28) in fissile shale units at Hass A (Figures 34) and Hass B (Figure 35). This result agrees with results in a previous study at Hass A (Krystyniak, 2003). Similarly, Hass A (Figure 19) has more net fissile shale relative to Hass B (Figures 19, 25) and Hass A has higher calculated gamma-ray magnitude (i.e. higher uranium concentration) relative to Hass B (Tables, 8, 9). Transitional shale was observed to have generally higher gamma-ray magnitude (i.e. higher uranium concentration) when compared to siliceous shale at Hass A (Figure 34). Transitional units (Hass A only) correspond to measurement points where the MS or gamma-ray sensor was

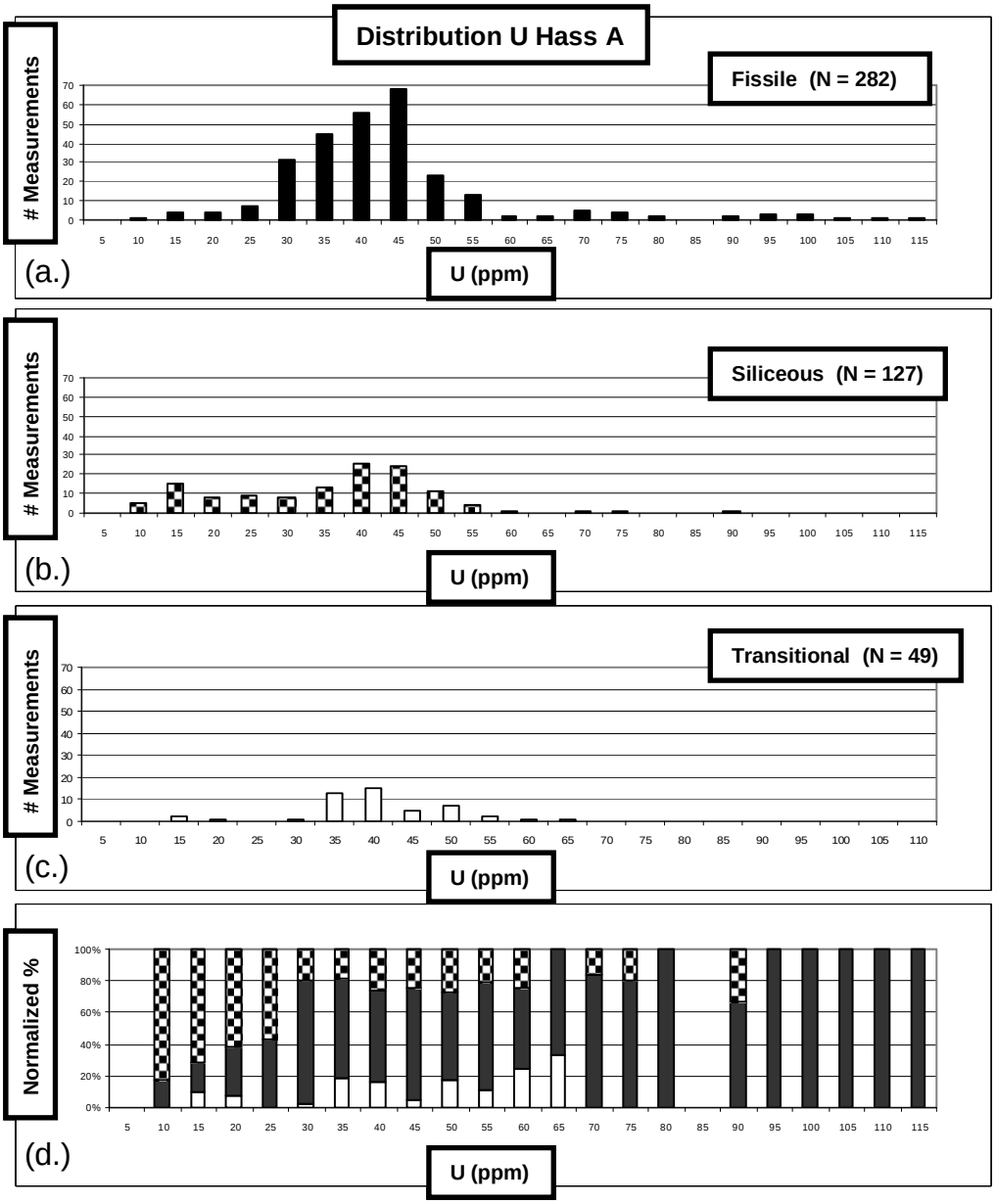

Figure 34. Distribution plots of uranium concentration from spectral gamma-ray data in select lithologies at Hass A including: fissile shale (a.), siliceous shale (b.), and transitional shale (c). Bottom plot (d.) combines all lithologies in a normalized distribution.

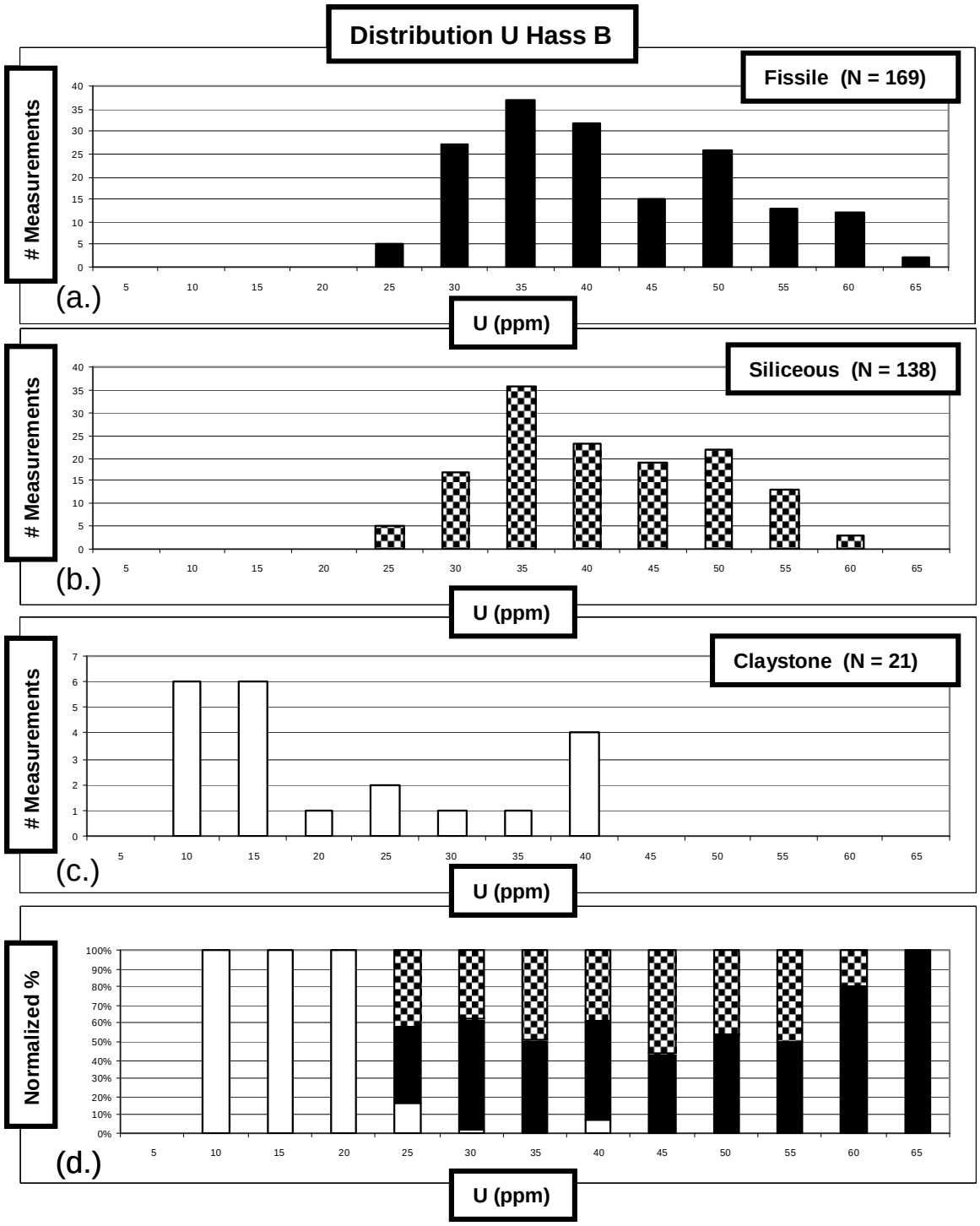

Figure 35. Distribution plots of uranium concentration from spectral gamma-ray data in select lithologies at Hass B including: fissile shale (a.), siliceous shale (b), and claystone (c.) found only found in basal beds at Hass B. Bottom plot (d.) combines all lithologies in a normalized distribution.

directly influenced by both siliceous and fissile shale. The upper siliceous shale at Hass A generally contains the lowest concentrations of uranium and lowest gamma-ray magnitude at the scale of the main interval (Figures 19, 27). The upper interval at Hass A is cliff-forming (Figure 16), overwhelmingly siliceous (Figure 19f.), and has the lowest concentrations of uranium (Figure 19c), thorium (Figure 19d), and potassium (Figure 19e) relative to other Hass A main intervals. In summary, lithology is strongly correlated with calculated gamma-ray magnitude.

At Hass B fissile shale has slightly higher gamma-ray magnitude (i.e higher uranium concentrations) relative to siliceous shale and much higher gamma-ray magnitude relative to the basal claystone (Figure 35). Siliceous shale also has higher gamma-ray magnitude when compared to the basal claystone at Hass B (Figure 35). Calculated gamma-ray magnitude in siliceous shale at Hass A was slightly higher when compared to siliceous shale at Hass B (Figure 35).

Distinct basal gamma-ray magnitude peaks were observed at Hass A and Hass B above the Acadian Unconformity surface (Figure 36). Within a few feet of both outcrop bases, gamma-ray magnitude almost doubles (Table 4). Hass A especially shows the characteristic variation in gamma-ray magnitude (e.g. gamma-ray profile) which is associated with well log response in the three main lithologic intervals typical of the Woodford Shale interval scale lithological variation (Figure 19).

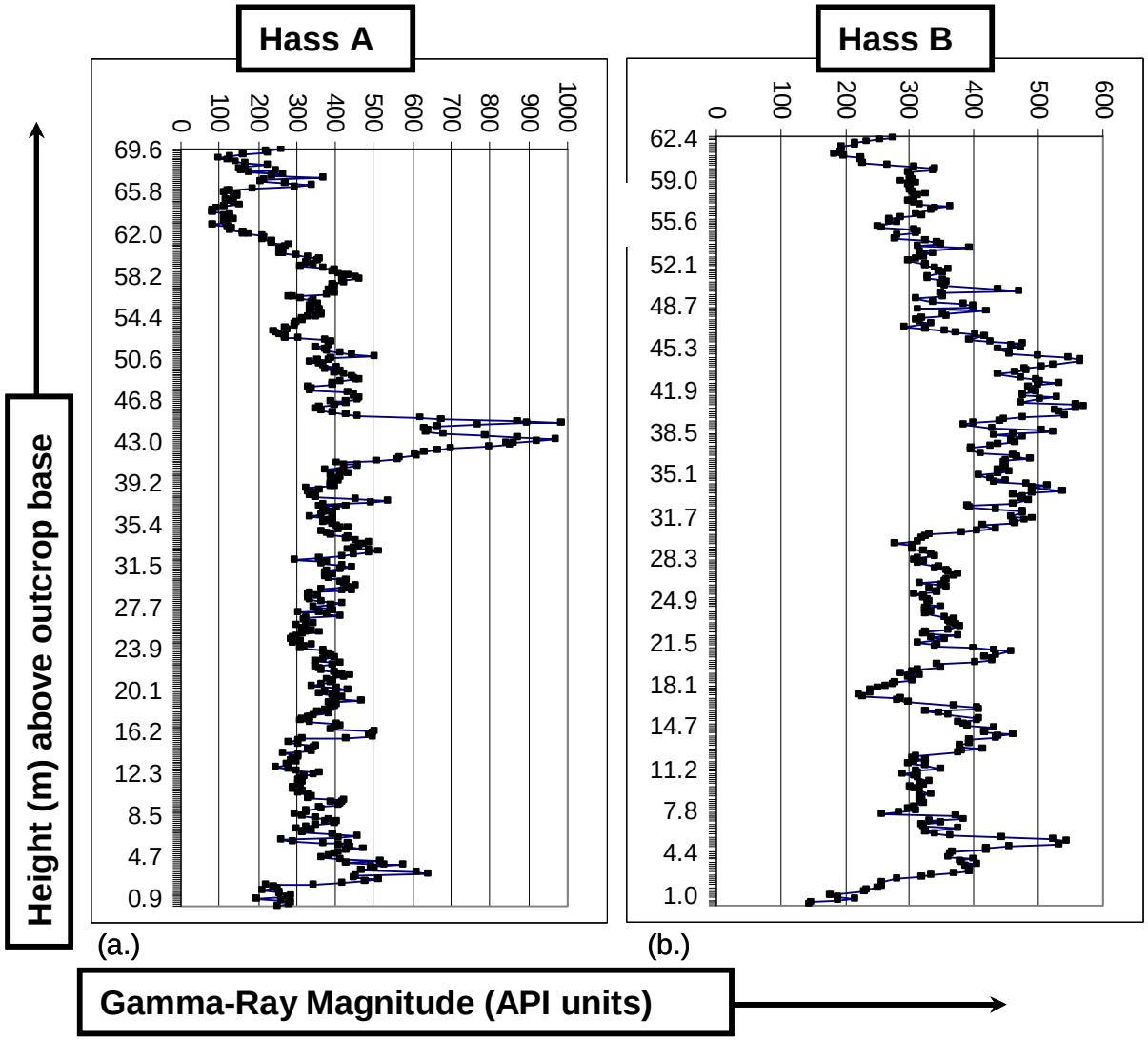

Figure 36. Comparison of gamma-ray magnitude profiles of Woodford Shale study outcrops. Hass A (a.) and Hass B (b.) are observed to have somewhat similar gamma-ray profiles especially near the outcrop base.

The base of the Woodford shale is characterized by a dramatic increase in gamma-ray magnitude with an immediate basal increase in uranium less significant than the corresponding relative increase in thorium (Figures, 19, 27). Therefore basal Woodford has a U/Th ratio much lower than any other interval in the formation. Potassium, along with U and Th (Figures, 19, 27) all increase in an absolute fashion resulting in significant increases in calculated gamma-ray magnitude increase immediately above the Devonian age Hunton Group Carbonates (Table 4).

Significant changes in several lithologically controlled parameters including potassium concentration, thorium concentration, MS magnitude, net shale (thickness shale/total thickness), total number of beds per meter (# beds/m) all occur in association with the largest lithologic, spectral gamma-ray, MS change at Hass A (Figure 19), the change from the middle fissile interval (mostly shale) to the upper siliceous interval. This change in lithology and rock properties occurs at approximately 44-46 m of section at Hass A. The large scale shift of the aforementioned parameters occurs in association with beds containing pyrite nodules a discrete pyrite bed as well as the uranium/gamma-ray magnitude and MS maximum point (112ppm); (Figure 37). Stratigraphically below the pyrite layers and nodules, the outcrop is pervasively stained with a rust colored residue. This residue exhibits highest magnitude MS response at Hass A. The residue is interpreted to be a weathering product of the abundant pyrite or marcasite.

Pattern correlation is observed in the separate plots of uranium, thorium and potassium at Hass A (Figure 19) and in separate plots of thorium and potassium at Hass B (Figure 27). Little correlation is observed between the plots of uranium concentration at

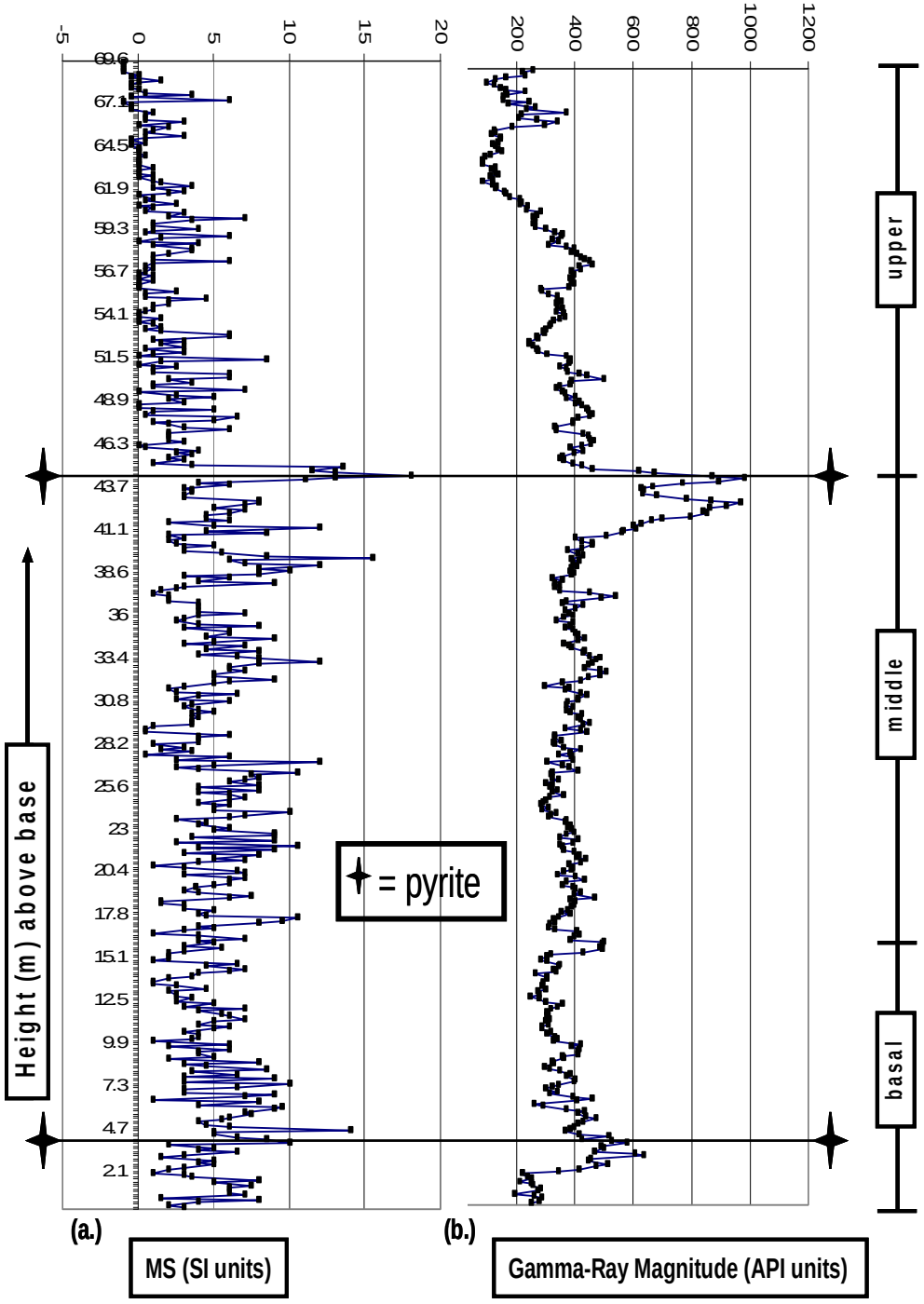

Figure 37. Comparison of MS (a.) and gamma-ray magnitude (b.) profiles at Hass A. Star indicates occurrence of pyrite nodules and/or discrete layers.

Hass B and corresponding plots of thorium and potassium (Figure 27). Despite the poor statistical correlations (R^2) between gamma-ray magnitude vs. thorium concentration (Figure 31) and gamma-ray magnitude vs. K (weight %); (Figure, 32), potassium and thorium concentration plots resemble uranium concentration (e.g. gamma-ray magnitude plot) when viewed at the outcrop scale at Hass A (Figure 19). At Hass B, the strong resemblance between gamma-ray specific element profile plots is limited to the basal interval (Figure 27).

At Hass A (Figure 38) and Hass B (Figure 39), distribution plots of K (weight %) show a strong relationship between potassium and lithology. Thorium concentration also varies with lithology at Hass A (Figure 40) and at Hass B (Figure 41). The distribution of K, Th, and U with lithotype for Hass A (Figure 42) and Hass B (Figure 43) show that thorium is more homogeneous with respect to lithology relative to potassium, and potassium is more homogeneous with respect to lithology relative to uranium. Uranium concentrations in transitional shale are never extremely high or low, and always intermediate in concentration between fissile and siliceous shale. Transitional shale is represented in several bins in the central portion of the Hass A uranium distribution plot (Figure 42).

At Hass B, the trend is obscured in terms of somewhat homogeneous uranium distribution in the selected lithologies (Figure 43). Fissile shale is enriched in uranium relative to other lithologies. Missing lithology includes the low gamma-ray magnitude phosphatic zone typical of upper Woodford Shale interval and possibly a small number of high magnitude gamma-ray measurements corresponding to fissile shale with the highest uranium concentrations. If the missing Hass B lithology and associated data

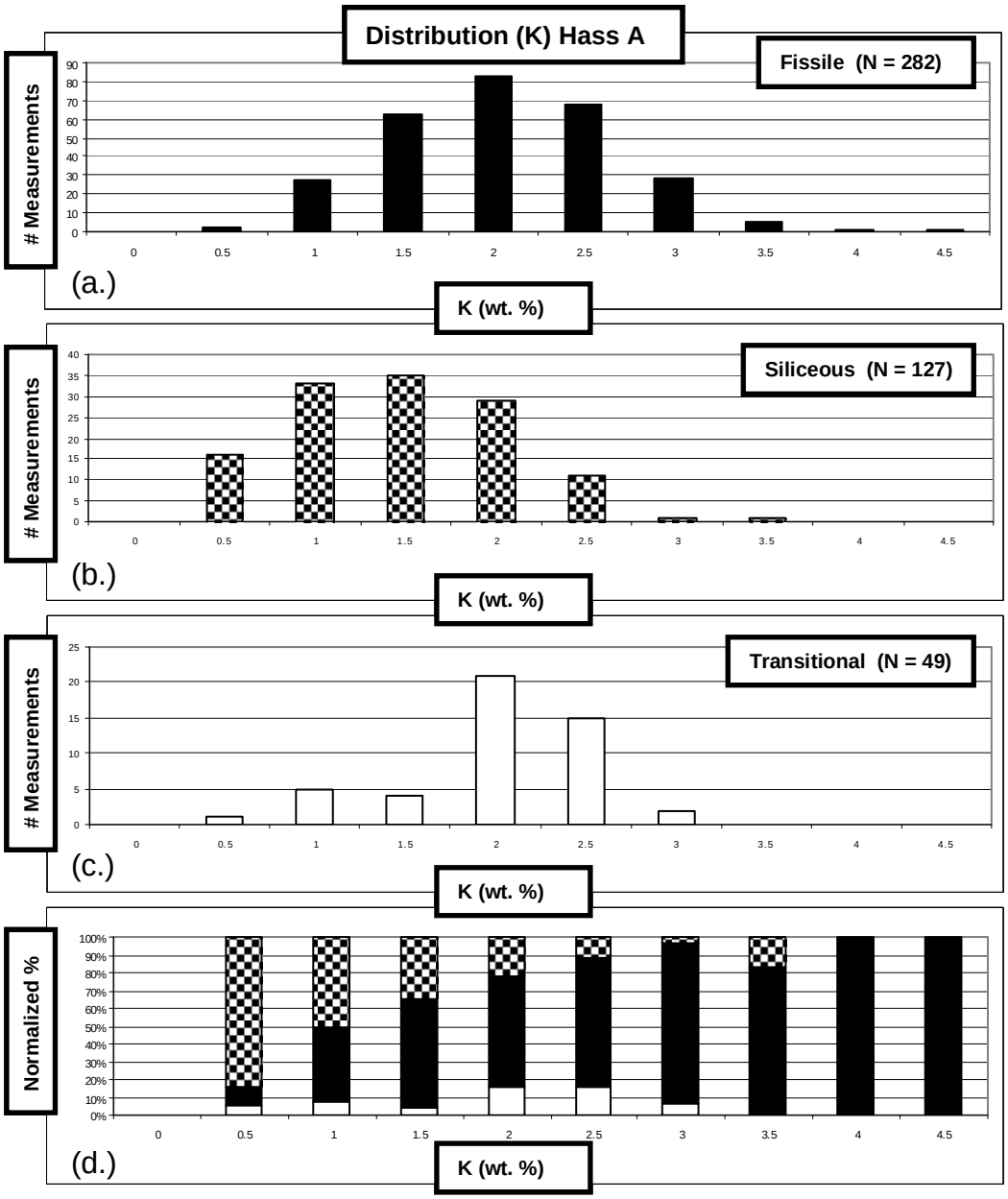

Figure 38. Distribution plots of potassium concentration from spectral gamma-ray data in select lithologies at Hass A. Note the unequal distribution of potassium (% gamma) in fissile shale (a.), siliceous shale (b.), and transitional shale (c.). Bottom plot (d.) combines all lithologies in a normalized distribution.

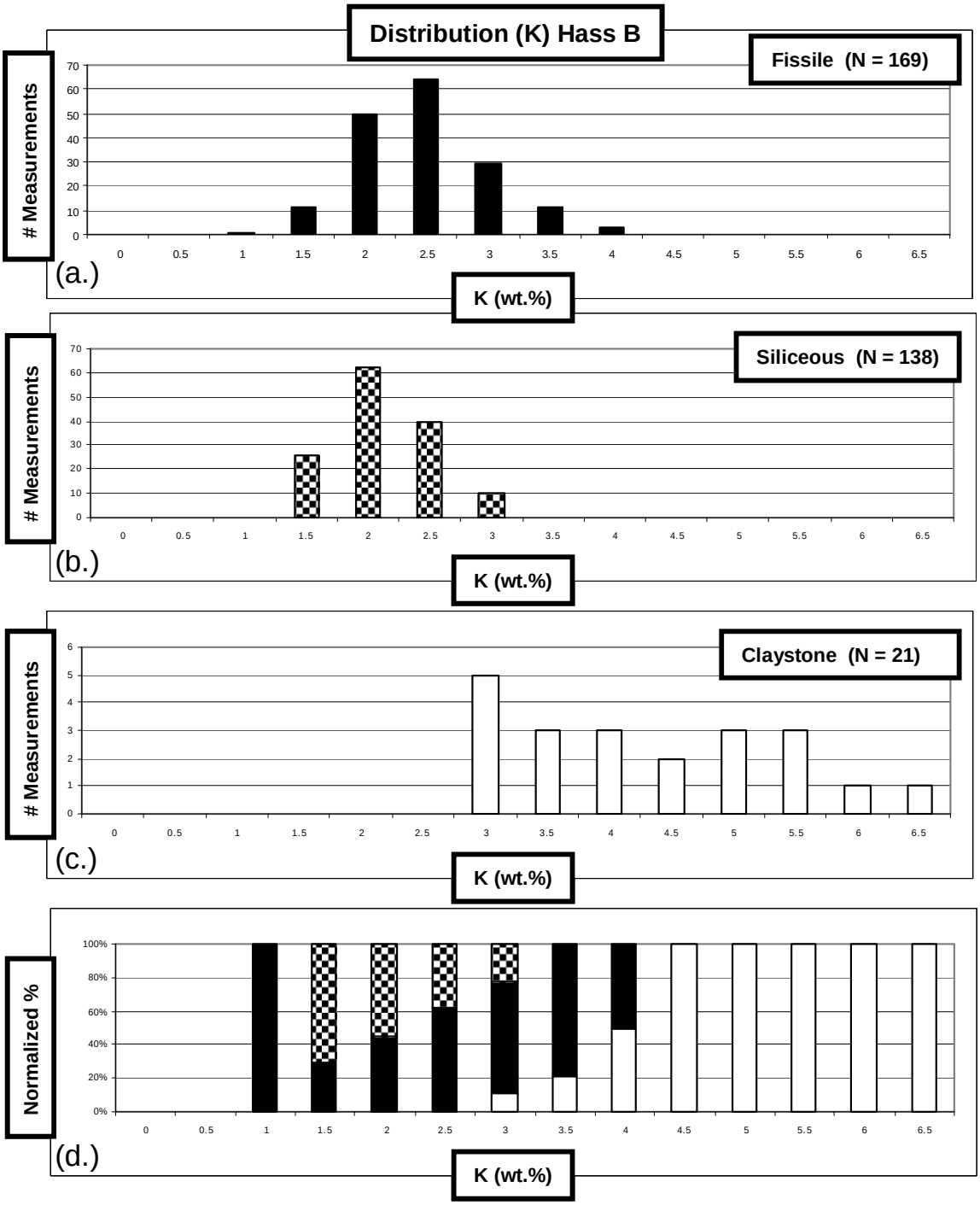

Figure 39. Distribution plots of potassium concentration from spectral gamma-ray data in select lithologies at Hass B including: fissile shale (a.), siliceous shale (b.) and basal claystone (c.). Bottom plot (d.) combines all lithologies in a normalized distribution.

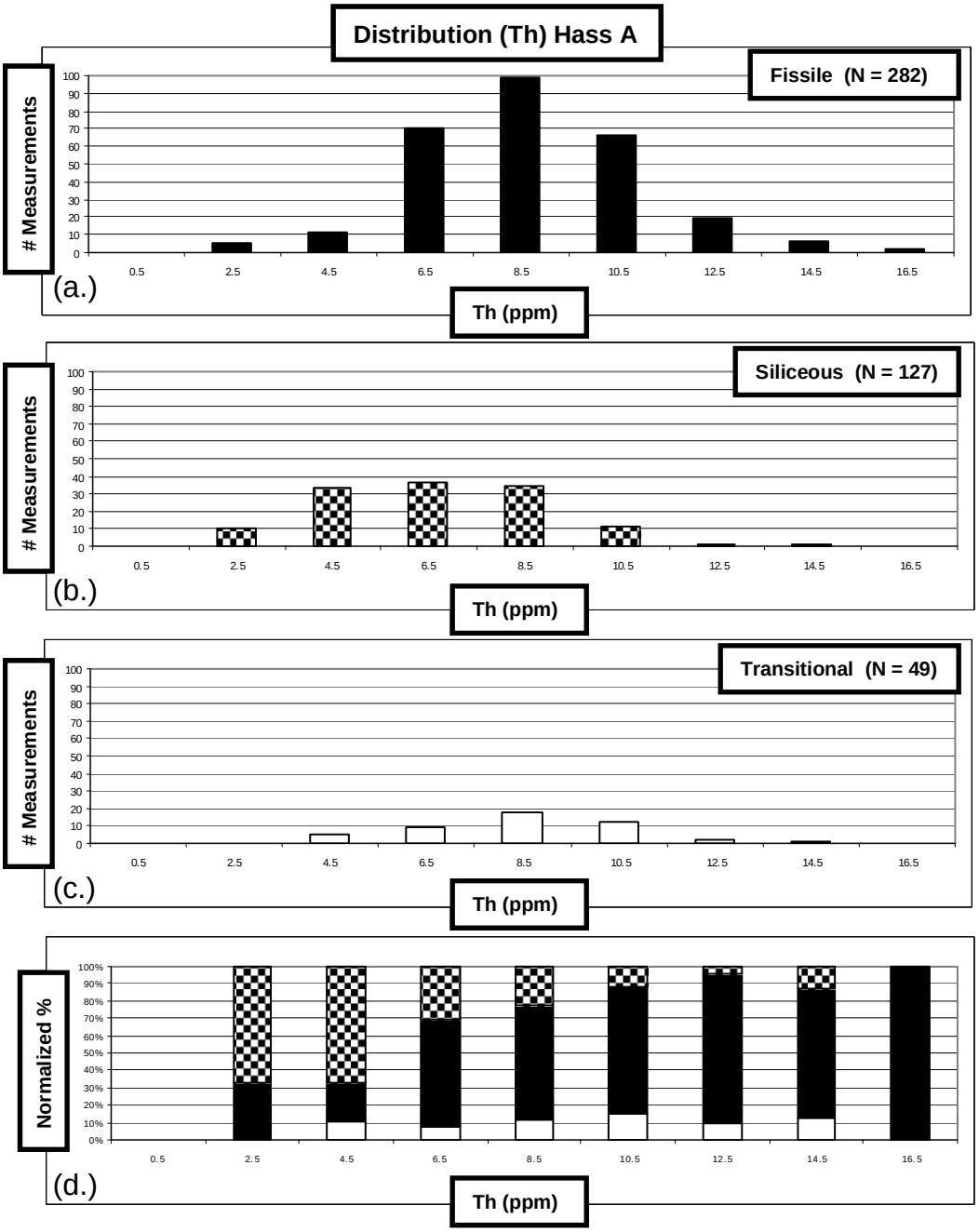

Figure 40. Distribution plots of thorium concentration from spectral gamma-ray data in select lithologies at Hass A including: fissile shale (a.), siliceous shale (b.), or transitional shale (c.). Bottom plot (d.) combines all lithologies in a normalized distribution.

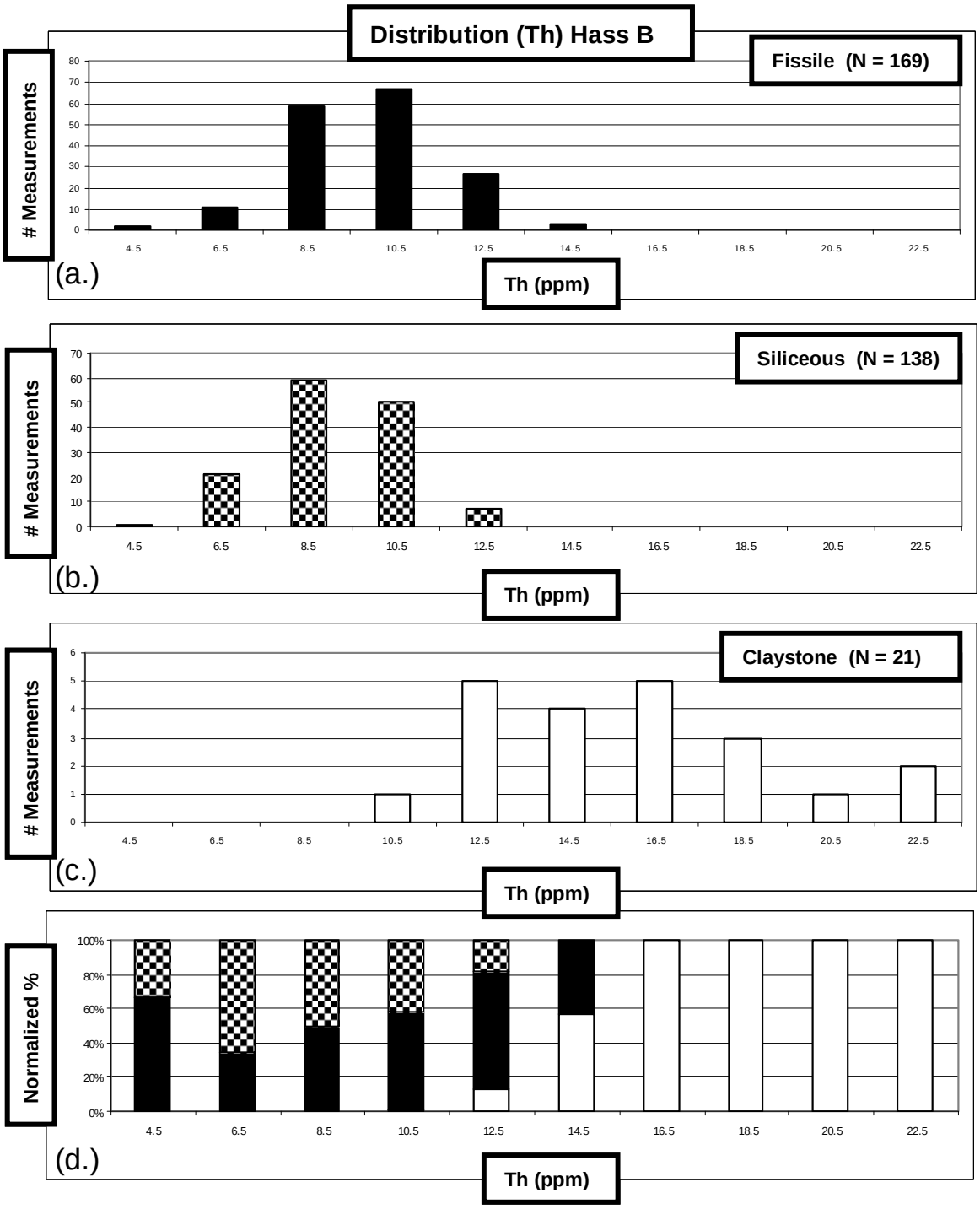

Figure 41. Distribution plots of thorium concentration from spectral gamma-ray data in select lithologies at Hass B including: fissile shale (a), siliceous shale (b), and claystone (c.). Bottom plot (d.) combines all lithologies in a normalized distribution.

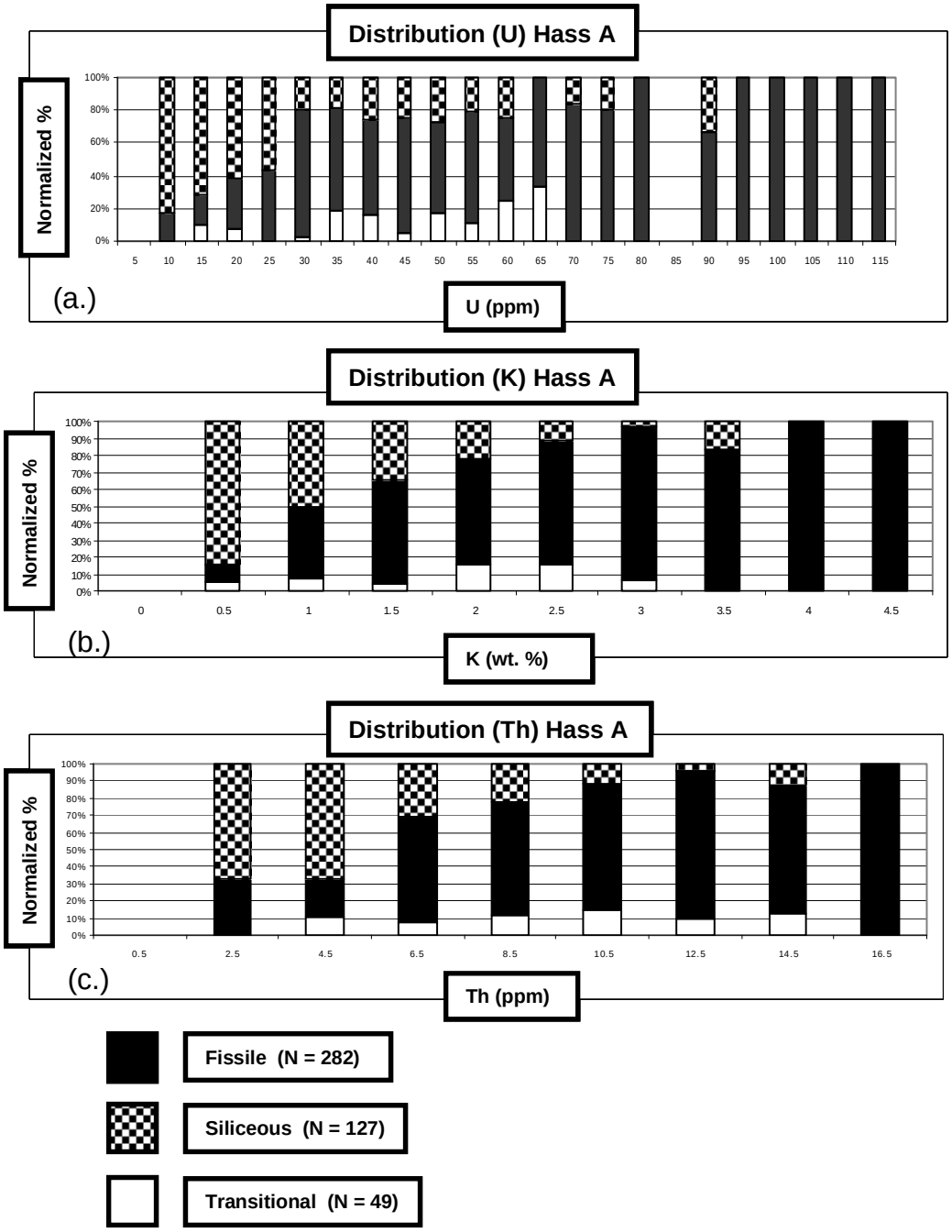

Figure 42. Distribution plots of gamma-ray specific elemental concentrations in select lithologies at HassA including: uranium (a.), potassium (b.), and thorium (c.).

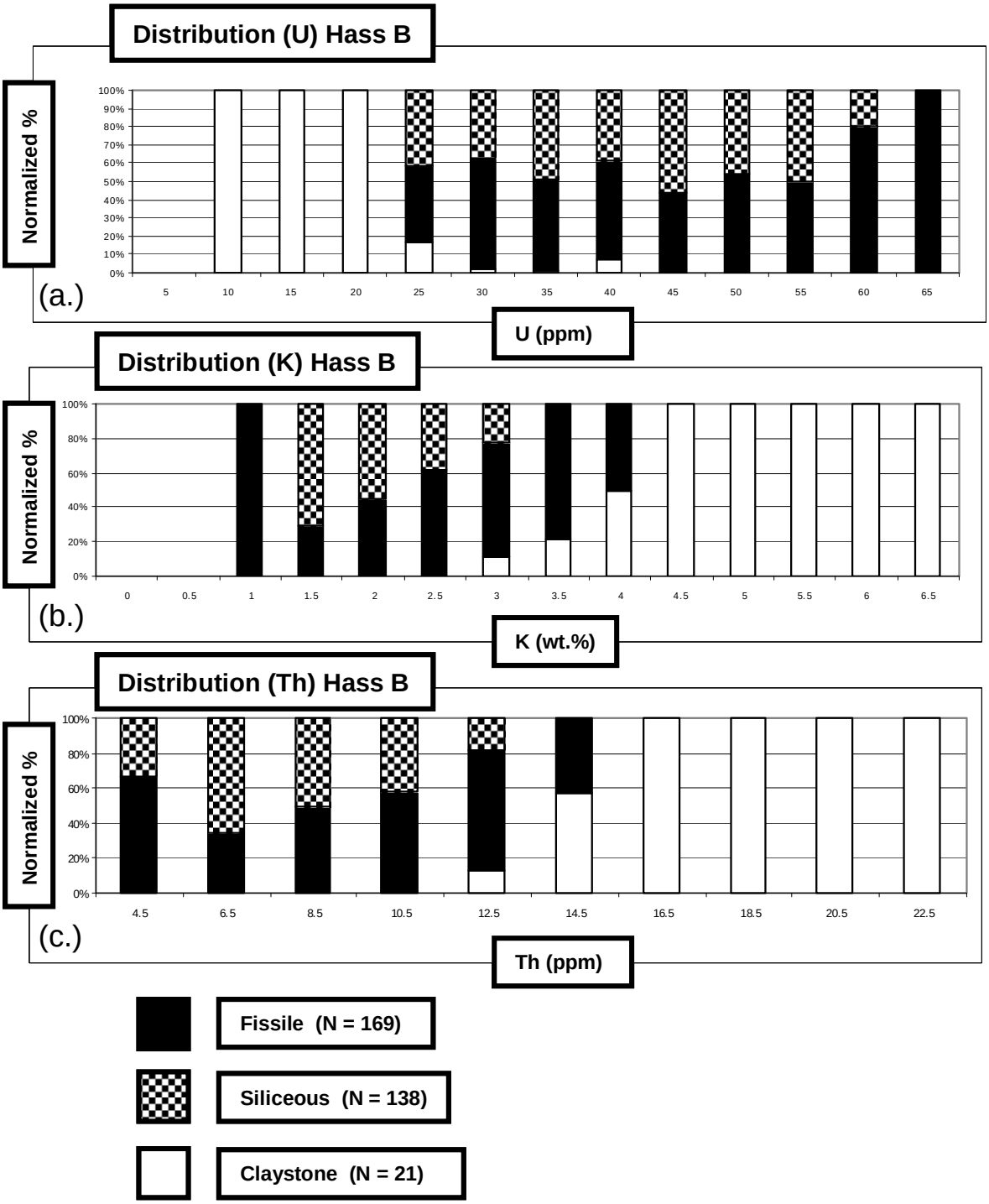

Figure 43. Distribution plots of gamma-ray specific elemental concentrations in select lithologies at Hass B including: uranium (a.), potassium (b.), and thorium (c.).

were included the summary statistics for gamma-ray magnitude and gamma-specific elemental assemblages would probably be different. Still, spectral gamma-ray data at the minor interval level (Tables 5, 6) and outcrop level (Table 7, 8) show Hass A has very different gamma-ray magnitude and gamma-ray specific elemental assemblage relative to Hass B, irrespective of the missing lithology at Hass B.

Fissile beds, ≤ 1.3 m at Hass A and ≤ 2.3 m at B, are generally much thicker than siliceous beds, ≤ 12.4 cm at Hass A and ≤ 46 cm at Hass B. Woodford intervals with the largest number of beds per meter (≥ 10) are consistently siliceous. Fissile beds larger than a meter thick are common at all Woodford Shale outcrops visited in the study. The intervals with highest concentration of all three radioactive gamma-ray specific elements are fissile intervals (≤ 10 beds/m) with the lowest number of beds/ meter and the highest gamma-ray magnitudes (Figures 19, 27). The correlation between thick fissile shale beds and uranium concentration was strongest at Hass A. The Hass A fissile middle main interval had the highest concentration of all gamma-ray specific elements, highest gamma-ray magnitude, highest MS, highest net shale (≈ 100%), and lowest cycle thickness (< 12 beds/meter) (Figure 19). At Hass A, the siliceous upper main interval had the lowest concentration of all three gamma-ray specific elements, lowest gamma-ray magnitude, lowest thorium/uranium ratio (ppm/ppm), lowest MS, lowest net shale, largest cycle thickness (> 35 beds/meter), and the highest net siliceous shale (net blocky chert/ total lithologic thickness) (Figure 19).

Gamma-Ray Magnitude: Variation between Outcrops

The Hass A maximum uranium composition is almost twice the maximum uranium concentration at Hass B (Tables 7, 8) and the R^2 value of gamma-ray magnitude vs. uranium concentration approaches one at both outcrops (Tables 9, 10). The maximum gamma-ray magnitude (γ_{max}) at Hass A is roughly twice that of Hass B (Figure 7, 8). However, the mean gamma-ray magnitude values of the two outcrops, and the mean uranium concentration values are almost equal. Plots of gamma-ray magnitude vs. height (ft.) above the outcrop base at study outcrops show limited pattern correlation near the base of the outcrops (Figure 36). The observations, that Hass A has higher uranium concentration and higher gamma-ray magnitude, are consistent with the observation that the Hass A outcrop is overall more fissile in terms of net shale (shale thickness/total lithologic thickness) relative to Hass B (Figures 19, 27). Finally all lithologic and gamma-ray specific elemental comparison between Hass A and Hass B must be considered in light of the missing Hass B lithology as the result of faulting, pervasive tectonic fracturing, and weathering.

Magnetic Susceptibility Observations:

MS vs. Gamma-Ray Magnitude

Magnetic susceptibility (MS) is observed to vary in a fashion that shows no significant statistical correlation to gamma-ray magnitude and uranium concentration (Tables 9, 10). Linear regression of MS vs. gamma-ray magnitude at Hass A (Figure 44) and Hass B (Figure 45) yielded low R^2 values. Despite low or no statistical correlation

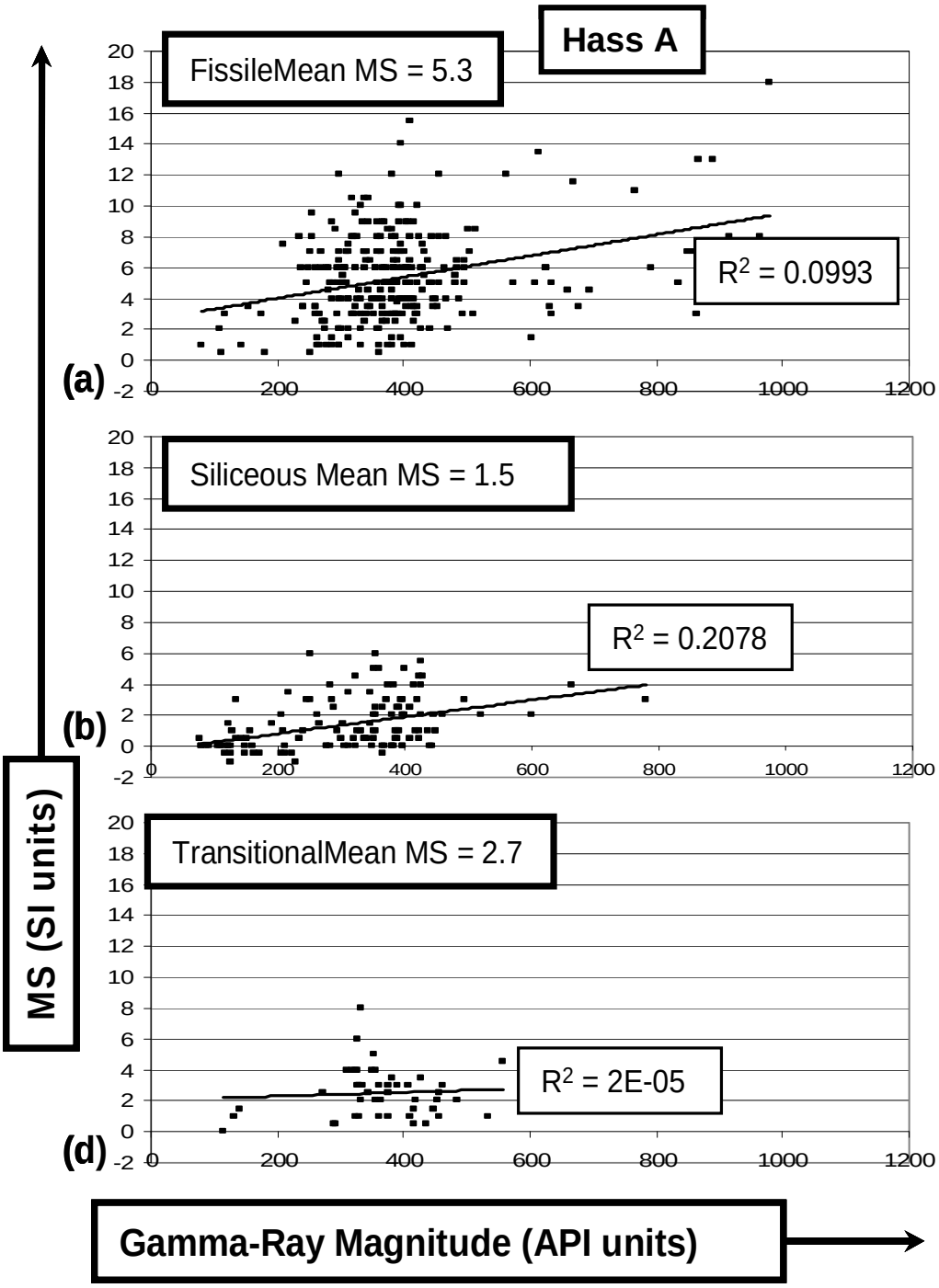

Figure 44. Plots of MS vs. gamma-ray magnitude in select lithologies at Hass A including: fissile shale (a.), siliceous shale (b.), and transitional shale (c).

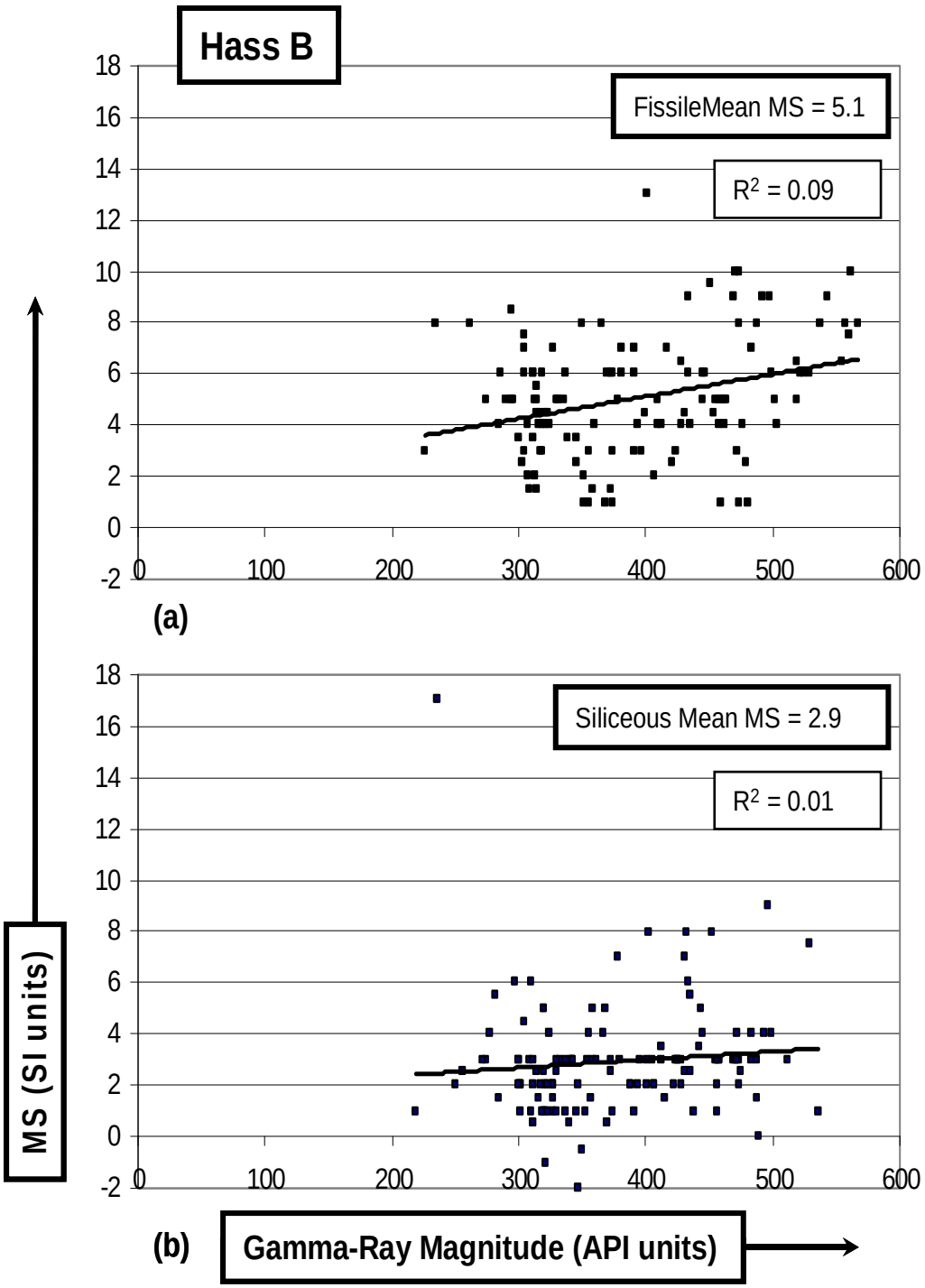

Figure 45. Plots of MS vs. gamma-ray magnitude in select lithologies at Hass B including: fissile shale (a.) and siliceous shale (b.).

between MS and gamma-ray magnitude, outcrop profiles show evidence of pattern correlation between the variables at Hass A (Figure 37). Pattern correlation between MS and gamma-ray magnitude at Hass B is problematic (Figure 46), partly due to the large number of missing MS measurements at Hass B. MS (Figure 47) and gamma-ray magnitude (Table 4) both strongly increase in the first few meters above the Hunton Limestone/Woodford Shale contact. Just as gamma-ray magnitude and gamma-ray specific elemental assemblage (Figures 42, 43) are controlled by lithology the change in MS magnitude across the Acadian Unconformity surface appears to be lithologically controlled (Figure 47).

MS vs. Lithology

Plots of uranium concentration vs. MS in select lithologies at Hass A (Figure 48) and Hass B (Figure 49) indicate that uranium concentration and MS variation are both strongly influenced by lithology. The plot of uranium concentration vs. MS select lithologies at Hass A shows that fissile and siliceous shales differ in terms of both uranium concentrations and MS (Figure 48). At Hass A, the mean value of MS in fissile shale is 5.3 SI units while the mean for siliceous shale is 1.5 SI units. MS differences between fissile and siliceous shale at Hass B (Figure 49) are less striking than those differences at Hass A (Figure 48), perhaps reflecting the large number of MS missing measurements. The distribution plot of MS magnitude in select lithologies at Hass A (Figure 50) also suggests strong lithologic control over MS. At Hass B, evidence from the distribution plot of MS magnitude in select lithologies is less conclusive (Figure 51). However, negative (-) MS at both outcrops is only observed in siliceous shale and mean MS in fissile shale (5.1 SI units) is much higher than mean MS in siliceous shale (2.9 SI units); (Figure 45).

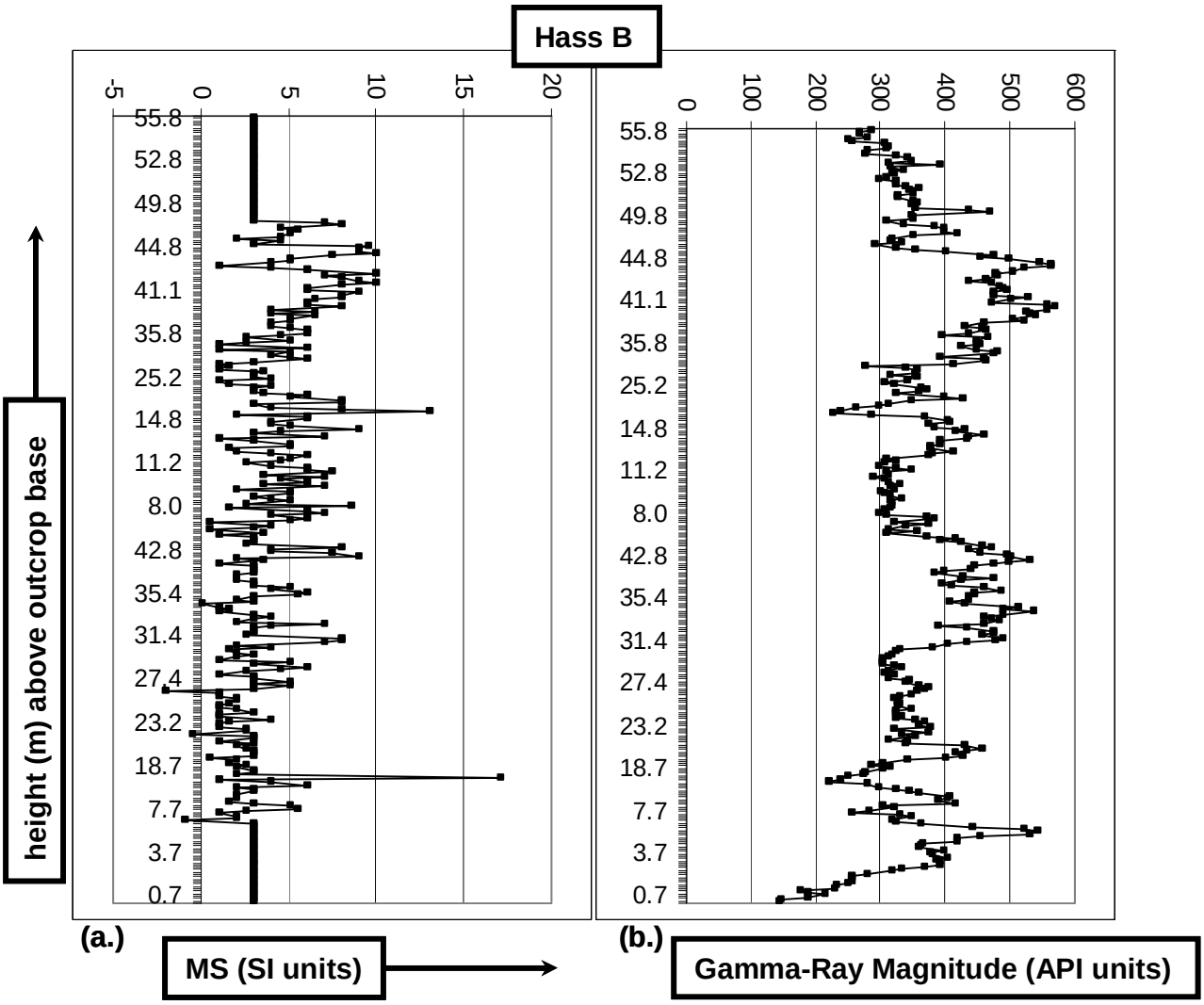

Figure 46. Comparison of MS and gamma-ray magnitude profiles at Hass B.

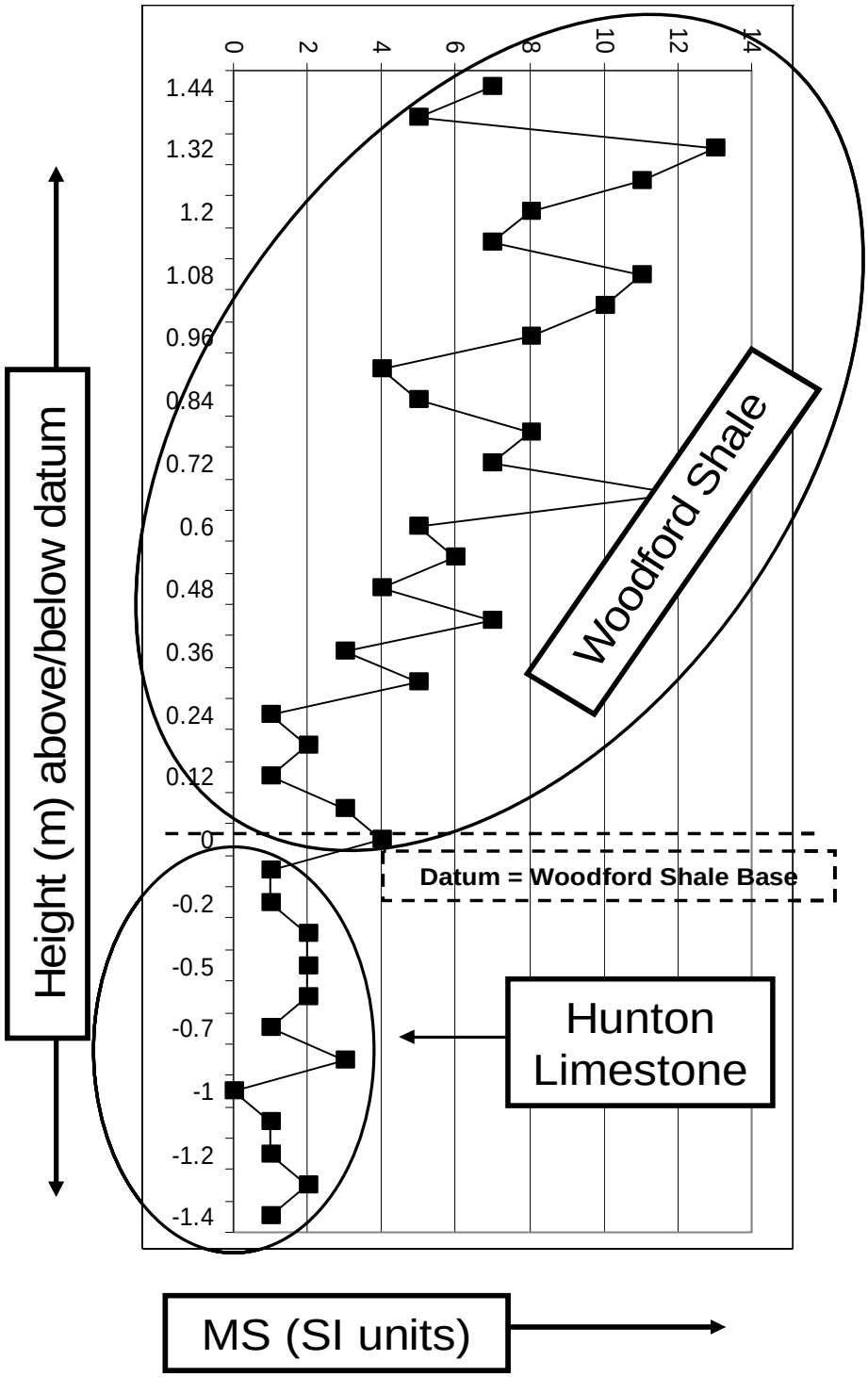

Figure 47. Lithologically controlled MS (κ) variation across the Acadian Unconformity.

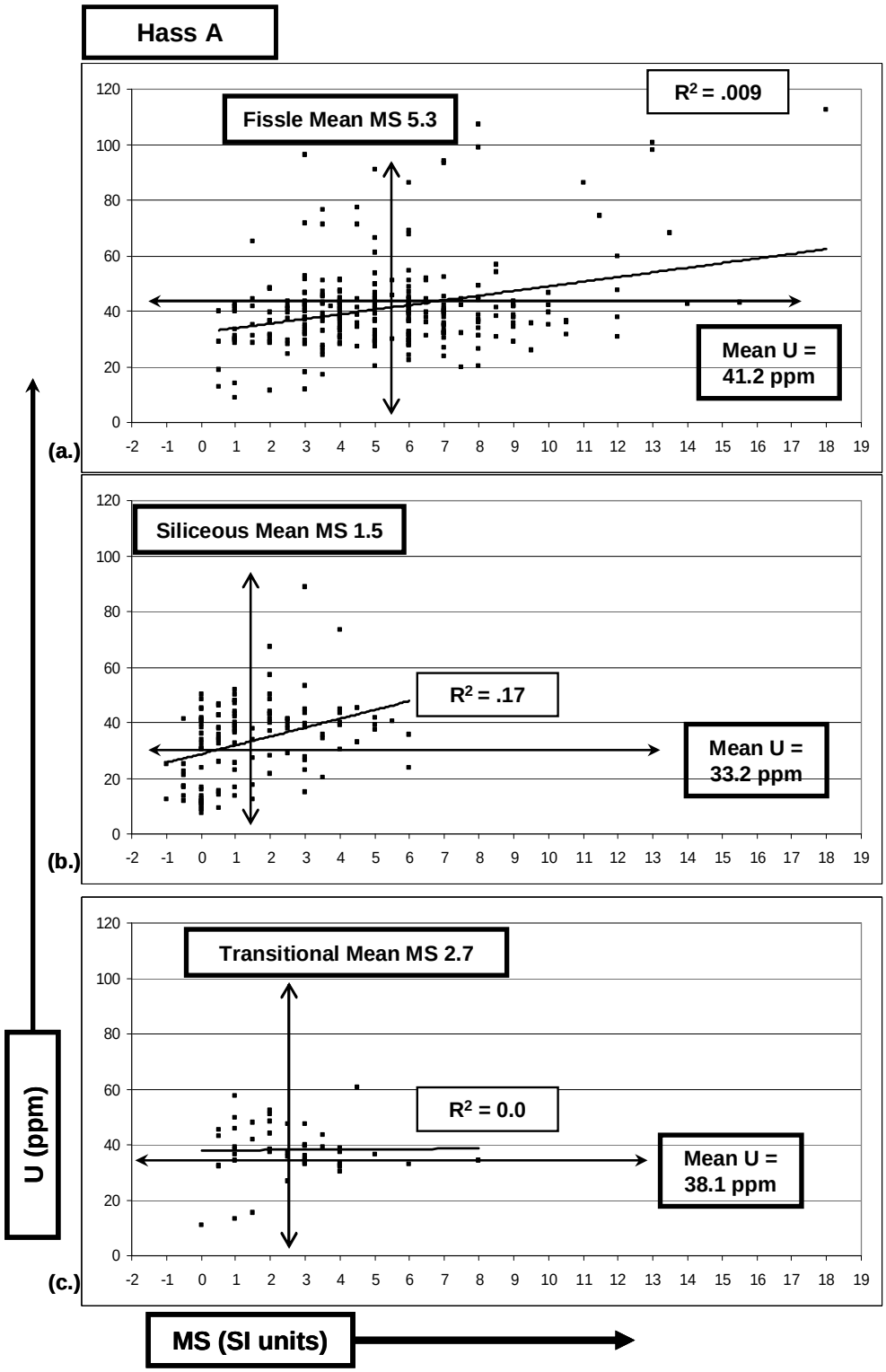

Figure 48. Plots of uranium concentration from spectral gamma-ray data vs. MS in select lithologies at Hass A including: fissile shale (a.), siliceous shale (b.) and transitional shale (c.).

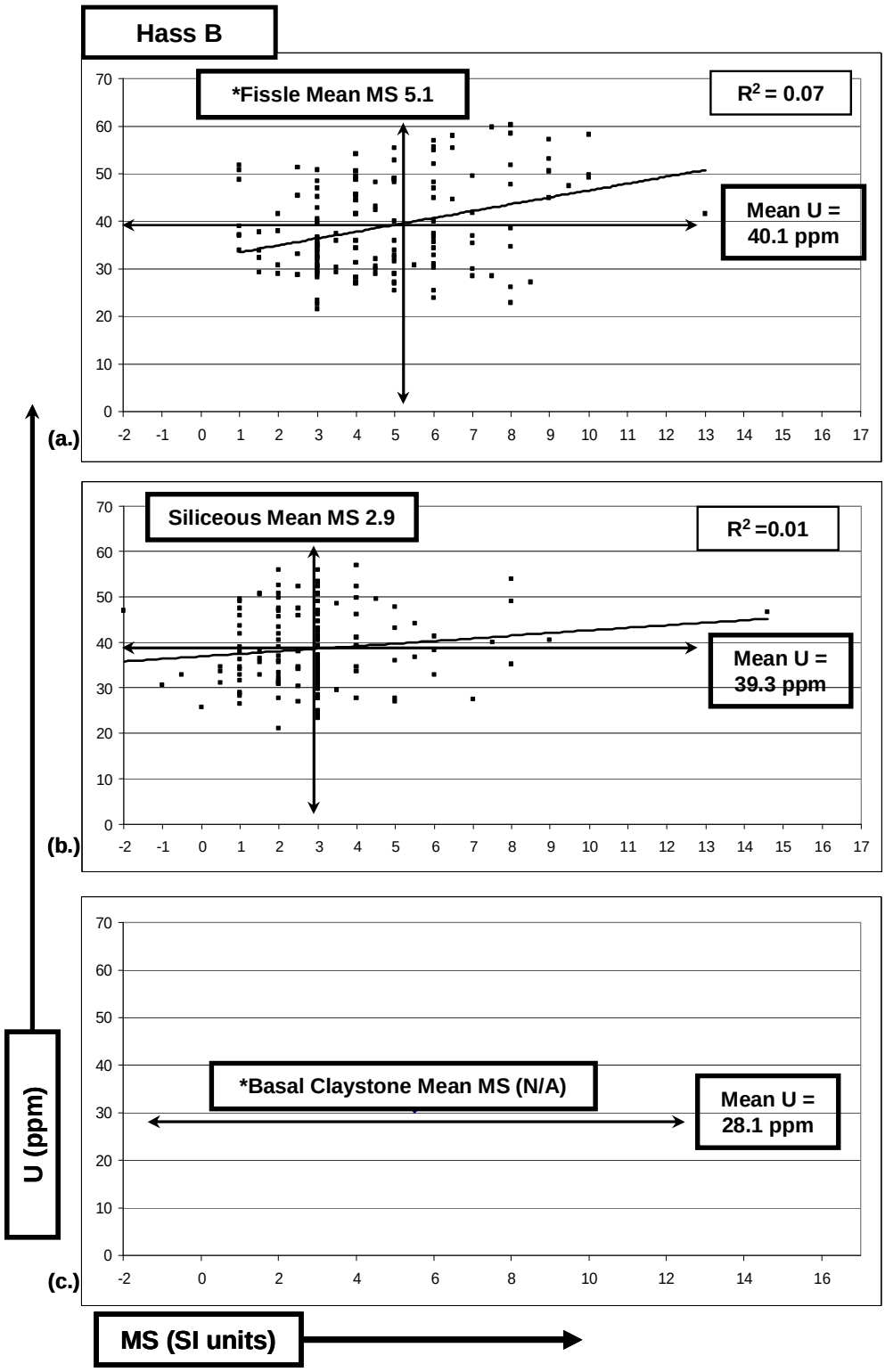

Figure 49. Plots of uranium concentration from spectral gamma-ray data vs. MS in select lithologies at Hass B including: fissile shale (a.), siliceous shale (b.), and basal claystone (c.). Includes uranium data using spectral gamma-ray data in intervals where no MS data was available*.

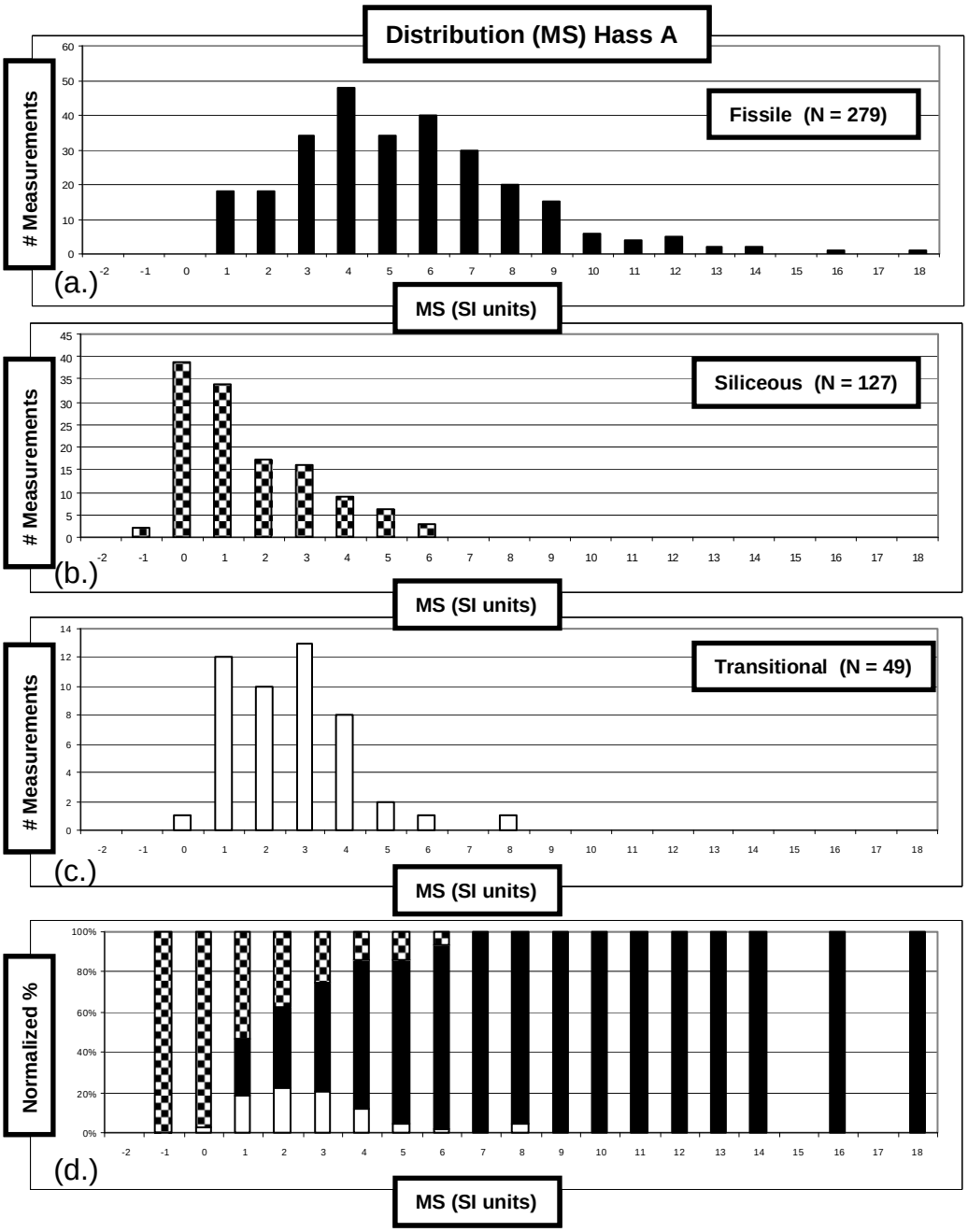

Figure 50. Distribution plots of MS in select lithologies at Hass A including: fissile (a.), siliceous (b.), and transitional shale (c.). Bottom plot (d.) combines all lithologies in a normalized distribution.

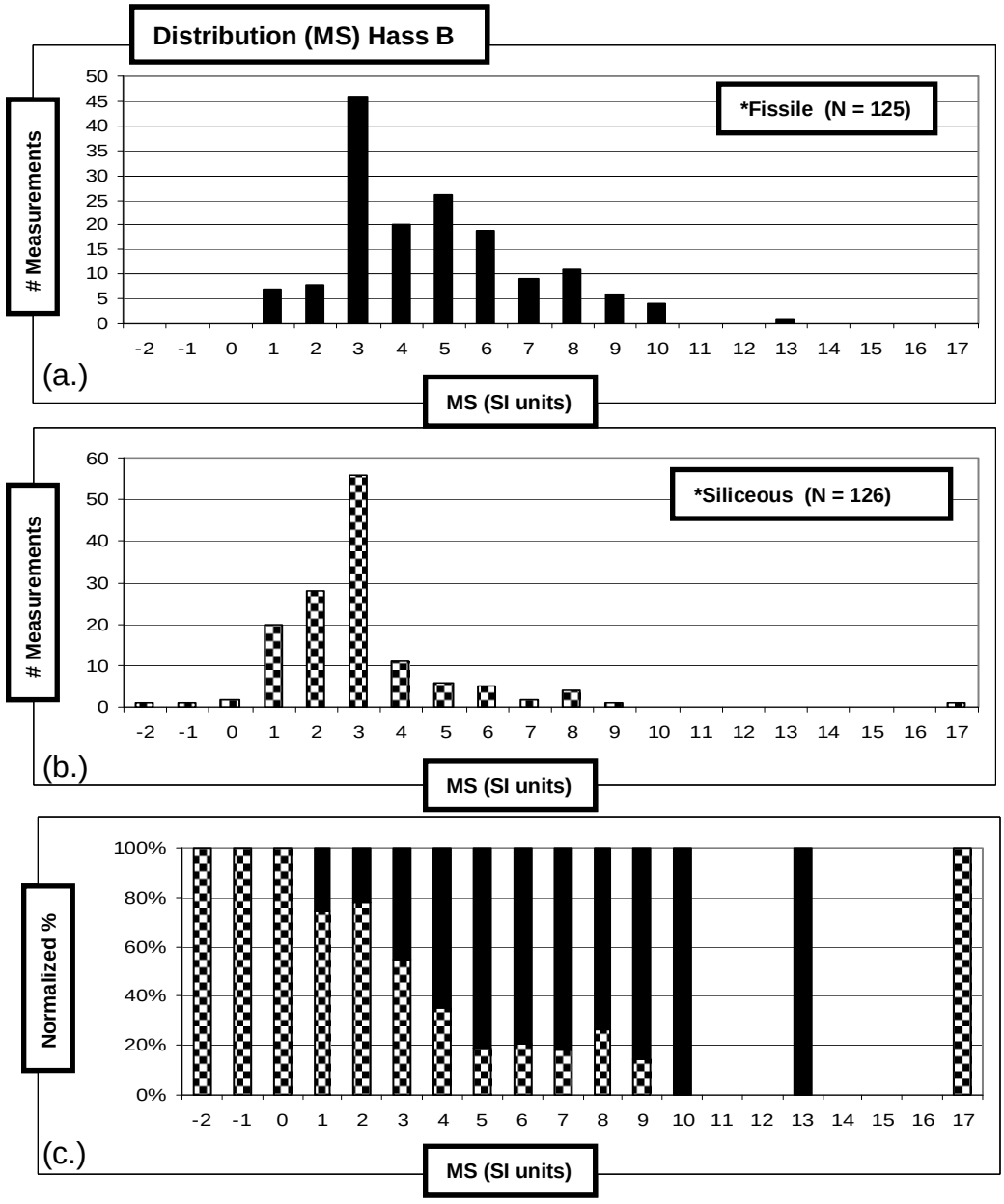

Figure 51. Distribution plots of MS in select lithologies at Hass A including: fissile (a.), siliceous (b.), and a normalized distribution plot of both lithologies (c.).

At least 5 types of variation in MS magnitude are observed within the Woodford Shale outcrops in the study. Descriptive statistics corresponding to MS variation at both study outcrops imply that MS varies with lithology (Table 11). At least some of the MS variation is related to the poor condition of the Hass B outcrop including: MS variation as a function of faulted, weathered, or covered section at Hass B where repeatable MS measurements were impossible. MS varies within individual main and minor intervals (Tables 12, 13) at individual study outcrops. MS varies between the three separate main intervals at individual study outcrops (Figure 52). MS varies between a given main interval at one study outcrop and the corresponding interval at the other study outcrop (Figure 52). Statistical MS variation at the outcrop scale is mostly restricted to small outcrop differences between MS in specific lithotypes (Table 11) and the MS profiles of Hass A and Hass B show little pattern correlation at the outcrop scale (figure 52).

A sixth type of MS variation was observed in the study. MS varies strongly between the Woodford Shale and the formations bounding the Woodford Shale (Figure 47). This observation shows that the MS response and lithology of the Woodford Shale is fundamentally different from the MS and lithology of the Hunton Limestone. The MS response of the Hunton Limestone, though not equal, was similar to MS response in the Sycamore Limestone. Likewise, Sycamore Limestone at Hass A and Hass B and Hunton Limestone, either Bois d'Arc Limestone at Hass A or Henryhouse-Harragan Limestone at Hass B, all have low magnitude MS relative to the MS of the Woodford Shale.

Table 11. Summary statistics for magnetic susceptibility in Woodford Shale.

M S Descriptive Statistics	Hass A all	Hass B all	Hass A Fissile	Hass A Siliceous	Hass A Transitional	Hass B Fissile	Hass B Siliceous	Hass B Claystone
Mean	3.9	4.0	5.3	1.4	2.5	5.1	2.9	N/A
Standard Error	0.1	0.2	0.2	0.1	0.2	0.2	0.2	N/A
Median	3.5	3.5	5.0	1.0	2.5	5.0	3.0	N/A
Mode	3.0	3.0	6.0	0	3.0	5.0	3.0	N/A
Standard Deviation	3.0	2.5	2.9	1.6	1.6	2.3	2.2	N/A
Sample Variance	9.3	6.3	8.2	2.7	2.5	5.5	4.9	N/A
Kurtosis	1.2	2.5	1.5	0	2.0	0.2	12.6	N/A
Skewness	0.9	1.1	0.9	0.9	1.0	0.4	2.5	N/A
Range	19.0	19.0	17.5	7.0	8.0	12.0	19.0	N/A
Minimum	-1.0	-2	0.5	-1.0	0	1.0	-2.0	N/A
Maximum	18	17	18.0	6.0	8.0	13.0	17.0	N/A
Count	455	251	279	127	49	125	126	N/A`

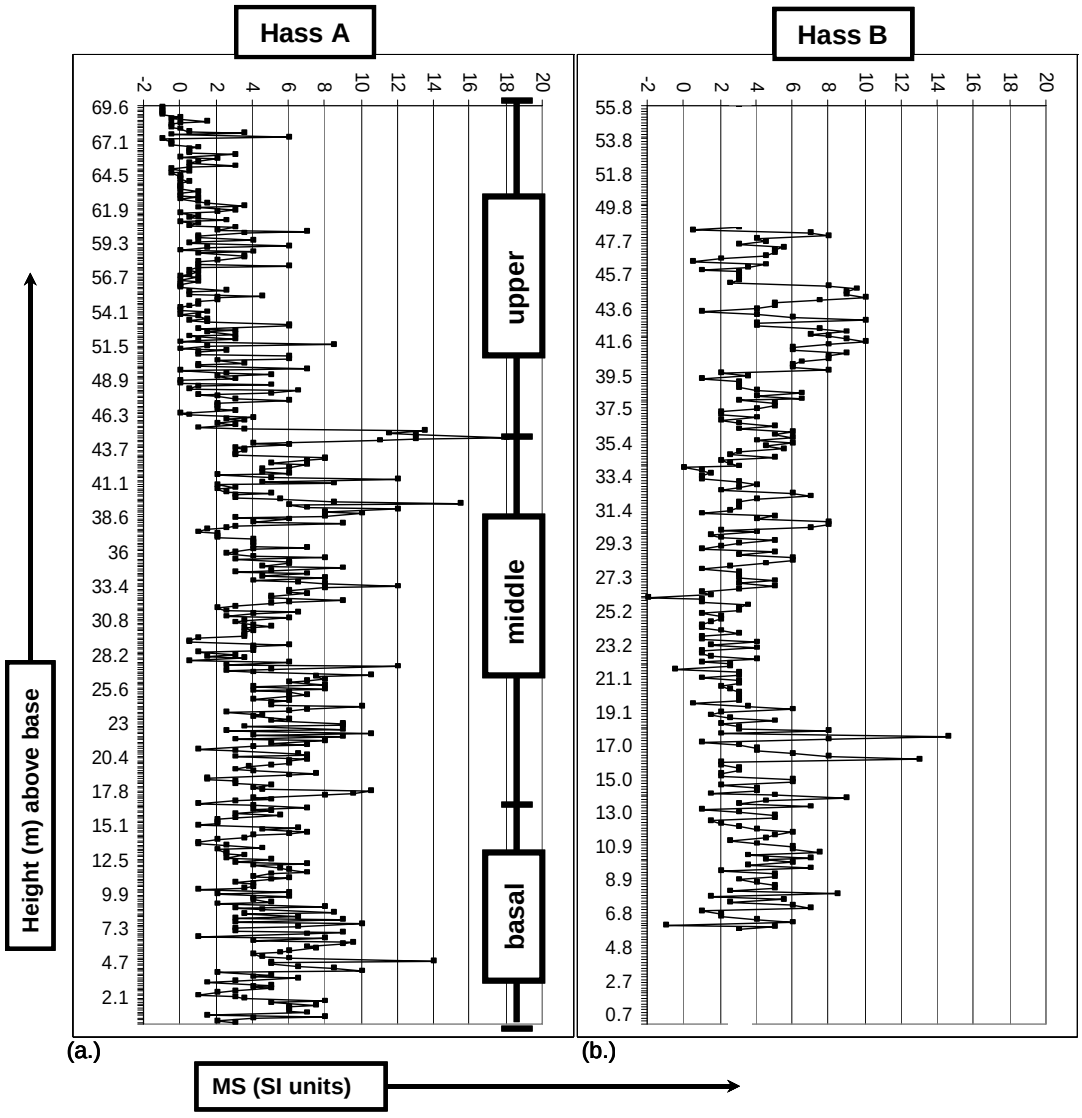

Figure 52. Comparison of MS profiles at Hass A (a.) and Hass B (b.).

Table 12. MS in lithological intervals (**from Table 2*) of Woodford Shale at **Hass A**

Interval	**Height Above Base** (m)	**Mean U_{ppm}**	**Mean Gamma** API	**Gamma Range** API	**Mean MS** **κ**	**MS Range** **κ**	
N (n = 1)	above Woodford	3	72.4	*	0	*	*
M	62.9 - 69.6	17.4	164	115 – 254	0.3	-1	+6
L	56.4 - 62.9	32.8	298	81 – 456	1.7	0	+7
K	45.7 - 56.4	39.5	360	238 – 496	2.2	0	+8.5
J	43 - 45.7	77.6	693	359 – 980	6.9	+1	+18
I	36 - 43	50.3	477	321 – 915	5.3	+1	+ 15.5
H	32.2 - 36	43.3	419	330 – 505	6.0	+2.5	+12
G	27.6 - 32.2	38.6	381	290 – 447	3.4	+0.5	6.5
F	25.6- 27.6	34.2	340	297 – 407	6.5	+ 2.5	+12
E	19.5 - 25.6	37.5	361	280 - 434	5.6	+1	+ 10.5
D	16.7 - 19.5	40.0	373	305 - 465	4.6	+1	+ 10.5
C	6.2- 16.7	35.1	340	242 – 498	4.4	+1	+ 10
B	0- 6.2	39.1	380	191 - 635	5.4	+1	+ 14.0
A (n = 12)	- 3.7 - 0	1.	34	29 - 52	1.5	0	+3

Table 13. MS in lithological intervals (*from Table 4*) of Woodford Shale at **Hass B**

Interval	**Height Above Base** (m)	**U** (ppm) range	**Mean Gamma** API units	**Gamma Range** API units	**Mean MS** **κ**	**MS Range** **κ**	
K	Covered zoned not exposed in spillway. No MS measurements after 48.2 m of section. No spectral gamma-ray measurements after 55.8 m of section.						
J**	47.2 – 55.8	14.0 – 39.4	286	181 - 362	N/A	N/A	N/A
I	40.2 – 47.2	28.4 – 53.2	468	290 - 498	5.8	0.5	10
H	32.7 – 40.2	40.4 – 60.3	480	380 - 561	5.5	1	10
G*	25.0 – 32.7	25.5 – 57.0	409	274 - 536	3.6	1	8
F*	17.4 – 25.0	31.5 – 48.9	352	301 - 456	2.3	-2	6
E	13.7 – 17.4	21.0 – 41.8	308	220 - 406	4.5	1	17
D	7.3 – 13.7	23.8 – 48.9	342	286 - 458	4.3	1	9
C	3.2 – 7.3	30.4 – 57.7	400	256 - 520	3.2	-1	6
B*	0 - 3.2	6.5 – 37.6	278	142 – 401	N/A	N/A	N/A
A (n =2)	below contact	2.8 – 2.9	143	143	0.5	0	1
No MS measurements from outcrop base to 5.8 m of section. Zones * B, F, G, and J are badly fractured and faulted. ** only 12 measuerments in the interval							

Inductively Coupled Plasma-Mass Spectrometry (ICP-MS):

Iron (Fe) vs. Aluminum (Al)

The concentration of several chemical elements was determined for 46 samples of Woodford Shale collected at Hass A. The elemental correlations from 4 of those elements are presented in Table 14. These elements include iron, aluminum, potassium, and uranium. This particular set of samples corresponds with paired MS/spectral gamma-ray measurement points. Iron/aluminum ratios (ppm/ppm) were calculated from the ICP-MS data corresponding to these samples. The iron aluminum ratios were compared against the North American Shale Composite (NASC) shale standard (Gromet et al., 1984), the Marine Sciences Group Black Shale Composite (BSC); (Vine and Tourtelot, 1970), and the Post Archaean Australian Shale Standard (PAASS); (Taylor and MCClennan, 1985). Aluminum is considered to be conservative in shale and therefore enhancement in iron or authigenic iron can be estimated by comparison to standards in the following way:

$$Fe_{auth.} = Al_{spl}\,(Fe_{std}/Al_{std}) \quad \text{(Eq. 5)}$$

where Fe_{auth} is the authigenic iron contained in the sample, Al_{spl} is the aluminum concentration (ppm) of the sample and Fe_{std} and Al_{std} are the concentrations of iron (ppm) and aluminum (ppm) from an appropriate shale standard (e.g. NASC); (Gromet, et al., 1984). The Woodford shale samples are found to be enriched when compared to the NASC, the standard with the highest Fe/Al ratio (0.45); (Figures 53, 54). The mean value of the Woodford Shale Fe/Al ratio was more than twice the

Table 14. Correlation of select elements from compositional analysis by inductively coupled plasma mass spectrometry in 42 Woodford Shale samples from Hass A

	K (ppm)	**Al (ppm)**	**Fe (ppm)**	**U (ppm)**
K (ppm)	**1**	**0.95**	**0.42**	**0.63**
Al (ppm)	**0.95**	**1**	**0.39**	**0.44**
Fe (ppm)	**0.42**	**0.39**	**1**	**0.37**
U (ppm)	**0.63**	**0.44**	**0.37**	**1**

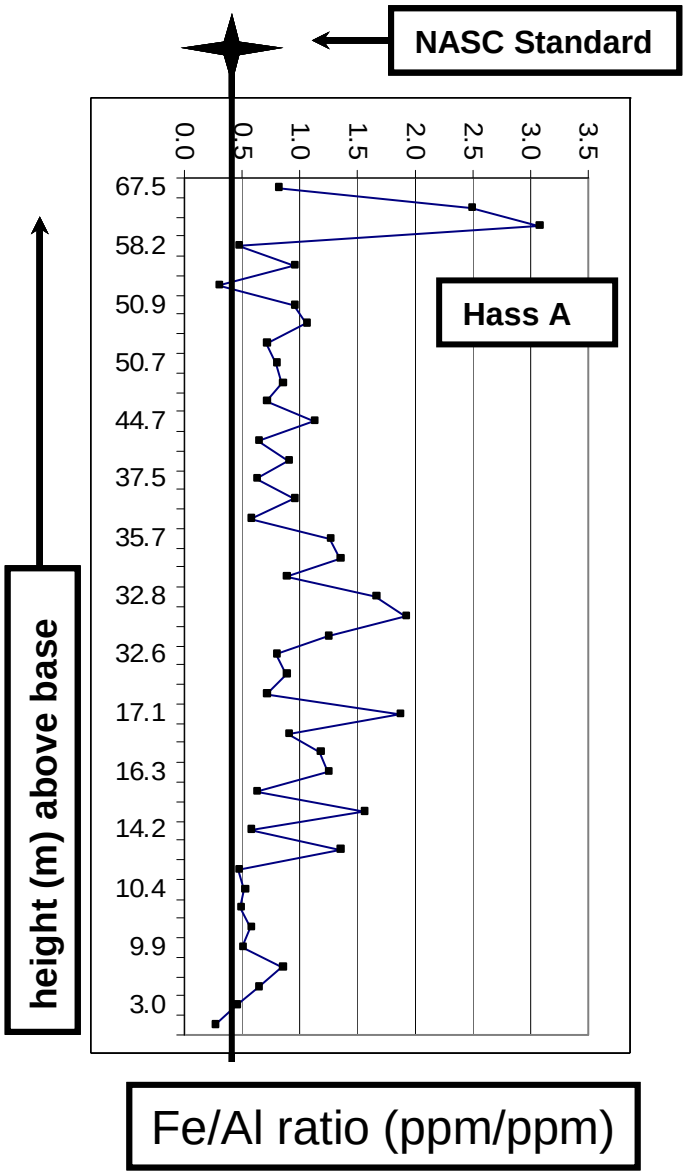

Figure 53. Woodford Shale iron/aluminum ratios calculated from inductively coupled plasma mass spectrometry data at Hass A. Note the value of the NASC shale standard (star); (Gromet et al., 1984).

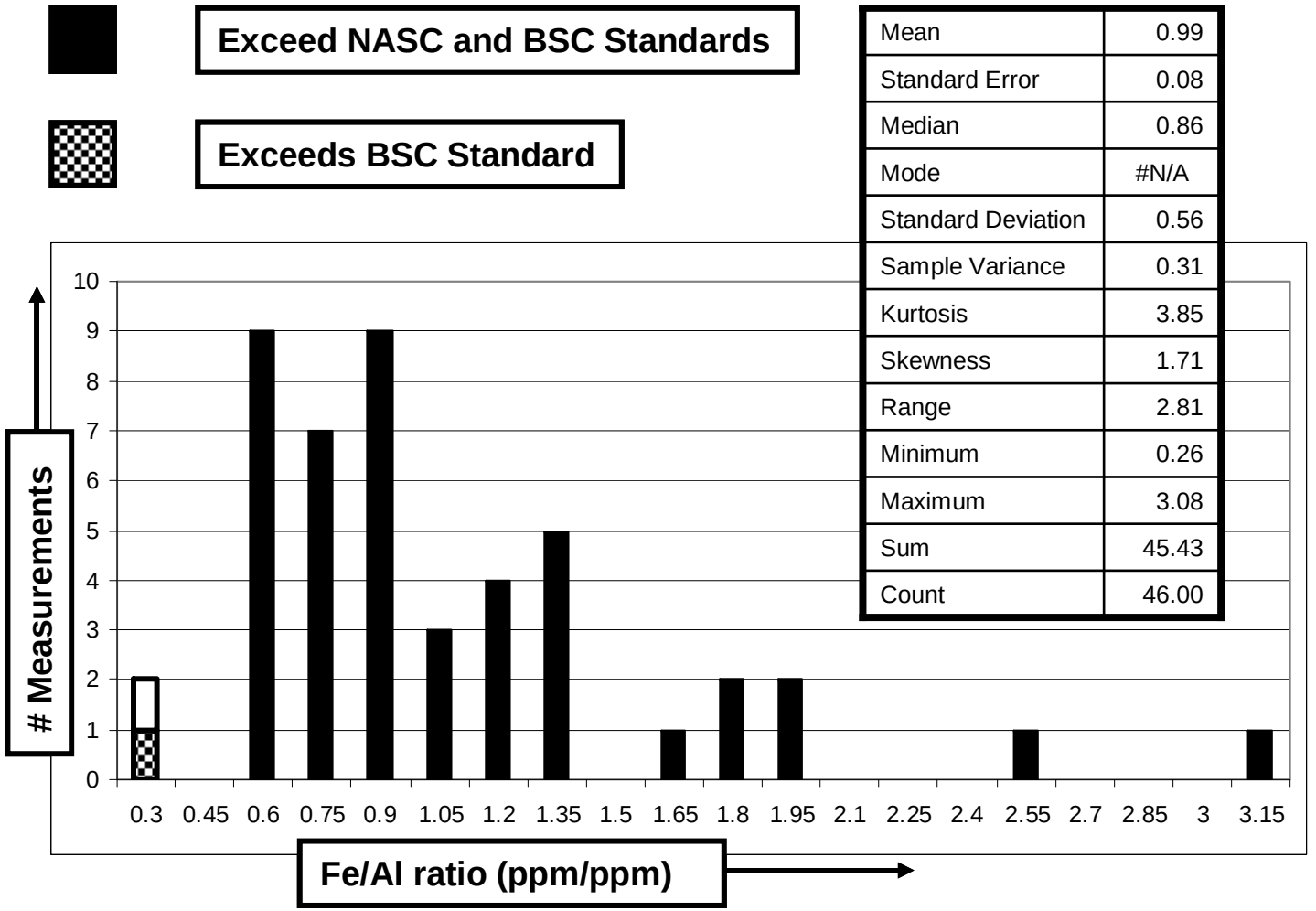

Figure 54. Distribution plot and summary statistics of iron/aluminum ratios in Woodford Shale at Hass A. Note shale standards including (Gromet et al, 1984; Vine and Tourtelot, 1970).

value of the Fe/Al ratio (0.45) of the North American Shale Composite (Figure 54). The maximum observed Fe/Al ratio in the Woodford Shale (3.1) was approximately 6.8 times the NASC standard (0.45). Only two of forty five calculated ratios (Figure 54) were lower than the NASC standard (0.45) or the PAAS standard (0.34) and only one calculated ratio was lower than the BSC standard (0.29).

Confidence in the ICP-MS based findings is somewhat increased through comparison of the Woodford Shale Al/Fe ratio mean (1.0) and median (.9) to the NASC (.45) (Figure 54) because both statistical parameters show significant enrichment relative to the NASC standard. Further, the mean (1.0) is similar to the median (0.9) Fe/Al ratio and both values are approximately twice the standard value despite skewness (1.71) in the distribution caused by a few extremely high Fe/Al values (e.g. Fe/Al_{max} = 3.1); (Figure 54). The sample with the highest Fe/Al ratio (3.1) has an estimated authigenic fraction authigenic fraction of 0.85 when the NASC is used for the estimate.

Summary statistics of Fe/Al ratios show that samples are enriched in authigenic iron relative to other shale standards including: the Post Archaean Australian Shale Standard (Fe_{std}/Al_{std} = 0.34); (Taylor & McClennan, 1985) and the Marine Sciences Group Black Shale Composite (BSC); (Fe_{std}/Al_{std} = 0.29); (Vine and Tourtelot, 1970). The mean estimated authigenic iron fraction of the samples ($Fe_{auth)}$ is: 0.44 when compared to the NASC, 0.58 when compared to the PAASS, and 0.64 when compared to the BSC. When compared to the BSC, the sample with the highest calculated Fe/Al ratio (Fe/Al_{max} = 3.1) has an estimated authigenic fraction (Fe_{auth} = .91).

ICP-MS Based Elemental Correlations

ICP-MS based elemental correlations among iron and aluminum along with uranium and potassium were analyzed (Table 14). Uranium, potassium, and thorium were also measured by the spectral gamma-ray method (Table 4). We were unable to produce usable results of thorium concentration using the ICP-MS method. Potassium concentration vs. aluminum concentration shows strong correspondence, with an R^2 = 0.95 (Figure 55). Aluminum is considered a conservative tracer in comparing elemental enrichments in shales (Taylor and McClennan, 1985). This plot implies that the Woodford Shale is not significantly enriched in potassium relative to aluminum. Other elemental correlations such as iron concentration vs. aluminum concentration, R^2 = 0.39 (Figure 56) and uranium concentration vs. aluminum concentration, R^2 = 0.44 (Figure 57), with low R^2 values, imply that the Woodford Shale is enriched in authigenic iron and uranium.

Since the plot of uranium concentration (ppm) vs. aluminum concentration from ICP-MS data shows weak correspondence, with an R^2 = .44 (Figure 65) and potassium strongly correlates with aluminum (Figure 63), these findings imply that the Woodford Shale is also enriched in uranium relative to potassium. A similar finding, R^2 = .44 (Figure 36c) for a plot of potassium vs. uranium derived from spectral gamma-ray data, also implies that uranium is enriched relative to potassium in Woodford Shale.

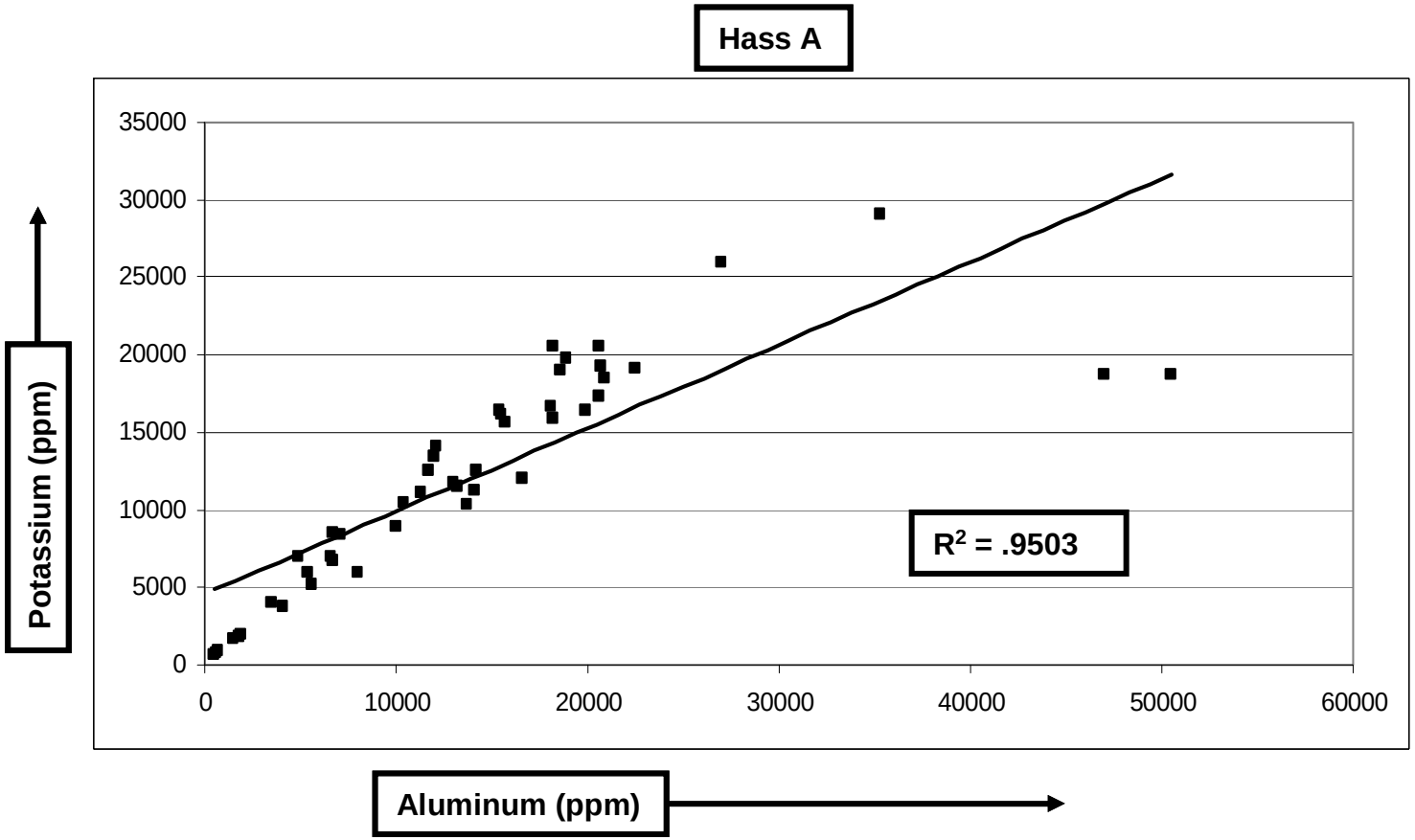

Figure 55. Plot of potassium concentration vs. aluminum concentration from inductively coupled plasma mass spectrometry data in the Woodford Shale at Hass A

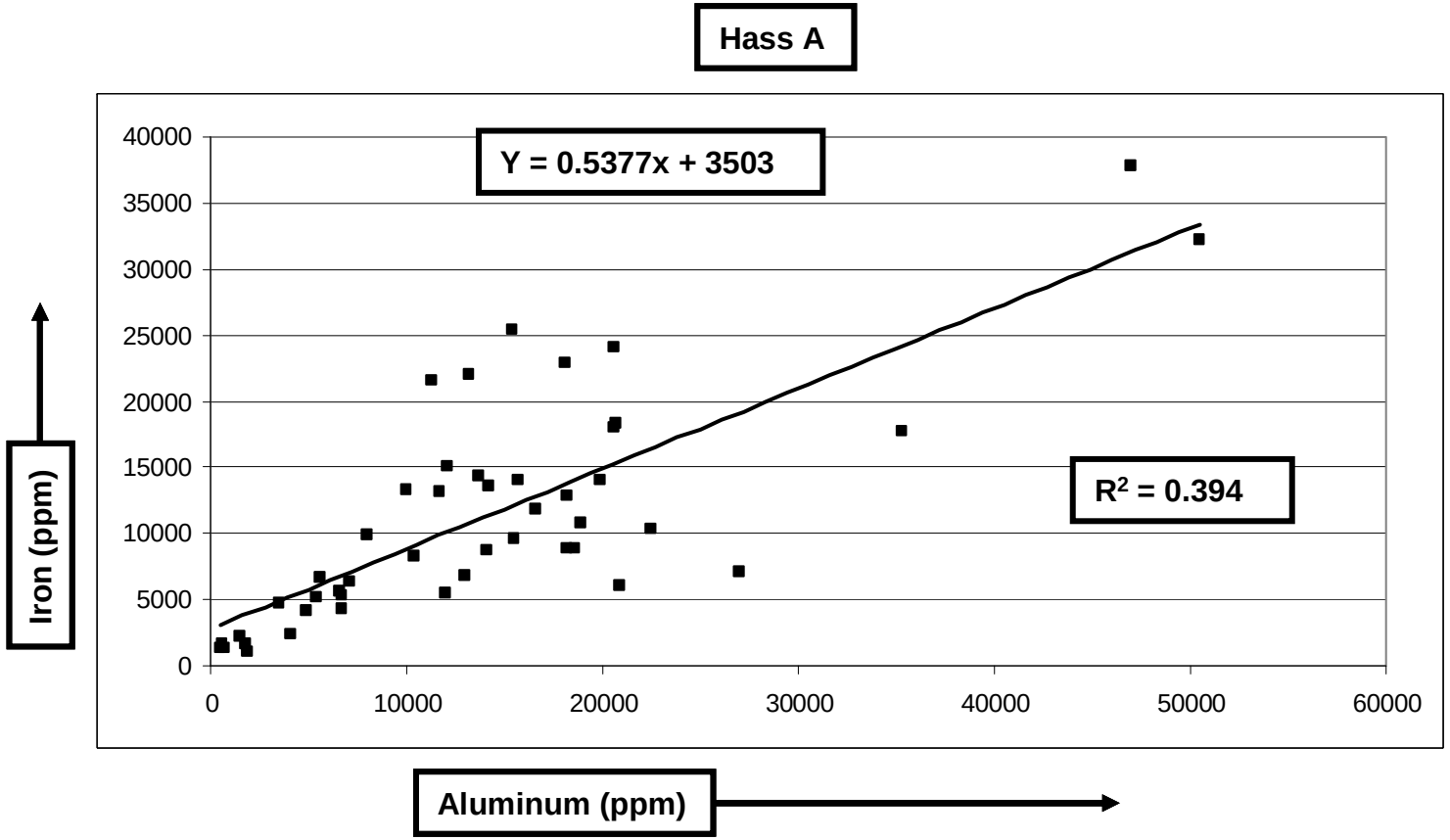

Figure 56. Plot of iron concentration vs. aluminum concentration from inductively coupled plasma mass spectrometry data in the Woodford Shale at Hass A.

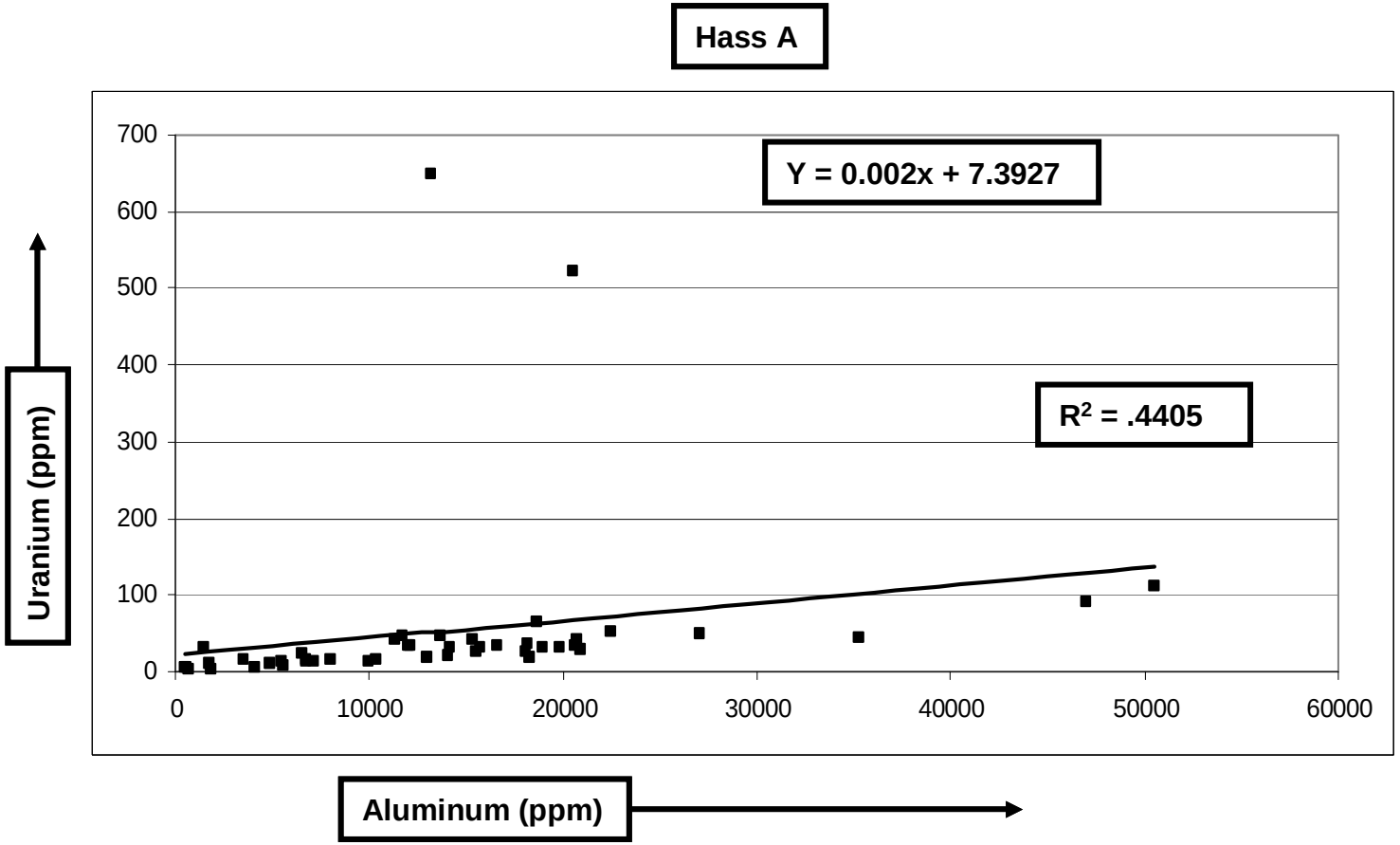

Figure 57. Plot of uranium concentration vs. aluminum concentration from inductively coupled plasma mass spectrometry data in the Woodford Shale at Hass A.

CHAPTER V

CONCLUSIONS

Study Variables: Lithologic Control

Based on 455 paired measurements of gamma-ray magnitude and MS at Hass A, lithology exerts a primary control over MS, gamma-ray magnitude, and variations in gamma-ray specific elemental assemblage. Trends at Hass B based on 251 paired spectral gamma-ray and MS measurements and 77 spectral gamma-ray measurements without corresponding MS measurements, reinforce the conclusion that lithology exerts control on over MS, gamma-ray magnitude, and gamma-ray elemental assemblage. Fissile shale beds and fissile shale intervals at both outcrops generally exhibit higher gamma-ray magnitude, MS and concentrations of uranium measured by the spectral gamma-ray method relative to siliceous shale, transitional shale, claystone and phosphatic intervals.

Highly indurated siliceous shale beds and siliceous intervals at both outcrops have the thinnest fissile beds, the lowest cycle thickness (highest number of beds per meter), and the lowest net fissile shale values (fissile thickness/total thickness). Siliceous intervals contain multiple repeated beds of siliceous shale, some with no discernable intervening fissile beds present. Siliceous beds and intervals generally have the lowest

gamma-ray magnitude, the lowest concentrations of all gamma-ray specific elements, and the lowest MS.

The cyclic Woodford Shale, alternating between fissile beds and siliceous beds, has a gamma-ray magnitude plot which contained oscillations that mirrored observed lithologic cyclicity at the outcrop face. The repeated observation that lithology can be inferred from gamma-ray magnitude and individual gamma-ray specific elemental concentrations confirmed the validity of the long-standing petroleum industry practice of using gamma-ray magnitude and spectral gamma-ray analysis to infer lithology.

The gamma-ray magnitude logs of the Woodford Shale have been interpreted as being comprised of three main intervals, each representing the characteristic gamma-ray magnitude and spectral gamma-ray specific elemental assemblage of one of the three large lithologic intervals observed in outcrops. The predictable nature of the association between Woodford Shale lithology and gamma-ray magnitude accounts for the formations use as a distinct and dependable stratigraphic marker within the Anadarko Basin. Gamma-ray magnitude in this study was observed to vary with lithology at the scale of the individual bed, in and between main intervals, and between study outcrops. All three of the individual radioactive elements sampled by spectral gamma-ray analysis (U, K, and Th) were observed to vary with lithology.

Gamma-Ray Magnitude, Elemental Control, and Geochemical Facies

The concentration of uranium had the largest control on gamma-ray magnitude in the Woodford Shale. R^2 values between uranium concentration and gamma-ray

magnitude approach a value of 1. Higher concentrations of uranium in fissile shale imply that it may be deposited in a more anoxic depositional environment relative to siliceous shale. The occurrence of pyrite nodules and discrete pyrite layers proximate to uranium concentration and gamma-ray magnitude maxima indicates that the Woodford Shale depositional environment was strongly reducing or anoxic and perhaps was even euxinic. The entire Woodford Shale is found to be enriched with authigenic iron, generally well above any published shale standard. It is important to note that the large pyrite nodules were excluded from the ICP-MS sampling. Although no speciation of iron was conducted in this study, the quantity of pyrite present and other evidence such as uranium and carbon concentrations makes it reasonable to assume that the degree of pyritization is nearly 100%.

The accumulation of apparently diagenetic pyrite layers, diagenetic pyrite nodules with euhedral pyrite crystals and marcasite nodules with radial crystals in intervals of highest MS, indicates that the Woodford Shale MS profile has been altered since deposition. The effect of diagenesis should be considered in global correlations of MS correlation employing the Woodford Shale. The exact source(s) of the pyrite and marcasite is beyond the scope of this study. However, if the pyrite and marcasite is sourced from intervals of the Woodford Shale itself, then diagenetic alteration of the Woodford Shale MS profile could also include diminution of MS in portions of the Woodford Shale.

Thorium and potassium also contribute to total gamma-ray magnitude and potassium and thorium concentrations are generally highest in fissile intervals generally concomitant with peak uranium concentration intervals at both outcrops. The ratio of

uranium to thorium (U_{ppm}/Th_{ppm}) is strongly related to lithology, with distinct differences observed between the three main intervals at both outcrops and between the outcrops. Since the sequestration of uranium and carbon is often geochemically related to high degrees of pyritization (DOP), the occurrence of discrete pyrite layers and nodules in the most uranium-rich intervals, helps to explain the coincidence of gamma-ray magnitude and MS peaks in fissile intervals containing generally high concentrations of all 3 radioactive elements measured in spectral gamma-ray analysis. Gamma-ray magnitude and gamma-ray specific elemental assemblage data collected in this study tend to agree with previous studies such that the concentrations and relative proportions of radioactive elements measured in spectral gamma-ray analysis can be used to define geochemical facies and lithofacies.

Gamma-Ray Magnitude Correlation with Magnetic Susceptibility

Through linear regression, it was found that gamma-ray magnitude, uranium concentration, potassium concentration, and thorium concentration all had poor statistical correspondence to MS at both outcrops. Consistent with previous studies, it was observed that both gamma-ray magnitude and MS response of the underlying Hunton Group carbonates was fundamentally different relative to the Woodford Shale. In the absence of spectral gamma-ray evidence related to uranium, one might wrongly conclude that bulk gamma-ray magnitude differences were only related to the increased detrital content of the Woodford Shale and increased inputs of clays containing potassium and resistate minerals containing thorium and minor uranium.

Uranium evidence gathered through spectral gamma-ray analysis and ICP-MS in this study shows that gamma-ray magnitude increases do not result from an increase in detrital content alone, but rather from fundamentally different geochemical context. Uranium dominates the API gamma response. While it is true that the Woodford Shale has a higher detrital content (e.g. Th and K) relative to Hunton Carbonate, authigenic uranium in the Woodford Shale exerts dominant control over gamma-ray magnitude. It is authigenic uranium rather than detrital thorium or potassium that controls the gamma-ray magnitude of the Woodford Shale. The Wignall and Myers method of estimating detrital contribution of uranium relative to total uranium concentration suggests that detrital uranium in the Woodford Shale is limited to a tiny percentage of the total uranium.

Controls on Magnetic Susceptibility in Woodford Shale

A strong relationship between MS and lithology was observed at both outcrops. Still, MS maxima are related to the large aggregates and discrete layers of diagenetic iron sulfide. Authigenic iron, here assumed to be pyrite, appears to control MS in the Woodford Shale. The lowest MS magnitudes in the Woodford Shale at Hass A, observed above 46 m of section, also appear to be controlled by lithology. Above 46 m of section, the lithology and MS of the Woodford Shale is fundamentally different relative to the basal or middle Woodford intervals. The siliceous, phosphatic, and dolomitic beds characteristic of the upper Woodford exhibit consistently low MS. Silica, phosphate, and carbonate are diamagnetic. The consistently low values of MS recorded in the siliceous and phosphatic beds of the upper interval of the Woodford Shale reflect that diamagnetic

nature. In this regard, the consistently low MS or MS minima in Woodford Shale are explained by magnetic physics and chemical composition (e.g. lithology) rather than domination by a detrital fraction of iron minerals contained of the formation. In summary, neither MS peaks nor MS background signal appear to be dominated by detrital iron. Likewise, there is no evidence that clay minerals dominate MS magnitude.

Previous studies have reported increases in the MS of carbonates as the result of increases in the detrital content. Other studies have also concluded that detrital magnetite, clays other detrital paramagnetic minerals containing iron control the MS response of rocks. Global correlations of MS based on these conclusions report that rock MS is controlled by soil-formed iron minerals and eustaticly controlled gradients of those minerals in ocean basins. These conclusions, while valid, fail to consider all of the geochemical changes to soil-formed sediment as it is chemically altered (weathered) and removed from proximal oxidizing continental environments and ultimately deposited in reducing marine depositional contexts. More importantly, the model of detrital control on MS fails to consider the action of biological agents in terrestrial and marine environments and the biogeochemical implications of carbon residuum that is characteristic of petroleum source rocks such as the Woodford Shale. Most importantly, the model of detrital control on MS fails to account for studies suggesting that the valence of magnetic species exerts greater potential control over MS than the concentration of magnetic species.

While increasing or decreasing the abundance of iron of given valence in a fixed volume of rock will cause a corresponding linear change in MS magnitude, the alteration of the valence of that iron alone, without accumulations or depletions in the total mass of

iron, is capable of inducing magnetic changes of several orders of magnitude. The claim that MS in black shale such as the pyrite rich Woodford Shale is controlled by detrital material, is at the very least, incomplete. The report that detrital iron such as clays or magnetite controls rock MS in black shale is contraindicated by the observed overall enrichment of the Woodford Shale in authigenic iron, even without accounting for diagenetic pyrite and marcasite nodules and layers observed at all study outcrops or previous studies that suggest dispersed pyrite is a major component in Woodford shale fabric. MS peaks are controlled by diagenetic iron sulfides. Magnetite and all iron (III) oxides are highly soluble and unstable in the biogeochemical depositional context of black shale or other depositional contexts containing organic carbon and low concentrations of oxygen.

Woodford Shale Iron: Pyrite Provenance

The results of compositional analysis of samples of the Woodford Shale by the method of inductively coupled plasma-mass spectrometry (ICP-MS) show that the Woodford Shale is enriched in authigenic iron relative to all shale standards. Based on that ICP-MS data alone, it would be difficult to conclude that detrital iron exerts the greatest control on MS in the Woodford Shale. Instead MS peaks are associated with authigenic or diagenetic pyrite.

Assuming a FeS_2 stochiometry for the nodules, with an iron weight fraction in excess 42 wt. %, detrital sources of that iron are not likely. More likely, the pyrite nodules are secondary structures and diagenetic in origin. Moreover, as diagenetic

features, the nodules are probably not directly related to the original depositional and environmental and their provenance is not detrital.

Although not firmly established by the data, the iron in the Woodford Shale pyrite nodules is most likely sourced from the Woodford Shale itself. As such the nodules probably represent secondary accumulations of iron, representing the probable diminution of iron in other portions of the Woodford formation. It might be reasonable to conclude that prior to formation of the nodules; the black shale of Woodford Formation was more enriched in authigenic iron, implying even less detrital control than is suggested by the current ICP-MS data. In any case, Woodford Shale pyrite sourced internally or externally during diagenesis or precipitated directly from seawater, will not support a conclusion of detrital control of MS by either clay or magnetite.

Whether sourced internally or externally, diagenetic nodular pyrite associated with MS maxima is not detrital. In either case above, the nodular pyrite is not related to primary depositional environment. Finally, if the pyrite nodules are indeed primary sedimentary structures (i.e authigenic pyrite), directly related to the original depositional context, our decision to exclude the nodules from ICP-MS analysis has strongly biased the results of that analysis. In this alternative but improbable scenario, the Woodford Shale iron enrichment would be greater than the ICP-MS data have implied, and a final conclusion of detrital MS control in Woodford Shale would be correspondingly marginalized. The inclusion of data from the pyrite nodules themselves would have several effects on the ICP-MS data set including; increasing the mean, median and mode iron concentrations, increasing the mean, median, and mode values of the Fe/Al ratio, and increasing the positive skewness of the distribution of calculated Fe/Al ratios. Even so, a

final conclusion of detrital control on MS is unsupported by the occurrence of pyrite nodules in excess of 133 g and discreet pyrite layers between shale beds where local and outcrop MS maxima are observed.

Hass B as a Possible Magnetic Type Section in the Unites States

The Hass B outcrop has been offered as a possible magnetic type section for the Frasnian/Famennian boundary (Crick et al, 2002). Several observations made in this study suggest that the Hass B outcrop is potentially a poor magnetic type section. One reason is related to the observation that MS correlation between Hass A and Hass B outcrops is problematic. Many of the problems with that A-B correlation are the direct result of the poor condition and incomplete stratigraphy, multiple faults, and repeated sections found at the Hass B outcrop. Observations made in this study indicate that Hass B is tectonically altered in a way that makes it inappropriate for some geological studies.

Additionally, welded breccia was observed north of the spillway. This cataclastic breccia implies that Hass B Woodford Shale near the many faults observed in this study, may have been subjected to temperatures high enough to induce magnetic changes to the rock. Another condition problem observed in the spillway was the presence of thick packages of pervasively shattered siliceous shale. The presence of multiple faults at and near the Hass B in the spillway calls into question whether a complete basal section occurs in the spillway where previous biostratigraphic studies have relied on first appearance of index conodonts in placement of the F/F boundary.

Study Hypothesis and Related Research Questions:

The study hypothesis, that "gamma-ray magnitude will vary inversely with magnetic susceptibility", is not supported by data and observations from this study. Instead the opposite conclusion is more reasonable. Despite the fairly poor statistical correlation (R^2) of gamma-ray magnitude vs. MS, MS and gamma-ray magnitude profiles have strong qualitative or pattern similarity. Some of the poor statistical correlation and unexplained variation between MS and gamma-ray magnitude could be explained by the fact that the gamma-ray instrument and MS instrument sample different volumes of rock, 0.5 m^3, and 8.0 cm^3 respectively (Dearing, 1991). Other explanations for the poor statistical correlation between MS and gamma-ray magnitude include the mutually variable thicknesses of adjacent fissile and siliceous beds, or the many instances (paired data points) where the MS instrument or gamma-ray instrument was influenced by both fissile and siliceous lithology, e.g. near a contact between a fissile bed and siliceous bed.

The conclusion that MS, gamma-ray magnitude, and GSEA are all controlled by lithology implies that MS may be suitable for lithocorrelation inside the Anadarko Basin. Data in this study and others imply that MS in carbonate rocks is generally much lower than MS in Black Shale. MS in the underlying Hunton limestone and the overlying Sycamore Limestone also appear to be fundamentally different than MS in Woodford shale. That finding implies that if MS could be logged along with other logging parameters, the fundamental change in MS between the Hunton Limestone and the Woodford Shale would be recognizable, as would be the fundamental change in MS between the Woodford Shale and the Sycamore Limestone.

The MS outcrop maximum at Hass A and the outcrop gamma-ray magnitude maximum are located in the same paired data point near maximum concentration of all three elements measured by spectral gamma-ray analysis, all associated with the highest weight fraction of iron, inferred from the occurrence of iron pyrite nodules. Finally the Hass A profile of gamma-ray magnitude has noteworthy qualitative similarity with the MS profile at the base of the outcrop where both parameters rapidly increase along with all elements employed in spectral gamma-ray analysis and another interval of pyrite nodules. Therefore, the MS profile of Hass A resembles the gamma-ray log of Hass A, the same type of evidence commonly used in lithocorrelation in the Anadarko Basin.

The finding that MS varies with lithology implies that MS lines may represent magnetic lithofacies or magnetofacies lines. In order for MS to be useful as a lithocorrelation tool in a specific basin, MS variation in that basin must be predictable in terms of magnetic variation as a function of lithologic change. Since lithology exerts control over MS, the use of MS in global correlation may be problematic. If MS were to arise as the result of high order globally controlled cycles, independent of lithology, then basin specific lithocorrelation might be problematic.

REFERENCES

Adams, J.A. and Weaver, C.E., 1958, Thorium-To-Uranium Ratios As Indicators OF Sedimentary Processes: Example of Geo-Chemical Facies: Bulletin Of The American Association Of Petroleum Geologists, v. 42, p. 387-430.

Adams, L.K., MacQuaker, J.H.S., and Marshall, J.D., 2006, Iron (III) Reduction in a Low-Organic-Carbon Brackish-Marine System: Journal of Sedimentary Research, v. 76, p. 919-925.

Algeo, T.J., 2004, Can marine anoxic events draw down the trace element inventory of seawater? Geology, v. 32, p. 1057-1060.

Amsden. T.W., 1960, Stratigraphy and paleontology of the Hunton Group in the Arbuckle Mountain region: Oklahoma Geological Survey Bulletin 84, 311 p.

Amsden, T.W. and Klapper, G., 1972, Misener Sandstone (Middle-Upper Devonian), North-Central Oklahoma: The American Association of Petroleum Geologists Bulletin, v. 56, p. 2323-2334.

Amsden, T.W., Klapper, G., and Ormiston, A.R., 1968, Lower Devonian Limestone of Post-Hunton Age, Turkey Creek Inlier, Marshall County, South-Central Oklahoma: The American Association of Petroleum Geologists Bulletin, v. 52, p. 162-173.

Archie, G.E., 1947, Electrical Resistivity An Aid In Core-Analysis Interpretation: American Association of Petroleum Geologists Bulletin, v. 31, p.350-366.

Aufill, M., Paxton, S.T., and Simms, A., 2006, Evaluation of Magnetic Susceptibility Relative to Spectral Gamma-Ray Response in the Upper Devonian - Lower Carboniferous Woodford Shale of South-central Oklahoma, (Abs.): Geological

Society of America Abstracts with Program, Annual Meeting, October 22-25, 2006, Philadelphia, Pennsylvania.

Aufill, M., Cruse, A.M., and Paxton, S.T., 2007, Timing Related to the Redoximorphic Properties of Iron and Uranium in Woodford Shale through Quantitative Microprobe Analysis of Pyrite Nodules (Abs.): Geological Society of America Abstracts with Program, South-Central and North Central Sections Joint Meeting, April 11-13, 2007, Lawrence, Kansas.

Badiozamani, K., 1973, The Dorag Dolomitization Model-Application To The middle Ordovician Of Wisconsin: Journal of Sedimentary Petrology, v. 43, p. 965-984.

Baldwin, B., and Butler, C.O., 1985, Compaction Curves: American Association of Petroleum Geologists Bulletin, v. 69, p. 622-626.

Ballard, R.D., Hekinian, R., and Francheteau, J., 1984, Geological setting of hydrothermal activity at 12^{o} 50' N on the East Pacific Rise: a submersible study: Earth and Planetary Science Letters, v. 69, p. 176-186.

Banerjee, S.K., King, J., and Marvin, J., 1994, A Rapid Method For Magnetic Granulometry With Applications To Environmental Studies: Geophysical Research Letters, v. 8, p. 333-336.

Barnes, C.E. and Cochran, J.K., 1990, Uranium removal in oceanic sediments and the oceanic U balance: Earth and Planetary Science Letters, v. 97, p. 94-101.

Bartington Instruments LTD. Operations Manual For MS2 Magnetic Susceptibility System: Oxford, UK: Bartington Instruments LTD, 1989.

Beier, J.A. and Hayes, J.M., 1989, Geochemical and isotopic evidence for paleoredox conditions during deposition of the Devonian-Mississippian New Albany Shale, southern Indiana: Geological Society of America Bulletin, v. 101, p.774-782.

Belknap, W.B., 1959, API Calibration Facility for Nuclear Logs: Drilling and Production Practices. Houston: API.

Berner, R.A., 1970, Sedimentary pyrite formation: American Journal of Science, v. 263, p. 1-23.

Berner, R.A., Baldwin, T., Holden, and G.R. Jr., 1979, Authigenic Iron Sulfides As Paleosalinity Indicators: Journal of sedimentary Petrology, v. 49, p. 1345-1350.

Bloxam, T.W., 1964, Uranium, thorium, potassium and carbon in some black shales from the South Wales coalfield: Geochimica et Cosmochimica Acta, v. 28, p. 1177-1185.

Braun, J.C, 1959, A Stratigraphic Study Of The Sycamore And Related Formations In The Southeastern Anadarko Basin: Oklahoma City Geological Survey Digest III, V. IX-XI, p. 150-164.

Broadhead, R.F., Kepferle, R.C., and Potter, R.C., 1982, Stratigraphic and Sedimentologic Controls of Gas in Shale-Example from Upper Devonian of Northern Ohio: American Association of Petroleum Geologists Bulletin, v. 66, p. 10-27.

Cardott, B.J. and Lambert, M.W., 1987, Thermal Maturation by Vitrinite Reflectance of Woodford Shale, Anadarko Basin, Oklahoma: The American Association of Petroleum Geologists Bulletin, v. 69, p.1983-1998.

Charpentier, R.R. and Schmoker, J.W., 1982, Volume of Organic-Rich Shale in the Appalachian Basin: Relating “Black” to Organic matter: The American Association of Petroleum Geologists Bulletin, v. 66, p. 375-378.

Chenouard, L. and Lalou, C., 1969, Gamma-Ray Spectrometry As A tool For A Rapid Investigation of Detritic Cores: Journal of Sedimentary Petrology, v. 39, p. 1477-1483.

Chitaley, S. and Chongyang, C., 2001, Permineralized Callixylon woods from the late Devonian Cleveland Shale of Ohio, U.S.A. and that of Kettle Point, Ontario, Canada: Review of Paleobotany and Palynology, v. 114, p. 127-144.

Christenson, S., Parkhurst, D.L., and Breit G.N., (1998) Summary of geochemical and geohydrologic investigations in Christenson, Scott, and Havens, J.S., eds., Ground-water quality assessment of the Central Oklahoma aquifer, Oklahoma-Results of investigations: United States Geological Survey Water-Supply Paper 2357-A, p. 107-117.

Cluff, R.M., 1980, Paleoenvironment Of The New Albany Shale Group (Devonian-Mississippian) of Illinois: Journal of Sedimentary Petrology, v. 50, p. 767-780.

Coffey, W.S., 2001, Lithostratigraphy And Porosity Characterization Of The Sycamore Formation (Mississippian), And It’s Relationship To Reservoir Performance, Carter-Knox Field, Grady and Stephens County, Oklahoma: Oklahoma City Geological Survey Shale Shaker Bulletin, V. 52, p. 9-17.

Cole, T., 1989, A Surface to Subsurface Study of the Sycamore Limestone (Mississippian) Along the North Flank of the Arbuckle Anticline: Oklahoma City Geological Survey The Shale Shaker Digest XII, v. XXXVI-XXXIX, p. 205-221.

Comer, J.B., 1991, Stratigraphic Analysis of the Upper Devonian Woodford Formation, Permian Basin, West Texas, and Southeastern New Mexico: Report of Investigations No.201, 63 p.

Comer, J.B. and Hinch, H.H., 1987, Recognizing and Quantifying Expulsion of Oil from the Woodford Formation and Age-Equivalent Rocks in Oklahoma and Arkansas: The American Association of Petroleum Geologists Bulletin, v. 71, p. 844-858.

Cooper, 1926, The Sycamore Limestone: Oklahoma Geological Survey Circular No. 9, 27 p.

Coveney, R.M. Jr., Watney, W.L., and Maples, C.G., 1991, Contrasting depositional models for Pennsylvanian black shale discerned from molybdenum abundances: Geology, v. 19, p. 147-150.

Crane, K. and Ballard, R.D., 1980, The Galapagos Rift At 86^{o} W: Structure And Morphology Of Hydrothermal Fields And Their Volcanic And Tectonic Processes Of The Rift Valley: Journal Of Geophysical Research, v. 85, p. 1443-1454.

Crick, R.E., Elwood, B.B., El Hasani, A., Feist, R., and Hindrich, J., 1997, MagnetoSusceptibility Event and Cyclostratigraphy (MSEC) of the Eifelian-Givetian GSSP and associated boundary sequences in North Africa and Europe: Episodes, v. 20, p. 167-175.

Crick, R.E., Ellwood, B.B., Feist, R., El Hasani, A., Schindler, E., Dreesen, R., Over, J.D., and Girard, C., 2002, Magnetostratigraphy susceptibility of the Frasnian/Famennian boundary: Palaeogeography, Palaeoclimatology, and Palaeoecology, v. 181, p. 67-90.

Cruse, A.M., and Seewald, J.S., 2001, Metal mobility in sediment-covered ridge-crest hydrothermal systems: experimental and theoretical constraints: Geochimica et Cosmochimica Acta, v. 65, p. 3233-3247.

Cruse A.M. and Lyons T.W., 2004, Trace metal records of regional paleoenvironmental variability in Pennsylvanian (Upper Carboniferous) black shales: Chemical Geology, v. 206, p. 319-345.

Cruse, A.M., Paxton, S.T., and Aufill, M., 2006, Uranium diffusion into the Proto-Woodford Shale (Abs.): Geological Society of America Abstracts with Program, Annual Meeting, October 22-25, 2006, Philadelphia, Pennsylvania.

Culp, C.K., 1961, Stratigraphic Relations of the Sycamore limestone in Southern Oklahoma: Oklahoma City Geological Survey The Shale Shaker Digest, v. IX-XI, p. 446-456.

Dearing J. Using the Bartington MS2 System, Kenilworth, UK: Chi Publishing, 1991

Dennis, N.F., 1997, The Woodford Shale In Portions Of Logan County, Oklahoma: Feasibility Of Defining An Algorithm For Mapping And Exploration: Oklahoma State University, M.S. thesis, 62 p.

Deer, W. A., Howie, R.A., and Zussman, L, The Rock Forming Minerals 2nd ed. Essex, UK 1999, p. 696.

Dillon, M. and Bleil, U., 2004, Rock Magnetic signatures in diagenetically altered sediments from the Niger deep-sea fan, Journal of Geophysical Research, v. 3, B03105, 12p.

Doveton, J.H. and Merriam, D.F., 2004, Borehole petrophysical chemostratigraphy of Pennsylvanian black shales in the Kansas subsurface: Chemical Geology, v. 206, p. 249-258.

Dunk, R.M., Mills, R.A., and Jenkins W.L., 2002, A reevaluation of the oceanic uranium budget for the Holocene: Chemical Geology, v.190, p. 45-67.

Ďurža, O., 2004, Interpretation of the magnetic susceptibility record of Senec brickyard loess/ paleosol sequence: Contributions to Geophysics and Geodesy, v. 34, p. 381-386.

Dypvik, H. and Harris, N.B., 2001, Geochemical facies analysis of fine-grained siliciclastics using Th/U, Zr/Rb, and (Zr+Rb)/Sr ratios: Chemical Geology, v. 181, p. 131-146.

Elias, M.K. and Branson, C.C., 1959, Type Section Of The Caney Shale: Oklahoma Geological Survey Circular no. 52, 24 p.

Ellis, D.V., Well Logging For Earth Scientists. New York, NY: Elsevier Science Publishing Co. Inc., 1987. 532p.

Ellwood, B.B., Peter, D.E., Balsam, W., and Scheiber, J., 1995, Magnetic and Geochemical Variations as Indicators of Paleoclimate and Archeological Site Evolution: Examples from 41TR68, Fort Worth, Texas: Journal of Archeological Sciences, v. 22, p. 409-415.

Ellwood, B.B., Crick, R.E., El Hassani, A., Benoist, S.L., and Young, R.H., 2000, Magnetosusceptibility event and cyclostragriphy method applied to marine rocks: Detrital input versus carbonate productivity: Geology, v. 28, p. 1135-1138.

Ellwood, B.B., Crick, R.E., Garcia-Alcalde Fernandez, J.L., Soto, F.M., Truyóls-Massoni, M., El Hassani, A., and Kovas, E.J., 2001, Global correlation using magnetic susceptibility data from lower Devonian rocks: Geology, v. 29, p. 583-586.

Ellwood, B.B., MacDonald, W.D., Wheeler, C., and Benoist, S.L., 2003a, The K-T boundary in Oman: identified using magnetic susceptibility field measurements with geochemical confirmation: Earth and Science Planetary Letters, v. 206, p. 529-540.

Ellwood, B.B., Harrold, F.B., Benoist, S.L., Thacker, P., Otte, M., Bonjean, D., Long, G.J., Shahin, A.M., Hermann, R., and Grandjean, F., 2003b, Magnetic susceptibility applied as an age-depth-climate relative dating technique using sediments from Scladina Cave, a late Pleistocene cave site in Belgium: Journal of Archeological Science, v. 31, p. 283-293.

Ellwood, B.B., Benoist, S.L., El Hassani, A., Wheeler, C., and Crick, R.E., 2003c, Impact Ejecta Layer from the Mid-Devonian: Possible Connection to Global Mass Extinctions: Science, v. 300, p. 1734-1740.

Ellwood, B.B., Garcia-Alcalde, J.L., Al Hassani, A., Hladil, J., Soto, F.M., Truyóls-Massoni, M., Weddige, K., and Koptikova, L., 2006, Stratigraphy of the Middle Devonian boundary: Formal definition of the susceptibility magnetostratotype in Germany with comparisons to sections in the Czech Republic, Morocco and Spain: Tectonophysics, v. 418, p. 31-49.

Ettensohn, F.R., Fulton, L.P., and Kepferle, R.C., 1979, Use of scintillometer and gamma-ray logs for correlation and stratigraphy in homogeneous black shales: Summary: Geological Society of America Bulletin, v. 90, p. 421-423.

Ettensohn, F.R., 1995, Global and Regional Controls on the Origin of Organic Matter in Devonian-Mississippian Black Shales of North America: Houston Geological Society Bulletin, January, 1995, p. 12-17.

Evans, M.A. and Elmore, R.D., 2006, Fluid control of localized mineral domains in limestone pressure solution structures: Journal of Structural Geology, v. 28, p. 284-301.

Faure, G., 1991, Principles And Applications Of Geochemistry 2nd ed. New Jersey: Prentice Hall, p. 600.

Fay, R.O., 1989, Geology Of The Arbuckle Mountains Along Interstate 35, Carter and Murray Counties, Oklahoma: Oklahoma Geological Survey Guidebook, v. 26, p. 1-50.

Fertl, W.H., 1979, Gamma-Ray Spectral Logging Data Assist in Geologic Studies: abstract *in* America Association of Petroleum Geologists Association Round Table, v. 63, p.499.

Fertl, W.H., and Chingilarian, G.V., 1989, Hydrocarbon resource evaluation in the Woodford Shale using well logs: Journal of Petroleum Science and Engineering, v. 4, p. 347-357.

Fisher, Q.J., and Wignall, P.B., 2001, Paleoenvironmental controls on the uranium distribution in an Upper Carboniferous black shale (Gastrioceras listeri marine band) and associated strata; England: Chemical Geology, v. 175, p. 605-621.

Fung, I.Y., Meyn, S.K., Tegen, I., Doney, S.C., John, J.G., and Bishop, K.B., 2000, Iron Supply and demand in the upper ocean: Global Biogeochemical Cycles, v. 14, p. 281-295.

Geršl, M., and Hladil, J., 2004, Gamma-ray and magnetic susceptibility across a Frasnian carbonate platform and the search for "punctata" equivalents in stromataporid coral limestone facies in Moravia: Geochemical Quarterly, v. 48, p. 283-292.

Gould, C.N., 1925, Index To The Stratigraphy of Oklahoma. (Decker, C.E., ed.) Norman, OK: Oklahoma Geological Survey. 115p.

Gromet, L.P., Dymek, R.F., and Kortev, R.L., 1984, The "North American Shale composite"- Its compilation, major and trace element characteristics: Geochimica et Cosmochimica Acta, v. 48, p. 2469-2482.

Hallam, A., 1966, The Depth Of Shales With Bituminous Laminae: Marine Geology, v. 5, p. 481-493.

Ham, W.E., 1955, Geology of the Arbuckle Mountains, Oklahoma: Oklahoma Geological Survey Guidebook 3, 61p.

Ham, W.E., 1986, Regional Geology of the Arbuckle Mountains: Oklahoma Geological Survey Special Publication 73-3, 61p.

Hass, W.H. and Huddle, J.W., 1965, Late Devonian And Early Mississippian Age Of The Woodford Shale In Oklahoma, As Determined From Conodonts, United States Geological Survey Professional Paper 525-D, P. D125-D132.

Hester, T.C., Schmoker, J.W., and Sahi, H.L., 1988, Cross sections based on gamma-ray, density, and resistivity logs showing stratigraphic units of the Woodford Shale,

Anadarko, Basin, Oklahoma: U.S. Geological Survey Miscellaneous Field Studies 2054.

Hester T.C., Schmoker, J.W., and Sahi, H.L., 1990, Log-Derived Regional Sourcerock Characteristics of the Woodford Shale, Anadarko Basin, Oklahoma: U.S. Geological Survey Bulletin1866-D, p. D1-D36.

Hester T.C., Schmoker, J.W., and Sahi, H.L., 1992, Tectonic Controls on Deposition and Sourcerock Properties of the Woodford Shale, Anadarko Basin, Oklahoma-Loading, Subsidence, and Forebulge Development: *in* Thormon, C.H. ed., Application of structural geology to mineral and energy resources of the central and western United States: U.S. Geological Survey Bulletin 2012, p. B1-B11.

Hollrah, T.L., 1977, Subsurface Lithostratigraphy Of The Hunton Group, In Parts Of Payne, Lincoln And Logan Counties, Oklahoma

Hoskins, J.H. and Cross, A.T., The Petrification Flora Of The Devonian-Mississippian Black Shale: The Paleobotanist, v. 1, p. 215-238.

Hosterman, J.W. and Whitlow, S.I., 1983, Clay Mineralogy of Devonian Shales in the Appalachian Basin: Geological Survey Professional Paper 1298, 31 p.

House, M.R., 2002, Strength, timing, setting and cause of mid-Palaeozoic extinctions: Palaeogeography, Palaeoclimatology, and Palaeoecology, v. 181, p. 1-25.

Ingall, E.D., Bustin, R.M., and Van Capellan, P., 1993, Influence of water column anoxia on the burial and preservation of carbon and phosphorous in marine shales: Geochimica et Cosmochimica Acta, v. 57, p. 303-316.

Ivanovich M. and Harmon, R.S. Uranium Series Disequilibrium Applications to Environmental Problems. Oxford, U.K.: Clarendon Press, 1982, 571 p.

Joachimski, M.M., and Buggisch, W., 1993, Anoxic events in the late Frasnian-Causes of the Frasnian-Famennian faunal crisis: Geology, v. 21, p. 675-678.

Johnson, J.G., et al., 1985, Devonian eustatic fluctuations in Euramerica: Geological Society of America Bulletin, v. 96, p. 567-587.

Kirkland, D.W., et al., 1992, Johnson, K.S. and Cardott, B.J. eds. Geology and Organic Geochemistry of the Woodford Shale in the Criner Hills and Western Arbuckle Mountains: Oklahoma Geological Survey Circular 93, p. 38-68.

Klemme, H.D. and Ulmishek, G.F., 1991, Effective Petroleum Source Rocks of the World: Stratigraphic Distribution and Controlling Depositional Factors: American Association of Petroleum Geologists Bulletin, v. 75, p. 1809-1852.

Krystyniak, A.M., 2003, Outcrop-Based Gamma-Ray Characterization Of The Woodford Shale Of South-Central Oklahoma, USA: Oklahoma State University, Masters Thesis, p. 160.

Krystyniak, A.M., Paxton, S.T., and Coffey, W.S., 2005, Detailed Outcrop Gamma-Ray Characterization of the Woodford Shale, South-central Oklahoma (Abs.): American Association of Petroleum Geologists Annual Convention, June 19-22, 2005, Calgary, Canada.

Lambert, M.W., 1991, Internal Stratigraphy and Organic Facies of the Devonian-Mississippian Chattanooga (Woodford) Shale in Oklahoma and Kansas: American Association of Petroleum Geologists Bulletin, v.75, p. 163-176.

Lambert, M.W., 1992, Lithology and geochemistry of shale members within the Devonian-Mississippian Chattanooga (Woodford) Shale, Midcontinent, USA: University of Kansas, Ph.D. Dissertation, p. 238.

Lambert, M.W., 1994, Revised Upper Devonian and Lower Mississippian Nomenclature in Kansas: Kansas Geological Survey Bulletin 230, p. 75-78.

Larasoaña, J.C., Roberts, A.P., Hayes, A., Wehausen, R., and Rohling, E.J., 2006, Detecting missing beats in the Mediterranean climate rhythm from magnetic identification of oxidized sapropels (Ocean Drilling Program Leg 160): Physics of the Earth and Planetary Interiors, v. 156, p. 283-293.

Ledbetter, M.T., 1986, Bottom-current pathways in the Argentine Basin revealed by mean silt particle size: Nature, v. 321, p. 423-425.

Leventhal, J.S., and Hosterman, J.W., 1982, Chemical and Mineralogical Analysis of Devonian Black Shale Samples from Martin County, Kentucky; Carroll and Washington Counties, Ohio; Wise County, Virginia; and Overton County, Tennessee, U.S.A.: Chemical Geology, v. 37, p.239-264.

Leventhal, J.S., Briggs, P.H., and Baker, J.W., 1983, Geochemistry of the Chattanooga Shale, Dekalb County, Central Tennessee: Chemical Geology: v. 37, p.101-116.

Li. Y. L., Vali, H., Yang. J., and Zhang, C.L., 2006, Reduction of Iron Oxides Enhanced by a Sulfate-Reducing Bacterium and Biogenic H_2S: Geomicrobiology Journal, v. 23, p. 103-117.

Liu, J., Zhu, R., and Li, G., et al., 2003, Rock magnetic properties of the fine-grained sediment on the outer shelf of the East China Sea: implication for provenance: Marine Geology, v. 193, p. 195-206.

Lüning, S., Loydell, D.K., Sutcliffe, A., Ait Salem, A., Zanella, E., Craig, J., and Harper, A.T., 2000, Silurian-Lower Devonian Black Shales In Morocco: Which Are The Richest Horizons? : Geology, v. 23, p. 293-311.

Lüning, S., Adamson, K., and Craig, J., 2003a, Frasnian organic-rich shales in Africa: regional distribution and depositional model in New Themes and Developing Technologies. In Arthur, T.J., et al., eds. Geological Society, London: Special Publications v.207, p. 165-184.

Lüning, S. and Kolonic, S., 2003, Uranium Spectral Gamma-Ray Response As A Proxy For Organic Richness in Black Shales: Applicability And Limitations: Journal of Petroleum Geology, v. 26, p. 153-174.

Lüning, S., Wendt, J., Belka, Z., and Kaufmann, B., 2004, Temporal-spatial reconstruction of the early Frasnian (Late Devonian) anoxia in NW Africa: new field data from the Ahnet Basin (Algeria): Sedimentary Geology, v. 163, p. 237-264.

Lyons, T.W., and Severmann, S., 2006, A critical look at iron paleoredox proxies: New insights from modern euxinic marine basins: Geochimica et Cosmochimica Acta, V. 70, p. 5698- 5722.

Maxwell, R.W., 1959, Post-Hunton Pre-Woodford Unconformity In Southern Oklahoma: in AAPG Special Publications, Petroleum Geology Of Southern Oklahoma, v. 2, p.101-126.

McCarthy, P.J., 2002, Micromorphology and development of interfluve paleosols: a case study from the Cenomanian Dunvegan Formation, NE British Columbia, Canada: Bulletin of Canadian Petroleum Geology, v. 50, p. 158-177.

McGee, G.R., 1996, The Late Devonian Mass Extinction The Frasnian/Famennian Crisis: New York, Columbia University Press, 1996. 303 p.

Meyer, B.L., and Nederlof, M.H., 1984, Identification of Source Rocks on Wireline Logs by Density/Resistivity and Sonic Transit Time/Resistivity Crossplots: The American Association of Petroleum Geologists Bulletin, v. 68, p. 121-129.

Michie, U.M. and Cooper, D.C., 1979, Uranium in the Old Red Sandstone: Institute Of Geological Sciences Report 78/16, 35 p.

Montgomery, S.L., et al., 2005, Mississippian Barnett Shale, Fort Worth basin, north central Texas: Gas-shale play with multi-trillion cubic foot potential; American Association of Petroleum Geologists Bulletin, v. 89, p. 155-175.

Moretti, I., Díaz Martínez, E., Montemurro, G., Aguilera, E., and Pérez, M., 1995, The Bolivian Source Rocks Sub Andean Zone Madre de Dios Chaco: Oil and Gas Science and Technology, v.50, p. 753-777.

Morgans-Bell, H.S. and Cohen, A.S., 2004, Organic-carbon burial, climate change and ocean chemistry (Mesozoic-palaeogene): Journal of the Geological Society, London, v. 161, p. 653-653

Morton, J.P., 1985, Rb/Sr dating of diagenesis and source age of clays in Upper Devonian black shales of Texas: v. 96, p. 1043-1049.

Nagata, T., 1961, Rock Magnetism: Tokyo, Japan: Maruzen Company LTD., 1961, 350 p.

Nash, A.J., and Pittman, E.D., 1975, Ferro-Magnesian Calcite Cement In Sandstones: Journal of Sedimentary Petrology, v. 45, p. 258-265.

Novosel, I., Spence, G.D., and Hyndman, R.D., 2005, Reduced magnetization produced by increased methane flux at a gas hydrate vent: Marine Geology, v. 216, p. 265-274.

O'Brien, N.R., 1995, Origin Of Shale Fabric-Clues From Framboids: Northeastern Geology and Environmental Sciences, v. 17, p. 146-150.

Olson, R.K., 1982, Factors Controlling Uranium Distribution in Upper Devonian-Lower Mississippian Black shales of Oklahoma and Arkansas: The University of Tulsa, M.S. thesis, p. 208.

Ormiston, A.R., and Oglesby, R.J., 1995, Effect of Late Devonian Paleoclimate on Source Rock Quality and Location in Alain-Yves Huc (ed.) Paleogeography, Paleoclimate, and Source Rocks: Special Publication, American Association of Petroleum Geologists. P. 105-132.

Over, D.J., 1992a, Conodont biostratigraphy of the Woodford Shale (late Devonian-Early Carboniferous) in the Arbuckle Mountains, south-central Oklahoma: Texas Tech University, M.S. Thesis, p. 190.

Over, D.J., 1992b, Conodonts and the Devonian-Carboniferous Boundary in the Upper Woodford Shale, Arbuckle Mountains, South-Central Oklahoma: Journal of Paleontology, V. 66, p. 293-311.

Over, D.J., 2000, Conodonts From The Upper Olentangy Shale (Upper Devonian Central Ohio) And Stratigraphy Across The Frasnian- Famennian Boundary: Journal of Paleontology, v. 74, p. 101-112.

Over, D.J., 2002, The Frasnian/Famennian boundary in central and eastern United States: Paleogeography, Palaeoclimatology, and Palaeoecology, v. 181, p. 153-169.

Over, D.J. and Barrick, J.E., 1990, The Devonian Carboniferous Boundary in the Woodford Shale, Lawrence Uplift, South-Central Oklahoma: Oklahoma Geological Survey Guidebook, # 27, p. 63-71.

Over, D.J. and Rhodes, M.K., 2000, Conodonts From The Upper Olentangy Shale (Upper Devonian, Central Ohio) and Stratigraphy Across The Frasnian Famennian Boundary: Journal of Paleontology, v. 74, p. 101-111.

Paxton, S.T., Cruse, A.M., and Krystyniak, A.M., 2006a, Detailed Fingerprints of Global Sea-level Change Revealed in Upper Devonian / Lower Mississippian Woodford Shale of South-central Oklahoma (Abs.): American Association of Petroleum Geologists Annual Convention, April 9-12, 2006, Houston, Texas.

Paxton, S.T., Cruse, A.M., and Krystyniak, A.M., 2006b, Detailed Fingerprints of Global Sea-level Change Revealed in Upper Devonian / Lower Mississippian Woodford Shale of South-central Oklahoma: Search and Discovery Article 4211, American Association of Petroleum Geologists, Posted September 21, 2006. (http://www.searchanddiscovery.net/documents/2006/06095paxton/index.htm).

Paxton, S.T., Cruse, A.M., Puckette, J.O., and Aufill, M., 2006, Depositional habitat for Paleozoic mudrock interpreted from analysis of spectral gamma-ray response (Abs.): Geological Society of America Abstracts with Program, Annual Meeting, October 22-25, 2006, Philadelphia, Pennsylvania.

Paxton, S.T., Cruse, A.M., Puckette, J.O., and Aufill, M., 2007, Discriminating Depositional Habitat and Provenance of Mudrock through Use of Spectral Gamma-Ray (Abs.): American Association of Petroleum Geologists Annual Convention, April 1-4, 2007, Long Beach, California

Peace, H.W., 1994, Mississippian Facies Relationships Eastern Anadarko Basin, Oklahoma: Oklahoma City Geological Society Shale Shaker Digest, v. XIII, p. 193-202.

Pearson, S.J., Marshall, J.E.A., and Kemp, E.S., 2004, The White Stone Band of the Kimmeridge Clay Formation, an integrated high-resolution approach to

understanding environmental change: Journal of the Geological Society, London, v. 161, p. 675-683.

Postma, G. and ten Veen, J.H, Astronomically and tectonically linked variations in gamma-ray intensity I Late Miocene hemipelagic successions of the Eastern Mediterranean Basin: Sedimentary Geology, v. 128, p. 1-12.

Prestridge, J.D., 1957, A Subsurface Stratigraphic Study of the Sycamore Formation in the Ardmore Basin: Unpublished MS Thesis, University of Oklahoma.

Pybas K., Cemen, I., and Al-Shaaieb, Z., 1995, The Collings Ranch Conglomerate of the Oklahoma Arbuckles: Its Origin and Tectonic Significance: Oklahoma Geological Survey Circular 97, p. 132-143.

Quinby-Hunt, M.S., Orth, C.J., and Berry, W.B.N, 1989, Elemental geochemistry of black shales-statistical comparison of low-calcic shales with other shales, Grauch, R.I. and Leventhal, J.S. Eds., Metalliferous Black Shales and Related Ore Deposits, United States Geological Survey Circular, v. 1037, p. 93-104.

Raiswell, R., Newton, R., and Wignall, P.B., 2001, An Indicator Of Water-Column Anoxia: Resolution Of Biofacies Variations In The Kimmeridge Clay (Upper Jurassic, U.K.): Journal of Sedimentary Research, v. 71, p. 286-294.

Raup, D.M., and Sepkowski, J.J. Jr., 1982, Mass extinction in the marine fossil record: Science, v. 215, p. 1501-1503.

Retallack, G.J., 1997, A Colour Guide To Paleosols. New York, NY: Wiley and Sons, Inc., p.175.

Retallack, J.G., 2001, Soils of the Past. London, UK: Blackwell Science Ltd., 404p.

Retallack, et al., 2003, Magnetic Susceptibility of Early Paleozoic and Precambrian paleosols: Paleogeography, Palaeoclimatology, Palaeoecology, v. 198, p. 373-380.

Rickard D.T., 1970, The origin of framboids: Lithos, v. 3, p. 269-293.

Rimmer, S.M., 2004a, Geochemical paleoredox indicators in Devonian-Mississippian black shales, Central Appalachian Basin: Chemical Geology, v. 206, p. 373-391.

Rimmer, S.M., 2004b, Multiple controls on the preservation of organic matter in Devonian-Mississippian marine black shales: geochemical and petrographic evidence: Paleogeography, Palaeoclimatology, Palaeoecology, v. 215, p. 125-154.

Rottman, K., 2000, Defining the Role of Woodford-Hunton Depositional Relationships in Hunton Stratigraphic Traps of Western Oklahoma: Oklahoma Geological Survey Circular 101, p. 139-146.

Russell, D.J., 1985, Depositional Analysis Of A Black Shale Using Gamma-Ray Stratigraphy: The Upper Devonian Kettle Point Formation Of Ontario: Bulletin Of Canadian Petroleum Geology, v. 33, p. 236-253.

Sachs, S.D. and Ellwood, B.B., 1988, Controls on magnetic grain-size variations and concentration in the Argentine Basin, South Atlantic Ocean: Deep-Sea Research, v. 35, p. 929-942.

Scheiber, J., 1994, Evidence for high energy events and shallow-water deposition in the Chattanooga Shale, Devonian, central Tennessee, USA: Sedimentary Geology, v. 93, p. 193-208.

Scheiber, J. and Baird, J., 2001, On the Origin and Significance of Pyrite Spheres in Devonian Black Shales of North America: v. 71, p. 155-166.

Scheiber, J., and Ellwood, B.B., 1993, Determination Of Basinwide Paleocurrent Patterns In A Shale Succession From Anisitropy Of Magnetic susceptibility (AMS) A Case Study Of The Mid-Proterozoic Newland Formation, Montana: Journal of Sedimentary Petrology, v. 63, p. 874-880.

Scheiber, J. and Riciputi, L., 2004, Pyrite ooids in Devonian Black Shales record intermittent sea-level drop and shallow-water conditions: Geology, v. 32, p. 305-308.

Schmoker, J.W., 1980, Organic content of Devonian Shales in Western Appalachian Basin: The American Association of Petroleum Geologists Bulletin, v. 64, p. 2156-2165.

Schmoker, J.W., 1981, Determination of Organic-Matter Content of Appalachian Devonian Shales from Gamma-Ray Logs: Schmoker: The American Association of Petroleum Geologists Bulletin, v. 65, p. 1205-1298.

Schmoker, J.W., 1993, Use of formation density logs to determine organic-carbon content in Devonian shales of the western Appalachian Basin and an additional example based on the Bakken Formation of the Williston Basin: US Geological Survey Bulletin 1909, p. J1-J14.

Schmoker, J.W. and Hester, T.C., 1983, Organic Carbon in Bakken Formation, United States Portion of Williston Basin: The American Association of Petroleum Geologists Bulletin, v. 67, p. 2165-2174.

Schumm, S., 1991, To Interpret the Earth Ten ways to be wrong: UK, Cambridge University Press p.133.

Schwartzapfel, J.A. and Holdsworth, B.K. Upper Devonian And Mississippian Radiolarian Zonation And Biostratigraphy Of The Woodford, Sycamore, Caney and Goddard Formations, Oklahoma. Cambridge, MA: Cushman Foundation For Foraminiferal Research, Inc., Department of Invertebrate Paleontology, Museum of Comparative Zoology, Harvard University, 1996, 275p.

Seewald, J., Cruse, A., and Saccocia, P., 2003, Aqueous volatiles in hydrothermal fluids from the Main Endeavour Field, northern Juan de Fuca Ridge: temporal variability following earthquake activity: Earth and Planetary Science Letters, v. 216, p. 575-590.

Sepkoski, J.J. Jr., 1986, Phanerozoic Overview of Mass Extinction *in* Patterns and Processes in the History of Life: Raup, D.M. and Jablonski eds., p. 277-295.

Siy, S.E., 1988, Geochemical and Petrographic Study of Phosphate Nodules of the Woodford Shale (UpperDevonian-Lower Mississippian) 0f Southern Oklahoma: Texas Tech University, M.S. thesis, p. 172.

Sorauf, J.E., 1986, Late Devonian rugose corals and the Frasnian-Famennian crisis: Canadian Journal of Earth Science, v. 23, p. 1265-1287.

Sternbach, C.A, 1984, Deep-Burial Diagenesis And Dolomitization In The Hunton Group Carbonate Rocks (Upper Ordovician To Lower Devonian) In The Anadarko Basin Of Oklahoma And Texas, USA: Rensselaer Polytechnic Institute, Ph.D. Dissertation, p. 158.

Sullivan, K.L., 1985, Organic Facies Variation of the Woodford Shale in Western Oklahoma: Oklahoma City Geological Survey Shale Shaker Digest XI, v. XXXIII-XXXV, p.185-198.

Swanson, V.E., 1961 Geology and Geochemistry of Uranium in Marine Black Shales: Geological Survey Professional Paper 356-C, 110 p.

Tarr, R.S., 1955, Paleogeologic Map At The Base of Woodford, And Hunton Isopachous Map Of Oklahoma: Bulletin Of The American Association Of Petroleum Geologists, v. 39, p. 1851-1858.

Taylor, S.R. and McClennan, S.M., 1985, The Continental Crust: Its Composition and Evolution., Blackwell, Oxford.

Tribovillard, N., Algeo, T.J., Lyons, T., and Riboulleau, A., 2006, Trace metals as paleoredox and paleoproductiivity proxies: An update: Chemical Geology, v. 232, p. 13-32.

Tyson, R.V., 2004, Variation in marine total organic carbon content through the type Kimmeridge Clay Formation (Late Jurassic), Dorset, UK: Journal of the Geological Society, London, V. 161, p. 667-673

Vlag, P.A., Kruvier, P.P., and Dekkers, M.J., 2004, Evaluating climate change by multivariate statistical techniques on magnetic and chemical properties of marine sediments (Azores region): Palaeogeography, Palaeoclimatology, and Palaeoecology: v. 212, p. 23-44.

Vine, J.D., and Tourtelot, E.B., 1970, Geochemistry of black shale deposits- A summary report: Economic Geology, v. 65, p. 253-272.

Watson, J.V. and Plant, J., 1979, Regional geochemistry of uranium as a guide to deposit formation: Phil. Trans. R. Soc. London A. 291, p. 321-338.

Weedon, G.P., Coe, A.L., and Gallois, R.W., 2004, Cyclostratigraphy, orbital tuning and inferred productivity for the type Kimmeridge Clay (Late Jurassic) Southern England: Journal of the Geological Society, London, v. 161, p. 665-681.

Wendt, J., Belka, Z., 1991, Age and Depositional Environment of Upper Devonian (Early Frasnian to Early Famennian) Black Shales and Limestone Kellwasser Facies in the Eastern Anti-Atlas, Morocco: Facies, v. 1991, p. 51-90.

Wignall, P.B. and Myers, K.J., 1988, Interpreting benthic oxygen levels in mudrocks: A new approach: Geology, v. 16. p. 452-455.

Zaback, D.A., Pratt, L.M., and Hayes, J.M., 1993, Transport and reduction of sulfate and immobilization of sulfide in marine black shales: Geology, v. 21, p. 141-144.

Zachara, J.M., Kukkadapu, R.K., Gassman, P.L., Dohnalkova, A., Fredrickson, J,K,, and Anderson, T., 2004, biogeochemical transformation of Fe minerals in a petroleum-contaminated aquifer: Geochimica et Cosmochimica, v. 68, p. 17.

APPENDIX

Appendix 1. Magnetic susceptibility and spectral gamma-ray data from Hass A.

Data pair #	MS SI Units *	K wt. %	U (ppm)	Th (ppm)	Gamma-Ray (API Units)	Lithology **	height above base (ft.)	height above base (m)
458	N	0.7	27.7	5.3	254	FN	228.5	69.6
457	N	0.6	23.8	4.7	218.8	FN	228	69.5
456	N	0.7	23.8	5.6	224	FN	227.5	69.3
455	-1	0.5	17.6	2.3	158	S	227	69.2
454	-1	0.7	12.3	3.8	124.8	S	226.5	69
453	0	0.5	8.9	3.2	92	S	226	68.9
452	-0.5	0.5	12	3.6	118.4	S	225.5	68.7
451	1.5	0.3	15.2	3.4	140	T	225	68.6
450	0	0.6	16.6	4.7	161.2	S	224.5	68.4
449	-0.5	0.4	25	4.4	224	S	224	68.3
448	-0.5	0.7	17.2	3.4	162.4	S	223.5	68.1
447	0	0.3	15.8	4.4	148.8	S	223	68
446	0.5	0.9	15.3	3.7	151.6	S	222.5	67.8
445	3.5	1.4	24.2	6.1	240.4	F	222	67.7
444	-0.5	1	17.1	4.4	170.4	S	221.5	67.5
443	6	1.1	28	5.2	262.4	F	221	67.4
442	-1	0.7	25.2	4.1	229.2	S	220.5	67.2
441	-0.5	0.6	41.4	6.3	366	S	220	67.1
440	-0.5	0.9	22.2	5.2	212.8	S	219.5	66.9
439	-0.5	1	21.3	4.5	204.4	S	219	66.8
438	1	0.9	29.3	3.7	263.6	F	218.5	66.6
437	0.5	1	38.2	3.8	336.8	S	218	66.4
436	0.5	1.3	32	3.9	292.4	T	217.5	66.3
435	0.5	1	18.8	3.8	181.6	F	217	66.1
434	3	0.8	11.8	2.9	118.8	F	216.5	66
433	0	0.5	13.8	1	122.4	S	216	65.8
432	2	0.7	11.6	1.3	109.2	F	215.5	65.7
431	1	0.6	14.2	5.1	143.6	F	215	65.5
430	0.5	0.4	15	4.2	143.2	S	214.5	65.4
429	3	0.4	14.8	2.4	134.4	S	214	65.2

Data pair #	MS SI Units *	K wt. %	U (ppm)	Th (ppm)	Gamma-Ray (API Units)	Lithology **	height above base (ft.)	height above base (m)
428	0.5	0.4	12.7	1.3	113.2	F	213.5	65.1
427	-0.5	0.4	13.6	2.3	124.4	S	213	64.9
426	0.5	0.6	14	2.9	133.2	S	212.5	64.8
425	-0.5	0.4	16.6	2	147.2	S	212	64.6
424	0	0.3	10.7	4.1	106.8	S	211.5	64.5
423	0	0.2	10	1.6	89.6	S	211	64.3
422	0	0.4	8.6	1.2	80	S	210.5	64.2
421	0.5	0.1	9.2	0.6	77.6	S	210	64
420	0	0.5	7.4	3.5	81.2	S	209.5	63.9
419	0	0.5	12.7	3.4	123.2	S	209	63.7
418	0	0.7	11.5	1.9	110.8	S	208.5	63.6
417	0	0.8	11.8	4.3	124.4	S	208	63.4
416	1	0.7	13.3	3.5	131.6	T	207.5	63.2
415	0	0.7	10.8	2.5	107.6	S	207	63.1
414	0	0.6	11.2	4	115.2	T	206.5	62.9
413	1	0.3	8.8	1.5	81.2	F	206	62.8
412	0	0.7	11.8	2.8	116.8	S	205.5	62.6
411	1	0.6	13.7	2.5	129.2	S	205	62.5
410	1.5	0.8	12.5	2.6	123.2	S	204.5	62.3
409	3.5	0.6	17	2.5	155.6	F	204	62.2
408	1	0.6	16.5	4.2	158.4	S	203.5	62
407	3	0.7	18	4.7	174	F	203	61.9
406	2	0.7	21.4	5.9	206	S	202.5	61.7
405	0	0.6	23.6	3	210.4	S	202	61.6
404	1	0.9	22.7	3.2	208.8	S	201.5	61.4
403	0.5	0.5	26	4.4	233.6	S	201	61.3
402	2.5	1	24.5	4.5	230	F	200.5	61.1
401	0	0.7	30.9	4.9	278	S	200	61
400	1	0.8	30.3	3	267.2	F	199.5	60.8
399	0.5	0.7	28.8	2.5	251.6	F	199	60.7
398	3	0.6	29.3	4.6	262.4	F	198.5	60.5
397	2	1	28	5.6	262.4	S	198	60.4

Data pair #	MS SI Units *	K wt. %	U (ppm)	Th (ppm)	Gamma-Ray (API Units)	Lithology **	height above base (ft.)	height above base (m)
396	7	1	26.9	5.5	253.2	F	197.5	60.2
395	3.5	1	27.9	5.3	260.4	F	197	60
394	1	1.2	32.5	4	295.2	S	196.5	59.9
393	1	0.7	37.7	3.4	326.4	S	196	59.7
392	4	1.1	38.3	7.5	354	F	195.5	59.6
391	1	1.4	38.9	4.4	351.2	S	195	59.4
390	0.5	0.9	35.7	5	320	S	194.5	59.3
389	6	0.6	39.1	4.3	339.6	F	194	59.1
388	1.5	1.2	34	3.2	304	S	193.5	59
387	0	1.4	39.4	7.3	366.8	S	193	58.8
386	4	1	44.9	5.1	395.6	F	192.5	58.7
385	1	1.2	44	4	387.2	S	192	58.5
384	3.5	1.3	45.2	5.4	404	F	191.5	58.4
383	3.5	1	47.1	5.5	414.8	F	191	58.2
382	2	1.4	48.3	5	428.8	F	190.5	58.1
381	1	1.6	50.1	5.6	448.8	S	190	57.9
380	1	1.6	49.7	8.2	456	T	189.5	57.8
379	6	1.5	45.4	6.7	414	F	189	57.6
378	1	1.1	46.9	6	416.8	S	188.5	57.5
377	0.5	1.4	42.5	6.1	386.8	S	188	57.3
376	1	1.7	42.9	5.6	392.8	S	187.5	57.2
375	0.5	0.9	42.5	8.7	389.2	S	187	57
374	0	1.6	40.9	6.9	380.4	S	186.5	56.8
373	1	1.4	42	6.7	385.2	S	186	56.7
372	0	0.9	45.1	5.2	396	S	185.5	56.5
371	1	1.6	40.6	6.2	375.2	F	185	56.4
370	0	1	30.6	4.1	277.2	S	184.5	56.2
369	0	1.2	30.4	5.4	284	S	184	56.1
368	0	1.6	32.6	4.9	306	S	183.5	55.9
367	2.5	1.1	37.5	5	337.6	F	183	55.8
366	0.5	1.8	34.3	8.5	337.2	S	182.5	55.6
365	0.5	1.3	37.7	7.4	352	S	182	55.5

Data pair #	MS SI Units *	K wt. %	U (ppm)	Th (ppm)	Gamma-Ray (API Units)	Lithology **	height above base (ft.)	height above base (m)
364	4.5	1.1	35.8	6.8	331.2	F	181.5	55.3
363	2	0.8	36.4	7.6	334.4	F	181	55.2
362	2	1.1	39.8	4.5	354	S	180.5	55
361	1	1.2	36.7	4.8	332	S	180	54.9
360	1	1.1	40.2	5.4	360.8	F	179.5	54.7
358	0.5	0.9	40.2	6.5	362	F	179	54.6
357	0	1.5	38.1	4.6	347.2	S	178.5	54.4
356	0	1.1	36	4.6	324	S	178	54.3
355	1.5	0.6	35.2	5.4	312.8	F	177.5	54.1
354	0	1	34	5.7	310.8	S	177	53.9
353	1	1.3	31.2	6.9	298	F	176.5	53.8
352	1.5	0.9	31.1	6.3	288.4	F	176	53.6
351	0.5	0.6	32.4	5.6	291.2	T	175.5	53.5
350	1.5	1.1	28.7	4.4	264.8	F	175	53.3
349	6	0.9	29.4	4.9	269.2	F	174.5	53.2
348	6	1.5	24.1	5.2	237.6	F	174	53
347	1	1.2	25.3	4.9	241.2	S	173.5	52.9
346	3	1.3	26.5	5	252.8	S	173	52.7
345	1.5	1.3	27.2	6.6	264.8	S	172.5	52.6
344	3	1	28	7	268	F	172	52.4
343	0.5	1.5	32.7	3.9	301.2	S	171.5	52.3
342	3	1.4	40.4	5.5	367.6	F	171	52.1
341	1	1.6	41.8	5.7	382.8	F	170.5	52
340	0	1.3	41.3	7.5	381.2	S	170	51.8
339	8.5	1.3	41.4	6.3	377.2	F	169.5	51.7
338	1.5	1.6	37.8	4.5	346	S	169	51.5
337	0	1.3	40.4	6.1	368.4	S	168.5	51.4
336	2.5	1.3	40.8	6.7	374	F	168	51.2
335	1	1.4	45.6	5.9	410.8	T	167.5	51.1
334	1	1.3	47.8	8.5	437.2	S	167	50.9
333	6	1.4	54.5	9.3	495.6	F	166.5	50.7
332	6	1.4	41.6	7.1	383.6	F	166	50.6

Data pair #	MS SI Units *	K wt. %	U (ppm)	Th (ppm)	Gamma-Ray (API Units)	Lithology **	height above base (ft.)	height above base (m)
331	2	1.2	41.5	7.3	380.4	S	165.5	50.4
330	3.5	1.1	39.3	3.9	347.6	F	165	50.3
329	1	1.3	36.9	4.1	332.4	S	164.5	50.1
328	1	1.2	39.2	5.7	355.6	S	164	50
327	7	1.7	39	6.5	365.2	F	163.5	49.8
326	0	1.3	44.8	4.8	398.4	S	163	49.7
325	2.5	0.9	41.6	5.2	368	F	162.5	49.5
324	5	1.1	46.4	5.4	410.4	F	162	49.4
323	2	1.4	43.8	5.9	396.4	S	161.5	49.2
322	3	1.1	46.7	6.9	418.8	F	161	49.1
321	0	1.4	48.3	7.9	440.4	S	160.5	48.9
320	0	1.2	50.1	5.8	443.2	S	160	48.8
319	5	1.7	49.8	7.7	456.4	F	159.5	48.6
318	1	0.9	51.7	4.8	447.2	S	159	48.5
317	0.5	1	46	5.9	407.6	S	158.5	48.3
316	6.5	1.3	43	6.1	389.2	F	158	48.2
315	5	1.4	43	5.8	389.6	F	157.5	48
314	1	0.8	36.4	5.4	325.6	T	157	47.9
313	2	1	37.4	4.5	333.2	T	156.5	47.7
312	3	1.4	35.3	6.8	332	F	156	47.5
311	6	1.7	47	5.8	426.4	F	155.5	47.4
310	2	1.7	48.4	6.7	441.2	F	155	47.2
309	2	1.8	48.5	7.1	445.2	S	154.5	47.1
308	2	1.7	50	8.2	460	S	154	46.9
307	2	1.4	50.9	5.8	452.8	T	153.5	46.8
306	3	1.4	46.6	6.6	421.6	F	153	46.6
305	0	1.6	41.7	5.8	382.4	S	152.5	46.5
304	0.5	1.7	46.7	5.8	424	S	152	46.3
303	4	1.4	43.6	5.4	392.8	F	151.5	46.2
302	2.5	1.3	39.1	5.2	354.4	S	151	46
301	3.5	1.2	38	5.3	344.4	F	150.5	45.9
300	2	1.5	39.4	4.9	358.8	F	150	45.7

Data pair #	MS SI Units *	K wt. %	U (ppm)	Th (ppm)	Gamma-Ray (API Units)	Lithology **	height above base (ft.)	height above base (m)
299	3	1	43.6	5.7	387.6	F	149.5	45.6
298	1	1.3	47.8	4.7	422	S	149	45.4
297	3.5	1.4	51.2	5.5	454	F	148.5	45.3
296	13.5	1.9	68.1	10	615.2	F	148	45.1
295	11.5	2	74.3	10.5	668.4	F	147.5	45
294	13	2	97.9	13.3	868.4	F	147	44.8
293	18	2.5	112.6	9.7	979.6	F	146.5	44.7
292	13	2.9	100.6	9.5	889.2	F	146	44.5
291	11	2.1	86.3	10.4	765.6	F	145.5	44.3
290	4	2.2	73.2	10.4	662.4	S	145	44.2
289	6	2.5	69.2	8.2	626.4	F	144.5	44
288	3	2.2	71.7	6.5	634.8	F	144	43.9
287	3.5	2	71.4	6.8	630.4	F	143.5	43.7
286	3.5	1.8	76.7	8.7	677.2	F	143	43.6
285	3	2.3	88.7	8.6	780.8	S	142.5	43.4
284	3	2.6	96.2	13.5	865.2	F	142	43.3
283	8	3	107.1	14.6	963.2	F	141.5	43.1
282	8	4.1	98.7	14.9	914.8	F	141	43
281	7	3.4	94	13.1	858.8	F	140.5	42.8
280	5	3.7	91.2	11.6	835.2	F	140	42.7
279	7	3.3	93.1	12.8	848.8	F	139.5	42.5
278	6	3.4	86.2	11.8	791.2	F	139	42.4
277	4.5	2.5	77.5	8.5	694	F	138.5	42.2
276	4.5	2.7	71.2	12.1	661.2	F	138	42.1
275	6	2.7	67.6	10.6	626.4	F	137.5	41.9
274	2	2.3	67.2	6.3	599.6	S	137	41.8
273	5	2.4	66.4	9.4	607.2	F	136.5	41.6
272	12	2.9	60	9	562.4	F	136	41.5
271	4.5	2.2	60.8	8.7	556.4	T	135.5	41.3
270	8.5	2.1	54	9.4	503.2	F	135	41.1
269	2	2	42.9	6.2	400	S	134.5	41
268	3	2	44.8	7.5	420.4	S	134	40.8

Data pair #	MS SI Units *	K wt. %	U (ppm)	Th (ppm)	Gamma-Ray (API Units)	Lithology **	height above base (ft.)	height above base (m)
267	2	2.3	48.2	7.9	454	T	133.5	40.7
266	2.5	2.4	47.4	9.4	455.2	T	133	40.5
265	5	1.7	45.5	7.4	420.8	F	132.5	40.4
264	3	2.2	38.2	7.4	370.4	S	132	40.2
263	3	2.6	40.2	11.2	408	T	131.5	40.1
262	5.5	3.3	40.3	12.9	426.8	S	131	39.9
261	8.5	2.5	38.4	9	383.2	F	130.5	39.8
260	15.5	2.2	43	8	411.2	F	130	39.6
259	6	2.1	39.8	9.4	389.6	F	129.5	39.5
258	7	2.9	40.1	8.8	402.4	F	129	39.3
257	12	2.7	37.7	9.6	383.2	F	128.5	39.2
256	8	2.8	36.5	11.3	382	F	128	39
255	10	2.8	39.7	8.2	395.2	F	127.5	38.9
254	8	2.4	38.6	9.8	386.4	F	127	38.7
253	3	2.1	32.3	7.2	320.8	F	126.5	38.6
252	6	2.5	35.5	7.9	355.6	S	126	38.4
251	4	2.1	32.8	7.8	327.2	F	125.5	38.3
250	9	2.4	34.2	8.1	344.4	F	125	38.1
249	3	1.9	34.6	5.6	329.6	T	124.5	37.9
248	2.5	2	35.4	7.3	344.4	T	124	37.8
247	1.5	2.1	48.1	7.1	446.8	T	123.5	37.6
246	1	2.1	57.5	10.2	534.4	T	123	37.5
245	2	1.9	52.5	8.9	486	T	122.5	37.3
244	2	2	38.2	7.1	366	T	122	37.2
243	2	1.8	38.4	5.1	356.4	T	121.5	37
242	4	2.1	44.7	8.4	424.8	S	121	36.9
241	4	2.1	41.7	8.3	400.4	F	120.5	36.7
240	4	1.9	38.2	6.7	362.8	F	120	36.6
239	4	1.9	39.3	7.4	374.4	S	119.5	36.4
238	7	2	41	7.6	390.4	F	119	36.3
237	4	1.8	36.8	9.2	360	F	118.5	36.1
236	3	2	33.2	8.1	330	T	118	36

Data pair #	MS SI Units *	K wt. %	U (ppm)	Th (ppm)	Gamma-Ray (API Units)	Lithology **	height above base (ft.)	height above base (m)
235	2.5	2.1	40.6	7.3	387.6	S	117.5	35.8
234	4	2.1	37.9	10.9	380.4	F	117	35.7
233	8	2.7	36.1	7.9	363.6	F	116.5	35.5
232	3	2	41.1	7.5	390.8	F	116	35.4
231	6	2.4	41.6	6.9	398.8	F	115.5	35.2
230	6	2.1	42.7	8	407.2	F	115	35.1
229	4.5	2.2	45.4	7.4	428	S	114.5	34.9
228	9	2.1	41.7	9.5	405.2	F	114	34.7
227	5	2.1	37	7.1	358	F	113.5	34.6
226	3	1.9	39.5	7.5	376.4	T	113	34.4
225	7	2.3	39.4	8.2	384.8	F	112.5	34.3
224	4.5	2.5	44.5	8.3	429.2	F	112	34.1
223	8	2	44.7	8.8	424.8	F	111.5	34
222	4	2.8	47.4	6.2	448.8	F	111	33.8
221	6.5	2.7	50.8	8.6	484	F	110.5	33.7
220	8	2.6	49.3	7.9	467.6	F	110	33.5
219	12	2.2	47.3	10.6	456	F	109.5	33.4
218	8	2.9	44.7	10	444	F	109	33.2
217	6	2.9	44.3	7.5	430.8	F	108.5	33.1
216	6	3.4	48.7	10.2	484.8	F	108	32.9
215	7	2.9	52.5	9.7	505.2	F	107.5	32.8
214	5	2.8	49.8	9.9	482.8	F	107	32.6
213	5	2.5	44.8	10.7	441.2	F	106.5	32.5
212	9	2.2	43.6	7.9	415.6	F	106	32.3
211	6	1.8	36.3	9.3	356.4	F	105.5	32.2
210	5	1.6	28.8	8.6	290.4	F	105	32
209	3	2.4	37.8	8.7	375.6	F	104.5	31.9
208	2	2.4	36.4	7.9	361.2	F	104	31.7
207	2.5	2.2	43.6	7.9	415.6	F	103.5	31.5
206	6.5	3	43.7	10.5	439.6	F	103	31.4
205	4	3.1	40.8	8.1	408.4	F	102.5	31.2
204	2.5	2.8	41.2	8.4	408	S	102	31.1

Data pair #	MS SI Units *	K wt. %	U (ppm)	Th (ppm)	Gamma-Ray (API Units)	Lithology **	height above base (ft.)	height above base (m)
203	6	2.5	36.8	9.7	373.2	F	101.5	30.9
202	3.5	2.2	36.3	10.4	367.2	F	101	30.8
201	3	2.5	37.9	11.1	387.6	F	100.5	30.6
200	4	3	35.2	9.5	367.6	F	100	30.5
199	5	2.9	36.6	10	379.2	F	99.5	30.3
198	3.5	2.7	43.1	8.3	421.2	F	99	30.2
197	4	2.7	40.7	10	408.8	F	98.5	30
196	3.5	2.4	42.6	9.6	417.6	F	98	29.9
195	3.5	2.5	45.6	10.5	446.8	F	97.5	29.7
194	3.5	2.3	43.3	11	427.2	T	97	29.6
193	1	1.8	38.1	7	361.6	T	96.5	29.4
192	0.5	2.3	42.9	8.9	415.6	T	96	29.3
191	0.5	2.2	45.1	10.1	436.4	T	95.5	29.1
190	6	2.1	33.1	7.5	328.4	T	95	29
189	4	1.9	33.4	7.1	326	T	94.5	28.8
188	4	2	37.3	4.9	350	T	94	28.7
187	4	2.3	32.3	7.5	325.2	T	93.5	28.5
186	1	2	34.3	5.7	329.2	T	93	28.3
185	3	2.3	35.9	9.1	360.4	T	92.5	28.2
184	1.5	2.8	41.8	9	415.2	T	92	28
183	3.5	2.1	39.2	8.9	382.8	T	91.5	27.9
182	0.5	1.9	33.9	9.4	339.2	S	91	27.7
181	6	1.9	41.3	5.8	384	F	90.5	27.6
180	2.5	2.4	39.7	8	388	F	90	27.4
179	12	1.7	30.6	6.8	299.2	F	89.5	27.3
178	5	2	36.3	7.7	353.2	T	89	27.1
177	2.5	2.5	36.9	10	375.2	T	88.5	27
176	4	3	40.4	9	407.2	F	88	26.8
175	10.5	1.8	31.8	9	319.2	F	87.5	26.7
174	7.5	2	32	6.3	313.2	F	87	26.5
173	8	2.2	31.2	8.3	318	F	86.5	26.4
172	7	2.2	33.1	9.7	338.8	F	86	26.2

Data pair #	MS SI Units *	K wt. %	U (ppm)	Th (ppm)	Gamma-Ray (API Units)	Lithology **	height above base (ft.)	height above base (m)
171	6	2.1	29.3	7.3	297.2	F	85.5	26.1
170	8	2	31	10.1	320.4	F	85	25.9
169	4	2	30.5	8.8	311.2	T	84.5	25.8
168	8	1.9	34.1	7.8	334.4	T	84	25.6
167	4	2	32.6	6.4	318.4	T	83.5	25.5
166	6	2	36.6	8	356.8	F	83	25.3
165	7	2.1	32.2	4.5	309.2	F	82.5	25.1
164	6	1.2	30.6	7.8	295.2	F	82	25
163	4	2.2	28.4	5.9	286	F	81.5	24.8
162	6	1.4	27.8	8.8	280	F	81	24.7
161	5	1.9	30.8	6.8	304	F	80.5	24.5
160	5	1.7	29.5	5.5	285.2	F	80	24.4
159	10	1.8	35.3	5.4	332.8	F	79.5	24.2
158	7	1.5	32	8.3	313.2	F	79	24.1
157	6	1.5	31.5	7.8	307.2	F	78.5	23.9
156	2.5	1.9	37.9	8.2	366.4	S	78	23.8
155	4.5	1.8	38.9	6	364	F	77.5	23.6
154	4	2.1	39	8.9	381.2	F	77	23.5
153	6	2.5	38.4	5.9	370.8	F	76.5	23.3
152	5	1.8	41.3	6.8	386.4	F	76	23.2
151	9	1.8	41.7	7.6	392.8	F	75.5	23
150	9	2.2	37.7	7.4	366.4	F	75	22.9
149	3.5	1.8	35.8	7.4	344.8	S	74.5	22.7
148	9	2.2	42.4	8.4	408	F	74	22.6
147	2.5	1.9	41.2	7.9	391.6	S	73.5	22.4
146	10.5	1.5	36.6	6.9	344.4	F	73	22.3
145	4	1.3	38.6	6.6	356	T	72.5	22.1
144	9	1.8	38	6.5	358.8	F	72	21.9
143	3	1.9	39.4	11.9	393.2	S	71.5	21.8
142	8	2	43.9	7.1	411.6	F	71	21.6
141	5	1.9	41.6	9.4	400.8	S	70.5	21.5
140	7	2.1	45.4	9.3	434	F	70	21.3

Data pair #	MS SI Units *	K wt. %	U (ppm)	Th (ppm)	Gamma-Ray (API Units)	Lithology **	height above base (ft.)	height above base (m)
139	4	1.9	43.3	10.1	417.2	F	69.5	21.2
138	1	1.8	39.2	8.1	374.8	T	69	21
137	3	2	39.6	10.1	389.2	T	68.5	20.9
136	6.5	2	39.7	8.5	383.6	F	68	20.7
135	7	2.4	35.4	9	357.6	F	67.5	20.6
134	3	2	32.8	10.5	336.4	T	67	20.4
133	7	1.9	42	7.8	397.6	F	66.5	20.3
132	6	2.2	44.2	10.1	429.2	F	66	20.1
131	6	1.4	39.7	7.2	368.8	F	65.5	20
130	5	1.9	37.4	5.7	352.4	S	65	19.8
129	3.75	1.5	41.8	7.9	390	F	64.5	19.7
128	3	1.7	42.3	8.1	398	F	64	19.5
127	4	2	43.5	8.8	415.2	S	63.5	19.4
126	7.5	1.6	42.3	7.8	395.2	F	63	19.2
125	6	2	51	6.3	465.2	F	62.5	19.1
124	1.5	1.4	41.9	6	381.6	F	62	18.9
123	1.5	1	44.4	6.4	396.8	F	61.5	18.7
122	3	1.5	42.7	6.7	392.4	F	61	18.6
121	3	1.5	42	6.4	385.6	F	60.5	18.4
120	5	1.6	39.2	7.8	370.4	F	60	18.3
119	4	1.8	36.7	6.9	350	F	59.5	18.1
118	4.5	1.5	41.4	6.3	380.4	F	59	18
117	10.5	1.7	35.9	6.2	339.2	F	58.5	17.8
116	9.5	1.2	35.7	4.8	324	F	58	17.7
115	8	1.6	33.8	8	328	F	57.5	17.5
114	4	1.1	34	5.5	311.6	F	57	17.4
113	5	1.3	33	5.1	305.2	F	56.5	17.2
111	3	1.6	34.3	7.1	328.4	T	55.5	16.9
110	1	1.4	42.8	9	400.8	F	55	16.8
109	4	2.1	43.2	7.7	410	F	54.5	16.6
108	7	1.9	40.3	10.4	394.4	F	54	16.5
107	4	1.9	39.9	8.1	382	S	53.5	16.3
106	5	2.2	53.6	8.4	497.6	F	53	16.2

Data pair #	MS SI Units *	K wt. %	U (ppm)	Th (ppm)	Gamma-Ray (API Units)	Lithology **	height above base (ft.)	height above base (m)
105	3	2.4	51.4	10.7	492.4	F	52.5	16
104	5.5	2	51	10.6	482.4	F	52	15.8
103	3	2.1	53.1	8.8	493.6	S	51.5	15.7
102	2	2.5	43	10.3	425.2	S	51	15.5
101	2	1.9	31.7	7.2	312.8	F	50.5	15.4
100	2	2	30	7.2	300.8	F	50	15.2
99	1	1.5	28.6	6.2	277.6	F	49.5	15.1
98	6.5	1.5	31.4	6.1	299.6	F	49	14.9
97	4.5	2	34.3	9.2	343.2	F	48.5	14.8
96	7	2.1	35.1	6.7	341.2	F	48	14.6
95	6	1.7	32.7	8.8	324	F	47.5	14.5
94	4	1.6	33.9	9.3	334	F	47	14.3
93	3.5	1.6	26.8	5.2	260.8	F	46.5	14.2
92	2	1.1	31.3	7.8	299.2	F	46	14
91	1	1.7	30.1	7.9	299.6	F	45.5	13.9
90	1	1.5	30.1	5.5	286.8	F	45	13.7
89	2.5	1.5	29.2	7.7	288.4	S	44.5	13.6
88	4.5	1.5	27.4	9.7	282	F	44	13.4
87	2	1.4	29.1	10.5	297.2	F	43.5	13.3
86	2.5	1.4	28	6.3	271.6	F	43	13.1
85	2.5	1.3	29.3	5.1	275.6	F	42.5	13
84	3.5	1.5	25.3	3.8	241.6	F	42	12.8
83	2.5	1.8	26.9	7.5	274	T	41.5	12.6
82	5	1.5	29.1	9.8	296	F	41	12.5
81	3	1.7	36.8	7.7	352.4	F	40.5	12.3
80	7	1.9	34.8	7.2	337.6	F	40	12.2
79	4	1.8	31.2	8.7	313.2	F	39.5	12
78	5.5	2	30.1	7.6	303.2	F	39	11.9
77	6	2.4	31.4	4.1	306	F	38.5	11.7
76	7	1.7	30.4	7.2	299.2	F	38	11.6
75	5	1.6	31.7	8	311.2	F	37.5	11.4
74	4	2.2	28.1	9.7	298.8	F	37	11.3
73	6	2.3	29.6	8.1	306	F	36.5	11.1

Data pair #	MS SI Units *	K wt. %	U (ppm)	Th (ppm)	Gamma-Ray (API Units)	Lithology **	height above base (ft.)	height above base (m)
72	5	2	27.2	8.5	283.6	F	36	11
71	3	1.9	27.5	8.5	284.4	S	35.5	10.8
70	4	2.2	30.7	7.9	312.4	F	35	10.7
69	4	1.7	30.5	7.9	302.8	F	34.5	10.5
68	3.5	2.3	33	6.2	325.6	F	34	10.4
67	1	2.1	33.5	8.2	334.4	F	33.5	10.2
66	6	2.1	32.4	7.8	324	F	33	10.1
65	2	2.3	43.8	7.7	418	T	32.5	9.9
64	6	1.9	40	8.3	383.6	F	32	9.8
63	4	2.5	42.1	9.2	413.6	F	31.5	9.6
62	4	2	42.8	8.5	408.4	F	31	9.4
61	5	1.8	42.3	9.6	405.6	F	30.5	9.3
60	2	1.9	36.9	6.8	352.8	S	30	9.1
59	8	1.7	36.9	8.9	358	F	29.5	9
58	3	1.6	33.4	6.5	318.8	F	29	8.8
57	4.5	1.3	33	9.4	322.4	S	28.5	8.7
56	8.5	1.4	30.6	6.3	292.4	F	28	8.5
55	3.5	0.9	34.1	6.2	312	S	27.5	8.4
54	6.5	0.9	37.7	7.5	346	F	27	8.2
53	3	1.4	40.2	9.1	380.4	F	26.5	8.1
52	9	1.6	38.7	8.5	369.2	F	26	7.9
51	3	1.5	43.3	7	398.4	S	25.5	7.8
50	10	1.5	42.2	8	393.6	F	25	7.6
49	6.5	1.4	36.2	7.6	342.4	F	24.5	7.5
48	3	1.5	34.5	5.1	320.4	F	24	7.3
47	3	1.3	31.5	6	296.8	F	23.5	7.2
46	9	1.5	35.4	7.5	337.2	F	23	7
45	7	1.6	31.9	7.2	309.6	F	22.5	6.9
44	1	2.2	39.9	8.7	389.2	S	22	6.7
43	8	1.8	49.3	8.1	455.6	F	21.5	6.6
42	4	1.7	44.2	5.3	402	F	21	6.4
41	9.5	1.7	25.9	5.2	255.2	F	20.5	6.2
40	9	1.9	29.2	6	288	F	20	6.1

Data pair #	MS SI Units *	K wt. %	U (ppm)	Th (ppm)	Gamma-Ray (API Units)	Lithology **	height above base (ft.)	height above base (m)
39	7	1.8	37.7	8.9	366	F	19.5	5.9
38	7.5	2	44.4	10.6	429.6	F	19	5.8
37	6	2.1	42.5	7.9	405.2	F	18.5	5.6
36	5.5	2.3	45.6	8.3	434.8	F	18	5.5
35	4	1.8	51.2	7.2	467.2	F	17.5	5.3
34	4.5	1.9	45.3	7.8	424	S	17	5.2
33	6	2	42.3	8.7	405.2	F	16.5	5
32	14	1.9	42.6	6.2	396	F	16	4.9
31	5	1.4	40.8	7.5	378.8	F	15.5	4.7
30	5	1.2	39.3	6.9	361.2	S	15	4.6
29	6.5	1.7	44.5	6.8	410.4	F	14.5	4.4
28	8.5	2	56.9	6.7	514	F	14	4.3
27	10	1.2	46.7	7.5	422.8	F	13.5	4.1
26	2	2	57.1	8.1	521.2	S	13	4
25	5	2.2	61.1	12.4	573.6	F	12.5	3.8
24	4	1.9	51.5	11.6	488.8	F	12	3.7
23	6.5	2.3	51.8	11.2	496	F	11.5	3.5
22	3	2.1	47.4	12.6	463.2	T	11	3.4
21	1.5	2.4	65	11.3	603.6	F	10.5	3.2
20	5	3	66.5	13.8	635.2	F	10	3
19	4	1.9	47.2	10.5	450	F	9.5	2.9
18	5	2.4	44.5	12.5	444.4	F	9	2.7
17	3	2.7	52.8	11	509.6	F	8.5	2.6
16	2	2.6	47.7	12	471.2	F	8	2.4
15	1	1.8	41.6	13.1	414	F	7.5	2.3
14	3	2.5	32.4	10.4	340.8	F	7	2.1
13	3.5	1.6	20.1	7.8	217.6	S	6.5	2
12	8	2.5	20.2	8.6	236	F	6	1.8
11	5	2.6	20.3	10.5	246	F	5.5	1.7
10	7.5	1.9	19.8	5.1	209.2	F	5	1.5
9	6	2	22.3	9.9	250	F	4.5	1.4
8	6	1.9	23.6	8.4	252.8	S	4	1.2
7	6	2.3	27.8	4.9	278.8	F	3.5	1.1

Data pair #	MS SI Units *	K wt. %	U (ppm)	Th (ppm)	Gamma-Ray (API Units)	Lithology **	height above base (ft.)	height above base (m)
6	7	2.5	23.6	10.4	270.4	F	3	0.9
5	1.5	1.4	17.7	6.7	190.8	S	2.5	0.8
4	8	0.9	26.4	7.4	255.2	F	2	0.6
3	4	1	30.3	6.1	282.8	S	1.5	0.5
2	2	1.4	28.6	6.2	276	F	1	0.3
1	3	1.7	22.7	9.3	246	S	0.5	0.2

* Denotes points where no MS measurement was possible
**F = Fissile Shale, S = siliceous shale, NF = Fissile w/no MS measurement

Appendix 2. Magnetic susceptibility and spectral gamma-ray data from Hass B.

Data pair #	MS SI Units *	K wt. %	U (ppm)	Th (ppm)	Gamma-Ray (API Units)	Lithology **	height above base (ft.)	height above base (m)
328	N	1.7	28.2	7.5	282.8	NS	164.0	55.8
327	N	2.1	24.9	8.6	267.2	NS	163.5	55.7
326	N	1.9	25.6	7.8	266.4	NS	163.0	55.6
325	N	1.9	26.3	9	276.8	NS	162.5	55.4
324	N	2	22.5	9.4	249.6	NF	162.0	55.2
323	N	2.1	23.3	8.3	253.2	NF	161.5	55.0
322	N	2.3	28.9	9	304	NF	161.0	54.9
321	N	1.9	30.7	8.7	310.8	NF	160.5	54.7
320	N	2.3	28.7	10.3	307.6	NF	160.0	54.5
319	N	1.7	27.8	7.4	279.2	NS	159.5	54.4
318	N	1.4	28.3	6.7	275.6	NF	159.0	54.2
317	N	2.2	31.4	9.3	323.6	NF	158.5	54.0
316	N	2.4	32	11.7	341.2	NF	158.0	53.8
315	N	2	34.4	9.4	344.8	NF	157.5	53.7
314	N	2.1	30.4	8.3	310	NF	157.0	53.5
313	N	2.7	39.4	8.2	391.2	NF	156.5	53.3
312	N	1.9	31.2	8	312	NS	156.0	53.2
311	N	2.5	32.8	7.8	333.6	NS	155.5	53.0
310	N	2.1	31.3	8.2	316.8	NS	155.0	52.8
309	N	1.8	32.9	7.1	320.4	NF	154.5	52.7
308	N	2.1	29.2	10.2	308	NF	154.0	52.5
307	N	1.8	28.4	9.6	294.4	NS	153.5	52.3
306	N	2.3	30.4	10.5	322	NF	153.0	52.1
305	N	2.1	32.5	7.1	322	NS	152.5	52.0
304	N	2.4	32.5	9.7	337.2	NF	152.0	51.8
303	N	2.4	34.1	11.6	357.6	NF	151.5	51.6
302	N	2.2	34.2	8.7	343.6	NS	151.0	51.5
301	N	1.7	36.3	7.6	348	NF	150.5	51.3
300	N	2	32.2	8.6	324	NF	150.0	51.1
299	N	2.8	29.4	11.1	324.4	NF	149.5	50.9
298	N	2.5	33.7	10.1	350	NF	149.0	50.8
297	N	2.7	34.9	8.3	355.6	NF	148.5	50.6

Data pair #	MS SI Units *	K wt. %	U (ppm)	Th (ppm)	Gamma-Ray (API Units)	Lithology **	height above base (ft.)	height above base (m)
296	N	2.3	35.2	7	346.4	NF	148.0	50.4
295	N	2.1	35.1	9.4	352	NF	147.5	50.3
294	N	2.7	45.2	7.3	434	NF	147.0	50.1
293	N	2.9	48.5	8.2	467.2	NF	146.5	49.9
292	N	2.4	35.3	6.5	346.8	NF	146.0	49.8
291	N	1.9	35.5	8.9	350	NF	145.5	49.6
290	N	1.7	35.9	8.7	349.2	NF	145.0	49.4
289	N	2	30.6	7.9	308.4	NF	144.5	49.2
288	N	1.9	34.5	6.7	333.2	NF	144.0	49.1
287	N	1.9	40	7.5	380.4	NF	143.5	48.9
286	N	2.3	40.6	8.9	397.2	NF	143.0	48.7
285	N	2.4	40	9.7	397.2	NS	142.5	48.6
284	0.5	1.7	32.8	5.4	311.2	S	142.0	48.4
283	7	2.3	41.9	11.1	416.4	F	141.5	48.2
282	8	2.1	34.6	9.7	349.2	F	141.0	48.1
281	4	1.9	36.3	8.8	356	S	140.5	47.9
280	4.5	2.5	30.4	8.4	316.8	F	140.0	47.7
279	3	2.4	29.7	8	308	S	139.5	47.5
278	5.5	2.3	30.7	7.9	314	F	139.0	47.4
277	5	1.8	33.9	7.5	330	F	138.5	47.2
276	5	1.9	29	6.9	290	F	138.0	47.0
275	4.5	2.2	32.1	7.6	322.4	F	137.5	46.9
274	2	1.5	38	5.9	351.6	F	137.0	46.7
273	0.5	1.8	39.2	6.8	369.6	S	136.5	46.5
272	4.5	1.6	42.4	8.6	399.2	F	136.0	46.3
271	3.5	2.2	42.9	8.6	412.8	S	135.5	46.2
270	1	1.8	41.1	8.4	391.2	S	135.0	46.0
269	3	1.6	45.8	7.9	423.6	S	134.5	45.8
268	3	1.9	50.7	9.1	472.4	F	134.0	45.7
267	3	2	48.5	8.6	454.4	S	133.5	45.5
266	3	1.7	49.7	11.2	469.6	S	133.0	45.3
265	2.5	2	47.4	6.1	435.6	S	132.5	45.2
264	8	1.6	49.6	7.6	452.8	S	132.0	45.0
263	9.5	2.1	47.5	9.4	451.2	F	131.5	44.8

Data pair #	MS SI Units *	K wt. %	U (ppm)	Th (ppm)	Gamma-Ray (API Units)	Lithology **	height above base (ft.)	height above base (m)
262	9	2.3	53.2	8.9	498	F	131.0	44.6
261	9	2.3	57.1	12.5	543.6	F	130.5	44.5
260	10	3	58.1	12.3	562	F	130.0	44.3
259	7.5	2.3	59.7	11.6	560.8	F	129.5	44.1
258	5	2.3	55.5	9.6	519.2	F	129.0	44.0
257	5	2.5	52.9	9.8	502.4	F	128.5	43.8
256	4	2	50.5	10.2	476.8	F	128.0	43.6
255	1	1.9	51.9	8.6	480	F	127.5	43.5
254	4	2.5	48.8	8	462.4	F	127.0	43.3
253	6	1.9	44.8	11.1	433.2	F	126.5	43.1
252	10	2.3	49.8	8.8	470.4	F	126.0	42.9
251	4	1.8	53.2	9.6	492.8	S	125.5	42.8
250	4	2.1	53.3	9.8	499.2	S	125.0	42.6
249	7.5	2.7	56	9.6	529.6	S	124.5	42.4
248	9	2.4	52.6	9.1	495.6	S	124.0	42.3
247	7	2.5	49.5	11.8	483.2	F	123.5	42.1
246	8	2.4	51.8	8.8	488	F	123.0	41.9
245	9	2.7	50.5	11.3	492.4	F	122.5	41.7
244	10	2.4	49.3	10.2	473.6	F	122.0	41.6
243	8	2.8	47.7	11.6	472.8	F	121.5	41.4
242	6	2.7	55.7	9	524.8	F	121.0	41.2
241	6	2.3	52	11.6	499.2	F	120.5	41.1
240	9	2	50.5	8.2	468.8	F	120.0	40.9
239	8	2.7	60.2	8	556.8	F	119.5	40.7
238	8	2.3	60.3	12.1	567.6	F	119.0	40.6
237	6.5	2.6	57.9	12.5	554.8	F	118.5	40.4
236	6	2.5	54.8	10.9	522	F	118.0	40.2
235	6	2.4	56.9	8.7	528.4	F	117.5	40.0
234	8	2	58.5	9.2	536.8	F	117.0	39.9
233	2	2.3	50.4	8.2	472.8	S	116.5	39.7
232	3.5	1.8	47.4	8.6	442.4	S	116.0	39.5
231	1	1.3	47.6	9.1	438	S	115.5	39.4
230	3	1.7	41.7	8.5	394.8	S	115.0	39.2
229	3	1.8	40.4	7	380	S	114.5	39.0

Data pair #	MS SI Units *	K wt. %	U (ppm)	Th (ppm)	Gamma-Ray (API Units)	Lithology **	height above base (ft.)	height above base (m)
228	3	1.6	46.7	6.4	424.8	S	114.0	38.9
227	4	1.9	54.1	10	503.2	F	113.5	38.7
226	6.5	2.6	55.5	8.3	518.8	F	113.0	38.5
225	4	2.1	49.6	7	458.4	F	112.5	38.3
224	6.5	2.1	44.6	9.4	428	F	112.0	38.2
223	3	2.2	49.8	9.8	472.8	S	111.5	38.0
222	5	2.2	48.6	7.7	454.8	F	111.0	37.8
221	5	1.9	48.9	9.7	460.4	F	110.5	37.7
220	4	2.1	45.5	9.3	434.8	F	110.0	37.5
219	2	2	44.2	9.3	422.8	S	109.5	37.3
218	2	2	41.2	8.2	394.4	S	109.0	37.1
217	4	1.8	41.5	8.2	393.6	F	108.5	37.0
216	2	1.9	43.4	7.3	406.8	S	108.0	36.8
215	3	1.7	48.9	9.9	458	S	107.5	36.6
214	5	2.1	48.9	9.7	463.6	F	107.0	36.5
213	3	2	52.2	8.5	483.6	S	106.5	36.3
212	6	1.9	48.2	7.5	446	F	106.0	36.1
211	5	1.8	46.4	11	444	S	105.5	36.0
210	6	2.4	46.9	8	445.6	F	105.0	35.8
209	4	2	47	9.2	444.8	S	104.5	35.6
208	6	2.1	45.6	8.9	434	S	104.0	35.4
207	4.5	1.9	48.2	9.3	453.2	F	103.5	35.3
206	5.5	1.8	46.2	9.3	435.6	S	103.0	35.1
205	3	1.8	42.2	9.8	405.6	S	102.5	34.9
204	2.5	1.6	45.4	8.1	421.2	F	102.0	34.8
203	5	1.8	48.3	7.5	445.2	F	101.5	34.6
202	2	1.9	46.1	7.2	428	S	101.0	34.4
201	2.5	2.1	51.2	9	479.2	F	100.5	34.3
200	3	2.3	55.8	7.1	511.6	S	100.0	34.1
199	0	2.3	52.6	7.7	488.4	S	99.5	33.9
198	1	2.1	57	11.5	535.6	S	99.0	33.7
197	1.5	1.6	53.9	7.6	487.2	S	98.5	33.6
196	1	1.6	50.8	6.2	456.8	S	98.0	33.4
195	1	1.9	50.7	9.2	472.8	F	97.5	33.2

Data pair #	MS SI Units *	K wt. %	U (ppm)	Th (ppm)	Gamma-Ray (API Units)	Lithology **	height above base (ft.)	height above base (m)
194	3	2.1	49	11.3	470.8	S	97.0	33.1
193	4	2	50.7	11.4	483.2	S	96.5	32.9
192	3	2.2	47.5	10.5	457.2	S	96.0	32.7
191	2	1.8	41.4	7	388	S	95.5	32.5
190	6	2.3	40.2	8	390.4	F	95.0	32.4
189	7	2.2	43.6	11.8	431.2	S	94.5	32.2
188	4	1.5	52.3	7.4	472	S	94.0	32.0
187	3	2	50.6	8.7	471.6	S	93.5	31.9
186	3	1.9	49.4	7.6	456	S	93.0	31.7
185	3	1.9	52.3	9.6	487.2	S	92.5	31.5
184	2.5	1.7	50.8	10.3	474.8	S	92.0	31.4
183	1	2.2	48.6	8.8	459.2	F	91.5	31.2
182	5	2.2	48.6	9.5	462	F	91.0	31.0
181	4	2	41.5	11.5	410	F	90.5	30.8
180	8	2.3	44.6	9.8	432.8	S	90.0	30.7
179	8	2.6	40.5	9.1	402	S	89.5	30.5
178	7	2.3	38.2	8.9	378	S	89.0	30.3
177	2	2.2	33	7.1	327.6	S	88.5	30.2
176	4	2.3	31.7	8.3	323.6	S	88.0	30.0
175	1.5	2.8	29.6	8.6	316	S	87.5	29.8
174	2	2.5	28.8	10.1	310.8	S	87.0	29.6
173	5	2.1	25.5	9.2	274.4	F	86.5	29.5
172	3	2.6	27.6	9.5	300.4	S	86.0	29.3
171	2	2.6	27	11	301.6	S	85.5	29.1
170	1	2.8	27.6	8.9	301.2	S	85.0	29.0
169	5	2.1	31.3	9	320	S	84.5	28.8
168	3	2.3	32.2	9.4	332	S	84.0	28.6
167	6	2.2	32.9	9.6	336.8	F	83.5	28.5
166	6	1.8	30.4	9.4	309.6	S	83.0	28.3
165	4.5	1.6	31	7.6	304	S	82.5	28.1
164	2.5	1.6	32.7	8.1	319.6	S	82.0	27.9
163	1	1.9	31.2	7.5	310	S	81.5	27.8
162	3	1.7	35.5	8	343.2	S	81.0	27.6
161	3	1.5	34.8	8.7	337.2	S	80.5	27.4

Data pair #	MS SI Units *	K wt. %	U (ppm)	Th (ppm)	Gamma-Ray (API Units)	Lithology **	height above base (ft.)	height above base (m)
160	3	1.9	36.6	7.9	354.8	F	80.0	27.3
159	5	2.3	35.4	9.4	357.6	S	79.5	27.1
158	3	1.9	39.2	7.2	372.8	S	79.0	26.9
157	5	2.1	38	7.5	367.6	S	78.5	26.8
156	3	2	36.1	8.2	353.6	S	78.0	26.6
155	1	1.4	36.9	8.5	351.6	F	77.5	26.4
154	1.5	1.9	32.4	6.2	314.4	F	77.0	26.2
153	-2	1.8	35.2	9.2	347.2	S	76.5	26.1
152	1	1.9	37.1	6.9	354.8	F	76.0	25.9
151	1	1.5	33.8	8.1	326.8	S	75.5	25.7
150	3.5	1.5	36	6.7	338.8	F	75.0	25.6
149	3	1.5	32.2	5.6	304	F	74.5	25.4
148	3	1.6	33.6	5.9	318	F	74.0	25.2
147	1	1.7	32.8	7.6	320	S	73.5	25.0
146	2	1.9	33.6	6.8	326.4	S	73.0	24.9
145	2	2.1	33.3	6.8	327.2	S	72.5	24.7
144	1.5	1.5	34.7	6.2	326.4	S	72.0	24.5
143	1	1.1	37.9	6.2	345.6	S	71.5	24.4
142	1	1.4	34.6	5.5	321.2	S	71.0	24.2
141	2	1.5	34.1	6.1	321.2	S	70.5	24.0
140	3	1.1	35.7	6.8	330.4	S	70.0	23.9
139	1	1.8	33.5	6.6	323.2	S	69.5	23.7
138	1	1.7	36.6	8.2	352.8	S	69.0	23.5
137	4	1.6	39	7.2	366.4	S	68.5	23.3
136	1.5	1.5	37.2	8.7	356.4	S	68.0	23.2
135	4	1.4	35.9	12.4	359.2	F	67.5	23.0
134	1	1.6	38.9	8	368.8	F	67.0	22.8
133	1	1.6	39	9.1	374	S	66.5	22.7
132	1.5	1.7	37.6	7.7	358.8	F	66.0	22.5
131	4	1.3	34.3	7.1	323.6	F	65.5	22.3
130	1	1.3	34	6.3	318	S	65.0	22.2
129	2.5	1.9	40.4	4.8	372.8	S	64.5	22.0
128	2.5	2	34.3	6	330.4	S	64.0	21.8
127	-0.5	1.5	38.1	5.4	350.4	S	63.5	21.6

Data pair #	MS SI Units *	K wt. %	U (ppm)	Th (ppm)	Gamma-Ray (API Units)	Lithology **	height above base (ft.)	height above base (m)
126	3	1.4	32.8	6.7	311.6	S	63.0	21.5
125	3	1.4	36.4	6.8	340.8	S	62.5	21.3
124	1	1.5	35.9	6.3	336.4	S	62.0	21.1
123	3	1.6	42.9	6.8	396	F	61.5	21.0
122	3	2.3	45.8	6.3	428.4	S	61.0	20.8
121	2	1.8	48.9	9.1	456.4	S	60.5	20.6
120	2.5	1.5	46.9	7.9	430.8	S	60.0	20.4
119	3	1.7	44.7	6.9	412.4	S	59.5	20.3
118	3	1.4	47	6.5	424.4	F	59.0	20.1
117	3	1.4	46.8	7.1	425.2	S	58.5	19.9
116	3	1.6	43.1	7.5	400.4	S	58.0	19.8
115	0.5	1.3	36	7.6	339.2	S	57.5	19.6
114	3.5	1.6	37.4	5.1	345.2	F	57.0	19.4
113	6	1.3	34.4	3.9	311.6	F	56.5	19.3
112	2	1.5	31.5	6.3	301.2	S	56.0	19.1
111	1.5	1.3	30.3	5.3	284.4	S	55.5	18.9
110	2.5	1.1	34.6	4.9	314	S	55.0	18.7
109	5	1	32.9	3.8	294.4	F	54.5	18.6
108	2	1.1	33.1	4.5	300.4	S	54.0	18.4
107	3	1.6	27.6	6.9	274	S	53.5	18.2
106	3	1.4	28.2	5.9	271.6	S	53.0	18.1
105	8	1.5	26.2	6.9	261.2	F	52.5	17.9
104	2	1.4	24.8	7.2	249.6	S	52.0	17.7
103	14.6	1.5	23.3	6.4	236	S	51.5	17.6
102	8	1.7	22.8	6.4	235.2	F	51.0	17.4
101	1	1.7	21	6.1	219.6	S	50.5	17.2
100	3	1.8	21.6	6.1	226	F	50.0	17.0
99	4	2.1	27.3	8.2	284.8	F	49.5	16.9
98	4	1.9	27.6	6.4	276.8	S	49.0	16.7
97	6	2.4	29	6.6	296.8	S	48.5	16.5
96	8	1.9	38.5	6.7	365.2	F	48.0	16.4
95	13	2.7	41.5	6.5	401.2	F	47.5	16.2
94	2	2	41.6	10.3	406	F	47.0	16.0
93	2	1.8	32.4	8.6	322.4	S	46.5	15.8

Data pair #	MS SI Units *	K wt. %	U (ppm)	Th (ppm)	Gamma-Ray (API Units)	Lithology **	height above base (ft.)	height above base (m)
92	3	1.4	35.6	8.7	342	S	46.0	15.7
91	3	2.1	37	7.3	358.8	S	45.5	15.5
90	2	2.7	41.8	7.2	406.4	S	45.0	15.3
89	2	2	41.4	9.4	400.8	S	44.5	15.2
88	6	2.7	37.4	7.8	373.6	F	44.0	15.0
87	6	2.1	40	7	381.6	F	43.5	14.8
86	2	2.2	40.4	7.4	388	S	43.0	14.7
85	4	2	45.6	7.8	428	F	42.5	14.5
84	4	1.9	44.4	6.8	412.8	F	42.0	14.3
83	1.5	2.2	43.1	8.7	414.8	S	41.5	14.1
82	5	2	48.9	8.8	458.4	F	41.0	14.0
81	9	2.9	44.9	7.1	434	F	40.5	13.8
80	4.5	2.8	43.2	10.1	430.8	F	40.0	13.6
79	3	3.3	36.5	11.7	391.6	F	39.5	13.5
78	7	3.3	36.8	10.8	390.4	F	39.0	13.3
77	1	3.1	33.8	13.6	374.4	F	38.5	13.1
76	3	3.8	34.5	9.3	374	F	38.0	13.0
75	5	3.2	39.9	9.9	410	F	37.5	12.8
74	5	3.5	36	8.7	378.8	F	37.0	12.6
73	1.5	3.1	33.9	12.9	372.4	F	36.5	12.4
72	2	2.6	29.1	8.3	307.6	F	36.0	12.3
71	3	2.8	27.5	8.9	300.4	S	35.5	12.1
70	4	3.7	27	11.4	320.8	F	35.0	11.9
69	6	4	23.8	12.4	304	F	34.5	11.8
68	5	3	26.8	8.4	296	F	34.0	11.6
67	4.5	3.3	29	9.2	321.6	F	33.5	11.4
66	2.5	2.5	33.2	9.8	344.8	F	33.0	11.2
65	4	2.5	28.3	10.1	306.8	F	32.5	11.1
64	6	2.4	30.2	7.7	310.8	F	32.0	10.9
63	6	2.7	25.5	9.8	286.4	F	31.5	10.7
62	7.5	2.4	28.5	9.3	303.6	F	31.0	10.6
61	3.5	3.1	29.2	6.9	310.8	F	30.5	10.4
60	7	2.8	29.9	10.9	327.6	F	30.0	10.2
59	4.5	2.6	29.9	8.3	314	F	29.5	10.1

Data pair #	MS SI Units *	K wt. %	U (ppm)	Th (ppm)	Gamma-Ray (API Units)	Lithology **	height above base (ft.)	height above base (m)
58	6	2.2	31.1	8.5	318	F	29.0	9.9
57	3.5	1.8	30.2	7.4	300	F	28.5	9.7
56	7	2.3	28.5	9.7	303.6	F	28.0	9.5
55	2	2.1	30.8	8.2	312.8	F	27.5	9.4
54	5	2.6	32.4	7.7	331.6	F	27.0	9.2
53	5	2.7	29	9.6	313.6	F	26.5	9.0
52	3	2.8	29.6	8.7	316.4	F	26.0	8.9
51	4	3	28.1	10.8	316	F	25.5	8.7
50	5	3.1	27.3	11.3	313.2	F	25.0	8.5
49	5	2.8	30.7	7.4	320	S	24.5	8.3
48	2.5	2.2	28.8	9.4	303.2	F	24.0	8.2
47	8.5	2.4	27.2	9.7	294.8	F	23.5	8.0
46	1.5	2.5	29.3	8.6	308.8	F	23.0	7.8
45	5.5	2.1	27	8.1	282	S	22.5	7.7
44	2.5	2.2	23.9	7.3	255.6	S	22.0	7.5
43	6	2.7	35.7	10.2	369.6	F	21.5	7.3
42	7	3.2	35.4	11.6	380.8	F	21.0	7.2
41	1	2.3	31.6	9.9	329.2	S	20.5	7.0
40	2	2.1	34.7	8.8	346.4	S	20.0	6.8
39	2	2.1	30.4	9.9	316.4	S	19.5	6.6
38	4	2	31.2	9.3	318.8	F	19.0	6.5
37	6	2.6	36.7	9.3	372.4	F	18.5	6.3
36	-1	2.4	30.7	9.3	321.2	S	18.0	6.1
35	5	2.9	31.5	9.3	335.6	F	17.5	6.0
34	3	2.7	35.7	8.2	361.6	S	17.0	5.8
33	N	2.6	45.6	8.4	440	NF	16.5	5.6
32	N	2	56.3	9.5	520.4	NF	16.0	5.5
31	N	2.3	56.7	12.9	542	NF	15.5	5.3
30	N	2.1	57.7	8.7	530	NF	15.0	5.1
29	N	2.3	46.5	11.2	453.6	NF	14.5	4.9
28	N	1.9	44.8	7	416.8	NF	14.0	4.8
27	N	1.7	45.5	6.6	417.6	NF	13.5	4.6
26	N	1.2	39.9	6.2	363.2	NF	13.0	4.4
25	N	1.9	37.3	7.6	359.2	NF	12.5	4.3

Data pair #	MS SI Units *	K wt. %	U (ppm)	Th (ppm)	Gamma-Ray (API Units)	Lithology **	height above base (ft.)	height above base (m)
24	N	2.3	35.6	9	357.6	NF	12.0	4.1
23	N	2.3	39.2	11.6	396.8	NF	11.5	3.9
22	N	3.2	35.4	10.2	375.2	NF	11.0	3.7
21	N	2.6	36.9	10.7	379.6	NC	10.5	3.6
20	N	3	37.6	13.2	401.6	NC	10.0	3.4
19	N	2.9	35.9	12.3	382.8	NC	9.5	3.2
18	N	3.3	36.5	11	388.8	NC	9.0	3.1
17	N	3.7	34.4	14.2	391.2	NC	8.5	2.9
16	N	4.4	28.4	16.9	365.2	NC	8.0	2.7
15	N	4.8	23.9	16	332	NC	7.5	2.6
14	N	4.9	21.7	16.3	317.2	NC	7.0	2.4
13	N	5.4	16	16.2	279.2	NC	6.5	2.2
12	N	5.3	12.7	17.2	255.2	NC	6.0	2.0
11	N	5.6	9.8	21.4	253.6	NC	5.5	1.9
10	N	6.1	10.4	18.5	254.8	NC	5.0	1.7
9	N	5	10.7	20.8	248.8	NC	4.5	1.5
8	N	5.4	10	15.7	229.2	NC	4.0	1.4
7	N	4.2	10.4	19.2	227.2	NC	3.5	1.2
6	N	3.4	7.9	13.9	173.2	NC	3.0	1.0
5	N	3.4	10.6	11.4	184.8	NC	2.5	0.9
4	N	3.8	10.9	16	212	NC	2.0	0.7
3	N	3.7	9	13.4	184.8	NC	1.5	0.5
2	N	2.9	6.5	11.3	143.6	NC	1.0	0.3
1	N	2.8	7.3	9.9	142.8	NC	0.5	0.2

* Denotes points where no MS measurement was possible

**F = Fissile Shale, S = siliceous shale, NF = Fissile w/no MS measurement, NS = Siliceous w/no MS measurement, NC = Claystone w/no MS measurement

Appendix 3. Elemental concentrations of select elements from inductively coupled plasma-mass spectromrtry data at Hass A.

Sample #	Al (ppm)	U (ppm)	Fe (ppm)	K (ppm	Fe/Al ratio (ppm/ppm)
1	20563.34	520.51	24098.65	17356.93	1.17
2	13161.52	648.57	21966.78	11482.89	1.67
3	1764.55	10.51	1682.11	1811.56	0.95
4	20915.86	29.66	5989.19	18451.19	0.29
5	22517.99	52.28	10364.39	19135.22	0.46
6	6583.93	24.43	5599.76	6948.24	0.85
7	6738.23	12.48	5332.30	8477.79	0.79
8	13650.67	45.40	14369.10	10391.53	1.05
9	5446.44	13.73	5169.90	5984.75	0.95
10	11683.39	45.78	13093.81	12567.22	1.12
11	50482.71	110.26	32218.55	18682.33	0.64
14	7088.63	13.79	6368.11	8399.77	0.90
15	4134.49	6.28	2331.31	3777.91	0.56
16	15533.24	24.63	9585.37	16111.73	0.62
17	14202.50	32.22	13522.80	12585.16	0.95
18	12091.66	34.21	15069.51	14040.78	1.25
19	20697.40	40.43	18299.53	19294.89	0.88
20	15378.37	41.43	25400.19	16343.39	1.65
21	11308.49	40.11	21621.12	11096.60	1.91
22	10399.07	16.20	8264.85	10466.54	0.79
23	20586.72	34.55	17943.68	20584.40	0.87
24	15740.50	29.71	14031.24	15670.19	0.89
25	14114.92	20.95	8649.68	11258.11	0.61
26	18915.51	30.17	10811.76	19773.88	0.57
27	7976.89	14.66	9901.31	5903.75	1.24
28	5572.66	8.36	6568.67	5134.97	1.18
29	1882.60	2.77	1056.26	1922.32	0.56
30	35312.13	45.10	17685.35	29052.29	0.50
31	13030.73	19.29	6837.59	11692.31	0.52
32	3472.42	14.82	4678.75	4003.11	1.35
33	18247.45	16.99	8907.11	15825.58	0.49
34	6743.27	14.40	4293.39	6766.65	0.64
35	4914.22	10.72	4163.29	6953.91	0.85
36	27022.78	48.13	7117.61	25942.47	0.26
37	12003.82	32.38	5452.82	13489.43	0.45
38	18616.01	64.03	8811.76	19042.55	0.47
39	18176.85	35.63	12893.53	20497.49	0.71
40	533.38	5.71	1322.85	679.26	2.48
41	551.06	4.10	1695.00	722.50	3.08
42	722.57	3.77	1341.37	898.32	1.86

VITA

Michael Gordon Aufill

Candidate for the Degree of

Master of Science

Thesis: Outcrop-Based Correlation Of Magnetic Susceptibility With Spectral Gamma-Ray Spectrometry In The Woodford Shale Of South-Central Oklahoma

Major Field: Geology

Biographical:

Personal Data: Born July 24, 1957 to William Robert Aufill and Katherine Elizabeth (Holley) Aufill in Alburquerque, New Mexico.

Education: Graduate Westside High School; Augusta, Georgia; May, 1975
BS Secondary Science Education; Oklahoma State University; May, 2004

Name: Michael Gordon Aufill Date of Degree: December, 2007

Institution: Oklahoma State University Location: Stillwater, Oklahoma

Title of Study: High Resolution Magnetic Susceptibility Of The Oklahoma Woodford Shale And Its Relationship To Variations In Outcrop Gamma Response

Pages in Study: 210 Candidate for the Degree of Master of Science

Major Field: Geology

In the present study, we quantify the correspondence between magnetic susceptibility (MS) and spectral gamma-ray measurements (SGR) in measured sections of the Woodford Shale. Paired MS/SGR measurements were made at 15 cm intervals. Shale samples were compositionally analyzed by inductively coupled plasma-mass spectrometry (ICP-MS). Iron/aluminum ratios (Fe_{ppm}/Al_{ppm}) from the ICP-MS data were compared to accepted shale standards in order to estimate the relative proportions of detrital iron and authigenic iron.

The data suggest that lithology exerts primary control on MS and SGR. Moreover, MS from some Woodford Shale sections varies with SGR. Fe/Al ratios calculated from ICP-MS suggest that Fe in the Woodford Shale is predominantly authigenic. The concomitant occurrence of diagenetic FeS_2 (pyrite) nodules, MS/SGR maxima, uranium concentrations over 100 ppm, and large quantities of dispersed pyrite appears to be common in distal anoxic environments characteristic of petroleum source rocks where Fe oxides are chemically unstable.

ADVISER'S APPROVAL: Dr. Alexander Simms